Therapeutic Potential of Adipose-Derived Stromal Cells for the Treatment of Senile Osteoporosis

Dissertation

zur

Erlangung der naturwissenschaftlichen Doktorwürde

(Dr. sc. nat.)

vorgelegt der

Mathematisch-naturwissenschaftlichen Fakultät

der

Universität Zürich

von

Ali Mirsaidi

aus dem

Iran

Promotionskomitee

Prof. Dr. med. vet. Michael O. Hottiger (Vorsitz)

PD Dr. Peter J. Richards (Leitung der Dissertation)

Prof. Dr. med. Francois Verrey

PD Dr. Paolo Cinelli

Zürich 2014

Summary

Impaired osteogenic differentiation of resident bone marrow stromal cells (BMSCs) of aged patients with low turnover osteoporosis is considered to be one of the major contributing factors in the development of structural and mechanical deficiencies associated with osteoporotic bone. As such, therapies designed to counteract these effects are currently being pursued with an aim to restoring the stem cell niche and enhancing bone quality. In the current thesis, evidence is provided which supports the use of autologous adipose-derived stromal cells (ASCs) as a means by which to combat age-related bone loss.

Initial studies were undertaken to compare the differentiation potential of ASCs from osteoporotic SAMP6 and non-osteoporotic SAMR1 mice in 2D *in vitro* culture systems. Their ability to differentiate towards osteoblast and adipocyte cell lineages was evaluated by histological, biochemical and molecular techniques. In contrast to BMSCs, the differentiation potential of ASCs was found to be comparable between both strains. Further *in vitro* studies were performed to assess the osteogenic potential of SAMP6-derived ASCs cultured under 3D conditions using long-term silk fibroin scaffold cultures and short-term scaffold free microtissue spheroid (ASC-MT) cultures. In both cases, ASCs underwent efficient osteogenesis resulting in mineralized tissue formation. In the final study, ASCs and ASC-MT were evaluated for their ability to enhance trabecular bone quality following a single intratibial injection in SAMP6 mice using micro-CT, histological and molecular based analyses. Both ASCs and ASC-MT could be identified within treated bones after 42 days and moreover, resulted in significant improvements in several parameters of trabecular bone quality. Furthermore, human ASCs harvested from osteoporotic patients were also demonstrated as having a positive influence on the osteogenic differentiation potential of dysfunctional osteoporotic patient-derived BMSCs *in vitro*.

In conclusion, these studies have demonstrated that adipose tissue may represent a promising autologous cell source for the development of novel bone regenerative therapeutic strategies for the treatment of age-related bone loss.

Zusammenfassung

Als einer der Hauptgründe für die strukturellen und mechanischen Defizite des Knochengewebes von Patienten mit altersbedingter Osteoporose wird eine beeinträchtigte Differenzierung von adulten Stammzellen aus dem Knochenmark (bone marrow stromal cells, BMSCs) zu knochenbildenden Osteoblasten angenommen. Dementsprechend werden gegenwärtig Therapieansätze verfolgt, die diese verminderte Differenzierungskapazität von Stammzellen kompensieren und dadurch die Knochenqualität verbessern sollen.

Im Rahmen dieser Promotion konnte gezeigt werden, dass autologe adulte Stammzellen aus dem Fettgewebe (adipose-derived stromal cells, ASCs) ein geeignetes Mittel zur Behandlung von altersbedingter Osteoporose darstellen könnten.

Zunächst wurde das Differenzierungspotential von ASCs aus osteoporotischen SAMP6- und nicht osteoporotischen SAMR1-Mäusen zu Osteoblasten und Adipozyten *in vitro* in 2D-Zellkulturen mit Hilfe von histologischen, biochemischen und molekularbiologischen Methoden untersucht. Im Gegensatz zu BMSCs konnte dabei kein Unterschied in der Differenzierungsfähigkeit von ASCs aus osteoporotischen und nicht-osteoporotischen Mäusen festgestellt werden.

Daraufhin wurde das osteogene Potential von ASCs aus osteoporotischen SAMP6-Mäusen in 3D-Zellkulturen untersucht. Zum einen wurden die Zellen auf einer Seidenfibroin-Matrix kultiviert, zum anderen Mikrogewebe ohne Matrix (ASC microtissues, ASC-MTs) hergestellt. ASCs zeigten unter beiden Kulturbedingungen eine effiziente Osteogenese mit einhergehender Mineralisierung.

Im abschliessenden Teil wurden ASCs und ASC-MT einmalig direkt in die Tibia von SAMP6-Mäusen injiziert und anschliessend die trabekuläre Knochenqualität mittels Mikro-CT sowie histologischen und molekularbiologischen Methoden bestimmt. Sowohl ASCs als auch ASC-MTs konnten noch 42 Tage nach der Injektion in den behandelten Knochen nachgewiesen werden, und ihre Applikation resultierte in einer signifikanten Verbesserung verschiedener Parameter der trabekulären Knochenqualität. Des Weiteren konnte gezeigt werden, dass ASCs osteoporotischer Patienten *in vitro* einen positiven Einfluss auf die osteogene Differenzierung von dysfunktionellen BMSCs von Osteoporose-Patienten haben.

Zusammenfassend kann gesagt werden, dass das Fettgewebe eine vielversprechende, autologe Quelle für adulte Stammzellen zur Entwicklung von neuen Therapieansätzen zur Behandlung von altersbedingter Osteoporose darstellen könnte.

Table of Contents

Abbreviations

MSC	multipotent stromal cell
BMSC	bone marrow stromal cell
ASC	adipose-derived stromal cell
ASC-MT	adipose-derived stromal cell microtissue spheroid
HSC	hematopoietic stem cell
SAMP6	senescence accelerated mouse strain prone 6
SAMR1	senescence-accelerated mouse resistant 1
ECM	extracellular matrix
Runx2	Runt-related transcription factor 2
Sp7	osterix
BMP	bone morphogenetic protein
c-fms	colony-stimulating factor 1 receptor
RANK	receptor activator of nuclear factor- κ B
RANKL	receptor activator of nuclear factor- κ B ligand
M-CSF	macrophage colony-stimulating factor
OPN	osteopontin
TRAP	tartrate resistant acid phosphatase
DMP	dentin matrix acidic phosphoprotein
MEPE	matrix extracellular phosphoglycoprotein
OPG	osteoprotegerin
PTH	parathyroid hormone
TGF β	transforming growth factor
BMD	bone mineral density
BMU	bone multicellular unit
C/EBP	enhancer binding protein
Ppar	peroxisome proliferator-activated receptor
FGF	fibroblast growth factor
WAT	white adipose tissue
BAT	brown adipose tissue
GVHD	graft-versus-host-disease

1 Introduction

The skeleton, which is composed of bone, soft tissue, and cartilage, is a dynamic organ, and it undergoes continuous bone remodeling throughout life. This process involves bone resorption coupled with bone formation which allows the skeleton to adapt bone mass and strength to external forces, as well as to modify the bone shape during growth and to regulate calcium homeostasis [1-3]. An imbalance between bone resorption and formation leads to metabolic bone diseases, such as osteoporosis.

Osteoporosis is the most common metabolic bone disorders affecting 200 million individuals worldwide, and due to shifts in the population pyramid towards old age, has since become the fourth most common disease [4, 5]. As such, it is a leading cause of mortality and morbidity, which is a key factor in the high cost of medical care in aged individuals. Osteoporosis constitutes the most common cause of fractures, with more than 1.5 million occurring per year in the United States, including over 500’000 cases of hospitalizations, 800’000 emergency room encounters, as well as visiting two million doctors, and placing of almost 180’000 individuals into nursing homes [6]. It has been further estimated that osteoporosis (especially in the hip) will occur in one out of two Americans over age of 50 by 2020, and will eventually result in a higher risk of developing osteoporosis in other skeletal sites [7]. In the European Union, it has been estimated that the total costs for medical care for osteoporotic patients, including hospitalization and rehabilitation, were over 36 billion Euros in 2000 and the corresponding projected costs in 2050 will be over 76 billion Euros [8, 9].

Osteoporosis can be classified as either primary or secondary. The main causes of primary osteoporosis consist of age and estrogen deficiency arising from the menopause, while secondary osteoporosis can occur as a consequence of disorders of energy metabolism such as anorexia nervosa, obesity, and diabetes mellitus [6, 10-12]. These individuals experience varying degrees of imbalance between bone deposition and bone resorption, resulting in progressive loss of bone mineral density (BMD) and increased skeletal fragility. This is primarily due to alterations in different factors such as bone microarchitecture, mineralization and mechanical properties [13]. This deviations may happen as a consequence of damage in the homeostatic control of the bone multicellular unit (BMU) in which the activities of bone forming osteoblasts and bone resorbing osteoclasts have become dysregulated [13].

The presence of functionally active BMSC-derived mature osteoblasts is crucial for bone formation. Studies have shown that BMSCs isolated from aged osteoporotic patients have a higher tendency to differentiate towards adipogenesis than osteogenesis, suggesting that the structural abnormalities associated with osteoporotic bone maybe as a result of inadequacies in bone cell differentiation [14, 15].

Available treatment options tend to be more supportive than curative and are often associated with persistent patient morbidity, further fractures, and eventually mortality [7, 16]. Therefore, stem cell-based therapies may represent a viable alternative to conventional treatment strategies for the management of bone loss and impaired bone quality in osteoporotic patients.

1.1 Bone tissue

Bone is an extremely dynamic mineralized tissue characterized by its hardness, resilience, growth mechanisms, high degree of vascularity and its capability to remodel itself throughout life.

Bone has several important functions within the body. It provides structural support and protection to vital organs in the body, as well as being responsible for maintaining mineral homeostasis. It is also the main organ to synthesis blood cells. Bone is also capable of maintaining optimal shape and structure, by means of continuous renewal and remodeling, through which it is able to respond to changes in the environment with different loading demands [17]. Bone also acts as a calcium store for the body and plays an impotent role in the regulation of plasma calcium levels [18]. The majority of calcium amount within the body is found in the skeleton (99%), and the remaining amount is found in cell membranes and extracellular fluid [19].

Anatomically, bones can be divided in two major types, including long bones (such as humerus, tibia, and femur), and flat bones (like skull, mandible, and sacrum). They are derived from either endochondral ossification or intramembranous during development.

Intramembranous ossification takes place during the development of flat bones and in peripheral sites of fracture healing. During intramembranous ossification, BMSCs undergo osteogenesis directly resulting in the production of mineralized osteoid tissue.

Endochondral ossification occurs during the development of short and long bones, growth plate, and the natural healing of bone fractures (callus ossification). Upon endochondral ossification, BMSCs aggregate and undergo chondrogenesis, forming a transitory hyaline cartilage tissue [20]. Chondrocytes within the cartilaginous tissue then undergo hypertrophy

and eventually apoptosis, giving way to osteoblasts and mineralized tissue formation. This is followed by formation of blood vessels, which transports the osteoprogenitor cells responsible for mineralization and the synthesis of the osteoid. There are two areas where ossification occurs during development of long bones, the primary center, which takes place within the diaphyseal, and the secondary center located in epiphyseal regions. In between these ossification centers, areas of proliferating chondrocytes (epiphyseal or growth plate) secure bone formation and growth [21].

At the histological level, bone may be further classified into two different types of tissue, namely cortical bone, and trabecular or cancellous bone. Cortical bone constitutes about 85% of the total bone tissue, of which 80 to 90% is calcified, and it is typically found in the long bones of the appendicular skeleton. Trabecular bone makes up about 15% of the skeleton and only 15 to 25% is calcified, and it is primarily located in the vertebrae as well as other sites of the axial skeleton (Figure 1). The relationship between trabecular architecture and bone strength serves as an important factor for predicting fracture risk [22].

Bone consists of three primary components, including extracellular matrix (ECM), cells, and bone marrow. The ECM of the bone is made up of mineralised tissue, which is important for providing mechanical strength. Chemically, inorganic minerals, mainly calcium phosphate, contribute to two-thirds of the composition of bone tissue and the rest is organic bone materials. Calcium together with phosphorus forms hydroxyapatite crystals which is the main component of bone tissue ($Ca_{10}(PO_4)_6(OH)_2$). These lie along the collagen fibrils, mainly collagen type I, and are embedded in an amorphous ground substance composed of proteoglycans and glycoproteins. Approximately 15% of total bone protein is non-collagenous endogenous and exogenous protein. Plasma is the main source for the majority of exogenous proteins, whereas endogenous proteins, such as osteonectin, osteopontin, fibronectin and osteocalcin are synthesized by bone cells [23-27]. These proteins are multi-functional, and play an important role in regulating bone mineralization and remodeling.

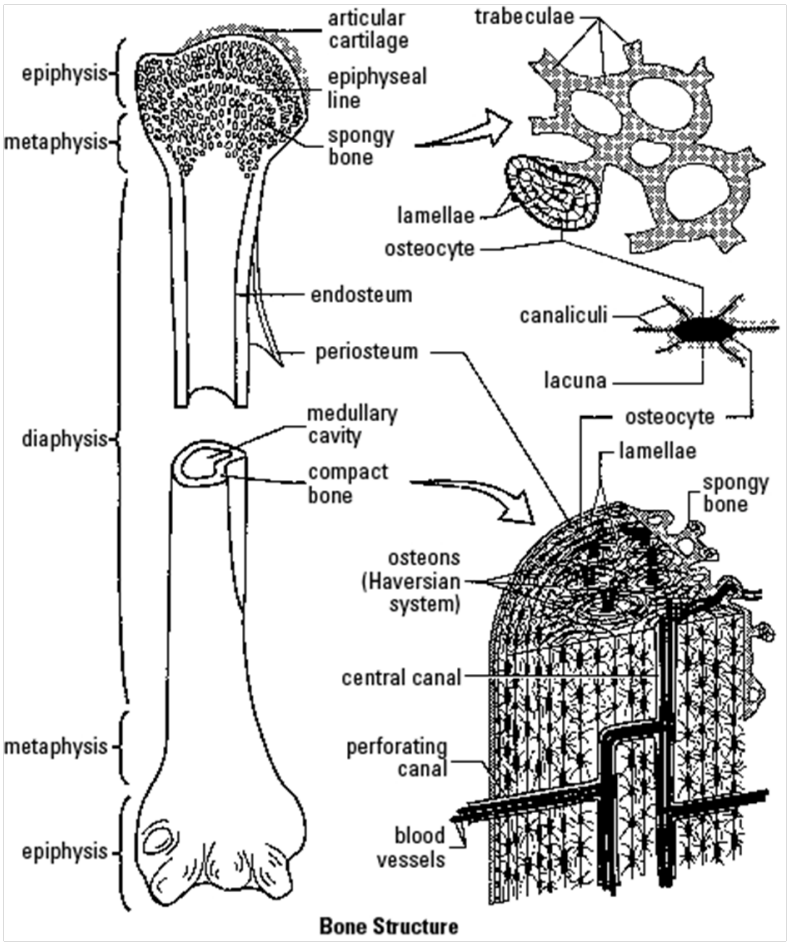

Figure 1: Schematic diagram of the bone microstructure [28].

1.1.1 Bone cells and their functions

Bone cells are derived from two distinct sources, one of which is BMSCs, which give rise to the osteoblastic lineage (osteoblasts, osteocytes and bone lining cells), and the other one is hematopoietic stem cells (HSCs) which gives rise to osteoclasts. Bone cells are responsible for maintaining the structure of the matrix.

The osteoblast is a cuboidal mononuclear cell, responsible for bone formation by synthesizing the main components of the ECM, including collagen and non-collagenous proteins. Osteoblasts are found in clusters along the bone surfaces, lining the layer of bone matrix. Morphologically, osteoblasts are characterized by a rounded nucleus, abundant rough endoplasmic reticulum, an extensive Golgi apparatus and lysosomes. They become embedded in their own synthesized osteoid through the process of bone formation, and have the capacity to either undergo apoptosis or differentiate further osteocytes.

Runt-related transcription factor 2 (Runx2) and a downstream factor, osterix (Sp7), are crucial for osteoblast differentiation [29, 30]. Bone morphogenetic proteins (BMPs) such as BMP2 have been observed to trigger the initiation of transcription factors that are crucial for the differentiation of osteoblasts [31]. Interaction between BMPs and Wnt proteins is one of the possible mechanisms by which BMPs regulate osteoblast differentiation [32]. Wnt protein binds to frizzled receptors and the lipoprotein receptor-related protein (LRP)-5 as a co-receptor on the cell surface. This interaction activates the binding of intracellular Axin protein to LRP-5, thereby blocking the degradation of β-catenin leading to activation of transcription [33]. Wnt stimulates the expression of BMP2, which increases osteogenesis and bone formation through BMP receptors on the cell surface. This pathway is regulated by sclerostin, which is an inhibitor of Wnt signaling [34]. Mutations in the sclerostin gene are responsible for sclerosteosis, an autosomal recessive disorder characterized by continues skeletal overgrowth [35].

Osteoclasts are large multinucleated cells responsible for bone resorption, formed by fusion of mononuclear progenitors of the monocyte-macrophage lineage. Morphologically, osteoclasts contain abundant Golgi complexes, mitochondria and transport vesicles loaded with lysosomal enzymes. Prior to bone resorption, osteoclasts polarize due to changes in the cytoskeleton and form three distinct plasma membrane domains, including the sealing zone, ruffled border, and functional secretory domain. The sealing zone occurs on the apical side where the cell membrane adheres tightly to the bone surface. In the cell membrane overlying this isolated compartment, numerous thin finger-like extensions form and make up the ruffled border, where the actual bone resorption occurs. Simultaneously, a functional secretory domain forms on the basolateral side of the cell. The initial attachment of osteoclasts to bone surfaces involves binding of integrins to specific amino acid sequences (RGD) within proteins such as osteopontin (OPN) at the matrix surface [36-38]. Protons are responsible for generating the acidic environment, and are produced by the help of Carbonic anhydrase II in the osteoclast cytoplasm. They are then subsequently transported into acidic vesicles via activation of a vacuolar type ATPase proton pump located in the membrane of the vesicles [39]. These acid-containing vesicles then fuse with the cell membrane to form the ruffled border, and the contents of the vesicles are released into the resorptive (Howship's) lacuna. The active secretion of protons acidifies the environment and solubilises the mineral crystals, exposing the organic matrix to degrading proteases, whilst providing the optimal pH for their activity [40]. The degradation products are endocytosed from the ruffled border, transported through the cell, and finally secreted into the extracellular space through the functional

secretory domain [41, 42]. Osteoclasts also contain large amounts of tartrate-resistant acid phosphatase (TRAP), a metallophosphatase secreted into the resorptive lacunae. When activated by proteolytic processing, TRAP exhibits protein phosphatase activity towards matrix proteins such as OPN, and regulates osteoclast motility by dephosphorylation of OPN in the matrix [43, 44].

The majority of the cells embedded within bone matrix are termed osteocytes, and they have several cellular extensions from their plasma membrane, which are necessary for interacting with other osteocytes and osteoblasts found on the bone surface. Osteocytes are differentiated osteoblasts enclosed in separate lacunae throughout the bone. They create a functional communicative network enabling cross-talk between the various types of bone cells by sending out thin cytoplasmic extensions traversing mineralized bone via thin canals termed canaliculi. Osteocytes are involved in the biomechanical regulation of bone mass and structure, most likely by sensing bone deformation, pressure, fluid flows and streaming potentials. Osteocytes typically express molecules such as dentin matrix protein 1 (DMP1) [45] and matrix extracellular phosphoglycoprotein (MEPE) [46]. MEPE is an inhibitor of mineralization [47], whereas DMP1 is produced by the osteocyte in a mechanically sensitive manner, and influences phosphate homeostasis through control of fibroblast growth factor [48].

The bone lining cells are flat elongated cells covering quiescent bone surfaces that develop from osteoblasts. One of their possible functions is to participate in the regulation of substrate exchange between the extracellular fluid of bone marrow and bone fluid compartment. They respond to mechanical signals and mediate communication between the osteocyte network and the pool of osteoclasts, thus initiating bone resorption [49]. The other functions of these cells is to remove the remaining collagen dissolved by osteoclasts in resorptive pits, and deposition of a thin layer of collagenous matrix before mature osteoblast begin the process of bone formation [50].

1.2 Bone remodeling

Bone remodeling is the process responsible for maintaining the shape, quality and size of the skeleton throughout life. Remodeling is essential for repairing microfractures before they accumulate and lead to fatigue fractures under repeated cyclic loading (targeted remodeling), as well as providing access to stores of calcium and phosphate and maintaining the mineral homeostasis (random remodeling). This process is regulated by different cytokines, hormones and mechanical forces [51, 52].

Osteoclast precursors initially express colony-stimulating factor 1 receptor (c-Fms) on their surface, as well as receptor activator of nuclear factor κB (RANK). Receptor activator of nuclear factor κB ligand (RANKL) and macrophage-colony stimulating factor (M-CSF) are two hematopoietic cytokines necessary for commitment and differentiation of macrophage precursors into mature osteoclasts (Figure 2) [53]. Osteoprotegerin (OPG) is produced by osteoblasts and represents a competitive soluble ligand for RANK [54]. The coupling of resorption and formation is based upon the RANK-RANKL-OPG axis. RANKL is a protein synthesized by osteoblasts, and is present both in a membrane-bound and a soluble form. RANKL binds to RANK on osteoclast precursors, thereby promoting osteoclast formation [37, 54-56]. Once RANKL binds to RANK, it triggers a signal transduction cascade that leads to the expression of a number of genes such as TRAP, cathepsin K, and calcitonin receptor [57]. This process is further regulated by OPG, which acts to block activation of RANK and thus formation of active osteoclasts. The synthesis of OPG is enhanced by estrogen and so the reduction in estrogen levels (e.g. at the onset of menopause) causes less synthesis of OPG as well as higher activity of osteoclast [56, 58].

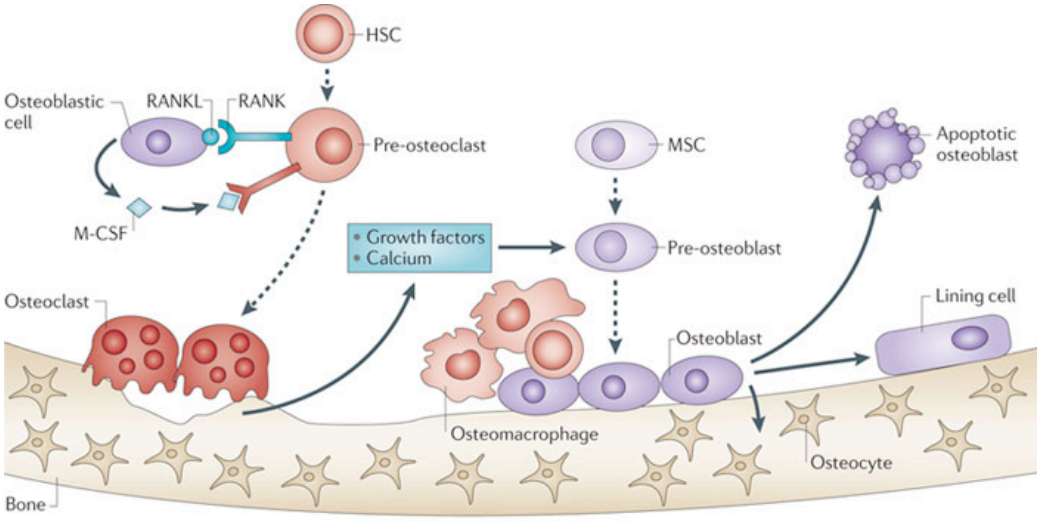

Figure 2: Bone remodeling process [59].

Systemic hormones, such as 1,25-dihydroxyvitamin D_3, and parathyroid hormone (PTH) can also regulate osteoclasts either directly, or through activation of osteoblasts and stromal cells [60, 61]. Following bone resorption, osteoclasts undergo apoptosis and are replaced by bone forming osteoblasts through the actions of transforming growth factor beta (TGFβ) [62]. Osteoblast activity is also controlled by both systemic hormones and a number of paracrine factors, one of which is platelet-derived growth factor BB (PDGF-BB) secreted by osteoclasts. PDGF-BB was also shown to induce the production of OPG (negative feedback of osteoclastogenesis) [63]. Following their attachment to bone, osteoblasts secrete both collagenous and non-collagenous proteins, leading to the production of new matrix. This requires about three months until the resorptive cavity is completely refilled, and is followed by the secretion of a number of proteins that are essential for regulating bone remodeling [64].

1.2.1 Pathology of the bone remodeling

Osteoporosis is a systemic disease affecting the whole skeleton, being characterized by reductions in bone mass and deterioration of the microarchitectural structure of bone tissue, resulting in loss of mechanical strength and increased risk of fracture [4].

An osteoporotic individual is defined by the World Health Organization (WHO) as someone who has a bone mineral density (BMD) of 2.5 standard deviations or more below the mean peak bone mass (average of healthy young adults) as measured by dual-energy X-ray absorptiometry. This is generally referred to as the T-score, which is defined as the measured BMD minus young adult mean BMD divided by the young adult standard deviation. Established osteoporosis includes T-scores bellow -2.5 and the presence of one or more fragility fractures, and can be classified as either primary or secondary [65-67].

Primary osteoporosis is further divided into type I, which occurs in postmenopausal women, appearing usually after the age of 50 years old. Type I osteoporosis mainly affects trabecular areas and contributes in particular to vertebral and wrist fractures. It is associated with low trabecular bone mass and disturbed trabecular architecture. In addition, cortical bone mass is decreased and the diameter of the modularly cavity is expanded due to increased endocortical bone resorption overriding periosteal apposition. Type II, also known as senile osteoporosis, affects both trabecular and cortical bone in aged men and women, typically from the 7th decade of life, and predisposes the hip to fractures.

Secondary osteoporosis is related to other conditions such as hypogonadism, endocrine disorders, renal failure, rheumatic diseases, gastrointestinal disorders, osteomalacia, rickets and Paget's disease [68].

After achieving peak bone mass in the late twenties, both men and women start to lose bone. Peak bone mass is mainly determined by genetic factors, but also influenced by environmental factors such as diet (e.g. vitamin D, calcium) and physical activity. Therefore, those who don't achieve their genetically optimal bone mass are at a greater risk of developing osteoporosis and associated fragility fractures later in life. The development of osteoporosis is dependent on several factors such as failure to reach peak bone mass in young adulthood, excessive resorption after peak bone mass, or impaired bone formation during remodeling [69].

Postmenopausal osteoporosis is a consequence of withdrawal of the bone-sparing effects of estrogen, where resorption overrides bone formation. Age-related bone loss occurs at most skeletal sites in adults although its pattern, magnitude and underlying cellular mechanisms are remarkably different. In men, trabecular bone volume decreases with age and the individual trabeculae become thinner, but remain connected [22]. This is associated with a decreased rate of matrix deposition and increased duration of the bone formation phase during remodeling. The same trabecular thinning is observed in women until menopause, where the rate of bone loss accelerates due to cessation of estrogen production. Lack of estrogens coupled with an enhancement of RANKL production by bone marrow osteoblastic, T and B cells [70], increases bone turnover rate and the osteoclastic resorption. There is also an increase in the activation frequency of basic multicellular units (BMUs), and the enhanced osteoclast activity could also leads to deeper Howship's lacunae. Thus, trabeculae are perforated and ultimately removed, resulting in reduced trabecular number and connectivity in women [71]. As osteoporosis disease advances, the bone volume reduces as a result of expanding marrow volume [72], and more adipose tissue is deposited within the bone marrow possibly due to an imbalance between osteogenesis and adipogenesis [73-75]. Therefore, osteoporosis has also been referred to as the bone obesity [6]. This concept is further supported by reports of osteopenia in a mouse model of accelerated adipogenesis which highlights the detrimental effect of imbalances between adipogenesis and osteogenesis on bone mass [76].

1.2.2 Effects of age on bone quality

One of the important elements to characterize bone quality is its resistance to fracture coupled with the incorporation of bone density and mechanical strength as well as architecture and mineralization [13, 77, 78], and are affected during aging due to alterations in bone turnover through the process of bone remodeling. As such, dealing with fracture repair in aged and osteoporotic bone is one of the main challenges for orthopaedic surgeons, as a result of inferior properties of the cancellous bone [79-81]. It is also further investigated that aging play an important role to regulate bone quality and potentially the initiation of osteoporosis by using combination knock out of both Werner (*Wrn*) and telomerase (*Terc*) genes in experimental models of accelerated aging. This mutation leads to reduce trabecular bone mass, which is one of the key elements in osteoporotic patients [82]. Another well recognized model of accelerated aging is klotho gene-deficient model that develops characteristics of age-related osteoporosis such as low-bone turnover osteoporosis with a highly reduction of bone formation rates as compared to bone resorption [83, 84]. Furthermore, this is associated with alterations in the age, number and spatial distribution of functionally active resident bone-forming cells [85]. The senescence accelerated mouse strain prone 6 (SAMP6) model has been extensively used for the purpose of investigating the detrimental effects of aging on bone quality. The SAMP6 mouse displays bone phenotype such as reduced trabecular bone volume, decreased bone strength [86] and reduced areal BMD [87]. An advantage of the SAMP6 model, compared with a true aging model, is that bone loss phenotype is clearly developed by 3 to 4 months and can be directly compared with the aged matched control, senescence-resistant mouse, strain R1 (SAMR1) [87]. Interestingly, as with human osteoporotic patients, although bone quality in these mice is severely impaired, the rate of fracture union remains unaffected [88]. It is evident therefore that the SAMP6 mouse encompasses many of the most salient features associated with the human condition and as such, maybe considered a suitable model with which to investigate both disease mechanisms and novel therapeutic strategies. Therefore, it is the intention of this thesis to utilize the SAMP6 model for the purpose of investigating the role and therapeutic potential of stem cells in osteoporosis. It is envisaged that the use of such an appropriate and well-defined osteoporotic model will allow us to more effectively translate our experimental results to the human condition.

1.3 Basic concept of stem cells

Stem cells represent the building blocks of our bodies and have been defined as the natural units of embryonic generation and adult regeneration [89]. Stem cells are distinguished from other cell types by two important characteristics. Firstly, they are unspecialized cells capable of undergoing self-renewal throughout an organism's lifetime, sometimes after long periods of inactivity. Secondly, they have the ability to become organ-specific cells with distinct functions. These two properties make somatic stem cells unique and ideal for tissue engineering applications [90].

Depending on the stage of development, stem cells may be classified as embryonic (derived from the totipotent cells of early embryo), fetal (derived from the developing foetus) and adult stem cells (derived from mature organs in the adult individual). Recently, pluripotent stem cells were artificially derived from somatic cells by specifically inducing the expression of genes involved in self-renewal and potency [48, 91, 92]. Stem cells receive various signals from their niche, including growth factors and secreted cytokines, as well as signals mediated by cell-cell interactions and interactions with ECM to control the process of stem cell characteristics [93].

Stem cells are not only necessary for development and organogenesis, but are also important for tissue maintenance and repair [94]. Apart from giving the full range of differentiated cells, stem cells can proliferate while maintaining their multipotent characteristics. This property of stem cells can also occur by so-called asymmetric cell division, suggesting that upon division one daughter cell becomes a committed progenitor cell that subsequently undergoes further differentiation, while the other daughter cell remains as a stem cell with the same characteristics as the mother cell [94, 95].

1.3.1 Stem cell niche

The idea of the stem cell niche was initially proposed over 30 years ago to explain the specialized microenvironment where a stem cell resides *in vivo* [96]. Under normal physiological conditions, the stem cell niche consists of a cellular and ECM component, which forms a functioning unit of tissue. At a more molecular level, the stem cell niche can be considered a dynamic entity in which complex interactions occur between stem cells and neighbouring cells, typically involving direct cell-cell interactions and release of diffusible soluble factors or cytokines (autocrine or paracrine signalling within the niche), extracellular matrix, oxygen tension and pH, amongst many other essential parameters [93, 97, 98]. The complex and highly dynamic relationship between stem cells and various components of its

surrounding microenvironment play an important role in the regulation of stem cell behaviour, with niche-specific signals serving to maintain the stem cell in its quiescent state. At selected time points, niche-specific signals can be modified accordingly to induce an appropriate response in the stem cell such as proliferation, migration and differentiation [93, 98].

1.3.2 Multipotent stromal cells (MSCs)

MSCs have the potential to undergo differentiation towards various cell lineages, giving rise to a variety of mesenchymal tissues, including bone (osteoblast), fat (adipocytes), muscle (myocytes), cartilage (chondrocytes) and tendon (tenocytes) [99] (Figure 3). This multipotency, together with their capacity for extensive expansion, has led to MSCs being considered as a very promising source of cells for regenerative medicine. This is primarily due to the ease by which these cells can be isolated and expanded *in vitro,* whilst still retaining their multipotential differentiation capacity under specific conditions [100, 101].

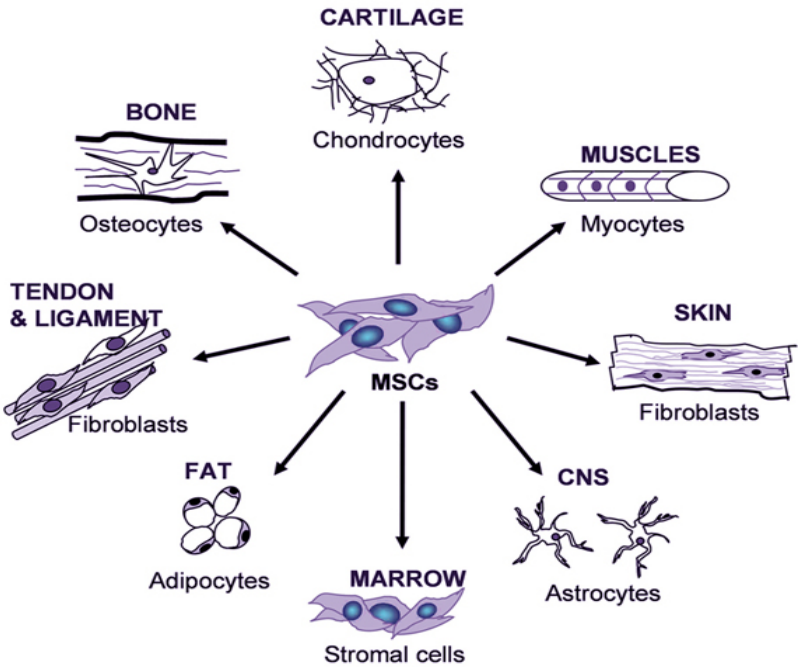

Figure 3: Multi-lineage potential of adult mesenchymal stem cells [102].

MSCs can be found ubiquitously throughout the body and are routinely isolated from sources such as bone marrow, adipose tissue, adult blood, umbilical cord blood, amniotic fluid, tendon and ligaments, synovial membranes, deciduous teeth, liver, lung and spleen [103-112].

MSC differentiation requires the activation of specific regulatory genes and subsequent signaling events. The key factors and important mechanisms known to be involved in adipogenic and osteogenic differentiation are detailed in the following sections (Figure 4).

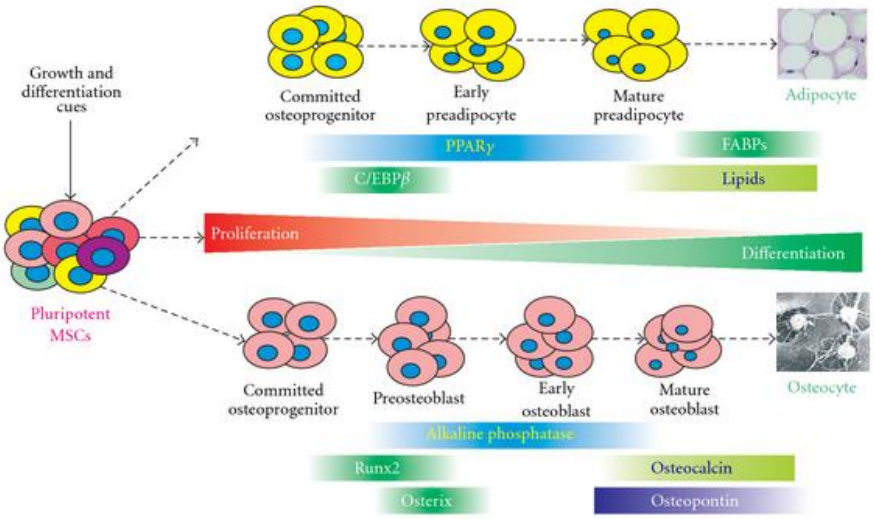

Figure 4: Adipogenic and osteogenic differentiation [113].

1.3.3 Adipogenesis

The transcriptional regulation of adipogenic differentiation has been studied using several *in vitro* models. In order for MSCs to undergo adipogenesis, a specific medium supplemented with 3-isobutyl-1-methylxanthine, insulin, indomethacin, and dexamethasone has frequently been used [114-116]. Upon differentiation, the fibroblast-like morphology of MSCs is converted into a more rounded shape as a result of changes in the ECM as well as the synthesizing of proteins associated with the cytoskeleton [117]. Furthermore, cytoplasmic formation of lipid droplets composed of triglycerides and cholesterol esters is enhanced during adipogenic differentiation. This is also involved in one or two rounds of clonal expansion followed by activation of adipogenic specific genes and achievement of the adipogenic phenotype [118]. Up-regulation of gene expression during adipogenic differentiation is accomplished by the chronological activation of peroxisome proliferator-activated receptor γ2 (PPARγ2) and enhancer binding proteins (C/EBPs). Intermediate activation of C/EBPβ and C/EBPδ stimulates expression of C/EBPα and PPARγ2 (Fig. 4) [117, 119], which then stimulates expression of target genes like fatty acid binding protein 4 (FABP4), facilitated glucose transporter member 4 (GLUT4), and lipoprotein lipase (LPL) [120-122]. Additionally, loss-of-function studies in chimeric mice and overexpression studies

in non-adipogenic fibroblasts suggest that PPARγ2 is necessary for induction of adipogenesis [123].

It has been shown that factors like fatty acids, M-CSF, insulin-like growth factor 1 (IGF1), prostaglandins, and glucocorticoids are involved in induction of adipogenic differentiation, while Wnt signaling and TGFβ play a more inhibitory role [118].

1.3.4 Osteogenesis

The mechanisms of osteogenesis, which is essential for bone formation, have been studied in different *in vitro* culture systems. One of the important components provided in differentiation culture medium is ascorbic acid. This is necessary for accumulation of collagen type I in the ECM of differentiating osteoblasts as well as for the expression of bone gamma-carboxyglutamate (Gla) protein (osteocalcin) and alkaline phosphatase (ALP). The other element is β-glycerophosphate which serves as an exogenous source of organic phosphate for matrix mineralization [124, 125].

At the transcriptional level, osteogenesis is induced by the transcription factors RUNX2 and SP7 [126, 127]. RUNX2 requires heterodimerisation with core-binding factor β to achieve its transcriptional activity to induce the differentiation of MSCs towards osteoblasts and chondroblasts and to inhibit their differentiation into adipocytes and myocytes [128, 129]. Furthermore, RUNX2 post-transcriptional regulation can be conducted via phosphorylation or protein-protein interactions, and its activity is enhanced by mitogen-activated protein kinase (MAPK) signaling as demonstrated in human MSCs stimulated with fibroblast growth factor (FGF)-2 [130, 131]. Sp7 is mainly expressed in osteoblasts, and is required for the differentiation of pre-osteoblasts into mature osteoblasts after initiation of osteogenesis by RUNX2 [30]. Furthermore, it has been shown that Sp7 inhibits expression of transcription factor (SOX9), which is necessary for chondrogenic induction.

Several hormones and signaling pathways also play important roles in the regulation of osteogenesis, including BMP and FGF signaling [132]. It has been reported that BMP2 enhances osteoblast commitment and affect stabilization of RUNX2 by acetylation. This process has an inhibitory effect on degradation of the transcription factor by the ubiquitination pathway [133]. FGFs together with their corresponding receptors (FGFRs) enhance osteogenic differentiation potential of adult MSCs and embryonic bone development [131, 134-139].

1.3.5 Inverse relationship between adipogenic and osteogenic differentiation

There is a close relationship between both osteogenic and adipogenic differentiation, as both pathways share a common progenitor cell. It has been shown that bone loss is accompanied by an increasing accretion of adipose tissue in the bone marrow cavity [72]. As such, an appreciation of the pathways that regulate both adipogenesis and osteogenesis may be critical to our understanding of how bone loss is controlled. Both RUNX2 and PPARγ are master transcriptional regulators and are present in low levels in undifferentiated MSCs, and are differentially regulated depending on which cell lineage is chosen [12, 140]. Differentiation towards either pathway is regulated by a complex set of paracrine signals, including BMPs, Wnts, PPARγ ligands, corticosteroids, and growth factors [74, 140]. Such factors are derived from cells in the neighbouring niche environment including osteoblasts, adipocytes, hematopoietic stem cells (HSCs), and endothelial cells [74, 141-143]. Additionally, MSC differentiation towards either adipogenesis or osteogenesis corresponds to unique intracellular redox profiles [144], and each cell type can further modify their extracellular redox environment to be more oxidizing (adipocytes) or reducing (osteoblasts), suggesting that differentiation into specific phenotypes may also be dependent on redox states [144]. Importantly, the pathogenesis of osteoporosis represents a significant imbalance between these reciprocally regulated differentiation programs, with excess marrow adipocytes being produced at the expense of osteoblasts [5, 6, 10-12, 74, 145-148]. These regulatory mechanisms are summarized in Figure 5.

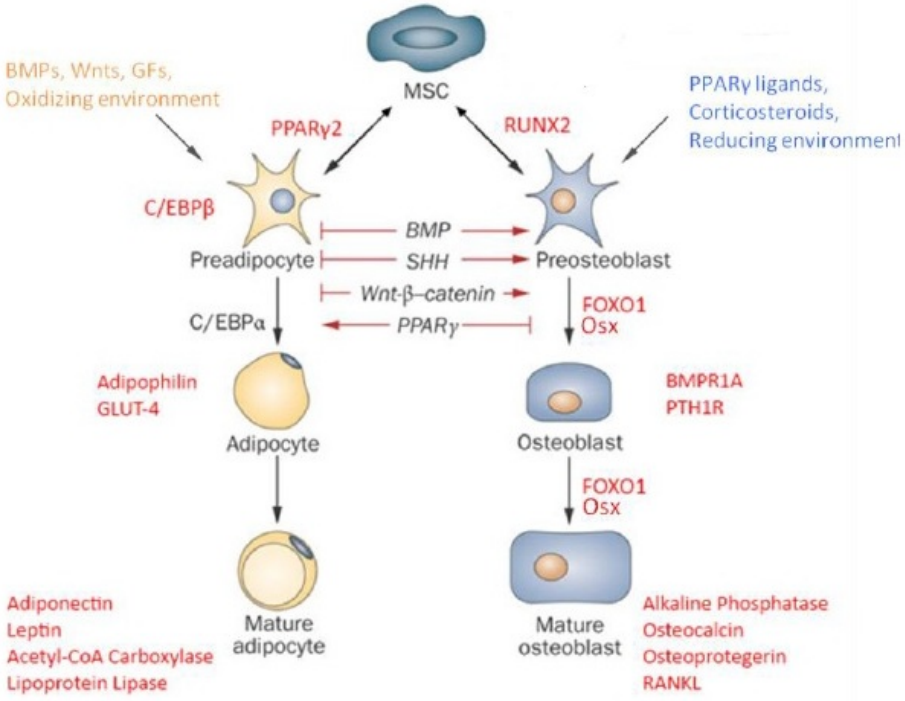

Figure 5: Schematic diagram differentiation number of regulators control MSC fate [148].

1.4 Potential therapeutic applications of MSCs

MSCs are promising candidates for clinical use in cellular therapies and tissue engineering strategies. Cellular therapies are medical processes, which utilize healthy, fully functional cells in order to replace dysfunctional cells that have been damaged or even destroyed by disease. The principle of tissue engineering is primarily the same, although it additionally involves culturing cells on three dimensional structures *in vitro*, in order to form functional units that more closely mimic the *in vivo* target tissue. A variety of different cell types may be used in cellular therapies and tissue engineering, including mature functional cells, genetically modified cells or even cells from different species. Optimal cells should be readily available and highly expandable *in vitro*, display consistent differentiation properties and be highly biosynthetic, preserve a stable phenotype after specification and not elicit any adverse immune response after implantation [149]. Among the cells that fit such a profile, MSCs are considered to be most suitable in situations of allogeneic and autologous transplantation [150].

Allogeneic transplantation can be clinically challenging, since the recipient's body may recognize the allergenic material as foreign, resulting in an immune response and possible rejection of the transplanted material. As such, allogeneic transplantation must be accompanied by rigorous immune suppression. MSCs are immunologically unique in that they express more major histocompatibility complex (MHC) Class I antigens than MHC Class II antigens [151]. It has also been reported that both undifferentiated MSCs and their differentiated derivatives lack the expression of MHC Class II antigens, strongly suggesting that MSCs are non-immunogenic and would not evoke an immune response upon transplantation [152]. In agreement with this observation, it has been shown that following allogeneic transplantation, MSCs evaded immune recognition and were readily detected in recipients after extended time periods [150]. A common complication of allogeneic transplantation is graft-versus-host-disease (GVHD), in which functional immune cells carried over from the donor in the transplanted material recognize the recipient as foreign and trigger an immune response. MSC transplantation has not only been shown to reduce the incidence of GVHD, but has also been used as a treatment for this disease [151]. Therefore, the potential of MSCs for use in allogeneic transplantation as well as autologous transplantation has major clinical significance, since material could be transplanted between mismatched individuals.

1.4.1 Use of adult MSCs in promoting new bone formation

Nowadays, the purpose of using adult MSCs for developing new bone reconstruction therapies is prevalent in areas of both experimental and clinical research. Several approaches have been utilized in the deployment of these cells to specific locations within dysfunctional or damaged bone to assist in restoring normal bone homeostasis. This has been shown by using biomaterial carriers seeded with BMSCs, which allow for the implantation of osteogenic differentiating cells directly into a defect site [153-155]. In a different approach, BMSCs can be introduced into the defect area either by a systemic or local injection. Such an approach has already been performed in clinical studies examining the effectiveness of BMSC treatment of the degenerative bone condition, osteogenesis imperfecta [156-160]. The successful outcome of such bone marrow infusions in children suffering from osteogenesis imperfecta was demonstrated by increases in osteoblast numbers and new lamellar bone formation [158]. Furthermore, it was also reported that the incidence of fractures among these children decreased.

The genetic alteration of MSCs to optimize both cellular delivery and also performance has been validated in several studies investigating the potential of cell-based therapies for the treatment of bone loss. It has been demonstrated that systemic transfer of genetically altered MSCs overexpressing receptor RANK-Fc and the CXC chemokine receptor-4 (CXCR-4) protected against bone loss in an ovariectomized mouse model [161]. Similarly, bone mineral density was increased in ovariectomized mice treated with BMSCs overexpressing BMP2 and α4 integrin [162]. In the case of mouse MSCs overexpressing β-galactosidase- or BMP4, cells were directly injected into the bone marrow, rather than intravenously, resulting in a much greater proportion of bone engrafted cells and significantly increased trabecular BMD [163]. This approach has also been adopted for the transfer of bone marrow cells to senile osteoporotic mice. It has been shown that following allogeneic bone marrow transplantation from normal mice into irradiated SAMP6 mice, bone mineral density was restored to levels comparable to non-osteoporotic mice [164]. However, one major drawback in the use of allogeneic bone marrow transplantation is the need for bone marrow ablation in recipients due to the presence of immunocompetent cells. One alternative therefore, is to use purified stem cell preparations free of contaminating immunoreactive cell types. This concept was further evaluated to investigate the effects of immortalized C3H/10T1/2 mouse embryonic fibroblasts on bone remodeling. Mouse C3H/10T/2 cells genetically induced to over express CXCR4, were shown to restore bone mass and enhance bone formation in glucocorticoid-

induced osteoporotic mice following either systemic or local intramedullary administration [165].

The local administration of osteocompetent MSCs directly into bone could therefore offer an alternative means by which to enhance bone quality, although the differentiation state of these cells and the microenvironment to which they are exposed, may play significant roles in determining their fate. In this thesis, adipose tissue will be evaluated as a potential source of therapeutic MSCs for the purpose of enhancing of bone quality in a mouse model for senile osteoporosis and determine the most appropriate means by which to transplant these cells.

1.4.2 Biological applications of adipose-derived stromal cells (ASCs)

In order to use adipose tissue for the purpose of stem cell therapy, one should first be aware of the composition of this tissue. Adipose tissue is the specific connective tissue which functions as the major storage site for fat in the form of triglycerides. The main portion of adipose tissue is composed of lipid-filled cells, maintained in a framework of collagen fibers. Adipose tissue contains endothelial cells, fibroblasts, blood cells, pericytes, adipocytes, and adipose precursor cells [166]. Fat tissue can be classified as two types; brown adipose tissue (BAT) and white adipose tissue (WAT), which is the larger proportion of the body fat. The morphology and function of brown adipocytes are distinct from white adipocytes. Phenotypically, brown fat cells are rich in mitochondria and accumulate lipids in multiple small droplets [167], and their function is to translate energy into heat production [168]. In the WAT, mature adipocytes have one large lipid droplet with the nucleus located at the cell periphery, and are also referred to as univacuolar adipocytes. WAT serves several functions such as heat insulation, mechanical cushion, and most importantly, a source of energy [166, 169, 170] (Figure 6). Moreover, WAT secretes hormones and signaling factors, which play an important role in several physiological and pathophysiological processes [171, 172]. The release of adipokines from adipocytes and adipose tissue influences insulin sensitivity, energy homeostasis, and vascular homeostasis of the organism [170, 173, 174].

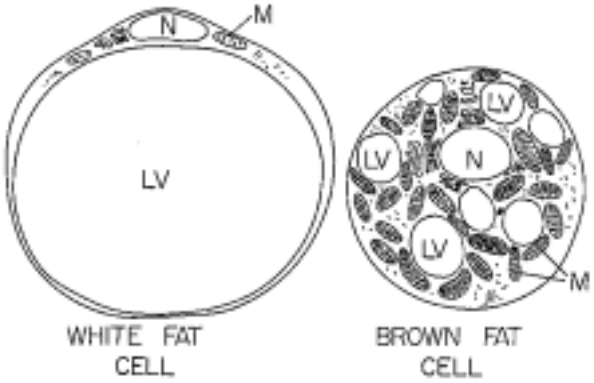

Figure 6: White fat cell and brown fat cell. LV: lipid vacuole; M: mitochondria; N: nucleus. [*Artwork courtesy of Dr. John Horwitz, U.C. Davis.S.*]

ASCs can be isolated from various fat stores throughout the body by minimally invasive liposuction or through enzymatic digestion of adipose tissue [175-177]. It has been demonstrated that ASC clones derived from lipoaspirates can differentiate towards adipogenesis, osteogenesis, and chondrogenesis [178]. These findings together with the fact that ASCs can undergo several population doublings while retaining their differentiation capabilities support the hypothesis that ASCs are a type of multipotent adult stem cell [178, 179]. In the case of using adipose tissue, deficiency of autologous donor tissue is very unlikely in most individuals. Subcutaneous fat extraction is one of the easiest ways for obtaining ASCs for generating different cell lineages [180].

Regarding osteogenesis, several studies have illustrated that there is a close relationship between osteogenic differentiation in bone marrow aspirates and adipose tissue [176, 181, 182]. It is conceivable therefore, that MSCs isolated from sources other than the bone marrow, may also have the potential to enhance the quality level of osteoporotic bone. Recent studies utilizing GFP-expressing ASCs have already confirmed that following a single intramedullary infusion in mice, not only do the cells become engrafted within the injected bones, but they also have many of the characteristic features associated with resident osteoblasts, confirming complete osteogenic differentiation of these cells [183]. Moreover, pre-exposure of these cells to bone microenvironment enhanced both cell migration and survival in the bones of recipient mice following systemic administration.

It has been shown that ASCs seeded on hydroxyapatite/tricalcium phosphate (HA-TPC) matrices are capable of forming bone in vivo, and the majority of the ASCs formed osteoid following implantation in mice [182]. Moreover, another study demonstrated that large

skeletal defects such as skull fracture, can be healed without genetic manipulation or the addition of any exogenous growth factors by using scaffolds seeded with ASCs [184, 185]. Information gleaned from such studies may enable us to identify suitably potent stem cell sources from which novel autologous stem cell-based therapeutic strategies could be developed with an aim to improving bone quality in elderly osteoporotic patients.

2 Hypothesis and aims of the thesis

The fundamental premise of this thesis is that resident BMSCs are centrally involved in the development of low turnover osteoporosis and that deficits in bone remodeling may be counteracted through manipulation or replacement of these cell populations, thereby resulting in improved bone quality.

Aim 1: Compare the differentiation potential of ASCs from osteoporotic (SAMP6) and non-osteoporotic (SAMR1) mice. ASCs were isolated from SAMP6 and SAMR1 mice and maintained in a 2D *in vitro* culture system. Their ability to differentiate towards osteoblast and adipocyte cell lineages was evaluated using histological, biochemical and molecular techniques.

Aim 2: Establish a 3D *in vitro* culture system using ASCs in scaffold-free microtissue spheroids (ASC-MTs). ASCs were cultured in an ASC-MT format and their osteogenic differentiation capacity was evaluated using histological, biochemical and molecular techniques.

Aim 3: Determine whether transplanted ASCs or ASC-MT have the capacity to promote new bone formation and enhance trabecular structure in osteoporotic mice. ASCs and ASC-MT were injected directly into the bone marrow of SAMP6 mice and their effects on bone quality evaluated by radiological and molecular analyses. Transplanted cells were identified through the use of CellTracker CM-Dil. The influence of ASCs on BMSC-mediated mineral formation was further assessed in *in vitro* studies utilizing osteoporotic patient-derived BMSCs and ASCs.

It was envisaged that the results gleaned from this study would not only improve our understanding of the role of MSCs in osteoporosis but would also allow for the development of more effective therapeutic strategies with which to combat bone loss and thus restore bone quality.

3 Results

3.1 Overview of published and submitted manuscripts

3.1.1 Telomere length, telomerase activity and osteogenic differentiation are maintained in adipose tissue-derived stromal cells from senile osteoporotic SAMP6 mice

Authors: **Mirsaidi A**, Kleinhans KN, Rimann M, Tiaden AN, Stauber M, Rudolph KL, Richards PJ.

Journal: Tissue Engineering and Regenerative Medicine, 2012; 6:378-90.

Contribution: Planning, performing and evaluating all the experiments.

3.1.2 Preparation and osteogenic differentiation of scaffold-Free mouse adipose-derived stromal cell microtissue spheroids (ASC-MT)

Authors: **Mirsaidi A**, Tiaden AN, Richards PJ.

Journal: Current Protocols in Stem Cell Biology, 2013, 27:2B.5.1–2B.5.12.

Contribution: Planning, performing and evaluating all the experiments.

3.1.3 Therapeutic potential of adipose-derived stromal cells in age-related osteoporosis

Authors: **Mirsaidi A**, Genelin K, Vetsch J, Stanger S, Lindtner RA, Blauth M, Müller R, Kuhn GA, Hofmann S, Ebner HL, Richards PJ.

Journal: Biomaterials, 2014, 35:7326-35.

Contribution: Planning, performing and evaluating all the *in vitro* and *in vivo* experiments.

3.1.4 ARTD1 deletion causes increased hepatic lipid accumulation in mice fed a high-fat diet and impairs adipocyte function and differentiation.

Authors: Erener S., **Mirsaidi A.**, Hesse M., Tiaden A.N., Ellingsgaard H., Kostadinova R., Donath M.Y., Richards P.J., and Hottiger M.O.

Journal: FASEB Journal, 2012, 26(6):2631-8.

Contribution: Planning and performing cell culture, including isolation and differentiation of ASCs as well as evaluation of differentiation by qRT-PCR and Oil red/ Alizarin red staining (Fig. 5, 6, S3).

3.1.5 Human serine protease HTRA1 positively regulates osteogenesis of human bone marrow-derived mesenchymal stem cells and mineralization of differentiating bone-forming cells through the modulation of extracellular matrix protein.

Authors: Tiaden AN, Breiden M, **Mirsaidi A**, Weber FA, Bahrenberg G, Glanz S, Cinelli P, Ehrmann M, Richards PJ.

Journal: Stem Cells, 2012, 30:2271-2282.

Contribution: Planning, performing cell culture, including isolation and differentiation of ASCs as well as evaluation of differentiation by qRT-PCR, alizarin red and immunofluorescence staining in 3D cell culture system (Fig. 2, 5c, S4).

3.1.6 Detrimental role for human high temperature requirement serine protease A1 (HTRA1) in the pathogenesis of intervertebral disc (IVD) degeneration.

Authors: Tiaden AN, Klawitter M, Lux V, **Mirsaidi A**, Bahrenberg G, Glanz S, Quero L, Liebscher T, Wuertz K, Ehrmann M, Richards PJ.

Journal: Journal of Biological Chemistry, 2012, 15; 287(25):21335-45.

Contribution: Preparing frozen tissue sections for histological analysis. RNA and protein isolation from disc tissue (Fig. 1).

JOURNAL OF TISSUE ENGINEERING AND REGENERATIVE MEDICINE
J Tissue Eng Regen Med (2011).
Published online in Wiley Online Library (wileyonlinelibrary.com) **DOI:** 10.1002/term.440

RESEARCH ARTICLE

Telomere length, telomerase activity and osteogenic differentiation are maintained in adipose-derived stromal cells from senile osteoporotic SAMP6 mice

Ali Mirsaidi[1†], Karin N. Kleinhans[2†], Markus Rimann[1], André N. Tiaden[1], Martin Stauber[3], K. Lenhard Rudolph[2] and Peter J. Richards[1,4*]

[1]*Bone and Stem Cell Research Group, CABMM, University of Zürich, Switzerland*
[2]*Institute of Molecular Medicine and Max-Planck Research Group on Stem Cell Ageing, University of Ulm, Germany*
[3]*b-cube AG, Bio-Technopark, Schlieren-Zürich, Switzerland*
[4]*Zürich Centre for Integrative Human Physiology (ZIHP), University of Zürich, Switzerland*

Abstract

Adipose tissue provides for a rich and easily accessible source of multipotent stromal cells and thus offers the potential for autologous cell-based therapy for a number of degenerative diseases. Senile osteoporosis is characterized by a reduction in bone quality, which is associated with inadequacies in bone marrow stromal cell (BMSC) differentiation. In the present study, we have characterized adipose-derived stromal cells (ASCs) isolated from aged osteoporotic mice and evaluated their suitability as a source of osteogenic precursor cells. Significant reductions in both tibia bone quality and telomere length in liver tissue were observed in the senescence-accelerated mouse prone 6 strain (SAMP6), as compared to the control age-matched senescence-accelerated mouse resistant 1 strain (SAMR1), thus confirming osteoporosis and accelerated ageing traits in this model. ASCs isolated from inguinal fat expressed mesenchymal surface markers and were capable of differentiating along the osteoblast, adipocyte and chondrocyte lineages. Telomere length was not compromised in ASCs from SAMP6 mice but was actually found to be significantly increased as compared to control SAMR1 mice. Furthermore, ASCs from both strains were comparable in terms of telomerase activity, *p21* mRNA expression, SA–β-gal activity and proliferative capacity. The overall osteogenic and adipogenic potential of ASCs was comparable between SAMP6 and SAMR1 strains, as determined by quantitative molecular, biochemical and histological analyses. In conclusion, adipose tissue may represent a promising autologous cell source for the development of novel bone regenerative therapeutic strategies in the treatment of age-related osteoporosis. **Copyright © 2011 John Wiley & Sons, Ltd.**

Received 9 December 2010; Accepted 5 May 2011

Keywords adipose; ageing; differentiation; mesenchymal stem cell; osteoporosis

1. Introduction

Bone quality is regarded as being the resistance of bone to fracture and reflects the incorporation of bone density and mechanical strength as well as architecture and mineralization (Lane, 2006; Seeman and Delmas, 2006; Recker and Barger-Lux, 2004). These elements of bone quality are severely affected in aged osteoporotic patients

*Correspondence to: Peter J. Richards, Bone and Stem Cell Research Group, Competence Centre for Applied Biotechnology and Molecular Medicine, Room 17-L-32, University of Zürich, Winterthurerstrasse 190, CH-8057 Zürich, Switzerland.
E-mail: peter.richards@cabmm.uzh.ch
†*These authors contributed equally to this study.*

by alterations in bone turnover through the process of bone remodelling. Such deviations may arise from a loss in the homeostatic control of the bone multicellular unit, where the activities of bone-forming osteoblasts and bone-resorbing osteoclasts are no longer balanced (Seeman and Delmas, 2006). Bone formation is reliant on the presence of functionally active mature osteoblasts derived from progenitor cells within the bone marrow, termed bone marrow stromal cells (BMSCs), through a process of osteogenic differentiation (Bruder *et al*., 1994). The observation that BMSCs isolated from aged osteoporotic patients have a reduced osteogenic capacity implies that the structural abnormalities associated with osteoporotic bone may be as a consequence of inadequacies in bone cell differentiation (Rodríguez *et al*., 1999, 2000). This is further supported by studies using the senescence-accelerated mouse prone 6 strain (SAMP6).

The SAMP6 strain was originally described by Matsushita *et al*. (1986), originating from crossbreeding between AKR/J mice and mice from an unknown strain. In addition to the SAMP6 strain, numerous other strains were also developed, including the resistant strain, termed SAMR1, which displayed no pathological phenotype. Unlike chronologically aged mouse models, osteoporosis-like traits, including reduced trabecular bone volume (Matsushita *et al*., 1986), decreased bone strength (Silva *et al*., 2002) and reduced areal bone mineral density (BMD) (Takeda, 1999) are clearly developed in the SAMP6 strain as early as 3–4 months of age, as compared to their age-matched SAMR1 strain counterparts. It is now well established that the osteoporotic phenotype observed in SAMP6 mice is associated with defects in the osteogenic differentiation capacity of resident BMSCs (Jilka *et al*., 1996; Silva *et al*., 2005). Additionally, data from our own studies have revealed that, in contrast to their reduced osteogenic potential, BMSCs from SAMP6 mice actually demonstrate an enhanced capacity for adipogenesis, thus lending some insight into the mechanisms responsible for reduced bone quality in these mice (Egermann *et al*., 2010).

The role of ageing in determining the quality of bone and potential onset of osteoporosis has also been highlighted through studies utilizing other experimental models of accelerated ageing. Compound knockout mice bearing mutations in both the Werner and telomerase genes result in mice with a significant decrease in trabecular bone mass and is directly related to an impairment in BMSC osteogenesis (Choi *et al*., 2008; Chang *et al*., 2004). Osteoporotic features are also apparent in *klotho* gene-deficient mice, a well-recognized model of accelerated ageing, and are associated with alterations in the age, number and spatial distribution of functionally active resident bone-forming cells (Kuro-o *et al*., 1997; Kawaguchi *et al*., 1999; Suzuki *et al*., 2005). It is essential, therefore, that therapeutic strategies employed to treat osteoporosis in elderly patients are effective not only in preventing further bone loss but also in stimulating the formation of high-quality bone through manipulation of the BMSC niche.

The use of stem cells from adipose tissue, termed adipose-derived stromal cells (ASCs), for the purpose of developing new bone reconstruction therapies is now prevalent in areas of both experimental and clinical research. This is primarily due to the ease by which these cells can be isolated and expanded in culture and their characteristic multipotency under specific conditions (Pittenger *et al*., 1999). ASCs have the capacity for osteogenic differentiation and may be easily accessed from subcutaneous fat stores through minimally invasive procedures (Halvorsen *et al*., 2000, 2001; Zuk *et al*., 2001; Schäffler and Büchler, 2007). Moreover, the proliferative capacity (Schipper *et al*., 2008; Zhu *et al*., 2009; Khan *et al*., 2009) and osteogenic potential (Shi *et al*., 2005; Weinzierl *et al*., 2006; Zhu *et al*., 2009; Khan *et al*., 2009) of ASCs appear not to be adversely affected by donor age. However, the application of ASCs as a cell-based therapy for the purpose of enhancing orthopaedic tissue repair and regeneration is at an early stage of research (Tapp *et al*., 2009) and, as such, no studies have yet been carried out to evaluate the possible therapeutic potential of autologous ASCs for the treatment of osteoporotic bone disease.

In the present study, we characterize ASCs isolated from aged osteoporotic mice and evaluate their potential as autologous bone regenerative stem cells for the treatment of senile osteoporosis. Initial quantitative analyses employing fluorescence *in situ* hybridization and μCT confirmed SAMP6 as a model for accelerated ageing and osteoporosis, respectively. ASCs isolated and expanded from both SAMP6 and SAMR1 mice displayed many of the key features associated with mesenchymal stem cells, such as specific surface marker expression and multipotent differentiation capabilities. There was no evidence of telomere shortening or increased cellular senescence in cultured ASCs isolated from SAMP6 mice as compared to SAMR1 mice. In fact, telomeric DNA levels were actually found to be significantly greater in ASCs from SAMP6 mice. Furthermore, in contrast to our previous studies, in which BMSCs from SAMP6 mice were shown to be defective in terms of their osteogenic capability (Egermann *et al*., 2010), ASCs from these mice demonstrated no such impairment in either the early or late phases of osteogenic differentiation. Similarly, ASC adipogenesis was comparable between the two mouse strains. These findings therefore highlight the potential for adipose tissue as a source of functional osteogenic precursor cells for the purpose of autologous cell-based therapy in aged bone disease.

2. Materials and methods

2.1. Animals

Experiments were performed using 20 week-old male SAMR1 and SAMP6 mice (Harlan Laboratories, Horst, The Netherlands). All animal research procedures were approved by the Animal Experimentation Committee of the Veterinary Office of the Canton of Zürich, Switzerland,

DOI: 10.1002/term

and followed the guidelines of the Swiss Federal Veterinary Office for the use and care of laboratory animals.

2.2. Microcomputed tomography (μCT)

Tibia were scanned by microcomputed tomography(μCT 40; Scanco Medical AG, Brüttisellen, Switzerland) and the measured data filtered using a three-dimensional (3D) constrained Gaussian filter with finite filter support (1 voxel) and filter width (s = 0.8). The system was operated in cone beam mode at 70 kVp, 114 μA and a focal spot size of 8 μm. The images were then binarized to separate the object from background, using a global thresholding procedure. A component-labelling algorithm was subsequently applied to remove all unconnected parts, which typically arise from image noise. A fully automated algorithm was used to identify three volumes of interest, the full bone (FULL), the metaphyseal trabecular bone (TRAB) and a cortical ring in the diaphysis (CORT). The FULL compartment identifies the outline of the whole organ. This compartment was used to estimate the total amount of bone in the tibia. The TRAB compartment identifies the trabecular bone in the proximal metaphysis. It is proximally limited by the growth plate and distally by 20% of the tibia length. The CORT compartment identifies a cortical ring of 1.0 mm height. This ring was placed at 50% of tibia length as measured from the proximal end of the tibia. The three compartments were then analysed with standard morphometric algorithms (Hildebrand *et al*., 1999; Odgaard, 1997).

2.3. Isolation and culture of mouse ASCs

Subcutaneous inguinal fat pads were removed, washed extensively in phosphate-buffered saline (PBS) and digested in Hepes buffer (with calcium and magnesium) containing 0.1% collagenase A (Roche Diagnostics, Rotkreuz, Switzerland) and 0.2% bovine serum albumin (BSA) for 40 min at 37 °C. Stromal cells were collected by centrifugation, filtered through a 40 μm sieve (Becton-Dickinson) and cultured in complete medium consisting of Dulbecco's modified Eagle's medium (DMEM-low glucose, with Glutamax; Invitrogen AG, Basel, Switzerland), supplemented with 10% fetal bovine serum (FBS; Invitrogen AG) and antibiotics. The supernatant was replaced after 1 day with fresh complete medium and cells were used between passage 1 and 4 unless otherwise stated.

2.4. Flow cytometry analysis of surface antigens

Cells were directly stained with phycoerythrin-labelled antibodies (Lucerna-Chem, Switzerland) specific for CD29, CD105, Sca1, CD34 and CD45. Specificity was confirmed through the use of appropriate phycoerythrin-labelled isotype control antibodies. Flow cytometry was carried out on a CyAn™ ADP flow cytometer, using Dako Summit software, v 4.3.

2.5. Telomere analysis

2.5.1. Telomere restriction fragment (TRF) length analysis

Genomic DNA was extracted and isolated from liver tissue by phenol–chloroform extraction, using standard protocols, and TRF analysis performed using pulsed-field gel electrophoresis (PFGE) as previously described (Wiemann *et al*., 2002). Briefly, 6 μg DNA was digested overnight at 37 °C, using *Hin*fI and *Rsa*1. Samples were run on a 1% agarose gel with a low-range PFG marker as a size standard, using a Gene Navigator System (GE Healthcare) at 11 V/cm with a 3 s pulse time. The gel was dried for 1 h in a vacuum drier, followed by 30 min denaturation and 30 min neutralization. After 1 h pre-hybridization, the gel was incubated in hybridization buffer with the $(TTAGGG)_3$ oligonucleotide radioactively labelled telomere probe overnight at 37 °C. The gel was washed three times with 0.25% SSC and 0.1%SDS and then exposed on a PhosphorImager-screen for 3 days. Telomere signals were calculated with PCbas 2.0 and Excel (Microsoft) computer programs.

2.5.2. Quantitative fluorescence in situ hybridization (Q-FISH)

Q-FISH was performed on interphase nuclei, as described previously with some modifications (Satyanarayana *et al*., 2003). In brief, paraformaldehyde-fixed paraffin-embedded tissue sections (7 μm) were dewaxed in xylene and rehydrated in a descending ethanol series. After washing in PBS, samples were boiled in citrate buffer for 15 min in a microwave. For ASCs grown on glass slides, cells were first fixed in methanol:acetic acid (3:1, v/v) and allowed to air-dry overnight. The hybridization mix containing the Cy3-telomere probe (Applied Biosystems) was applied to the samples and denatured at 80 °C for 3 min, followed by a 2 h incubation at room temperature in a humid chamber. Samples were mounted in DAPI containing mounting solution and images (×200 magnification) captured, using the Leica DMI6000B automated inverted research microscope system (Leica Microsystems), and telomere fluorescence intensity (TFI) was quantified using the TFL-TELO V1.0 telomere analysis program developed by P. Landsdrop.

2.6. Induction and quantification of differentiation

2.6.1. Osteogenesis

ASCs were plated at 5000 cells/cm^2 and incubated in α-minimum essential medium (α-MEM; Invitrogen AG), supplemented with 10% FBS, 50 μM L-ascorbic acid 2-phosphate sesquimagnesium salt hydrate (Sigma-Aldrich, Buchs, Switzerland), 10 mM β-glycerophosphate (Sigma-Aldrich) and 5 μM retinoic acid (Sigma-Aldrich)

DOI: 10.1002/term

for up to 14 days, with regular changes of medium. Alkaline phosphatase (ALP) activity was determined in cell lysates, using *p*-nitrophenylphosphate (pNPP) liquid substrate (Sigma-Aldrich). Optical densities measured at 405 nm were converted to molar units using a standard curve of known concentrations of *p*-nitrophenol (pNP; Sigma-Aldrich) and normalized to total protein content and reaction time. Mineralization in cell colonies was identified using alizarin red S (Sigma-Aldrich) and was quantified by colorimetric analysis at 570 nm, following extraction using 10% cetylpyridinium chloride (Sigma-Aldrich). Values were converted to molar units using a standard curve of known concentrations of alizarin red S and normalized to total DNA content. All differentiation studies were carried out using ASCs at passage 3–4.

2.6.2. Adipogenesis

ASCs were plated at 10 000 cells/cm^2 and incubated in adipogenic medium consisting of DMEM supplemented with 10% FBS, 1 μM dexamethasone (Sigma-Aldrich), 10 μg/ml insulin (Sigma-Aldrich), 0.1 mM indomethacin (Sigma-Aldrich) and 0.5 mM isobutylmethylxanthine (IBMX; Sigma-Aldrich) for 2 days. The cells were then maintained in adipogenic medium without IBMX for up to 14 days. Triglyceride content in differentiated cells was identified using 0.3% oil red O (Sigma-Aldrich), and the number of adipocytes was counted per 30 fields of view by fluorescence microscopy and normalized to total cell number, following counterstaining with Hoechst 33 342 (Sigma-Aldrich). All differentiation studies were carried out using ASCs at passage 3–4.

2.6.3. Chondrogenesis

For chondrogenic differentiation, 2×10^5 cells were grown in pellet cultures and incubated in DMEM-high glucose (Invitrogen AG) supplemented with 1% FBS, 50 μM L-ascorbic acid 2-phosphate sesquimagnesium salt hydrate, 0.5 μg/ml insulin and 10 ng/ml human TGFβ1 (Peprotech, UK) for 28 days. Paraffin wax sections (5 μm) of fixed pellet cultures were stained with toluidine blue (Sigma-Aldrich) in order to visualize proteoglycans. All differentiation studies were carried out using ASCs at passage 3–4.

2.7. Quantitative reverse-transcription–polymerase chain reaction (qRT–PCR)

Total RNA was isolated and purified using TRIzol reagent (Invitrogen AG) according to the manufacturer's instructions. RNA (0.5 μg) was reverse-transcribed to cDNA, using superscript II (Invitrogen AG) and random hexanucleotide primers (Promega AG, Dübendorf, Switzerland). Quantification of mRNA expression was performed with TaqMan Gene Expression Assays (Applied Biosystems) specific for *p21* (Mm00432448_m1), *Alpl* (Mm01187117_m1), *Spp1* (Mm01611440_mH), *Pparγ2* (Mm00440940_m1) and *Fabp4* (Mm00445878_m1), using the StepOnePlus Real-Time PCR System (Applied Biosystems), and values normalized to the 18S ribosomal RNA (Hs03003631_g1). Each 10 μl reaction consisted of 1× TaqMan Fast Universal PCR Master Mix (Applied Biosystems), 1× TaqMan Gene Expression Assay and 10 ng cDNA. All reactions were performed in fast optical 96-well reaction plates (Applied Biosystems) at 95 °C for 20 s, 40 cycles of 95 °C for 1 s and 60 °C for 20 s. ASCs were used at passage 3–4 and all assays were performed in triplicate.

2.8. Analysis of senescence

2.8.1. Telomerase assay

Telomerase activity in cell lysates was determined using the TeloTAGGG Telomerase PCR ELISA (Roche Diagnostics, Rotkreuz, Switzerland) according to the manufacturer's instructions. A total of 1×10^4 cells were used per measurement and optical densities measured at 450 nm were normalized to a standard cell lysate supplied with the kit. The mean absorbance readings from negative control cell extracts heated at 85 °C for 10 min were subtracted from all measurements.

2.8.2. Senescence-associated β-galactosidase (SA-β-gal) assay

SA–β-gal activity was determined in ASCs using the Senescence Cells Histochemical Staining Kit (Sigma-Aldrich), according to the manufacturer's instructions, and counterstained with Hoechst 33 342. The percentage of SA–β-gal-positive cells was determined from at least 20 fields of view, using the Leica DMI6000B automated inverted research microscope system. ASCs were used at passage 3 and the assay performed in triplicate.

2.8.3. WST-1 proliferation assay

ASC proliferation was tested at various time points over a 14 day incubation period, using the WST-1 assay (Roche, Switzerland) according to the manufacturer's instructions. ASCs were plated at 3×10^3 cells/cm^2, incubated with WST-1 for 2 h at selected time points and absorbance measured at 450 nm. ASCs were used at passage 3–4 and the assays were performed in triplicate.

2.9. Statistical analysis

All statistical analyses were carried out using SPSS17.0 (SPSS Inc., Chicago, IL, USA). Parametric analysis of Normally distributed data was performed using the two-tailed unpaired Student's *t*-test for comparison of two groups or one-way analysis of variance (ANOVA) for multiple group comparisons. The non-parametric

DOI: 10.1002/term

Table 1. Quantitative μCT analysis of SAM tibia

Index	SAMP6 ($n = 8$)	SAMR1 ($n = 8$)	p^a
AVD (%)	62.73 (±0.512)	70.79 (±0.52)	<0.001
BV/TV (%)	4.723 (±0.33)	8.437 (±0.52)	<0.001
BS/TV (1/ mm)	2.012 (±0.14)	3.219 (±0.18)	<0.001
Tb.Th (mm)	0.0685 (±0.002)	0.0736 (±0.001)	=0.064
Tb.Sp (mm)	0.682 (±0.02)	0.480 (±0.01)	<0.001
Tb.N (1/ mm)	1.38 (±0.05)	1.90 (±0.06)	<0.001
Conn.D (1/ mm^3)	13.77 (±1.59)	19.68 (±2.4)	=0.059
BV (%)	70.49 (±0.87)	76.08 (±0.5)	<0.001
Ct.Th (mm)	0.27 (±0.005)	0.28 (±0.003)	=0.092
J (mm^4)	0.1585 (±0.007)	0.119 (±0.004)	<0.001
I_{max} (mm^4)	0.09 (±0.004)	0.07 (±0.002)	<0.001
I_{min} (mm^4)	0.07 (±0.003)	0.049 (±0.0008)	<0.001

AVD, apparent volume density; BV/TV, trabecular bone volume density; BS/TV, trabecular bone surface density; Tb.Th, trabecular thickness; Tb.Sp, trabecular separation; Tb.N, trabecular number; Conn.D, trabecular connectivity density; BV, cortical bone volume density; Ct.Th, cortical thickness; J, polar moment of inertia; I_{max} and I_{min}, second moment of inertia.
[a]p values determined using one-way ANOVA. All results are expressed as mean ± S.E.M.

Mann–Whitney U-test was used to determine differences between frequencies observed in Q-FISH analysis of telomere length and in the assessment of oil red O staining. In all cases, $p < 0.05$ was considered statistically significant, and all data were expressed as mean ± standard error of the mean (SEM).

3. Results

3.1. Analysis of bone loss and ageing in SAMP6 mice

Initial studies were carried out to confirm that the SAMP6 strain used in the current study displayed osteoporotic traits similar to those reported for the human condition. Bone volume and structure were initially compared in tibias from SAMP6 and SAMR1 strains by the use of quantitative μCT analysis (Table 1). SAMR1 mice displayed significant increases ($p < 0.001$) in bone volume density in both the full compartment (AVD) and the trabecular compartment (BV/TV) as compared to their SAMP6 counterparts. Such differences in BV/TV levels were reflected by the increased trabecular number (Tb.N; $p < 0.001$) and decreased spacing between the trabeculae (Tb.Sp; $p < 0.001$). Similarly, bone surface density (BS/TV; $p < 0.001$) was also significantly elevated in SAMR1 mice. In the cortical compartment, bone volume density (BV) was significantly increased ($p < 0.001$) in SAMR1 mice. Furthermore, reduced values for the second moment of inertia (I_{min} and I_{max}; $p < 0.001$) and the polar moment of inertia (J; $p < 0.001$) in SAMR1 mice indicated an increase in bending stiffness and a higher torsion strength, respectively.

Telomere shortening is now regarded as being a key determinant of an organism's life expectancy and overall health and, as such, has significant pathological implications in numerous degenerative disorders (Sahin and Depinho, 2010). In addition to its osteoporotic phenotype, the SAMP6 strain has also been proposed as a model of accelerated ageing, due primarily to its shortened life span as compared to the longer-lived SAMR1 control strain (Takeda, 1999). However, no studies have yet sought to determine whether telomere length is also compromised in these animals. We therefore conducted a series of studies to examine and quantify telomere length in native tissue, using paraffin wax-embedded liver sections. Quantitative analysis of interphase nuclei by fluorescence *in situ* hybridization (Q-FISH) demonstrated a significant reduction in fluorescence intensity measurements in SAMP6 (91.68 ± 1.4; $p < 0.001$; Figure 1A) as compared to SAMR1 (111.8 ± 1.9; Figure 1B). Deficiencies in telomere length were also confirmed in SAMP6 mice, using quantitative southern blot analysis of genomic DNA. TRF length was significantly reduced in SAMP6 (36.34 ± 0.22; $p < 0.001$) as compared to SAMR1 (44.23 ± 0.85) (Figure 1C). A significant increase in the ratio of loaded genomic DNA to telomere signal was also observed in SAMP6 (1.6 ± 0.2; $p < 0.01$) as compared to SAMR1 (0.6 ± 0.13) (Figure 1D), thus signifying an overall loss of telomeric DNA in SAMP6 samples. These data therefore reinforce the notion of SAMP6 as a model for age-related bone disease and introduce the concept of telomere deficiencies as being a potential contributory factor to premature ageing in these mice.

3.2. Characterization of ASCs from SAM strains

ASCs offer an appealing source of cells for tissue-engineering strategies, due to their ease of isolation, expansion and ability to differentiate into several types of mesenchymal tissue. In the present study, we investigated whether ASCs isolated from the SAM strains also possessed such attributes by examining surface marker expression and multipotent capabilities. Subcutaneous adipose tissue was harvested and ASCs isolated and expanded. ASC populations from SAMP6 and SAMR1 mice expressed high levels of several markers considered

DOI: 10.1002/term

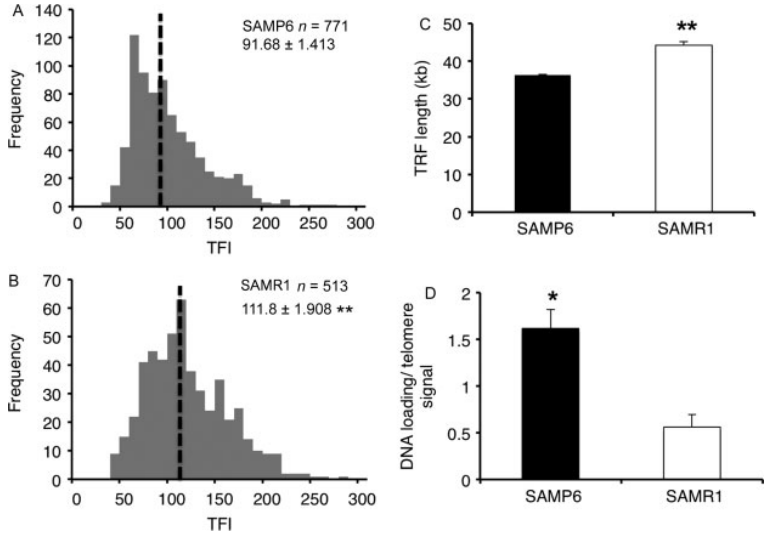

Figure 1. Telomere length in liver tissue from SAMP6 mice is significantly reduced as compared to SAMR1 controls. (A, B) Frequency distributions of telomere fluorescence intensity in SAMP6 ($n = 6$ animals) (A) and SAMR1 ($n = 4$ animals) (B) mice following Q-FISH analyses on paraffin wax-embedded liver sections. Average telomere fluorescence intensity (indicated by dashed line) was calculated from measuring a total of 771 and 513 nuclei from SAMP6 and SAMR1 mice, respectively. (C, D) The mean TRF length in DNA samples from SAMP6 ($n = 6$ animals) and SAMR1 ($n = 6$ animals) was analysed using a specific radiolabelled telomeric probe and pulsed-field gel electrophoresis (C), and the ratio of loaded DNA to telomere signal determined (D). All data are expressed as mean ± SEM. $^{*}p < 0.01$; $^{**}p < 0.001$

to be representative of mesenchymal stem cells, including CD29, CD105 and Sca1, but were almost completely negative for the well-known haematopoietic markers CD34 and CD45 (Figure 2A). Cell morphology was comparable in freshly isolated undifferentiated ASCs from SAMP6 and SAMR1 mice and multipotency was demonstrated through their ability to differentiate into adipocytes, osteoblasts and chondrocytes (Figure 2B). Therefore, the stromal vascular fraction of adipose tissue derived from both SAMP6 and SAMR1 mice contains mesenchymal stem cells with multipotent capabilities.

3.3. Analysis of ageing and senescence in ASCs from SAM strains

The effect of ageing on BMSC and ASC function has already been extensively studied in both rodent and human cell systems. BMSCs isolated from aged donors are generally considered to have a lower proliferative capacity than those from young donors, and this has been associated with telomere shortening and increased levels of senescence markers (Stenderup *et al.*, 2003; Baxter *et al.*, 2004; Stolzing *et al.*, 2008). By contrast, the proliferation capacity of ASCs does not appear to be significantly affected by donor age, with only a moderate decrease being reported in cells from aged donors (Schipper *et al.*, 2008; Zhu *et al.*, 2009; Khan *et al.*, 2009). We therefore set out to examine and compare various parameters of ageing in ASCs isolated from SAMP6 and SAMR1 mice. Q-FISH analysis was initially carried out to compare telomere length in cultured undifferentiated ASCs isolated from SAMP6 (Figure 3A) and SAMR1 mice (Figure 3B). Unexpectedly, ASCs isolated from SAMP6 mice actually demonstrated a small, but significant, increase in the mean telomere fluorescence intensity as compared to cells from SAMR1 mice ($p < 0.001$). Despite these differences in telomere length, ASCs from both strains maintained equivalent levels of telomerase activity (Figure 4A), expressed comparable levels of mRNA specific for the senescence marker *p21* (Figure 4B) and demonstrated similar proliferative capacities (Figure 4C). The actual level of senescence in ASCs from both strains was deemed to be very low, as demonstrated by an almost complete absence of any positive staining for senescence-associated-β-galactosidase (SA–β-Gal) activity (Figure 4D). Therefore, short-term cultures of ASCs isolated from SAMP6 mice do not appear to show any signs of accelerated ageing, as compared to ASCs from control SAMR1 mice when grown under standard conditions.

3.4. Osteogenic potential of ASCs from aged osteoporotic SAMP6 mice

There is now a growing body of evidence to suggest that ASCs have the potential to retain their differentiation

DOI: 10.1002/term

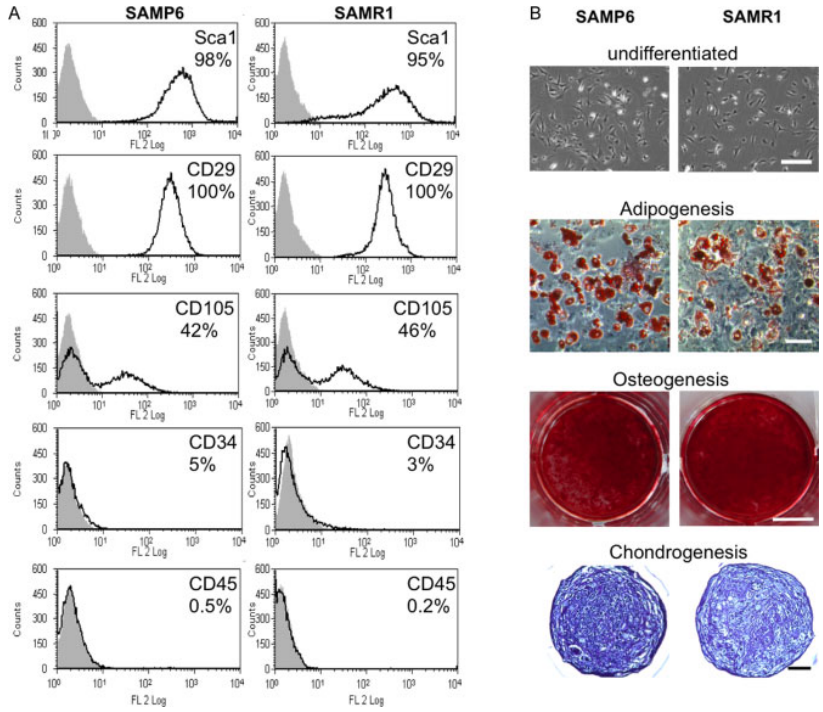

Figure 2. ASCs isolated from SAM strains express mesenchymal surface markers and are multipotent. (A) FACS analysis was used to determine the proportion of ASCs expressing mesenchymal (CD29, CD105, Sca-1) or haematopoietic (CD34, CD45) cell surface antigen markers. (B) Freshly isolated undifferentiated ASCs at passage 0 (P0) showed similar cell morphologies between SAMP6 and SAMR1 strains (scale bar = 100 μm). Multipotent differentiation was induced under specific culture conditions for adipogenesis, osteogenesis and chondrogenesis and visualized using oil red O (scale bar = 100 μm), alizarin red S (scale bar = 5 mm) and toluidine blue (scale bar = 200 μm), respectively. In all cases, experiments were carried out in triplicate

capacity with ageing. Studies using ASCs isolated from adult mice demonstrated that osteogenic potential was maintained when cells were grown in osteogenic medium supplemented with retinoic acid and BMP-2 (Shi *et al.*, 2005). Similarly, studies investigating the osteogenic potential of human ASCs have found no direct correlation between differentiation capacity and donor age (Weinzierl *et al.*, 2006; Zhu *et al.*, 2009; Khan *et al.*, 2009) We therefore sought to identify whether osteogenesis in ASCs isolated from SAMP6 mice was also maintained, thus offering a potentially abundant source of bone regenerative autologous stem cells in osteoporotic individuals.

Quantitative PCR analysis was initially performed in order to examine the relative expression levels of various early- and mid-phase markers of osteogenic differentiation, including genes encoding for liver/bone/kidney-type alkaline phosphatase (*Alpl*) (Figure 5A) and osteopontin (*Spp1*) (Figure 5B). Increases in *Alpl* expression were observed in both strains during the early stages of osteogenesis and, at day 3, were significantly elevated in SAMP6 as compared to SAMR1 ($p < 0.001$). Expression levels of *Alpl* in SAMP6 gradually decreased and had returned to baseline by day 14. In contrast, *Alpl* expression remained upregulated in SAMR1 and was significantly increased as compared to SAMP6 at day 14 ($p < 0.001$). A gradual increase in *Spp1* expression was also observed over the course of the experiment in both strains. Expression levels were significantly greatest in SAMR1 during the first half of induction, reaching a maximum at day 7 ($p < 0.01$). However, by day 14, *Spp1* mRNA expression in SAMR1 was significantly reduced as compared to SAMP6 ($p < 0.05$).

Alkaline phosphatase (ALP) activity was also shown to increase during the early phase of osteogenic induction reaching a maximum by day 7 in both strains (Figure 5C). As with *Alpl* mRNA expression, ALP protein activity was significantly enhanced in SAMP6 during the early phase of osteogenesis at day 3 as compared to SAMR1 ($p < 0.05$).

ASCs incubated in osteogenic medium for up to 14 days also showed extensive mineralization, as visualized by alizarin red S staining (Figure 5D). The development of a mineralized matrix appeared to parallel the pattern of osteopontin expression in these cultures, whereby a

DOI: 10.1002/term

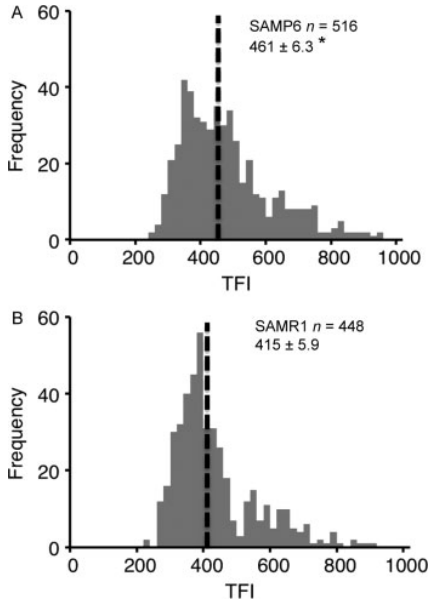

Figure 3. Telomere length is maintained in ASCs isolated from SAMP6 mice. Frequency distributions of telomere fluorescence intensity in interphase ASCs from SAMP6 ($n = 4$ animals) (A) and SAMR1 ($n = 4$ animals) (B) mice, as determined by Q-FISH analyses. Average telomere fluorescence intensity (indicated by dashed line) was calculated by measuring a total of 516 and 448 nuclei from SAMP6 and SAMR1 mice, respectively. $^{*}p < 0.001$

marked reduction in alizarin red S-positive staining was observed in ASCs from SAMP6 as compared to SAMR1 mice up until the late phase of differentiation at day 14. At this time point, quantitative measurement of the alizarin red S bound to cellular matrix revealed comparable levels between both SAM strains (Figure 5E). Therefore, although some variations are observed between SAMP6 and SAMR1 during both the early and mid-phases of osteogenic induction, it would appear that osteogenesis as a whole is maintained in ASCs isolated from aged osteoporotic SAMP6 mice.

3.5. Adipogenic potential of ASCs from aged osteoporotic SAMP6 mice

We have previously shown that BMSCs isolated from the SAMP6 strain differentiate towards adipocytes to a much greater degree than those isolated from SAMR1 mice (Egermann *et al*., 2010), and as such may represent a significant contributory factor to the osteoporotic phenotype observed in SAMP6 mice. Therefore, we investigated whether this alteration in adipogenesis was also apparent in ASCs isolated from SAMP6 mice. The expression of adipogenic markers peroxisome proliferator-activated receptor $\gamma 2$ (*Pparγ2*) (Figure 6A) and fatty acid binding protein 4 (*Fabp4*) (Figure 6B) were highly upregulated in ASCs following adipogenesis induction. Expression levels of both markers were generally found to be comparable between the two strains, with a small significant increase ($p < 0.05$) in *Fabp4* mRNA being observed in ASCs from SAMP6 mice at day 5 only (Figure 6B). Further analysis using oil red O staining revealed no significant differences in the number of adipocytes in SAMP6 and SAMR1 ASC cultures at day 10 (Figure 6C, D). Therefore, as with ASC osteogenesis, although some variations were observed between ASCs from SAMP6 and SAMR1 mice during adipogenesis, their overall potential to form mature adipocytes was comparable.

4. Discussion

Bone marrow stromal cells (BMSCs) are regarded as being key components of the bone multicellular unit, due to their potential for osteogenic differentiation, and thus play a central role in the overall maintenance of bone quality. However, their general fitness appears to decline with donor age and passage number, as evidenced by increases in cellular ageing markers and an inability to maintain osteogenic potential under normal conditions and following exposure to stress (Roura *et al*., 1999; D'Ippolito *et al*., 2006; Stolzing *et al*., 2008). Such observations have therefore led to speculation that deficiencies in resident BMSC differentiation may play a significant role in the development of age-related osteoporotic phenotypes.

The concept of defective bone marrow cells as an underlying cause of aged osteoporosis was originally introduced by Meunier *et al*. (1971) and has since been corroborated by a series of studies examining bone quality, using various experimental models, where BMSC performance is impaired. Bonyadi *et al*. (2003) have reported that BMSCs isolated from *Sca-1*$^{-/-}$ mice had a reduced tendency towards osteogenic differentiation and that these mice displayed many of the features associated with senile osteoporosis. Similarly, a low turnover osteoporosis is evident in the *klotho* mouse strain, where bone marrow osteogenesis is also significantly reduced (Kuro-o *et al*., 1997). Perhaps more striking are the results from investigations utilizing the senile osteoporotic SAMP6 model, where the osteogenic differentiation potential of resident BMSCs has consistently been shown to be defective in comparison to BMSCs isolated from the age-matched SAMR1 control strain (Jilka *et al*., 1996; Silva *et al*., 2005; Egermann *et al*., 2010). These observations therefore highlight the fact that age-related inadequacies in cellular differentiation must be taken into account when considering the potential impact of therapeutic strategies aimed at restoring bone quality in osteoporotic patients.

Adipose-derived stromal cells (ASCs) represent a readily available population of cells, with the ability to differentiate into osteoblasts both *in vitro* and *in vivo*

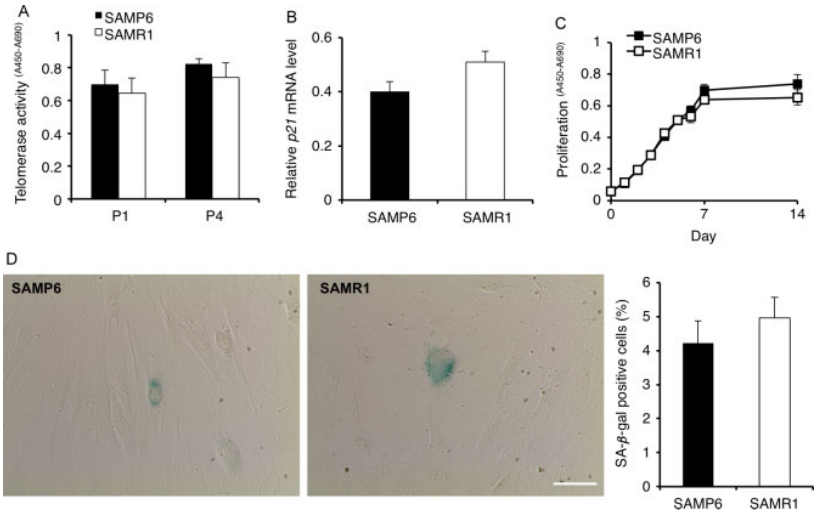

Figure 4. Senescence state of ASCs from SAMP6 and SAMR1 mice. (A) Telomerase activity was measured in ASCs (1×10^4) from SAMP6 ($n = 3$–4 animals) and SAMR1 ($n = 3$–4 animals) at passage 1 (P1) and passage 4 (P4), using the TeloTAGGG telomerase PCR ELISA. All measurements are expressed as arbitrary units and were normalized to a positive standard following the subtraction of basal values. (B) The expression level of the senescence marker p21 was determined in ASCs ($n = 3$ animals) by qRT–PCR. The expression value of *p21* was normalized to the amount of 18S ribosomal RNA in order to calculate the relative amount of mRNA. (C) ASC proliferation was compared between SAMP6 ($n = 3$–5 animals) and SAMR1 ($n = 3$–5 animals) over 14 days, using the WST-1 proliferation assay and values expressed as optical densities (OD). (D) SA–β-gal staining of ASCs from SAMP6 ($n = 3$) and SAMR1 ($n = 3$) mice (scale bar = 50 μm). In all cases, data are expressed as mean ± SEM

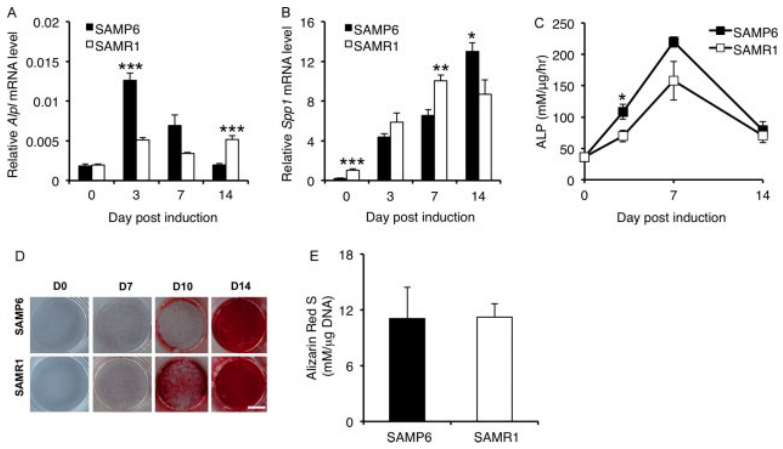

Figure 5. ASCs from SAMP6 maintain their osteogenic potential *in vitro*. The mRNA expression levels of *Alpl* (A) and *Spp1* (B) were determined in ASCs from both SAMP6 ($n = 4$ animals) and SAMR1 ($n = 3$ animals) by qRT–PCR, following osteogenic induction. The expression value of each gene was normalized to the amount of 18S ribosomal RNA in order to calculate relative amounts of mRNA. (C) ALP activity was quantified in protein lysates from ASCs over the course of osteogenic differentiation and normalized to total protein content ($n = 3$–4). (D) Alizarin red S staining was used to visualize mineralization over the course of osteogenic differentiation. Representative images are shown from two separate experiments. Scale bar = 5 mm. (E) Quantitative analysis of alizarin red S staining in ASC cultures at day 14 after osteogenic induction ($n = 4$–5 animals). All tests were carried out in triplicate and data expressed as mean ± SEM. $^*p < 0.05$; $^{**}p < 0.01$; $^{***}p < 0.001$

DOI: 10.1002/term

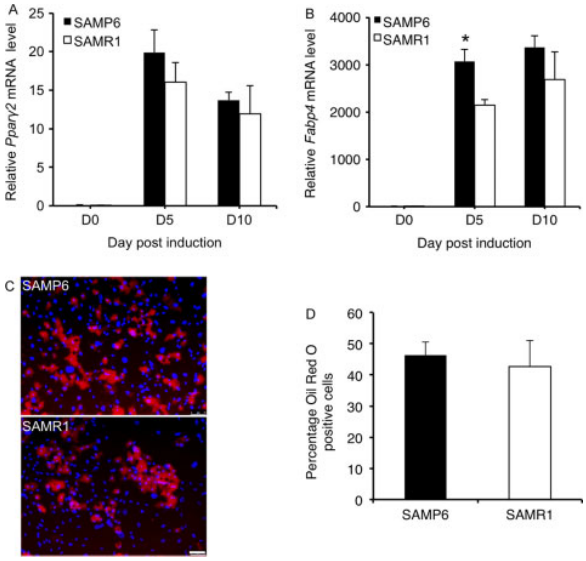

Figure 6. ASCs from SAMP6 and SAMR1 mice demonstrate comparable adipogenic potential *in vitro*. The mRNA expression levels of *Pparγ2* (A) and *Fabp4* (B) were determined in ASCs from both SAMP6 ($n = 4$ animals) and SAMR1 ($n = 4$ animals) mice by qRT–PCR, following adipogenic induction. The expression value of each gene was normalized to the amount of 18S ribosomal RNA in order to calculate relative amounts of mRNA. (C) Representative fluorescent images of ASCs stained with oil red O (red) and Hoechst 33342 nuclear stain (blue). (D) The percentage of cells demonstrating triglyceride accumulation was quantified in ASCs at day 10 ($n = 3$). Scale bar = 75 μm. All tests were carried out in triplicate and data expressed as mean ± SEM. $^*p < 0.05$

(Justesen *et al*., 2004; Hicok *et al*., 2004), and fulfil all criteria deemed necessary for regenerative applications involving stem cells (Gimble, 2003). As such, there is now a growing clinical interest in the use of ASCs as a novel therapeutic approach in bone tissue engineering (Helder *et al*., 2007). Indeed, the *in vivo* application of ASCs to treat a variety of bone defects has already shown promising results (Dudas *et al*., 2006; Li *et al*., 2007; Yoon *et al*., 2007; Mesimaki *et al*., 2009). However, the use of ASCs as a potential stem cell-based therapeutic strategy for the treatment of age-related osteoporotic bone loss has not yet been addressed. In the present study, we isolated and characterized ASCs from SAMP6 and SAMR1 mice and assessed their osteogenic and adipogenic differentiation capabilities. Initial studies confirmed that the SAMP6 mice used in the current study displayed both osteoporosis- and accelerated ageing-related traits as compared to the age-matched control SAMR1 strain. ASCs isolated from both SAMP6 and SAMR1 strains were easily accessed from subcutaneous inguinal fat pads and could be expanded in culture over several passages. They consistently expressed the characteristic surface markers associated with mesenchymal stem cells and readily differentiated into adipocytes, osteoblasts and chondrocytes, thus confirming their multipotency. Due to the premature ageing-like features associated with the SAMP6 model, we also analysed ASCs for various biological markers of advanced ageing. ASCs isolated from both SAMP6 and SAMR1 strains expressed similar levels of *p21* mRNA and displayed an almost complete absence of staining for SA–β-gal activity, both of which are intrinsically linked to cellular senescence. Interestingly, ASCs from SAMP6 mice actually demonstrated a significant increase in telomeric DNA as compared to SAMR1 mice. It is unclear as to why ASCs isolated from what are considered to be biologically younger SAMR1 mice should display signs of telomere shortening in culture. It is generally accepted that telomere length is maintained in part through the actions of the telomerase reverse transcriptase (Tert) (Chan and Blackburn, 2002) and that the differentiation potential of both BMSCs and ASCs is dependent on telomerase activity (Simonsen *et al*., 2002; Lu *et al*., 2004; Kang *et al*., 2004). In the present study, no significant differences were observed in ASC telomerase activity between SAMP6 and SAMR1 mice when tested at various passages. As such, alterations in telomere length cannot be attributed to differences in telomerase activity in these cells. This is supported by findings from studies using human and non-human primate ASCs, where telomere length was maintained for as long as 30 passages despite significant reductions in telomerase activity (Izadpanah *et al*., 2006). The multipotent and proliferative capacity of ASCs from SAMR1 mice also appeared not to be adversely affected by the reduced telomeric DNA levels. Therefore, it seems more likely that mechanisms acting independently of

DOI: 10.1002/term

telomerase are responsible for the differences observed in telomere length between ASCs from SAMP6 and SAMR1 mice, the specific determination of which awaits further investigation.

Maintenance of ASC functionality with increasing chronological age has already been alluded to in several studies comparing ASCs isolated from animal and human subjects (Shi *et al*., 2005; Weinzierl *et al*., 2006; Schipper *et al*., 2008; Zhu *et al*., 2009; Khan *et al*., 2009; Yu *et al*., 2011). However, the effects of genuine biological ageing on the functional properties of ASCs have not yet been fully addressed. The fact that SAMP6 mice show several defining features associated with advancing age, as compared to their chronologically age-matched SAMR1 counterparts, implies that the age-related phenotypes observed in this mouse strain are related to biological ageing. We therefore compared ASCs from chronologically age-matched SAMP6 and SAMR1 mice in terms of their potential to differentiate along the osteoblast lineage and ability to generate mineralized matrix. We demonstrated that, unlike BMSCs, ASCs isolated from aged osteoporotic SAMP6 mice had the capacity to retain their overall osteogenic differentiation potential when compared to age-matched SAMR1 control mice. However, differences between strains were observed during both the early and mid-phases of osteogenesis, as determined by quantitative analysis of molecular markers of osteogenic differentiation as well as through measurements of ALP activity and mineral deposition. Levels of ALP expression and activity were actually found to be greatest in ASCs from SAMP6 mice during the first week of osteogenesis and reduced to a level equal to or below that of SAMR1 mice by day 14. Conversely, levels of osteopontin expression were highest in ASCs from SAMR1 mice for the first 7 days but were superseded by SAMP6 cultures at day 14. Similarly, SAMR1 cultures mineralized at a faster rate as compared to ASCs from SAMP6 mice, although by day 14, the level of alizarin red S staining was comparable between strains. It is unclear why mineralization was delayed in SAMP6 cultures as compared to SAMR1 mice. It is possible that the increased osteopontin expression levels observed in SAMR1 cultures may be partly responsible for the early appearance of mineralized matrix. This is supported by the fact that only at the later stage of differentiation, where osteopontin expression levels become significantly increased, do SAMP6 cultures demonstrate matrix deposition. The importance of osteopontin as an instigator of matrix mineralization in differentiating osteoblasts has previously been reported in studies using both mouse and rat osteoblast precursor cells (Beck *et al*., 1998; Kojima *et al*., 2004). Furthermore, a mineralizing phenotype was evident in differentiating MC3T3-E1 cell lines expressing high levels of osteopontin, even in the absence of ALP activity (Beck *et al*., 1998). Therefore, although equivalent levels of mineralization are observed in SAM cultures during the final stages of differentiation, a delay in mineral deposition is nevertheless apparent in SAMP6 cultures and would seem to be independent of ALP activity.

In addition to their osteogenic potential, ASC adipogenesis must also be taken into account when considering their use in the regeneration of osteoporotic bone. We have previously shown that BMSCs from SAMP6 mice have an increased tendency towards adipogenesis rather than osteogenesis when compared to SAMR1 mice (Egermann *et al*., 2010) and, as such, give rise to higher levels of fat marrow. We therefore compared adipogenesis in ASCs from both strains in order to ascertain whether such abnormalities in adipogenic differentiation were also evident in these cells. Despite there being some variations between the two strains in terms of the expression levels of the early adipogenic markers *Pparγ2* and *Fabp4*, the actual number of mature adipocytes present at completion of the experiment was not significantly different.

In summary, our findings demonstrate that ASCs isolated from a recognized murine model for aged osteoporosis maintain telomere length, show no signs of premature cellular senescence, retain a high capacity for osteogenic differentiation and show no alterations in expected adipogenic differentiation potential. Such observations therefore support the notion of adipose tissue being a valuable source of osteoprogenitor cells, and that the ability of such cells to proliferate and differentiate does not appear to be adversely affected by the biological age or osteoporotic status of the donor from which they were isolated. Further analysis of ASC function in chronologically aged mice from different genetic backgrounds, as well as from human subjects, is needed in order to confirm these observations and thus validate the use of autologous stem cell-based therapeutic strategies for the treatment of bone loss in aged patients.

Acknowledgements

This work was partially financed with the help of the Forschungskredit, University of Zürich, and Stiftung Osteoporose Schweiz.

References

Baxter MA, Wynn RF, Jowitt SN, *et al*. 2004; Study of telomere length reveals rapid aging of human marrow stromal cells following *in vitro* expansion. *Stem Cells* **22:** 675–682.

Beck GR Jr, Sullivan EC, Moran E, *et al*. 1998; Relationship between alkaline phosphatase levels, osteopontin expression, and mineralization in differentiating MC3T3-E1 osteoblasts. *J Cell Biochem* **68:** 269–280.

Bonyadi M, Waldman SD, Liu D, *et al*. 2003; Mesenchymal progenitor self-renewal deficiency leads to age-dependent osteoporosis in Sca-1/Ly-6A null mice. *Proc Natl Acad Sci USA* **100:** 5840–5845.

Bruder SP, Fink DJ, Caplan AI. 1994; Mesenchymal stem cells in bone development, bone repair, and skeletal regeneration therapy. *J Cell Biochem* **56:** 283–294.

Chan SW, Blackburn EH. 2002; New ways not to make ends meet: telomerase, DNA damage proteins and heterochromatin. *Oncogene* **21:** 553–63.

Chang S, Multani AS, Cabrera NG, *et al*. 2004; Essential role of limiting telomeres in the pathogenesis of Werner syndrome. *Nat Genet* **36:** 877–882.

Choi Y, Wright AC, Johnson FB. 2008; Defects in telomere maintenance molecules impair osteoblast differentiation and promote osteoporosis. *Aging Cell* **7:** 23–31

D'Ippolito G, Schiller PC, Ricordi C, *et al*. 1999; Age-related osteogenic potential of mesenchymal stem cells from human vertebral bone marrow. *J Bone Miner Res* **14:** 1115–1122.

Dudas JR, Marra KG, Cooper GM, *et al*. 2006; The osteogenic potential of adipose-derived stem cells for the repair of rabbit calvarial defects. *Ann Plast Surg* **56:** 543–548.

Egermann M, Heil P, Tami A, *et al*. 2010; Influence of defective bone marrow osteogenesis on fracture repair in an experimental model of senile osteoporosis. *J Orthop Res* **28:** 798–804.

Gimble JM. 2003; Adipose tissue-derived therapeutics. *Expert Opin Biol Ther* **3:** 705–713.

Halvorsen YC, Wilkison WO, Gimble JM. 2000; Adipose-derived stromal cells – their utility and potential in bone formation. *Int J Obes Relat Metab Disord* **24**(suppl 4): S41–44.

Halvorsen YD, Franklin D, Bond AL, *et al*. 2001; Extracellular matrix mineralization and osteoblast gene expression by human adipose tissue-derived stromal cells. *Tissue Eng* **7:** 729–741.

Helder MN, Knippenberg M, Klein-Nulend J, *et al*. 2007; Stem cells from adipose tissue allow challenging new concepts for regenerative medicine. *Tissue Eng* **13:** 1799–1808.

Hicok KC, Du Laney TV, Zhou YS, *et al*. 2004; Human adipose-derived adult stem cells produce osteoid *in vivo*. *Tissue Eng* **10:** 371–380.

Hildebrand T, Laib A, Müller R, *et al*. 1999; Direct three-dimensional morphometric analysis of human cancellous bone: microstructural data from spine, femur, iliac crest, and calcaneus. *J Bone Miner Res* **14:** 1167–1174.

Izadpanah R, Trygg C, Patel B, *et al*. 2006; Biologic properties of mesenchymal stem cells derived from bone marrow and adipose tissue. *J Cell Biochem* **99:** 1285–1297.

Jilka RL, Weinstein RS, Takahashi K, *et al*. 1996; Linkage of decreased bone mass with impaired osteoblastogenesis in a murine model of accelerated senescence. *J Clin Invest* **97:** 1732–1740.

Justesen J, Pedersen SB, Stenderup K, Kassem M. 2004; Subcutaneous adipocytes can differentiate into bone-forming cells *in vitro* and *in vivo*. *Tissue Eng* **10:** 381–391.

Kang SK, Putnam L, Dufour J, *et al*. 2004; Expression of telomerase extends the lifespan and enhances osteogenic differentiation of adipose tissue-derived stromal cells. *Stem Cells* **22:** 1356–1372.

Kawaguchi H, Manabe N, Miyaura C, *et al*. 1999; Independent impairment of osteoblast and osteoclast differentiation in klotho mouse exhibiting low-turnover osteopenia. *J Clin Invest* **104:** 229–237.

Khan WS, Adesida AB, Tew SR, *et al*. 2009; The epitope characterization and the osteogenic differentiation potential of human fat pad-derived stem cells is maintained with ageing in later life. *Injury* **40:** 150–157.

Kojima H, Uede T, Uemura T. 2004; *In vitro* and *in vivo* effects of the overexpression of osteopontin on osteoblast differentiation using a recombinant adenoviral vector. *J Biochem* **136:** 377–386.

Kuro-o M, Matsumura Y, Aizawa H, *et al*. 1997; Mutation of the mouse *klotho* gene leads to a syndrome resembling aging. *Nature* **390:** 45–51.

Lane NE. 2006; Epidemiology, etiology, and diagnosis of osteoporosis. *Am J Obstet Gynecol* **194**(2, suppl): S3–11.

Li H, Dai K, Tang T, Zhang X, *et al*. 2007; Bone regeneration by implantation of adipose-derived stromal cells expressing BMP-2. *Biochem Biophys Res Commun* **356:** 836–842.

Lu L, DiGirolamo CM, Navarro PAA, *et al*. 2004; Telomerase deficiency impairs differentiation of mesenchymal stem cells. *Exp Cell Res* **294:** 1–8.

Matsushita M, Tsuboyama T, Kasai R, *et al*. 1986; Age-related changes in bone mass in the senescence-accelerated mouse (SAM), SAM-R/3 and SAM-P/6 as new murine models for senile osteoporosis. *Am J Pathol* **125:** 276–283.

Mesimäki K, Lindroos B, Törnwall J, *et al*. 2009; Novel maxillary reconstruction with ectopic bone formation by GMP adipose stem cells. *Int J Oral Maxillofac Surg* **38:** 201–209.

Meunier P, Aaron J, Edouard C, *et al*. 1971; Osteoporosis and the replacement of cell populations of the marrow by adipose tissue. A quantitative study of 84 iliac bone biopsies. *Clin Orthop Relat Res* **80:** 147–154.

Odgaard A. 1997; Three-dimensional methods for quantification of cancellous bone architecture. *Bone* **20:** 315–328.

Pittenger MF, Mackay AM, Beck SC, *et al*. 1999; Multilineage potential of adult human mesenchymal stem cells. *Science* **284:** 143–147.

Recker RR and Barger-Lux MJ. 2004; The elusive concept of bone quality. *Curr Osteoporosis Rep* **2:** 97–100.

Rodríguez JP, Garat S, Gajardo H, *et al*. 1999; Abnormal osteogenesis in osteoporotic patients is reflected by altered mesenchymal stem cells dynamics. *J Cell Biochem* **75:** 414–423.

Rodríguez JP, Montecinos L, Ríos S, *et al*. 2000; Mesenchymal stem cells from osteoporotic patients produce a type I collagen-deficient extracellular matrix favoring adipogenic differentiation. *J Cell Biochem* **79:** 557–565.

Roura S, Farré J, Soler-Botija C, *et al*. 2006; Effect of aging on the pluripotential capacity of human $CD105^{+}$ mesenchymal stem cells. *Eur J Heart Fail* **8:** 555–563.

Sahin E and Depinho RA. 2010; Linking functional decline of telomeres, mitochondria and stem cells during ageing. *Nature* **464:** 520–528.

Satyanarayana A, Wiemann SU, Buer J, *et al*. 2003; Telomere shortening impairs organ regeneration by inhibiting cell cycle reentry of a subpopulation of cells. *EMBO J* **22:** 4003–4013.

Schäffler A and Büchler C. 2007; Concise review: adipose tissue-derived stromal cells – basic and clinical implications for novel cell-based therapies. *Stem Cells* **25:** 818–827.

Schipper BM, Marra KG, Zhang W, *et al*. 2008; Regional anatomic and age effects on cell function of human adipose-derived stem cells. *Ann Plast Surg* **60:** 538–544

Seeman E and Delmas PD. 2006; Bone quality – the material and structural basis of bone strength and fragility. *N Engl J Med* **354:** 2250–2261.

Shi YY, Nacamuli RP, Salim A, *et al*. 2005; The osteogenic potential of adipose-derived mesenchymal cells is maintained with aging. *Plast Reconstr Surg* **116:** 1686–1696.

Silva MJ, Brodt MD, Ettner SL. 2002; Long bones from the senescence accelerated mouse SAMP6 have increased size but reduced whole-bone strength and resistance to fracture. *J Bone Miner Res* **17:** 1597–1603.

Silva MJ, Brodt MD, Ko M, *et al*. 2005; Impaired marrow osteogenesis is associated with reduced endocortical bone formation but does not impair periosteal bone formation in long bones of SAMP6 mice. *J Bone Miner Res* **20:** 419–427.

Simonsen JL, Rosada C, Serakinci N, *et al*. 2002; Telomerase expression extends the proliferative life-span and maintains the osteogenic potential of human bone marrow stromal cells. *Nat Biotechnol* **20:** 592–596.

Stenderup K, Justesen J, Clausen C, *et al*. 2003; Aging is associated with decreased maximal life span and accelerated senescence of bone marrow stromal cells. *Bone* **33:** 919–926.

Stolzing A, Jones E, McGonagle D, *et al*. 2008; Age-related changes in human bone marrow-derived mesenchymal stem cells: consequences for cell therapies. *Mech Ageing Dev* **129:** 163–173.

Suzuki H, Amizuka N, Oda K, *et al*. 2005; Histological evidences on altered distribution of osteocytes and bone matrix synthesis in *klotho*-deficient mice. *Arch Histol Cytol* **68:** 371–381.

Takeda T. 1999; Senescence-accelerated mouse (SAM): a biogerontological

resource in aging research. *Neurobiol Aging* **20:** 105–110.
Tapp H, Hanley JR EN, Patt JC, *et al*. 2009; Adipose-derived stem cells: characterization and current application in orthopaedic tissue repair. *Exp Biol Med* **234:** 1–9.
Weinzierl K, Hemprich A, Frerich B. 2006; Bone engineering with adipose tissue derived stromal cells. *J Craniomaxillofac Surg* **34:** 466–471.
Wiemann SU, Satyanarayana A, Tsahuridu M, *et al*. 2002; Hepatocyte telomere shortening and senescence are general markers of human liver cirrhosis. *FASEB J* **16:** 935–942.
Yoon E, Dhar S, Chun DE, *et al*. 2007; *In vivo* osteogenic potential of human adipose-derived stem cells/polylactide-co-glycolic acid constructs for bone regeneration in a rat critical-sized calvarial defect model. *Tissue Eng* **13:** 619–627.
Yu JM, Wu X, Gimble JM, *et al*., 2011; Age-related changes in mesenchymal stem cells derived from rhesus macaque bone marrow. *Aging Cell* **10:** 66–79.
Zhu M, Kohan E, Bradley J, *et al*. 2009; The effect of age on osteogenic, adipogenic and proliferative potential of female adipose-derived stem cells. *J Tissue Eng Regen Med* **3:** 290–301.
Zuk PA, Zhu M, Mizuno H, *et al*. 2001; Multilineage cells from human adipose tissue: implications for cell-based therapies. *Tissue Eng* **7:** 211–228.

DOI: 10.1002/term

Preparation and Osteogenic Differentiation of Scaffold-Free Mouse Adipose-Derived Stromal Cell Microtissue Spheroids (ASC-MT)

Ali Mirsaidi,[1] André N. Tiaden,[1] and Peter J. Richards[1]

[1]Bone and Stem Cell Research Group, CABMM, University of Zurich, Zurich, Switzerland

ABSTRACT

In this unit, previously described methods are expanded upon, where procedures relating to the preparation, culturing, and osteogenic differentiation of scaffold-free mouse adipose-derived stromal cell microtissue spheroids (ASC-MT) are outlined. Not only is a detailed methodology of how to engineer such spheroids are presented, but a full account of how to induce and analyze osteogenesis in these ASC-MT constructs is given along with relevant figures to help better illustrate the methods described. *Curr. Protoc. Stem Cell Biol*. 27:2B.5.1-2B.5.12. © 2013 by John Wiley & Sons, Inc.

Keywords: adipose-derived stromal cells • osteogenesis • 3D-culture

INTRODUCTION

The use of adipose-derived stromal cells (ASCs) in tissue engineering and regenerative medicine is becoming increasingly popular due to the ease by which these cells can be isolated from donor fat tissue and their capacity for multipotent differentiation (Tapp et al., 2009). Microtissue spheroids (MTs) represent an alternative cell culture technique with which to investigate tissue-specific processes in vitro, and are believed to represent a more physiologically relevant environment for cells than the traditional two-dimensional (2-D) culture system (Friedrich et al., 2009; Kelm and Fussenegger, 2010). Here, the methodology of how to engineer and analyze scaffold-free mouse ASC-MTs undergoing osteogenic differentiation is described. The first protocol section delivers an extended guideline for the preparation and expansion of ASCs isolated from murine subcutaneous inguinal fat pads followed by an extensive description of how to successfully establish, culture, and harvest mouse ASC-MTs using the hanging drop technology. Furthermore, the outlined protocols for generating 2-D ASC monolayers and ASC-MT hanging drop cultures include detailed instructions on how to differentiate mouse ASCs towards the osteogenic lineage. Support protocols are also provided to describe analysis of mouse ASC osteogenic differentiation in both experimental settings using Alizarin Red S staining to visualize mineralized matrix formation.

NOTE: Aseptic technique is required for the handling of all solutions and equipment in contact with living cells.

NOTE: All animal research procedures were approved by the Animal Experimentation Committee of the Veterinary Office of the Canton of Zürich, Switzerland, and followed the guidelines of the Swiss Federal Veterinary Office for the use and care of laboratory animals.

Current Protocols in Stem Cell Biology 2B.5.1-2B.5.12, November 2013
Published online November 2013 in Wiley Online Library (wileyonlinelibrary.com).
DOI: 10.1002/9780470151808.sc02b05s27

BASIC PROTOCOL 1

ASC ISOLATION AND EXPANSION

The procedures described here allow for the standardization of methodologies employed for the isolation of multipotent mouse stromal cells derived from adipose tissue and will ensure a high level of consistency between individual experiments and investigators.

Materials

Male mice (8- to 12-weeks old)
70% ethanol
Betadine (Mundipharma Medical Company)
Growth medium I (see recipe)
Dulbecco's phosphate-buffered saline (D-PBS, Life Technologies, cat. no. 14190-094)
Digestion solution (see recipe)
0.25% trypsin-EDTA (Life Technologies, cat. no. 25200-056)

Sterile surgical instruments (forceps, tweezers, clamps, micro-scissors, scalpels)
15- and 50-ml tubes (Falcon)
Sterile petri dishes
Stereomicroscope
Shaker, 37°C
Centrifuge
40-µm cell strainer (BD Falcon, cat. no. 352340)
25- and 75-cm^2 culture flasks (Nunclon, cat. nos. 734-2064 and 734-2066)
37°C, 5% CO_2 humidified incubator
5- and 10-ml serological pipets, sterile

Prepare mice and dissect inguinal fat pad

1. Prepare 8- to 12-week-old male mice prior to dissection by shaving lower ventral surface and cleaning skin area with 70% ethanol and Betadine.

   In female rodents, the mammary glands, which also reside within the inguinal fat pad may represent a source of contaminating cells and should be avoided. For this reason, male rodents are the better choice for ASC isolation.

2. Lay mouse dorsal side down (face up), and make incision into skin with scissors along ventral surface from femoral part of hind limb upwards.

   It is important to perform this step carefully and to not puncture the peritoneal cavity.

3. Retract skin on one side and hold in place with needles to expose inguinal fat pad as made evident by the presence of the inguinal lymph node (Fig. 2B.5.1).

4. Remove portion of inguinal pad from upper leg all the way through the abdominal cavity (from lateral to medial) while avoiding removal of lymph node if present.

5. Place fat tissue into a 50-ml tube containing 25 ml growth medium while extracting the contralateral fat pad.

   Fat tissue floats.

Process fat tissues

6. Transfer fat tissues to a sterile petri dish, cut into pieces using micro-scissors, and then transfer back into a 50-ml tube containing 25 ml growth medium.

   Performing this step under a stereomicroscope to visualize and remove major blood vessels and connective tissue, which may act as a source of contaminating cells, is recommended.

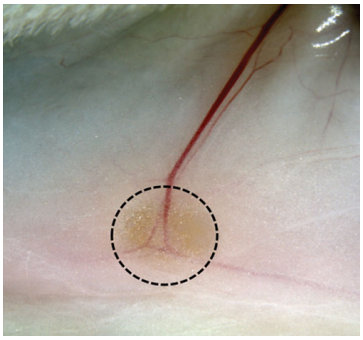

Figure 2B.5.1 Mouse inguinal fat pad including lymph node (dashed circle).

7. Wash the minced tissue quickly by transferring floating tissue with forceps into a fresh 50-ml tube containing 25 ml D-PBS.
8. Transfer the washed floating minced tissue pieces into a 15-ml tube with sterile tweezers and add 5 ml digestion solution to release the stem cells embedded within the fat tissue matrix.
9. Incubate tissues 30 min on a 37°C shaker to allow full exposure of minced tissue to the digestion solution (low speed rotary shaker at 80 rpm).

   For an efficient digestion of the tissue, periodically remove tubes from rotary shaker and mix vigorously.

10. Add 5 ml of D-PBS to bring the total volume up to 10 ml and centrifuge 5 min 400 × *g*, room temperature, to separate the population of mature adipocytes from the pelleted stromal vascular fraction. Repeat this step two additional times for a total of three times.

    Mature adipocytes float due to intracellular accumulation of lipid vesicles.

Process adipose stromal fraction

11. Remove supernatant and resuspend pellets in 5 ml growth medium to inactivate collagenase activities.
12. Pass the medium through a 40-µm cell strainer to remove undigested particles, then wash the filter with an additional 5 ml growth medium, and centrifuge 5 min at 400 × *g*, room temperature.
13. Remove supernatant and resuspend the adipose stromal fraction in 5 ml of growth medium.
14. Transfer cell suspension to 25-cm^2 culture flask and incubate in a 37°C, 5% CO_2 humidified incubator to allow the adipose stromal cells to adhere to plastic.
15. After 24 hr, change the growth medium to remove non-adherent cells from culture.
16. Grow ASCs to 60% confluency in a 25-cm^2 culture flask, rinse with D-PBS, and detach ASCs with trypsin-EDTA (0.25%) for 2 min in a 37°C, 5% CO_2 incubator.

    Incubate until cells are released from the surface (~2 min). Verify that cells are detached under a light microscope.

17. Inactivate the trypsin by adding growth medium (with 1:10 dilution factor), then mix gently with a pipet and directly transfer to a 75-cm^2 culture flask. When ASCs are 60% confluent, split further at a ratio of 1:3.

Growth medium is used to quench the proteolytic activity of trypsin.

SUPPORT PROTOCOL 1

INDUCTION OF OSTEOGENIC DIFFERENTIATION IN ASC 2-D CULTURES

The protocol described here will allow for standardization of methodologies employed for the induction of osteogenic differentiation in ASCs and will ensure a high level of consistency between individual experiments and investigators.

Materials

ASCs (see Basic Protocol 1)
Growth medium II (see recipe)
Osteogenic induction medium (see recipe)
Dulbecco's phosphate-buffered saline (D-PBS, Life Technologies, cat. no. 14190-169)
10% (v/v) formaldehyde solution (Sigma, cat. no. F1635) in D-PBS
Alizarin Red S working solution (see recipe)

5- and 10-ml serological pipets, sterile
37°C, 5% CO_2 humidified incubator
Rocking platform
Light microscope

1. For osteogenic differentiation, plate ASCs in growth medium II at 5000 cells/cm^2 in sterile tissue culture plates and incubate in a 37°C, 5% CO_2 humidified incubator to allow ASCs to adhere to tissue culture plastic.
2. After 24 hr, change the growth medium II to osteogenic induction medium and replace half of the osteogenic medium every 3 days thereafter.
3. After 14 days, remove the osteogenic induction medium and wash ASCs three times with D-PBS.
4. Fix ASCs with 10% (v/v) formaldehyde solution for 60 min at room temperature.
5. Remove fixative and wash ASCs three times with distilled water.
6. Add Alizarin Red S working solution (0.5 ml/cm^2) to ASCs, and incubate 10 min at room temperature with gentle rocking.

It is important to ensure that the Alizarin Red S working solution is at pH 4.2.

7. Remove the stain and wash thoroughly with distilled water. Repeat for a total of three washes.
8. Visualize Alizarin Red S staining under a light microscope (Fig. 2B.5.2).

BASIC PROTOCOL 2

GENERATION OF OSTEOGENIC ASC-MTs

ASC-MTs are produced using the hanging drop technique. The procedures described here will allow for standardization of methodologies employed for culturing ASCs in hanging drops and will ensure a high level of consistency between individual experiments and investigators.

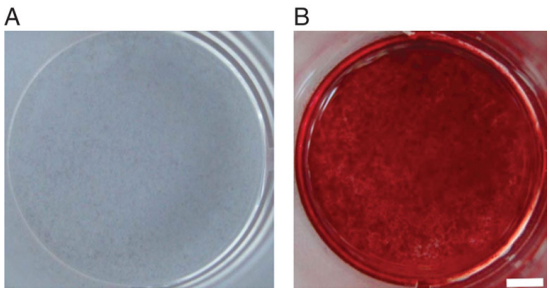

Figure 2B.5.2 Osteogenic differentiation. ASCs were grown in control medium (**A**) or osteogenic induction medium (**B**) and stained with Alizarin Red S after 14 days. Scale bar = 2.5 mm.

Materials

ASCs (see Support Protocol 1)
Dulbecco's phosphate-buffered saline (D-PBS, Life Technologies, cat. no. 14190-169)
0.25% trypsin-EDTA (Life Technologies, cat. no. 25200-056)
Growth medium I or II (see recipe)
Osteogenic induction medium (see recipe)
Trypan blue solution (Sigma, cat. no. T8154)

Light microscope
5- and 10-ml serological pipets, sterile
15-ml tubes (Falcon)
Centrifuge
Hemacytometer
Terasaki plates (Nunc, cat. no. 734-2079)
Reagent reservoir (Thermo Scientific, cat. no. 8093-11)
Multichannel electronic pipettor (Thermo Scientific, cat. no. 2034)
1250-µl tips (Thermo Scientific, cat. no. 8041)
37°C, 5% CO_2 humidified incubator

1. Plate ASCs at 5000 cells/cm^2 and induce toward osteogenesis under sterile conditions in a 37°C, 5% CO_2 humidified incubator (see Support Protocol 1).
2. On day 3, rinse ASCs with D-PBS and detach with 0.25% trypsin-EDTA. Incubate until cells are released from the surface (~2 min). Verify that cells are detached under a light microscope.
3. Inactivate the trypsin by adding growth medium I using a 1:10 dilution ratio, mix gently, and transfer into a clean 15-ml tube.

   Growth medium is used to quench the proteolytic activity of trypsin.
4. Centrifuge ASCs 5 min at 300 × *g*, room temperature, to obtain a cell pellet.
5. Aspirate the supernatant and gently resuspend the ASCs in an appropriate volume of osteogenic induction medium to allow for accurate cell counting.
6. Determine cell number from a 50-µl aliquot of the cell suspension using a hemacytometer and determine viability through dye exclusion with Trypan blue solution. Adjust cell concentration to allow for 5000 cells per ASC-MT.

7. Dilute ASCs in osteogenic induction medium to 2×10^5 cells/ml, and then transfer a maximum of 25 ml cell suspension into a reagent reservoir for plating ASCs into Terasaki plates using a multichannel pipettor.

   In cases where higher volumes (e.g., several plates) are required, refill the reservoir with the remaining cell suspension for the next pipetting run.

8. Adjust pipet tip distances in a way that each tip fits perfectly into every second well of the Terasaki plate.

9. For pipetting, use the maximum possible pipetting speed. Aspirate cell suspension into each pipet tip, release the first round of droplets into the reservoir to remove air bubbles and then pipet 25 µl of suspension into each well.

   The droplet size range is very limited and should lie between 23 to 27 µl. The force generated by larger volumes makes the droplets heavier and therefore more likely to merge together, while smaller volumes do not provide either enough space for cell assembly or sufficient nutrients.

10. Begin pipetting while approaching the well from the side, then move to straight above the well, deposit droplet, and pull out towards the top very gently, since fast movement can also destroy the droplet. Refill tips prior to becoming empty.

    Avoid using the last remnants of the medium in the tips, as the accuracy of the volume, and thus cell number, in the last droplets cannot be guaranteed.

11. When a Terasaki plate is completely filled, replace the lid and, while holding one edge to the surface of the working area, carefully turn the plate upside down without destroying the droplets (this will enable gravity-enforced ASC-MT spheroid formation).

    Careful consideration of the working space is essential as it is important to avoid excessive vibrations.

12. Transfer plates to a 37°C, 5% CO_2 incubator for an incubation period up to 6 days.

    Over the course of culture time, the ASC-MTs will become more spherical and more defined, but also the droplets will shrink in size due to evaporation.

BASIC PROTOCOL 3

HARVESTING AND PROCESSING OF ASC-MT FOR HISTOLOGICAL ANALYSIS OF OSTEOGENIC DIFFERENTIATION

The procedures described here will allow for standardization of methodologies employed for the harvesting and tissue processing of osteogenic ASC-MTs from hanging drop culture and will ensure a high level of consistency between individual experiments and investigators. As detailed assessment of tissue morphology is required for characterization of ASC-MT differentiation, development of an efficient protocol for histological analysis of ASC-MTs is essential.

Materials

Dulbecco's phosphate-buffered saline (D-PBS, Life Technologies, cat. no. 14190-169)
Terasaki plates containing osteogenic ASC-MTs (see Basic Protocol 2)
10% (v/v) formaldehyde solution (Sigma, cat. no. F1635) in D-PBS
Low-melting-point agarose (Sigma, cat. no. A9414)
Hematoxylin blue
Paraffin wax (Paraplast, Sigma, cat. no. P3558)

Sterile petri dishes (12-cm diameter)

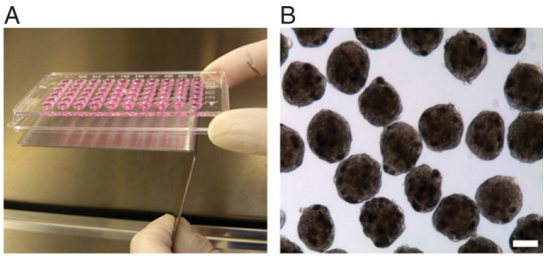

Figure 2B.5.3 Harvesting ASC-MTs from Terasaki plates. (**A**) The ASC-MT-harvesting device was prepared in-house using a polished stainless-steel plate, which was angled to allow for ease of placement during harvesting. Once in contact with the harvesting device, the droplets readily detach from the Terasaki plates thus allowing for optimized transfer to the appropriate collection vessel. (**B**) Visualization of ASC-MTs under phase-contrast microscope. Scale bar = 100 μm.

Sterile, non-adhesive, stainless-steel ASC-MT harvesting device
Light microscope
Sterile 0.2- and 1.5-ml microcentrifuge tubes (Eppendorf)
Tweezers
Microcentrifuge
Disposable needles
Tissue processing/embedding cassettes with lid (Sigma, cat. no. Z672122)
Tissue processor (Leica Histoprocessor, cat. no. ASP200S)
Paraffin embedding station (Leica, cat. no. EG1150H)
Embedding moulds (VWR Scientific)

1. Add sterile D-PBS to a sterile petri dish until it is half full.
2. Carefully remove the Terasaki plate lid while keeping plate in the same orientation as incubated (upside down).
3. Approach the hanging drops from below with the sterile harvesting device, and allow the droplets to come into contact with the harvesting device (Fig. 2B.5.3A).
4. Immerse the ASC-MT-laden surface of the harvesting device into the D-PBS-filled petri dish. Repeat this step two to three times until every ASC-MT is extracted out of the Terasaki plate. Repeat for all Terasaki plates.
5. Gently swirl petri dishes for up to 10 sec until the ASC-MTs start accumulating in the center of the plate (see Fig. 2B.5.3B).

   For an efficient harvest of all ASC-MTs from the petri dish, perform the swirling motion under a light microscope to gain better visibility of the floating ASC-MTs.

6. Carefully pipet the ASC-MTs located in the center of the petri dish into a 1.5-ml microcentrifuge tube. Allow the ASC-MTs to sediment for up to 5 sec inside the microcentrifuge tube for further processing.
7. Remove any excess D-PBS and fix ASC-MTs with 0.5 ml 10% formaldehyde solution in D-PBS for 60 min at room temperature.
8. Prepare 1% agarose solution in double deionized water, boil, and allow it to cool down while monitoring the temperature.

   It is important to cool down the agarose solution to a temperature between 40° and 45°C to protect ASC-MTs.

Table 2B.5.1 Processing Program using the Leica Histoprocessor

Reagent	Duration (min)[a]	Temperature (°C)
Ethanol (70%)	00:10	37
Ethanol (90%)	00:10	37
Ethanol (absolute)	00:10	37
Ethanol (absolute)	00:10	37
Ethanol (absolute)	00:10	37
Ethanol (absolute)	00:20	37
Xylene	00:10	37
Xylene	00:10	37
Xylene	00:15	37
Histowax	00:10	62
Histowax	00:10	62
Histowax	00:20	62

[a]Total duration = 3:21 hr.

9. Remove fixative and wash ASC-MTs three times with 1 ml D-PBS. Resuspend ASC-MTs with 100 µl of D-PBS and transfer them into a 0.2-ml microcentrifuge tube and pulse spin for 5 sec in a microcentrifuge.
10. Remove the supernatant, and resuspend ASC-MTs quickly in 50 µl of 1% agarose solution using a 200-µl tip enlarged by removing the tip with scissors.
11. Pulse spin the ASC-MTs for 5 sec in a microcentrifuge, and place tube on ice for 20 min to allow for the agarose to solidify.
12. Remove the agarose plug from the 0.2-ml microcentrifuge tube with disposable needles. Dip the tip of the agarose plug into a dye solution (e.g., hematoxylin blue) to facilitate localization of the ASC-MTs during tissue sectioning.
13. Transfer the agarose plugs into a conventional paraffin-embedding cassette, and place them into automated tissue processor (Leica Histoprocessor) for processing using the program detailed in Table 2B.5.1.
14. Embed tissue in molten paraffin wax and store at room temperature.

SUPPORT PROTOCOL 2

ANALYSIS OF OSTEOGENESIS IN ASC-MT PARAFFIN WAX SECTIONS

Materials

Alizarin Red S working solution (see recipe)
DPX mountant (Sigma, cat. no. 44581)

Microtome (Leica, cat. no. RM2235)
Superfrost Plus slide (Thermo Scientific, cat. no. J1800AMNZ)
37°C incubator
60°C heating block
Light microscope

Additional reagents and equipment for hanging drop generation of ASC-MTs (see Basic Protocol 2) and ASC-MTs in paraffin wax (see Basic Protocol 3)

1. Generate ASC-MTs in osteogenic medium for up to 6 days in hanging drop format using four Terasaki plates (see Basic Protocol 2).

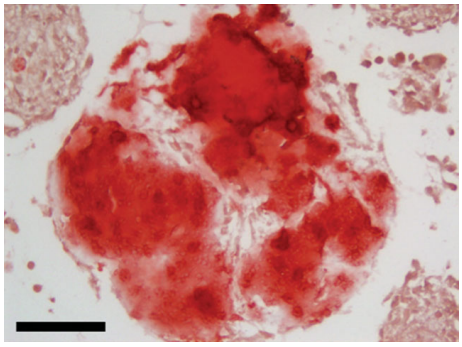

Figure 2B.5.4 Alizarin Red S staining of paraffin wax sections of ASC-MTs. Scale bar = 50 μm.

2. After 4 to 6 days, harvest ASC-MTs and process for tissue sectioning (see Basic Protocol 3).
3. Trim paraffin blocks as necessary and cut 3- to 5-μm sections using a microtome and transfer onto a Superfrost Plus slide. Allow slides to dry overnight at 37°C and store them at room temperature until use.
4. Before staining slides for Alizarin Red S, place 1 hr at 60°C.
5. Remove paraffin wax from tissue sections on slides by incubating in 300 ml of xylene for 5 min. Repeat step for a total of two times.
6. Rehydrate in two steps by dipping slides for 5 min in 100% ethanol, and then for 5 min in 90% ethanol.

   Water may remove calcium prior to Alizarin Red S staining.
7. Allow sections to dry for 20 min at room temperature.
8. Add slides to 2% Alizarin Red S working solution for 5 min.
9. Rinse sections quickly in distilled water.
10. Dry sections for 20 min at room temperature and mount them with DPX mountant.
11. Visualize Alizarin Red S under a light microscope (Fig. 2B.5.4).

    Red staining is a positive indicator of mineral deposition within the tissue sections.

REAGENTS AND SOLUTIONS

For culture recipes and steps, use sterile tissue culture–grade water. For other purposes, use deionized, distilled water or equivalent in recipes and protocol steps. For suppliers, see SUPPLIERS APPENDIX.

Alizarin Red S working solution

Prepare 2% (w/v) Alizarin Red S (Sigma, cat. no. A5533) in double deionized water; adjust pH to 4.2 with 10% (v/v) ammonium hydroxide (Sigma, cat. no. 221228). Store up to 1 month at room temperature in the dark.

Digestion solution

Hank's balanced salt solution (HBSS, Life Technologies, cat. no. 14025-050)

continued

0.1% (w/v) collagenase A (Roche, cat. no. 10103586001)
0.2% (w/v) bovine serum albumin (Roche, cat. no. 10735086001)

Fixative solution

Prepare 10% (v/v) formaldehyde solution (Sigma, cat. no. F1635) in D-PBS
Store up to 6 months at room temperature

Growth medium I

Dulbecco's modified Eagles medium (DMEM, Life Technologies, cat. no. 21885-025)
10% (v/v) fetal bovine serum (Biowest, cat. no. S05081S1830)
1% (v/v) penicillin/streptomycin (Sigma, cat. no. P4333151140)
Store up to 3 months at 4°C

Growth medium II

Minimum essential medium alpha (α-MEM, Life Technologies, cat. no. 22561-021)
10% (v/v) fetal bovine serum (Biowest, cat. no. S05081S1830)
1% (v/v) penicillin/streptomycin (Sigma, cat. no. P4333151140)
Store up to 3 months at 4°C

Osteogenic induction medium

Growth medium II (see recipe) supplemented with:
1 M β-glycerol phosphate (Sigma, cat. no. G9422) in DMEM (Life Technologies; cat. no. 21885-025)
50 mM L-ascorbic acid 2-phosphate (Sigma, cat. no. A8960) in double deionized water
10 mM retinoic acid (Sigma, cat. no. R2625) in DMSO (Sigma, cat. no. D2650)
Filter sterilize using a 0.2-μm filter
Store up to 12 months at −80°C

COMMENTARY

Background Information

Multipotent mesenchymal stem cells, including adipose-derived stromal cells (ASCs), represent a promising source of bone-forming cells for the treatment of various musculoskeletal disorders, including age-related bone loss (Tapp et al., 2009; Mirsaidi et al., 2012). Cell culture-based studies investigating the osteogenic differentiation of mesenchymal stem cells are routinely performed in 2-D cell culture systems. However, microtissue spheroids (MTs) may represent an alternative means by which to investigate cellular behavior in a more tissue-specific context (Kelm and Fussenegger, 2010; Tiaden et al., 2012). They can be produced from a variety of different cell types, including cell lines (Kelm et al., 2003; Friedrich et al., 2009) as well as primary stem cells (Keller, 1995; Tiaden et al., 2012). In contrast to cells grown in a standard 2-D monolayer system, cells cultured in MTs are maintained in a three-dimensional (3-D) configuration. This 3-D arrangement is considered to be potentially more representative of the native cellular environment, where the surrounding cellular milieu and extracellular matrix (ECM) can significantly influence cell shape (Goldmann, 2002), polarity (Boudreau, 2003), tension (Tarone et al., 2000), and differentiation (Bokel and Brown, 2002). Moreover, ECM is essential to organize the communication between single cells and drives developmental as well as differentiation processes (Schenk and Quaranta, 2003). Furthermore, the 3-D configuration is believed to support osteoblast formation and matrix mineralization through the process of cellular condensation (Dunlop and Hall, 1995). As such, MTs offer an alternative means by which to investigate osteogenic differentiation and bone formation in vitro, and in the case of ASC-MTs, could represent a novel therapeutic strategy for the treatment of bone disorders such as age-related osteoporosis.

Critical Parameters and Troubleshooting

Using ASCs to generate osteogenic microtissues is primarily dependent on the purity of the cell population isolated from mouse

Table 2B.5.2 Troubleshooting Guide for Common Problems Encountered During Preparation, Culturing, and Osteogenic Differentiation of ASC-MTs

Problem	Possible cause	Solution
Heterogeneous cell culture after ASC isolation from inguinal fat pad	Female mice used	Use male mice
	Contamination of culture with immune cells, epithelial cells, and fibroblasts	Remove lymph nodes, blood vessels, and connective tissues prior to tissue digestion
Low cell recovery after tissue digestion	Amount of initial fat tissue used too low	Increase amount of fat tissue extracted from mouse
	Insufficient collagenase digestion	Prepare fresh digestion solution just prior to usage and include manual shaking step to increase cell dissociation from fat tissue
No Alizarin Red S staining in ASC 2-D culture or osteogenic ASC-MTs	Induction medium too old	Prepare fresh osteogenic induction medium before each induction experiment
	Using Alizarin Red S working solution with wrong pH	Ensure Alizarin Red S working solution is pH 4.2
Droplets merge together during generation of osteogenic ASC-MTs	Force generated by larger volumes makes the droplets heavier and mixes them together	Only use volumes from 23 µl to 27 µl per well of Terasaki plate
Low numbers of ASC-MTs harvested for histology	Not all of the ASC-MTs have accumulated in center of Petri dish	Perform swirling motion of Petri dish and view under a light microscope to gain better visibility of the floating ASC-MTs
Inconsistent morphology of ASC-MT upon histological analysis	Temperature of agarose mold too high	Cool agarose solution to 45°C before adding to ASC-MTs

inguinal fat pads. Procedures relating to the preparation and culturing of ASCs to yield a homogeneous cell culture with the desired number of cells while retaining a low passage number are described. After extracting fat pads, it is recommended to remove major blood vessels and connective tissue, which may act as a source of contaminating cell types. Therefore, the visualization of tissue using a stereomicroscope and removal of non-fat tissue is recommended. As ASC isolation from one mouse is limited to two fat pads only, it is important to manually shake harvested tissues during digestion to increase the efficiency of ASC isolation and thus maximize cell numbers. In addition, it is advisable to allow ASCs to reach at least 60% confluency prior to further passaging, thus ensuring a better proliferation rate in further passages. For induction of ASC osteogenesis, it is advisable to prepare fresh medium, which can be stored at 4°C for the duration of the study (usually 2 weeks). To perform Alizarin Red S staining, adjusting the Alizarin Red S working solution pH to 4.2 is critical to ensure specific staining of the mineralized matrix. The other important parameter in this assay is the use of high-purity distilled water in each of the washing steps, as alkaline buffers (such as PBS) can remove the Alizarin Red S stain. In the case of ASC-MT generation, it is essential to pipet the correct volume and to avoid any unnecessary vibrations or movement, which may disturb the hanging drop. Once osteogenic ASC-MTs

are harvested, preparation of an agarose mold at 45°C is an important requirement for the preservation of ASC-MTs for further processing. To analyze osteogenic differentiation in ASC-MT paraffin wax sections, it is necessary to rehydrate the sections in up to 90% ethanol only, as water may remove calcium prior to Alizarin Red S staining. Common problems and solutions encountered during the preparation, culturing, and osteogenic differentiation of ASC-MTs are described in Table 2B.5.2.

Anticipated Results

The protocol for ASC isolation from inguinal fat pads from both the left and right side of one male mouse is expected to generate $\sim 0.9 \pm 0.2 \times 10^6$ cells per 75-cm^2 culture flask at passage one with ~60% to 80% confluency after 5 days expansion. Performing 3 days of osteogenic induction of ASCs in monolayer culture, followed by generation of osteogenic ASC-MTs using the hanging drop technique with an initial seeding density of 5000 cells, gives spherical tissues in the range of 100 µm and 250 µm in diameter. These ASC-MTs can be harvested and further processed for various histochemical analyses such as Alizarin Red S staining in which osteogenic differentiation can be determined by visualizing calcium deposition after 4 to 6 days.

Time Considerations

The amount of time needed to complete the isolation of ASCs from inguinal fat pads varies greatly with user experience and the number of mice needed per experiment. Preparation of all necessary surgical instruments and solutions should be done 1 hr prior to dissection of mice. The minimum time required to isolate ASCs from 4 to 6 mice is ~4 hr. Once the ASCs have been seeded into monolayer culture and induced towards osteogenesis, it usually takes at least 10 to 14 days to observe matrix mineralization as determined by Alizarin Red S staining. Once osteogenic ASC-MTs have been harvested, an additional 2 hr should be necessary for embedding in agarose solution and a further 4 hr for tissue processing and embedding in paraffin wax.

Literature Cited

Bokel, C. and Brown, N.H. 2002. Integrins in development: Moving on, responding to, and sticking to the extracellular matrix. *Dev. Cell* 3:311-321.

Boudreau, N.J. 2003. Organized living: From cell surfaces to basement membranes. *Sci STKE* 2003:pe34.

Dunlop, L.L. and Hall, B.K. 1995. Relationships between cellular condensation, preosteoblast formation and epithelial-mesenchymal interactions in initiation of osteogenesis. *Int. J. Dev. Biol.* 39:357-371.

Friedrich, J., Seidel, C., Ebner, R., and Kunz-Schughart, L.A. 2009. Spheroid-based drug screen: Considerations and practical approach. *Nat. Protoc.* 4:309-324.

Goldmann, W.H. 2002. Mechanical aspects of cell shape regulation and signaling. *Cell Biol. Int.* 26:313-317.

Keller, G.M. 1995. In vitro differentiation of embryonic stem cells. *Curr. Opin. Cell Biol.* 7:862-869.

Kelm, J.M. and Fussenegger, M. 2010. Scaffold-free cell delivery for use in regenerative medicine. *Adv. Drug Deliv. Rev.* 62:753-764.

Kelm, J.M., Timmins, N.E., Brown, C.J., Fussenegger, M., and Nielsen, L.K. 2003. Method for generation of homogeneous multicellular tumor spheroids applicable to a wide variety of cell types. *Biotechnol. Bioeng.* 83:173-180.

Mirsaidi, A., Kleinhans, K.N., Rimann, M., Tiaden, A.N., Stauber, M., Rudolph, K.L., and Richards, P.J. 2012. Telomere length, telomerase activity and osteogenic differentiation are maintained in adipose-derived stromal cells from senile osteoporotic SAMP6 mice. *J. Tissue Eng. Regen. Med.* 6:378-390.

Schenk, S. and Quaranta, V. 2003. Tales from the crypt[ic] sites of the extracellular matrix. *Trends Cell Biol.* 13:366-375.

Tapp, H., Hanley, E.N. Jr., Patt, J.C., and Gruber, H.E. 2009. Adipose-derived stem cells: Characterization and current application in orthopaedic tissue repair. *Exp. Biol. Med.* 234:1-9.

Tarone, G., Hirsch, E., Brancaccio, M., De Acetis, M., Barberis, L., Balzac, F., Retta, S.F., Botta, C., Altruda, F., and Silengo, L. 2000. Integrin function and regulation in development. *Int. J. Dev. Biol.* 44:725-731.

Tiaden, A.N., Breiden, M., Mirsaidi, A., Weber, F.A., Bahrenberg, G., Glanz, S., Cinelli, P., Ehrmann, M., and Richards, P.J. 2012. Human serine protease HTRA1 positively regulates osteogenesis of human bone marrow-derived mesenchymal stem cells and mineralization of differentiating bone-forming cells through the modulation of extracellular matrix protein. *Stem Cells* 30:2271-2282.

Biomaterials 35 (2014) 7326–7335

Contents lists available at ScienceDirect

Biomaterials

journal homepage: www.elsevier.com/locate/biomaterials

Therapeutic potential of adipose-derived stromal cells in age-related osteoporosis

Ali Mirsaidi [a, b, 1], Konstantin Genelin [c, 1], Jolanda R. Vetsch [d], Scott Stanger [d], Felix Theiss [e], Richard A. Lindtner [c], Brigitte von Rechenberg [e], Michael Blauth [c], Ralph Müller [d], Gisela A. Kuhn [d], Sandra Hofmann Boss [d, f, g], Hannes L. Ebner [c], Peter J. Richards [a, b, *]

[a] Bone and Stem Cell Research Group, CABMM, University of Zurich, 8057 Zurich, Switzerland
[b] Institute of Physiology and Zurich Center for Integrative Human Physiology (ZIHP), University of Zurich, 8057 Zurich, Switzerland
[c] Department of Trauma Surgery and Sports Medicine, Innsbruck Medical University, A-6020 Innsbruck, Austria
[d] Institute for Biomechanics, ETH Zurich, 8093 Zurich, Switzerland
[e] Musculoskeletal Research Unit, CABMM, University of Zurich, 8057 Zurich, Switzerland
[f] Department of Biomedical Engineering, Eindhoven University of Technology, P.O. Box 513, 5600 MB Eindhoven, The Netherlands
[g] Institute for Complex Molecular Systems, Eindhoven University of Technology, P.O. Box 513, Eindhoven 5600 MB, The Netherlands

ARTICLE INFO

Article history:
Received 24 April 2014
Accepted 5 May 2014
Available online 2 June 2014

Keywords:
Osteoporosis
Osteogenesis
Stem cell
Bone regeneration
Transplantation

ABSTRACT

Adipose-derived stromal cells (ASCs) are increasingly being used for orthopedic-based tissue engineering approaches due to their ability to readily undergo osteogenic differentiation. In the present study, we used *in vitro* and *in vivo* approaches to evaluate the use of ASCs as a treatment strategy for age-related osteoporosis. Molecular, histological and micro-computed tomography (micro-CT) based approaches confirmed that ASCs isolated from 18-week-old osteoporotic senescence-accelerated mice (SAMP6) were capable of undergoing osteogenesis when cultured in either silk fibroin (SF) scaffolds or scaffold-free microtissues (ASC-MT). A single intratibial injection of CM-Dil-labeled isogeneic ASCs or ASC-MT into SAMP6 recipients significantly improved trabecular bone quality after 6 weeks in comparison to untreated contralateral bones, as determined by micro-CT. Injected ASCs could be observed in paraffin wax bone sections at 24 h and 6 weeks post treatment and induced a significant increase in several molecular markers of bone turnover. Furthermore, a significant improvement in the osteogenic potential of osteoporotic patient-derived human bone marrow stromal cells (BMSCs) was observed when differentiated in conditioned culture media harvested from osteoporotic patient-derived human ASCs. These findings therefore support the use of ASCs as an autologous cell-based approach for the treatment of osteoporosis.

1. Introduction

Osteoporosis is characterized by significant deficits in both bone mass and bone quality, resulting in low bone strength and a reduced resistance to fractures [1]. There is now a mounting body of scientific evidence to suggest that impaired osteogenic differentiation of resident bone marrow stromal cells (BMSCs) may play a decisive role in mediating osteoporotic bone loss. Deficiencies in osteogenesis have previously been reported in BMSCs isolated from osteoporotic patients, where significant decreases in osteoblast-mediated mineral deposition were observed [2–4]. Inadequacies in the osteogenic capacity of BMSCs have also been linked to osteoporotic bone phenotypes associated with various animal models of aging [5–9]. Furthermore, the diminished osteogenic differentiation potential of BMSCs from osteoporotic patients appears to be in direct contrast to their ability to form adipocytes, thereby introducing the concept of fat marrow accretion as a potential confounding factor in the regulation of bone quality [7,9–11]. Nevertheless, despite these observations, the most widely prescribed treatments for osteoporosis are focused on inhibiting bone resorption [12]. The fact that BMSCs represent a critical component of the homeostatic machinery controlling bone turnover [13], alternative therapeutic strategies designed at targeting the BMSC niche in osteoporotic bone marrow may therefore warrant further consideration.

* Corresponding author. CABMM, University of Zurich, Winterthurerstrasse 190, CH-8057 Zürich, Switzerland. Tel.: +41 44 635 3801; fax: +41 44 635 6840.
E-mail address: peter.richards@cabmm.uzh.ch (P.J. Richards).
[1] Authors contributed equally.

http://dx.doi.org/10.1016/j.biomaterials.2014.05.016
0142-9612/

The use of adipose-derived stromal cells (ASCs) for the purpose of enhancing orthopedic tissue repair and regeneration is now widespread in areas of both experimental and clinical research [14,15]. ASCs have several advantages over other multipotent stem cell sources in that they are easily accessed non-invasively and have been shown to maintain both their proliferative [16–18] and osteogenic [17–19] potential with age. Moreover, we and others have recently reported that unlike their BMSC counterparts, the osteogenic differentiation capabilities of ASCs isolated from osteoporotic humans and mice remain intact [4,20], thereby highlighting their potential as an autologous cell-based therapy for treating age-related bone loss. Indeed, encouraging results have already been obtained from several studies investigating the therapeutic effects of systemically and locally administered ASCs on experimental osteoporosis [21–23]. However, to date, all studies investigating the therapeutic potential of ASCs in osteoporosis have focused on the prevention of bone loss in ovariectomized (OVX) mouse models, and have utilized cells obtained from non-osteoporotic animals.

In the present study, we hypothesize that ASCs isolated from osteoporotic SAMP6 mice have the capacity to generate mineralized matrix when induced to undergo osteogenesis in three-dimensional (3-D) culture systems, and can significantly enhance various parameters of bone quality *in vivo* following a single low dose intratibial injection. We use molecular, biochemical, histological and micro-CT analyses to evaluate the osteogenic potential of osteoporotic SAMP6-derived ASCs in 3-D scaffold-based and scaffold-free systems, and to validate their use as a therapeutic intervention for treating age-related bone loss in a mouse model for senile osteoporosis. Furthermore, we assess the capacity of ASCs to influence the osteogenic differentiation of BMSCs isolated from aged osteoporotic patients.

2. Materials & methods

2.1. Animals

Experiments were performed using 18-week-old male and female senescence accelerated mouse prone 6 (SAMP6) mice (Institute for Laboratory Animal Science, University of Zurich, Switzerland). All animal research procedures were approved by the Animal Experimentation Committee of the Veterinary Office of the Canton of Zurich, Switzerland and followed the guidelines of the Swiss Federal Veterinary Office for the use and care of laboratory animals.

2.2. Human patients

Human ASCs and BMSCs were harvested from a total of $n = 6$ non-osteoporotic and $n = 9$ osteoporotic female donors (>65 years of age) undergoing routine surgery. Osteoporosis was confirmed by dual energy X-ray absorptiometry (DXA; Hologic QDR 4500) according to WHO guidelines. All procedures were carried out in accordance with the ethics commission guidelines for Innsbruck Medical University.

2.3. Cell isolation and culture

ASCs isolated from inguinal fat pads of 18-week-old male SAMP6 mice were purified and characterized according to previously published protocols established in our laboratory [20,24]. Human BMSCs or ASCs were harvested from the femoral medullary cavity or subcutaneous adipose tissue respectively, as previously described [20,24,25]. In all cases, cells were maintained in normal growth medium consisting of Dulbecco's modified eagle medium (DMEM-low glucose, with Glutamax; Life Technologies, Zug, Switzerland), supplemented with 10% fetal bovine serum (FBS; Life Technologies) and penicillin (50 units/ml) and streptomycin (50 μg/ml) (Life Technologies). Cells were used between passage 2 and 4 unless otherwise stated.

2.4. Osteogenesis of SAMP6-derived ASCs in 3-D culture systems

The osteogenic induction of mouse ASCs was performed using protocols previously established in our laboratory [20,24]. ASC-seeded SF scaffolds were prepared as previously described [26,27]. Briefly, silk cocoons from *Bombyx Mori L.* were cooked twice in sodium carbonate for 1 h to extract sericins. Dried silk was dissolved in 9M lithium bromide and dialyzed against ultrapure water for 36 h. Frozen, dialyzed silk solution was lyophilized for four days and dissolved in hexafluoroisopropanol (HFIP) at 17% (w/v). Silk solution (1 ml) was pipetted onto 2.5 g sodium chloride granules of 300–400 μm diameter and left for 3 days until the HFIP had completely evaporated. Sodium chloride was leached out for 24 h in water and scaffolds cut into discs of 5 mm in diameter and 2 mm in height. For cell cultivation on SF scaffolds, 3×10^6 ASCs per scaffold were seeded by pipetting a droplet of 50 μl of cell suspension on top of each scaffold. Constructs were placed in an incubator at 37 °C, 5% CO_2, 100% humidity for 90 min and a drop of culture medium was applied every 20 min to prevent scaffolds from drying out. Five cell seeded constructs were fixed on the bottom of a bioreactor applicable for micro-CT monitoring. Each bioreactor was filled with 5 ml of osteogenic induction medium consisting of normal growth medium supplemented with 50 μM L-ascorbic acid 2-phosphate sesquimagnesium salt hydrate (Sigma–Aldrich, Buchs, Switzerland), 10 mM β-glycerophosphate (Sigma–Aldrich) and 5 μM retinoic acid (Sigma–Aldrich). Medium was exchanged three times per week for up to 6 weeks. ASC-MT cultures were prepared as previously described [24,28]. Briefly, 2.5×10^3 ASCs were cultured in 25 μl hanging drops of osteogenic medium in Terasaki plates (VWR, Switzerland) for up to 6 days. In all cases, osteogenic differentiation was evaluated by Alizarin red (Sigma–Aldrich) staining of paraffin wax tissue sections and by the analysis of osteogenic gene expression using quantitative reverse-transcription polymerase chain reaction (qRT-PCR). Fully formed ASC-MT were also cultured in sterile plastic culture plates under normal growth conditions or in osteogenic medium for up to 14 days, and the ability of ASCs to migrate out from the microtissues and also induce mineralization determined by microscopic analysis.

2.5. Osteogenesis of human BMSCs from osteoporotic patients

Age-matched BMSCs harvested from osteoporotic (OP; $n = 9$) or non-osteoporotic (non-OP; $n = 6$) patients were cultured for up to 21 days in osteogenic medium (OM) consisting of 50 μM L-ascorbic acid 2-phosphate sesquimagnesium salt hydrate, 10 mM β-glycerophosphate and 10 nM dexamethasone (Sigma–Aldrich), and osteogenesis compared at selected time points using the alkaline phosphatase (ALP) activity assay or by Alizarin red staining as previously described [25]. For studies investigating the influence of osteoporotic patient-derived ASCs on the osteogenic potential of osteoporotic patient-derived BMSCs, cultures of human BMSCs ($n = 4$) or ASCs ($n = 4$) isolated from age-matched osteoporotic patients were initially used to generate conditioned medium. Supernatants from cells cultured in normal growth medium (GM) were harvested at 48 h to generate conditioned medium (CM) designated ASC-CM or BMSC-CM. For osteogenic differentiation, human osteoporotic patient-derived BMSCs ($n = 4$) were

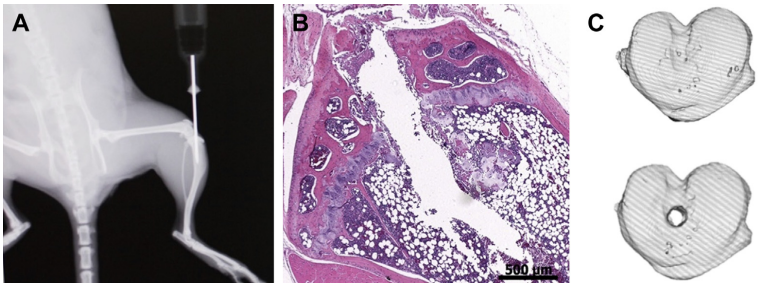

Fig. 1. (A) Digital radiograph illustrating an intratibial injection into the left proximal tibia of a SAMP6 mouse. (B) Representative hematoxylin & eosin stained paraffin wax section of decalcified tibia 1 day after injection. Scale bar = 500 μm. (C) Micro-CT analysis of tibial plateau from non-injected (upper panel) and injected (lower panel) bones at 24 h post treatment.

Table 1
List of TaqMan Gene Expression Assays used in RT-PCR analysis.

Gene symbol	Protein product	Assay ID[a]
Alpl	Alkaline phosphatase	Mm01187117_m1
Col1a2	Collagen type 1A 2	Mm00483888_m1
Ctsk	Cathepsin K	Mm00484039_m1
Gapdh	Glyceraldehyde-3-phosphate dehydrogenase	Mm99999915_g1
HtrA1	High temperature requirement protease A1	Mm00479887_m1
Ibsp	Integrin binding sialoprotein	Mm00492555_m1
Mrps12	Mitochondrial ribosomal protein S12	Mm00488728_m1
Opn	Osteopontin	Mm01611440_m1
Tnfa	Tumor necrosis factor alpha	Mm00443258_m1

[a] TaqMan Expression Assay identity code according to supplier (Life Technologies, Zug, Switzerland).

cultured for up to 14 days in OM supplemented with 100% of either ASC-CM or BMSC-CM in triplicates, and osteoblast formation determined by Alizarin red staining as previously described [25].

2.6. Intratibial injection

SAMP6 mice were anaesthetized with an i.p. injection of Fentanyl (0.05 mg/kg), Midazolam (5 mg/kg) and Medetomidin (0.5 mg/kg) in 0.9% NaCl, and the left tibia injected with either undifferentiated ASCs ($n = 9$), ASCs pre-differentiated for 3 days in osteogenic medium either as a monolayer ($n = 13$) or as ASC-MT ($n = 13$), or PBS/EDTA (vehicle; $n = 9$). Prior to implantation, cells were labeled with CM-Dil (Life Technologies) according to the manufacturer's recommendations. A pre-drilled hole was created in the left proximal tibia of 18-week-old female SAMP6 mice using a 26-gauge needle. Following brief flushing of the cavity with heparin (10 IE/ml), 10 μl of cells (15×10^4) or vehicle were injected directly into the medullary canal using a Hamilton syringe (Fig. 1A–C). The contralateral tibia remained untreated and served as the control. Tracking of injected CM-Dil-labeled ASCs was performed in dewaxed DAPI-stained paraffin sections of tibia taken at 24 h and 42 days following injection and analyzed using the Leica DMI6000B automated inverted research microscope system (Leica Microsystems, Heerbrugg, Switzerland).

2.7. Micro-CT monitoring of SF scaffolds

Bioreactors containing cell seeded scaffolds ($n = 5$ per bioreactor) were scanned weekly for up to 6 weeks on a micro-CT40 (Scanco Medical AG, Brüttisellen, Switzerland). Scans were operated at 45kVp energy level, 177 μA intensity, 200 ms integration time, 2-fold frame-averaging at high resolution mode leading to an isotropic resolution of 18 μm. The bioreactors were removed from the incubator for 1 h during the measurement. Greyscale images were filtered by applying a 3-D Gaussian filter (sigma 1.2, support 1) and a global threshold of 12.8% of the maximal grey values (corresponding to a density value of 127.59 mg HA/cm^3). Unconnected objects smaller than 50 voxels were not analyzed. Samples were evaluated morphometrically for mineralized tissue volume density (BV/TV).

2.8. Micro-CT analysis of mouse tibia

Tibia were excised and stored in 70% ethanol. Micro-CT40 (Scanco Medical AG, Brüttisellen, Switzerland) scans were performed with the X-ray tube operating at an energy of 55 kVp and an intensity of 145 μA. Three-dimensional images with an isotropic voxel size of 15 μm were reconstructed from 1000 projection images taken over 180° and an integration time of 300 ms. A 3-D Gaussian filter (sigma 0.8, support 1) was then applied to all images, and a global threshold corresponding to 22.4% of the maximum grey values was used to separate bone from marrow and surrounding soft tissues. Three compartments were selected for the evaluation. Full bone and cortical bone (5% of bone length located at 50% of length) were determined by an automated algorithm [29]. A trabecular compartment of 150 slices located distal of the growth plate was selected by manual contouring. Bone morphometric parameters were calculated within each compartment as described previously [30,31].

2.9. qRT-PCR analysis

Total RNA was purified from either mouse ASCs or mouse bone tissue using TRIzol reagent and treated with TURBO DNase (Life Technologies) as previously described [20,28]. RNA (0.5 μg) was reverse transcribed to cDNA using superscript II (Life Technologies) and random hexanucleotide primers (Promega AG, Dübendorf, Switzerland), and quantification of mRNA expression performed using TaqMan Gene Expression Assays (Life Technologies) (Table 1). For all *in vitro* studies, values were normalized to *Mrps12* mRNA levels and presented as fold change according to the $2^{-\Delta\Delta CT}$ method unless otherwise stated. For the measurement of gene expression levels in bone tissue, total RNA was harvested from the diaphysis of 5–6 bone samples and values normalized to *Gapdh* mRNA levels and presented as $2^{-\Delta CT}$. Each 10 μl reaction consisted of 1x TaqMan Fast Universal PCR Master Mix (Life Technologies), 1x TaqMan Gene Expression Assay and 10 ng cDNA (based upon initial RNA concentrations). All reactions were performed in triplicate in fast optical 96-well reaction plates (Life Technologies) at 95 °C for 20 s and 40 cycles of 95 °C for 1 s and 60 °C for 20 s.

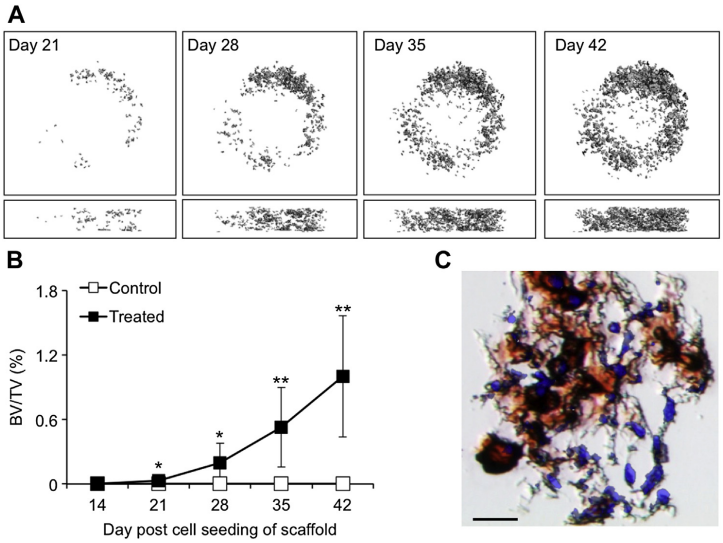

Fig. 2. (A) Representative micro-CT images of SF scaffolds seeded with ASCs (1×10^6) at selected time points following incubation in osteogenic induction medium. *Top panel*, transverse cross section; *bottom panel*, longitudinal cross section. (B) Micro-CT analysis of mineralized tissue volume density (BV/TV) in ASC-seeded SF scaffolds (Treated) ($n = 5$) as compared to SF scaffolds alone (Control) ($n = 5$). *$p < 0.05$, **$p < 0.01$ as determined by the Student's *t*-test (mean ± S.D.). (C) Representative image of an Alizarin red and DAPI stained paraffin wax section of ASC-seeded SF scaffold 42 days after osteogenic induction. Scale bar = 25 μm. *Red*, mineral deposition; *blue*, cell nuclei. (For interpretation of the references to colour in this figure legend, the reader is referred to the web version of this article.)

2.10. Histology

Paraffin wax sections of ASC microtissue spheroids were incubated with polyclonal rabbit anti-HTRA1 (1:50) or rabbit anti-osteocalcin (1:1000) using the conditions previously described [27]. Samples were then washed and incubated with goat anti-rabbit-Cy3 (1:400) for 1 h and mounted in DAPI containing Mowiol solution and images captured using the Leica DMI6000B system.

2.11. Statistical analysis

All statistical analyses were carried out using SPSS19.0 (SPSS Inc., Chicago, IL). Parametric analysis of normally distributed data was performed using either the two-tailed unpaired or paired Student's *t*-test for comparison of two groups or one-way analysis of variance (ANOVA) with Tukey's post hoc test for multiple group comparisons. In all cases, a *p*-value of <0.05 was considered statistically significant, and all data were expressed as mean ± standard deviation (S.D).

3. Results

3.1. Osteogenic differentiation of ASCs in 3-D culture systems

The ability of ASCs to grow and differentiate under 3-D culture conditions was initially evaluated using SF scaffolds. Micro-CT analysis revealed significant increases in mineralized tissue formation in SF scaffolds seeded with ASCs after 21 days ($p < 0.05$), and this continued to increase up until completion of the study at day 42 ($p < 0.01$) (Fig. 2A and B). Alizarin red staining of paraffin sections at day 42 confirmed localization of seeded ASCs in areas of mineralized matrix (Fig. 2C). Further analysis of ASC osteogenesis was also performed using ASC-MT. ASCs readily formed spheroid microtissues when cultured in hanging drops (Fig. 3A and B). Under osteogenic conditions, ASC-MT produced mineralized matrix within 6 days (Fig. 3C and D) and stained positive for known markers of osteogenic differentiation including HTRA1 (Fig. 3E and F) and osteocalcin (Fig. 3G and H). Furthermore, several genetic markers of osteogenesis including alkaline phosphatase (*Alpl*) ($p < 0.01$), osteopontin (*Opn*) ($p < 0.01$), and high temperature requirement serine protease A1 (*HtrA1*) ($p < 0.01$) were significantly upregulated in comparison to undifferentiated ASC-MT after 3 days in culture (Fig. 3I). Additional studies revealed that ASCs initially grown as ASC-MT retained both their proliferative capacity as well as their potential to undergo osteogenesis when transferred to tissue culture plates (Fig. 4). Cells were observed to migrate out from the microtissues and could induce mineral formation within the 2-D culture system already after 7 days.

3.2. Tracking of injected ASCs

CM-Dil positive ASCs were easily identified within the bone marrow of mice 24 h following a single intratibial injection of either undifferentiated ASCs (Fig. 5A) or pre-differentiated ASC-MT

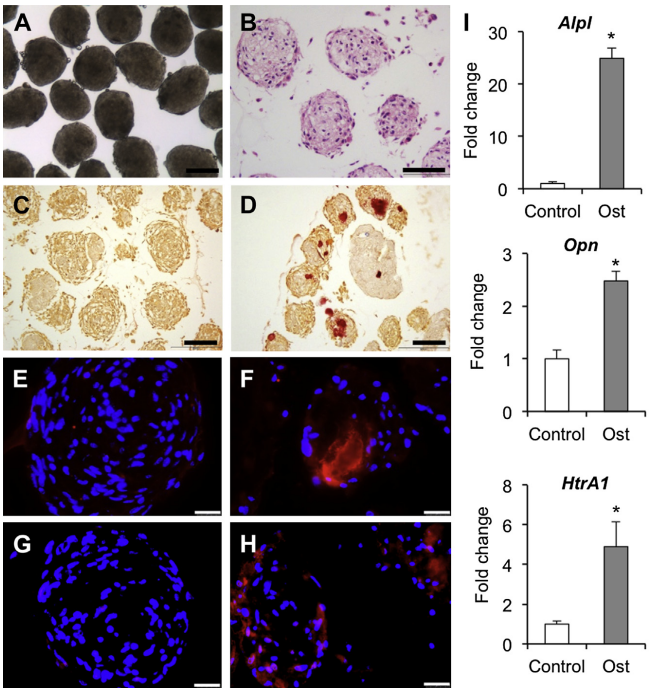

Fig. 3. (A) Undifferentiated ASC-MT after 6 days in hanging drops visualized *in situ*. Scale bar = 100 μm. (B) Hematoxylin & eosin stained paraffin wax section of undifferentiated ASC-MT after 6 days in hanging drops. Scale bar = 100 μm. (C–D) Representative images of Alizarin red stained paraffin wax sections of ASC-MT cultured for 6 days in growth medium (C) or osteogenic induction medium (D). Scale bar = 100 μm. (E–H) Representative immunofluorescence images of paraffin wax sections of ASC-MT cultured for 6 days in growth medium (E, G) or osteogenic induction medium (F, H) and stained with anti-HTRA1 (E, F) or anti-osteocalcin (G, H). Positive staining was detected using an anti-rabbit Cy3 antibody (*red*). Nuclei were stained with DAPI (*blue*). Scale bar = 25 μm. (I) qRT-PCR analysis of alkaline phosphatase (*Alpl*), osteopontin (*Opn*) and high temperature requirement protease A1 (*HtrA1*) in ASC-MT cultured for 3 days in growth medium (Control) or osteogenic induction medium (Ost). Values were normalized to *Mrps12* and the fold change as compared to undifferentiated controls determined using the $2^{-\Delta\Delta CT}$ method (mean ± S.D.). *$p < 0.01$ as determined by the Student's *t*-test.

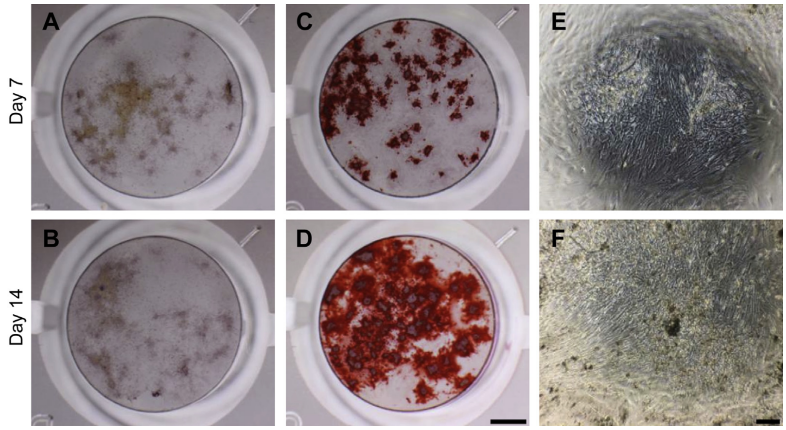

Fig. 4. Analysis of ASC outgrowth from ASC-MT. Undifferentiated ASCs were cultured in ASC-MT for 4 days, and then transferred to culture plates and incubated for 7 days (A, C, E) or 14 days (B, D, F) in normal growth medium (A, B) or osteogenic induction medium (C–F). Cells were stained with Alizarin red (A–D) or left unstained and visualized by phase contrast light microscopy (E–F). *A–D*, scale bar = 2 mm; *E–F*, scale bar = 500 μm.

(Fig. 5B). At 42 days post injection, CM-Dil positive cells were still evident within all of the treated bones, although to a much lesser extent than bone sections at 24 h post injection (Fig. 5C and D). Untreated contralateral bones remained absent of CM-Dil-labeled cells at all time points.

3.3. Influence of ASCs on bone quality in SAMP6 mice

In order to determine the effects of ASCs on bone quality, micro-CT was performed on bone samples taken at day 42 following treatment. Animals injected with undifferentiated ASCs, pre-differentiated ASC-MT or PBS/EDTA showed no adverse reactions and treatments were generally well tolerated. However, intratibial injections of ASCs that had been pre-differentiated as monolayers for 3 days prior to implantation resulted in >50% mortality, with death occurring immediately after the administration of these cells. As such, we were unable to accurately assess the influence of these cells on bone quality in SAMP6 mice. Histological analysis revealed that the most likely cause of death was due to pulmonary embolism as evidenced by both cartilaginous and fibrous deposits within lung vacuoles taken from mice that died shortly after receiving an intratibial injection of pre-differentiated mouse ASCs (Suppl. Fig. 1).

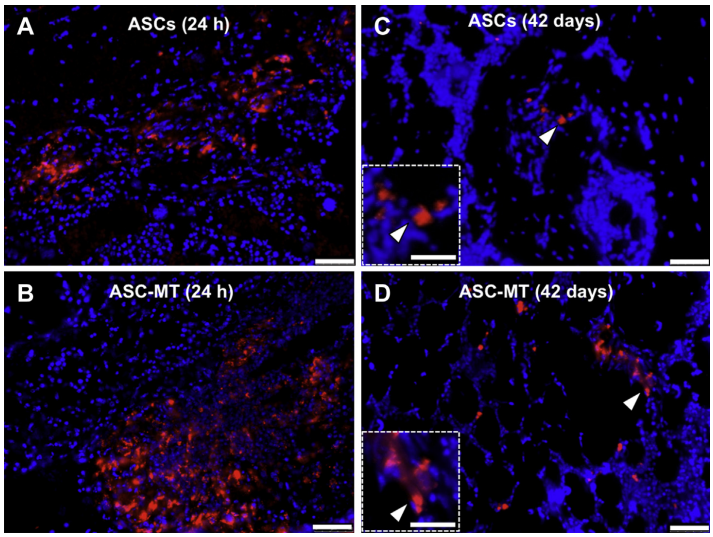

Fig. 5. Representative fluorescence images of paraffin wax sections of tibia injected with undifferentiated ASCs (A, C) or ASC-MT (B, D) at 24 h (A, B) and 42 days (C, D) post treatment. Scale bar = 50 μm. *Inset and arrowhead*, high magnification images of CM-Dil labeled cells. Scale bar = 25 μm. *Red*, CM-Dil; *blue*, DAPI.

When compared to untreated contralateral tibia, undifferentiated ASC-treated and pre-differentiated ASC-MT-treated tibia demonstrated significant increases in trabecular bone volume density (BV/TV) (ASC, $p = 0.01$; ASC-MT, $p = 0.002$) and trabecular number (Tb.N) (ASC, $p = 0.01$; ASC-MT, $p = 0.01$), although trabecular thickness (Tb.Th) (ASC, $p = 0.3$; ASC-MT, $p = 0.1$), was not significantly affected (Fig. 6A and B). Furthermore, the distance between trabeculae (Tb.Sp) was significantly reduced in both treatment groups (ASC, $p = 0.01$; ASC-MT, $p = 0.02$). By contrast, no significant changes in BV/TV ($p = 0.07$), Tb.N ($p = 0.89$), Tb.Sp ($p = 0.77$) or Tb.Th ($p = 0.30$), were observed in tibia treated with PBS/EDTA when compared to the respective untreated contralateral tibia. Additionally, no significant changes in cortical bone parameters were observed in any of the treatment groups tested (data not shown).

3.4. Effect of ASCs on gene expression in vivo

RNA was harvested from the tibia of mice after 14 days following treatment with either PBS/EDTA or ASCs, and analyzed for various genetic markers using qRT-PCR. The expression levels of all genetic markers analyzed were found to be significantly upregulated in ASC-treated bones as compare to untreated contralateral controls (Fig. 7). Similarly, with the exception of *Tnfa*, PBS/EDTA treatment also induced significant increases in the expression levels of all gene markers. However, in comparison to PBS/EDTA-treated bones, ASC-treated bones showed significant increases in genetic markers associated with osteogenesis, including, *Opn* ($p < 0.01$), *Ibsp* ($p < 0.05$), *Col1a2* ($p < 0.01$), *HtrA1* ($p < 0.01$), as well as resorption-associated markers, *Tnfa* ($p < 0.01$) and *Ctsk* ($p < 0.01$). No significant differences in the expression profiles of any of the genes tested were observed between the untreated contralateral control bones of PBS/EDTA- and ASC-treated mice.

3.5. Osteogenic differentiation of human osteoporotic BMSCs

The osteogenic potential of human BMSCs isolated from aged osteoporotic patients was confirmed as being impaired as demonstrated by marked reductions in both ALP activity (Fig. 8A) and Alizarin red staining (Fig. 8B) in comparison to BMSCs from non-osteoporotic patients. Supplementation of osteogenic medium (OM) with conditioned medium harvested from osteoporotic patient-derived ASCs (ASC-CM) cultured under normal growth conditions, significantly enhanced mineral formation of osteoporotic patient-derived BMSCs after 14 days as compared to cells cultured in OM alone, or OM supplemented with conditioned medium from osteoporotic patient-derived BMSCs (BMSC-CM) (Fig. 8C).

4. Discussion

ASCs represent an easily accessible population of multipotent stromal cells, and unlike their BMSC counterparts, have the potential to readily undergo osteogenic differentiation independently of donor age and status of bone quality [18–20]. As such, the use of ASCs in bone tissue engineering is becoming more commonplace [32–37] and investigators have now started to recognize their potential as a therapeutic strategy for the treatment of osteoporosis [21–23]. Indeed, previous findings from our own studies have demonstrated that ASCs isolated from osteoporotic SAMP6 mice

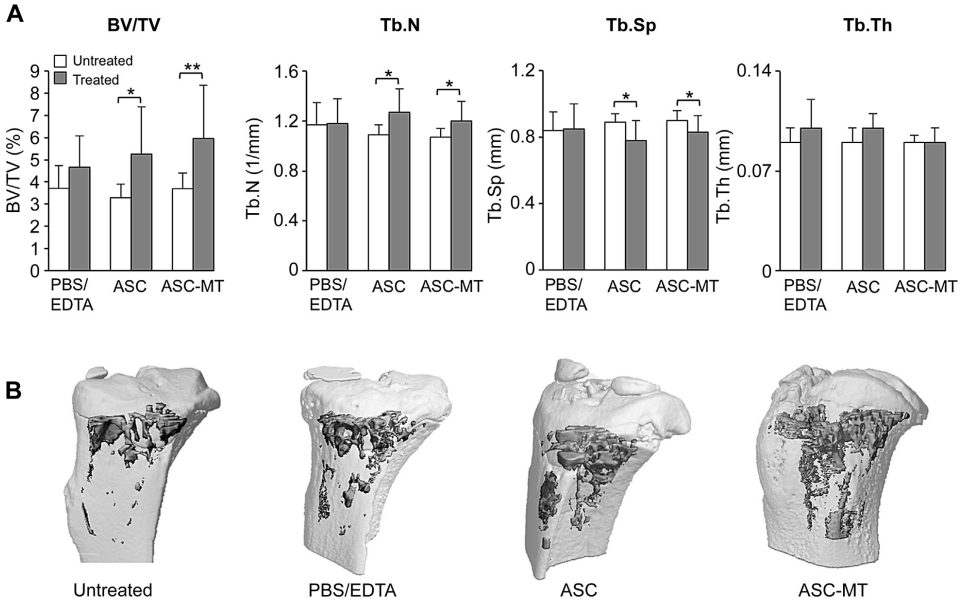

Fig. 6. (A) Micro-CT analysis of treated and untreated tibia from SAMP6 mice 42 days after surgical intervention. Tibia were treated (Treated) with either PBS/EDTA (PBS/EDTA) ($n = 9$), undifferentiated ASCs (ASC) ($n = 9$), or pre-differentiated osteogenic ASC-MT ($n = 13$). In all cases, treatments were compared to the contralateral control tibia (untreated). BV/TV, trabecular bone volume density; Tb.N, trabecular number; Tb.Sp, trabecular spacing; Tb.Th, trabecular thickness. All results are expressed as mean ± S.D. $^{*}p < 0.05$, $^{**}p < 0.01$ as determined by the paired Student's *t*-test. (B) Representative 3-D micro-CT images of control tibia (untreated), PBS/EDTA-treated tibia (PBS/EDTA), ASC-treated tibia (ASC) and ASC-MT-treated tibia (ASC-MT).

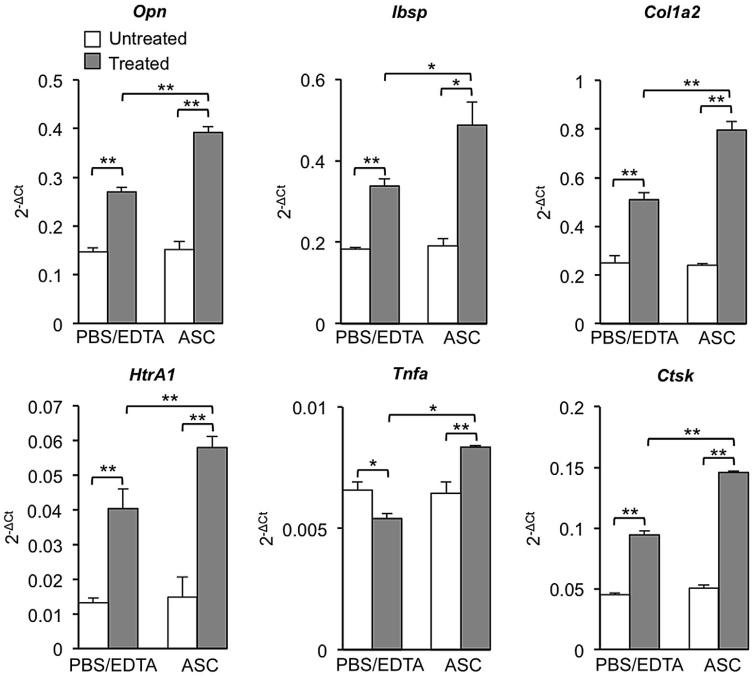

Fig. 7. qRT-PCR analysis was performed on mRNA isolated from tibia treated (Treated) with either PBS/EDTA or ASC and the corresponding contralateral control tibia (Untreated) of SAMP6 mice 14 days after surgical intervention. Values were normalized to *Gapdh* and presented as $2^{-\Delta CT}$ (RNA of 5–6 mice pooled, technical triplicates, mean ± S.D.). $^{*}p < 0.05$, $^{**}p < 0.01$, as determined by one-way ANOVA. *Opn*, osteopontin; *Ibsp*, Integrin binding sialoprotein; *Col1a2*, Collagen type 1A2; *HtrA1*, high temperature requirement protease A1; *Tnfa*, tumor necrosis factor alpha; *Ctsk*, Cathepsin k.

were able to retain their osteogenic potential under 2-D culture conditions when compared to ASCs from non-osteoporotic SAMR1 control mice [20]. However, no studies have yet sought to evaluate the therapeutic potential of isogeneic ASCs on bone quality in this mouse model for senile osteoporosis.

In the present report, *in vitro* 3-D culture systems were initially used to evaluate the osteogenic potential of SAMP6-derived ASCs in order to simulate a more accurate natural physiological environment. Preliminary investigations were carried out using a scaffold-based approach, whereby micro-CT was used to monitor the mineral formation in long-term cultures of SAMP6-derived ASCs seeded on SF scaffolds. A gradual increase in mineralized tissue formation was observed in ASC-seeded scaffolds over the 42 day culture period. Additional histological analysis using Alizarin red and DAPI staining confirmed that cells could still be identified within the scaffolds after 42 days, being localized to areas of mineral deposition. Short-term osteogenic differentiation of ASCs grown in scaffold-free microtissue spheroids was observed after only 3 days in osteogenic induction medium as evidenced by significant increases in osteogenic markers *Alpl*, *Opn* and *HtrA1*. By day 6, mineral deposition was apparent in the majority of tissues, along with the expression of osteogenic proteins HTRA1 and osteocalcin. Furthermore, cells cultured within spheroid microtissues were confirmed as being able to retain their proliferative capacity as well as their osteogenic potential following outgrowth onto a plastic surface. These preliminary findings therefore confirmed that SAMP6-derived ASCs were capable of maintaining their functional capacity for osteogenesis when cultured in 3-D environments and thus encouraged us to further investigate their capacity to influence bone formation *in vivo*.

The underlying premise for using ASCs to treat osteoporotic bone, stems from the concept that resident BMSCs are defective in terms of their ability to maintain a normal osteogenic potential and thus have a reduced tendency to generate bone-forming osteoblasts [2,3,7–9]. Supplementation of osteoporotic bone with competent osteoprogenitor cells may therefore represent a viable means by which to re-establish normal bone homeostasis and enhance bone quality. Indeed, this concept has already been tested by several independent research groups and has been shown to have significant benefits in terms of preventing bone loss in various experimental OVX mouse models. Human ASCs demonstrated a protective effect on OVX-induced bone loss in nude mice when intravenously injected at the time of surgical intervention [21]. These effects were hypothesized as being mediated mainly through paracrine effects of the transplanted ASCs based on the fact that no cells could be visualized within bone after 48 h post injection. Similarly, the systemic administration of genetically modified mouse ASCs restored normal bone parameters in immunocompetent mice after 28 days, although no data was presented to indicate whether ASCs could be detected within the bones of treated animals [22]. More recently, it was demonstrated that a single intratibial injection of ASCs into the femur of OVX SAMP8 mice, an aging animal model primarily used in studies of learning and memory, resulted in significant increases in bone mineral density as

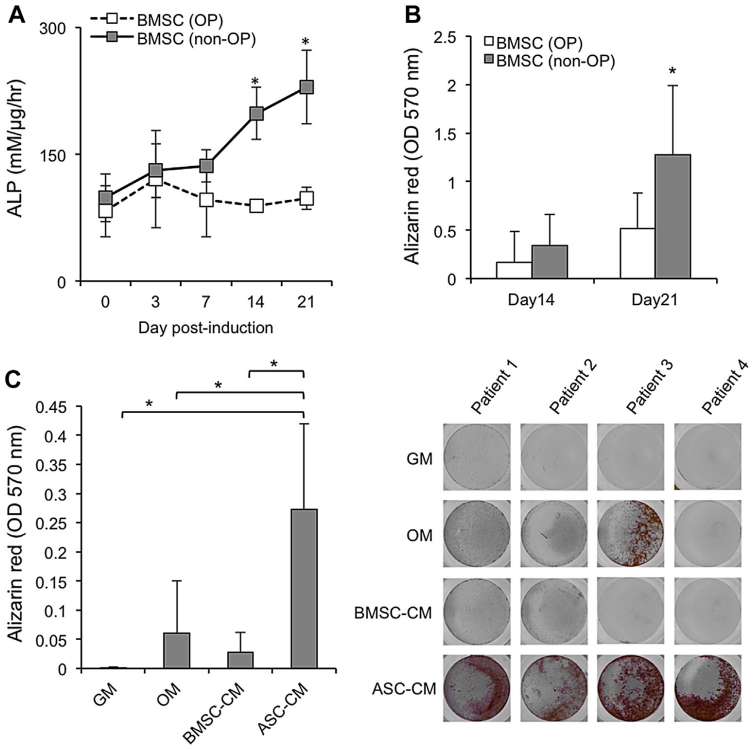

Fig. 8. (A–B) Osteogenic differentiation of human BMSCs isolated from osteoporotic (OP) ($n = 5–9$) or non-osteoporotic (non-OP) ($n = 5–6$) patients was compared using the ALP activity assay (A) and Alizarin red staining (B). *$p < 0.05$ as determined by Student's *t*-test. (C) The osteogenic potential of osteoporotic patient-derived BMSCs ($n = 4$) cultured in osteogenic medium (OM) or OM supplemented with either conditioned medium from osteoporotic patient-derived ASCs (ASC-CM) or BMSCs (BMSC-CM) was determined by Alizarin red staining at day 14 after osteogenic induction. Undifferentiated cells cultured in growth medium (GM) served as negative controls. *$p < 0.01$ as determined by one-way ANOVA. All experiments were performed in triplicate and results expressed as mean ± S.D.

compared to control groups, which was evident at 4 months following the initial treatment [23]. However, these effects appeared to require the *in vitro* osteogenic differentiation of ASCs prior to implantation. In the present study, we observed a significant improvement in the trabecular bone quality of SAMP6 mice 42 days following a single intratibial injection of either undifferentiated SAMP6-derived ASCs or pre-differentiated osteogenic ASC-MT as compared to untreated contralateral bones. Furthermore, CM-Dil labeled cells could still be detected within the bone marrow of treated tibia even at this late time point. Attempts were also made to assess the effects of a single intratibial injection of a cell suspension of pre-differentiated osteogenic ASCs, but unexpectedly, this resulted in high mortality rates associated with pulmonary embolism. It remains unclear as to why such adverse events should have occurred following the use of these cells, especially as other studies using pre-differentiated mouse ASCs reported no untoward effects [23]. However, one possible explanation may relate to the size of cells that were injected into the bone cavity. A recent study evaluating the therapeutic potential of human placenta-derived mesenchymal stem cells (hMSCs) in ischemic stroke, demonstrated high incidences of embolism and neurological abnormalities following the intra-carotid injection of hMSCs previously cultured as monolayers [38]. By contrast, the injection of hMSC suspensions derived from 3-D microtissue spheroids, led to a subsequent improvement in neurological function with no reports of vascular obstruction. These opposing effects were attributed to differences in the size of hMSCs produced, with microtissue-derived hMSCs showing a noticeable decrease in diameter as compared to hMSCs grown as monolayers. Such alterations in cell dimension may therefore go someway to explaining why osteogenic ASCs cultured as monolayers, but not as ASC-MT, resulted in embolism. Certainly, this could represent an important point of concern when considering such an approach in humans and may therefore warrant further investigation. It would appear therefore that incorporation of ASCs into microtissue spheroids may represent one possible means by which to overcome this potentially detrimental effect of pre-differentiated osteogenic ASCs when injected directly into the bone marrow cavity.

In addition to improvements being made in trabecular bone, we also observed significant increases in the gene expression of bone turnover markers in the tibia of ASC-treated mice as compared to PBS/EDTA-treated mice. This is in line with previous investigations in which the beneficial effects of locally administered ASCs on mouse bone quality have been associated with alterations in genetic markers of osteogenesis [23]. However, it should be mentioned that in the current study, the majority of genes tested

were significantly upregulated in both ASC- and PBS/EDTA-treated mice when compared to untreated contralateral bones, thus indicating that the mere act of injecting into the tibia alone was sufficient to upregulate gene expression.

It is interesting to note, that the capacity of pre-differentiated osteogenic ASC-MT to enhance trabecular bone quality was comparable to undifferentiated ASCs, despite them having already been induced along the osteogenic lineage. This would therefore imply that the transplanted ASCs may have mediated their effects through the stimulation of resident cells, rather than instigating new bone formation directly. This concept was further tested *in vitro* utilizing ASCs and BMSCs isolated from human osteoporotic patients. Initial observations confirmed that the osteogenic potential of osteoporotic patient-derived BMSCs was significantly impaired as compared to normal, age-matched non-osteoporotic control samples. Furthermore, we could demonstrate that conditioned media harvested from osteoporotic patient-derived ASCs was able to better support osteoporotic patient-derived BMSC osteogenesis. Although similar findings were reported in studies utilizing human ASCs with either human BMSCs or mouse osteoblastic cell lines [21,39], as far as we are aware, this is the first direct evidence that human osteoporotic ASCs have the capacity to impart a pro-osteogenic paracrine effect on human osteoporotic patient-derived BMSCs *in vitro*. It is possible therefore, that the increases in SAMP6 trabecular bone quality following ASC treatment were due, in part, to the paracrine actions of injected ASCs on resident BMSC populations.

5. Conclusion

We have demonstrated that ASCs isolated from osteoporotic SAMP6 mice have the capacity to undergo osteogenic differentiation and induce mineralized tissue formation in short- and long-term 3-D cultures, and that a single intratibial injection of undifferentiated ASCs or pre-differentiated ASC-MT, significantly enhanced parameters of bone quality in SAMP6 mice. Furthermore, *in vitro* data utilizing human osteoporotic patient-derived BMSCs and ASCs is provided, which supports the concept of transplanted ASCs influencing bone formation in a paracrine manner. Our data therefore highlights the potential benefits of using ASCs as an autologous cell-based therapeutic strategy to treat osteoporosis.

Acknowledgements

The authors would like to acknowledge Dr. Matthias Arlt (Balgrist University Hospital, University of Zurich), Dr. med. vet. Katja Nuss (Clinics for Horses, University of Zurich), and Dr. med. vet. Paula Grest (Institute for Veterinary Pathology, University of Zurich) for their assistance with the *in vivo* studies. This work has been partially financed with the help of the Forschungskredit University of Zurich and the Stiftung Osteoporose Schweiz.

Appendix A. Supplementary data

Supplementary data related to this article can be found online at http://dx.doi.org/10.1016/j.biomaterials.2014.05.016.

References

[1] Lane NE. Epidemiology, etiology and diagnosis of osteoporosis. Am J Obstet Gynecol 2006;194(Suppl. 2):S3–11.
[2] Rodríguez JP, Garat S, Gajardo H, Pino AM, Seitz G. Abnormal osteogenesis in osteoporotic patients is reflected by altered mesenchymal stem cells dynamics. J Cell Biochem 1999;75:414–23.
[3] Rodríguez JP, Montecinos L, Ríos S, Reyes P, Martínez J. Mesenchymal stem cells from osteoporotic patients produce a type I collagen-deficient extracellular matrix favoring adipogenic differentiation. J Cell Biochem 2000;79:557–65.
[4] Chen HT, Lee MJ, Chen CH, Chuang SC, Chang LF, Ho ML, et al. Proliferation and differentiation potential of human adipose-derived mesenchymal stem cells isolated from elderly patients with osteoporotic fractures. J Cell Mol Med 2012 Mar;16(3):582–93.
[5] Bonyadi M, Waldman SD, Liu D, Aubin JE, Grynpas MD, Stanford WL. Mesenchymal progenitor self-renewal deficiency leads to age-dependent osteoporosis in Sca-1/Ly-6A null mice. Proc Natl Acad Sci U S A 2003;100:5840–5.
[6] Kuro-o M, Matsumura Y, Aizawa H, Kawaguchi H, Suga T, Utsugi T, et al. Mutation of the mouse klotho gene leads to a syndrome resembling aging. Nature 1997;390:45–51.
[7] Jilka RL, Weinstein RS, Takahashi K, Parfitt AM, Manolagas SC. Linkage of decreased bone mass with impaired osteoblastogenesis in a murine model of accelerated senescence. J Clin Invest 1996;97:1732–40.
[8] Silva MJ, Brodt MD, Ko M, Abu-Amer Y. Impaired marrow osteogenesis is associated with reduced endocortical bone formation but does not impair periosteal bone formation in long bones of SAMP6 mice. J Bone Miner Res 2005;20:419–27.
[9] Egermann M, Heil P, Tami A, Ito K, Janicki P, Von Rechenberg B, et al. Influence of defective bone marrow osteogenesis on fracture repair in an experimental model of senile osteoporosis. J Orthop Res 2010;28:798–804.
[10] Astudillo P, Ríos S, Pastenes L, Pino AM, Rodríguez JP. Increased adipogenesis of osteoporotic human-mesenchymal stem cells (MSCs) characterizes by impaired leptin action. J Cell Biochem 2008 Mar 1;103:1054–65.
[11] Pino AM, Rosen CJ, Rodríguez JP. In osteoporosis, differentiation of mesenchymal stem cells (MSCs) improves bone marrow adipogenesis. Biol Res 2012;45:279–87.
[12] Rachner TD, Khosla S, Hofbauer LC. Osteoporosis: now and the future. Lancet 2011;377:1276–87.
[13] Seeman E, Delmas PD. Bone quality – the material and structural basis of bone strength and fragility. N Engl J Med 2006;354:2250–61.
[14] Tapp H, Hanley Jr EN, Patt JC, Gruber HE. Adipose-derived stem cells: characterization and current application in orthopaedic tissue repair. Exp Biol Med 2009;234:1–9.
[15] Antebi B, Pelled G, Gazit D. Stem cell therapy for osteoporosis. Curr Osteoporos Rep 2014;12:41–7.
[16] Schipper BM, Marra KG, Zhang W, Donnenberg AD, Rubin JP. Regional anatomic and age effects on cell function of human adipose-derived stem cells. Ann Plast Surg 2008;60:538–44.
[17] Zhu M, Kohan E, Bradley J, Hedrick M, Benhaim P, Zuk P. The effect of age on osteogenic, adipogenic and proliferative potential of female adipose-derived stem cells. J Tissue Eng Regen Med 2009;3:290–301.
[18] Khan WS, Adesida AB, Tew SR, Andrew JG, Hardingham TE. The epitope characterization and the osteogenic differentiation potential of human fat pad-derived stem cells is maintained with ageing in later life. Injury 2009;40:150–7.
[19] Shi YY, Nacamuli RP, Salim A, Longaker MT. The osteogenic potential of adipose-derived mesenchymal cells is maintained with aging. Plast Reconstr Surg 2005;116:1686–96.
[20] Mirsaidi A, Kleinhans KN, Rimann M, Tiaden AN, Stauber M, Rudolph KL, et al. Telomere length, telomerase activity and osteogenic differentiation are maintained in adipose-derived stromal cells from senile osteoporotic SAMP6 mice. J Tissue Eng Regen Med 2012;6:378–90.
[21] Cho SW, Sun HJ, Yang JY, Jung JY, Choi HJ, An JH, et al. Human adipose tissue-derived stromal cell therapy prevents bone loss in ovariectomized nude mouse. Tissue Eng Part A 2012;18:1067–78.
[22] You L, Pan L, Chen L, Chen JY, Zhang X, Lv Z, et al. Suppression of zinc finger protein 467 alleviates osteoporosis through promoting differentiation of adipose derived stem cells to osteoblasts. J Transl Med 2012;10:11.
[23] Liu HY, Chiou JF, Wu AT, Tsai CY, Leu JD, Ting LL, et al. The effect of diminished osteogenic signals on reduced osteoporosis recovery in aged mice and the potential therapeutic use of adipose-derived stem cells. Biomaterials 2012;33:6105–12.
[24] Mirsaidi A, Tiaden AN, Richards PJ. Preparation and osteogenic differentiation of scaffold-free mouse adipose-derived stromal cell microtissue spheroids (ASC-MT). Curr Protoc Stem Cell Biol 27:2B.5.1–2B.5.12.
[25] Lindtner RA, Tiaden AN, Genelin K, Ebner HL, Manzl C, Klawitter M, et al. Osteoanabolic effect of alendronate and zoledronate on bone marrow stromal cells (BMSCs) isolated from aged female osteoporotic patients and its implications for their mode of action in the treatment of age-related bone loss. Osteoporos Int 2014;25:1151–61.
[26] Hofmann S, Hagenmüller H, Koch AM, Müller R, Vunjak-Novakovic G, Kaplan DL, et al. Control of in vitro tissue-engineered bone-like structures using human mesenchymal stem cells and porous silk scaffolds. Biomaterials 2007;28:1152–62.
[27] Thimm BW, Wüst S, Hofmann S, Hagenmüller H, Müller R. Initial cell precultivation can maximize ECM mineralization by human mesenchymal stem cells on silk fibroin scaffolds. Acta Biomater 2011;7:2218–28.
[28] Tiaden AN, Breiden M, Mirsaidi A, Weber FA, Bahrenberg G, Glanz S, et al. Human serine protease HTRA1 positively regulates osteogenesis of human bone marrow-derived mesenchymal stem cells and mineralization of differentiating bone-forming cells through the modification of extracellular matrix protein. Stem Cells 2012;30:2271–82.

[29] Kohler T, Stauber M, Donahue LR, Muller R. Automated compartmental analysis for high-throughput skeletal phenotyping in femora of genetic mouse models. Bone 2007;41:659–67.
[30] Hildebrand T, Ruegsegger P. A new method for the model-independent assessment of thickness in three-dimensional images. J Microsc 1997;185:67–75.
[31] Hildebrand T, Laib A, Muller R, Dequeker J, Ruegsegger P. Direct three-dimensional morphometric analysis of human cancellous bone: microstructural data from spine, femur, iliac crest, and calcaneus. J Bone Miner Res 1999;14:1167–74.
[32] Helder MN, Knippenberg M, Klein-Nulend J, Wuisman PI. Stem cells from adipose tissue allow challenging new concepts for regenerative medicine. Tissue Eng 2007;13:1799–808.
[33] Dudas JR, Marra KG, Cooper GM, Penascino VM, Mooney MP, Jiang S, et al. The osteogenic potential of adipose-derived stem cells for the repair of rabbit calvarial defects. Ann Plast Surg 2006;56:543–8.
[34] Li H, Dai K, Tang T, Zhang X, Yan M, Lou J. Bone regeneration by implantation of adipose-derived stromal cells expressing BMP-2. Biochem Biophys Res Commun 2007;356:836–42.
[35] Yoon E, Dhar S, Chun DE, Gharibjanian NA, Evans GR. In vivo osteogenic potential of human adipose-derived stem cells/poly lactide-co-glycolic acid constructs for bone regeneration in a rat critical-sized calvarial defect model. Tissue Eng 2007;13:619–27.
[36] Liu Y, Zhou Y, Feng H, Ma GE, Ni Y. Injectable tissue-engineered bone composed of human adipose-derived stromal cells and platelet-rich plasma. Biomaterials 2008;29:3338–45.
[37] Zhou Y, Ni Y, Liu Y, Zeng B, Xu Y, Ge W. The role of simvastatin in the osteogenesis of injectable tissue-engineered bone based on human adipose-derived stromal cells and platelet-rich plasma. Biomaterials 2010;31:5325–35.
[38] Guo L, Ge J, Zhou Y, Wang S, Zhao RC, Wu Y. Three-dimensional spheroid-cultured mesenchymal stem cells devoid of embolism attenuate brain stroke injury after intra-arterial injection. Stem Cells Dev 2014;23:978–89.
[39] Kim KI, Park S, Im GI. Osteogenic differentiation and angiogenesis with cocultured adipose-derived stromal cells and bone marrow stromal cells. Biomaterials 2014;35:4792–804.

Supplementary Fig. 1. Hematoxylin and eosin stained paraffin wax sections of lung tissue taken from a mouse shortly after death due to a single intratibial injection of pre-differentiated osteogenic ASCs. (A) Large numbers of eosinophils were often observed in fibrillar masses within blood vacuoles throughout the lung tissue (*). (B) In some cases, vacuoles were observed containing large emboli consisting of cartilage and mineralized tissue (*). Scale bar = 50 µm

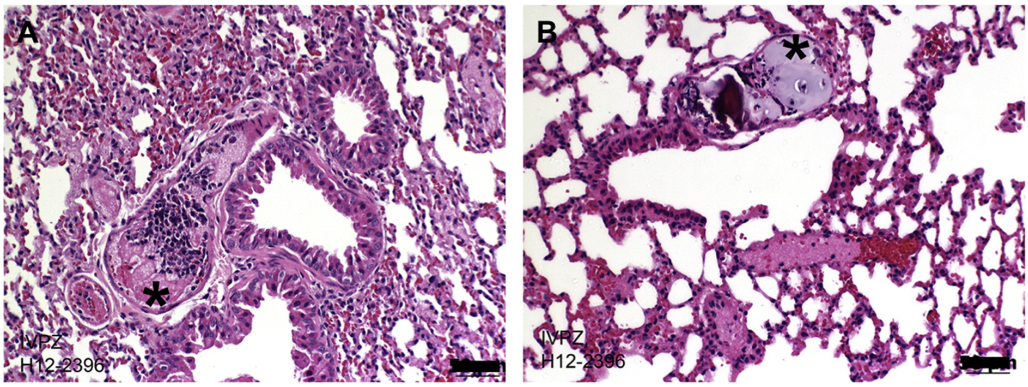

The FASEB Journal • Research Communication

ARTD1 deletion causes increased hepatic lipid accumulation in mice fed a high-fat diet and impairs adipocyte function and differentiation

Süheda Erener,[*,†] Ali Mirsaidi,[‡,§] Mareike Hesse,[*,†] André N. Tiaden,[‡] Helga Ellingsgaard,[‖] Radina Kostadinova,[*] Marc Y. Donath,[‖] Peter J. Richards,[‡,§] and Michael O. Hottiger[*,§,1]

*Institute of Veterinary Biochemistry and Molecular Biology, †Life Science Zurich Graduate School, Molecular Life Science Program, ‡Competence Centre for Applied Biotechnology and Molecular Medicine, Bone and Stem Cell Research Group, and §Zurich Centre for Integrative Human Physiology (ZIHP), Institute of Physiology, University of Zürich, Zurich, Switzerland; and ‖Clinic for Endocrinology, Diabetes and Metabolism, University Hospital Basel, Basel, Switzerland

ABSTRACT **ADP-ribosyltransferase *Diphtheria* toxin-like 1 [ARTD1; formerly called poly-ADP-ribose polymerase 1 (PARP1)] is a chromatin-associated enzyme involved in regulating metabolic homeostasis. The liver is at the core of glucose and lipid metabolism and is significantly affected by obesity and the metabolic syndrome. Here, we show that when fed a high-fat diet (HFD), mice lacking *ARTD1* developed exacerbated hepatic steatosis. *ARTD1*$^{-/-}$ mice had a 19% higher liver weight than wild-type (*WT*) animals and exhibited a significantly increased serum concentration of cholesterol (38%) and impaired glucose tolerance. In addition, adipocyte function and size were significantly reduced in *ARTD1*$^{-/-}$ mice fed an HFD (7794 μm^2 for *WT* and 5579 μm^2 for *ARTD1*$^{-/-}$ mice). The significantly reduced adipogenic differentiation of adipose-derived stromal cells (ASCs) isolated from *ARTD1*$^{-/-}$ mice (28 *vs.* 11% Oil red O-positive cells in *WT* and *ARTD1*$^{-/-}$ ASCs, respectively) suggested that impaired adipogenesis as the underlying cause for this adipose tissue malfunction. This function of ARTD1 was specific for adipogenesis, since osteogenic differentiation was not affected by the *ARTD1* deletion. In summary, we show that *ARTD1*$^{-/-}$ mice fed an HFD display impaired adipogenesis and show exacerbated hepatic steatosis, which can have important implications for nonalcoholic fatty liver disease.—Erener, S., Mirsaidi, A., Hesse, M., Tiaden, A. N., Ellingsgaard, H., Kostadinova, R., Donath, M. Y., Richards, P. J., Hottiger, M. O. *ARTD1* deletion causes increased hepatic lipid accumulation in mice fed a high-fat diet and impairs adipocyte function and differentiation. *FASEB J.* 26, 2631–2638 (2012). www.fasebj.org**

Key Words: adipogenesis · ADP-ribosylation · liver · PARP-1

Obesity is a complex metabolic disorder characterized by an excess of body fat that is closely associated with other serious health conditions, such as heart disease and diabetes (1). White adipose tissue (WAT) is the predominant storage site for excess energy in the form of fat in adult humans, but also functions as an important endocrine organ (2, 3). However, it appears that low-grade chronic inflammation (metaflammation) in metabolic tissues is the underlying mechanism leading to the disruption of nutrient and energy metabolism (4, 5).

ADP-ribosyltransferase *Diphtheria* toxin-like 1 [ARTD1; formerly called poly-ADP-ribose polymerase 1 (PARP1); ref. 6] is a chromatin-associated enzyme that modifies itself and target proteins by transferring the ADP-ribose moieties from nicotinamide adenine dinucleotide (NAD^+) to specific acceptor residues on target proteins (7). ARTD1 is thus able to regulate protein function, chromatin compaction, and gene expression (7, 8) and is subsequently involved in numerous biological phenomena, such as stress response, inflammation, and differentiation or cell cycle regulation, as well as in infectious diseases and cancer (9). Mice lacking *ARTD1* also exhibit metabolic phenotypes, such as

Abbreviations: aP2, adipocyte protein 2; ARTD, ADP-ribosltransferase *Diphtheria* toxin-like; ASC, adipocyte-derived stromal cell; ATGL, adipose triglyceride lipase; CD36, cluster of differentiation 36; DMEM, Dulbecco's modified eagle medium; FBS, fetal bovine serum; FFA, free fatty acid; Glut4, glucose transporter type 4; GTT, glucose tolerance test; H&E, hematoxylin and eosin; HFD, high-fat diet; HSL, hormone sensitive lipase; ITT, insulin tolerance test; NAD^+, nicotinamide adenine dinucleotide; NAFLD, nonalcoholic fatty liver disease; ND, normal diet; PAR, poly-ADP-ribose; PPARγ, peroxisome proliferator-activated receptor γ; PARP, poly-ADP-ribose polymerase; PBS, phosphate-buffered saline; WAT, white adipose tissue; WT, wild type

[1] Correspondence: Institute of Veterinary Biochemistry and Molecular Biology, University of Zürich, Winterthurerstrasse 190, Zürich 8057, Switzerland. E-mail: hottiger@vetbio.uzh.ch

doi: 10.1096/fj.11-200212

This article includes supplemental data. Please visit *http://www.fasebj.org* to obtain this information.

alterations in body weight, WAT formation, and the development of high-fat diet (HFD)-induced obesity, although these vary depending on the strain background (10–12). The deletion of *ARTD1*, a major NAD^+-consuming enzyme, can lead to increased cellular NAD^+ levels (10). Consequently, *ARTD1* deletion can activate NAD^+-dependent enzymes, such as sirtuins, and thereby indirectly induce phenotypes, such as increased mitochondrial biosynthesis and altered energy metabolism (10, 13). Furthermore, the enzymatic activity of ARTD1 also directly partakes in the sustained expression of the key regulator of adipocyte function, peroxisome proliferator-activated receptor γ (PPARγ; ref. 14). In cell culture, ARTD1 modulates PPARγ-dependent gene expression [such as cluster of differentiation 36 (*CD36*) or adipocyte protein 2 (*aP2*)] and adipocyte function (14) and may thus also be involved in adipogenesis *in vivo*.

To identify and characterize such direct *in vivo* functions of ARTD1 in metabolism, we analyzed *ARTD1*$^{-/-}$ and wild-type (*WT*) mice of the C57BL/6 background fed an HFD. Here, we report that deletion of *ARTD1* caused increased hepatic fat accumulation and dyslipidemia in mice exposed to HFD. These effects correlated with increased PPARγ2 target gene expression in liver samples from *ARTD1*$^{-/-}$ mice fed an HFD as well as with elevated serum levels of cholesterol, smaller adipocyte size, and impaired adipocyte differentiation. These results define a novel function for ARTD1 in the development of hepatic steatosis, as well as in the modulation of adipocyte differentiation and in adipose tissue function *in vivo*. These findings may thus provide novel insights into the molecular pathways that govern the onset, development, and progression of prevalent human diseases such as nonalcoholic fatty liver disease (NAFLD).

MATERIALS AND METHODS

Animals and animal care

In the *ARTD1*$^{-/-}$ male C57BL/6 mice used in this study and obtained from Zhao-Qi Wang (Leibniz Institute for Age Research–Fritz Lipmann Institute, Jena, Germany), part of the second exon and second intron of the *ARTD1* gene is replaced with the neomycin resistance gene (15). *ARTD1*$^{-/-}$ and *WT* mice were fed an HFD consisting of 60% of calories from fat (S3282; Bio-Serv, Frenchtown, NJ, USA) starting at 6–8 wk of age for 14 wk. Control mice were fed a normal diet (ND) consisting of 4.5% fat. Animals were housed in a specific pathogen-free facility with a 12-h light-dark cycle and given free access to food and water. Animal experiments were performed according to the regulations of the Cantonal Veterinary Office (Zurich, Switzerland).

Culture and analysis of mouse adipocyte-derived stromal cells (ASCs)

ASCs were isolated, cultured, and analyzed as described previously (16). In short, fat pads were removed from male mice and digested with 0.1% collagenase A (Roche Diagnostics, Rotkreuz, Switzerland). Stromal cells were collected by centrifugation and cultured in supplemented Dulbecco's modified eagle medium (DMEM; low glucose with Glutamax; Invitrogen AG, Basel, Switzerland), 10% fetal bovine serum (FBS; Invitrogen), and antibiotics. Supernatant was replaced after 1 d with fresh complete medium and cells were used between passage 3 and 4. Total RNA was isolated and purified using TRIzol reagent (Invitrogen) and reverse transcribed using superscript II (Invitrogen) and random hexanucleotide primers (Promega AG, Dübendorf, Switzerland). mRNA expression analysis was performed with primers specific for *ARTD1* (Mm01321084_m1), *PPARγ2* (Mm00440940_m1), *aP2* (Mm00445878_m1), and glucose transporter type 4 (*GLUT4*; Mm00436615_m1) and by using the StepOnePlus Real-Time PCR System (Applied Biosystems/Life Technologies, Zug, Switzerland). All values were normalized to the *RPS12* ribosomal RNA (Mm00488728_m1).

Adipogenesis

To assess adipogenesis, ASCs were plated at 10,000 cells/cm^2 and incubated in adipogenic medium (DMEM supplemented with 10% FBS and 1 μM dexamethasone; Sigma-Aldrich, Buchs, Switzerland), 10 μg/ml insulin (Sigma-Aldrich), 0.1 mM indomethacin (Sigma-Aldrich), and 0.5 mM isobutyl methylxanthine (IBMX; Sigma-Aldrich). After 2 d, cells were switched to adipogenic medium without IBMX for up to 14 d. Triglyceride content was determined using 0.3% Oil Red O (Sigma-Aldrich), and adipocytes were counted in 30 fields of view by fluorescence microscopy.

Osteogenesis

ASCs were plated at 5000 cells/cm^2 and incubated in α-minimum essential medium (α-MEM; Invitrogen), supplemented with 10% FBS, 50 μM L-ascorbic acid 2-phosphate sesquimagnesium salt hydrate (Sigma-Aldrich), 10 mM β-glycerophosphate (Sigma-Aldrich), and 5 μM retinoic acid (Sigma-Aldrich) for up to 14 d with regular changes of medium. Mineralization in cell colonies was identified using Alizarin Red S (Sigma-Aldrich).

RNA extraction and real-time PCR analysis from WAT

Mouse tissues were isolated, rinsed in phosphate-buffered saline (PBS), frozen in liquid nitrogen and stored at −80°C until extraction. Total RNA was extracted from WAT using the RNeasy Lipid Tissue Kit (Qiagen, Hombrechtikon, Switzerland) according to the manufacturer's instructions, with the inclusion of a DNase digestion step. Total RNA from liver and also from 3T3-L1 cells was extracted using the Total RNA isolation mini kit (Macherey Nagel, Oensingen, Switzerland) with a DNase step. Equal amounts of RNA from 5–8 mice were pooled and reverse-transcribed using the high-capacity cDNA reverse transcription kit (Applied Biosystems/Life Technologies, Zug, Switzerland). Real-time PCR was performed using the Rotor-Gene 3000 (Corbett Life Science, now Qiagen) and SYBR Green using the primers listed in Supplemental Table S1. *Cyclophilin* was chosen as the internal control for normalization and for the relative quantification of gene expression.

Whole-cell extraction

Tissues were lysed in RIPA buffer (50 mM Tris, pH 8; 400 mM NaCl; 0.5% Triton Nonidet P-40; 1% DOC; 0.1% SDS; 1 μg/ml pepstatin; 1 μg/ml bestatin; 2 μg/ml leupeptin; 2 mM

PMSF; 10 mM β-glycerophosphate; 1 mM NaF; and 1 mM DTT), homogenized with a needle and syringe, and rotated for 20 min at 4°C. Lysate was centrifuged for 20 min at 4°C at 14,000 rpm. Total proteins were loaded on 7.5% SDS gels and blotted with anti-PAR and anti-tubulin antibodies.

Serum measurements

Serum insulin concentrations were measured with the insulin ELISA kit (Mercodia Inc., Uppsala, Sweden). Blood glucose was determined by using the FreeStyle Lite glucometer (Abbott, Baar, Switzerland).

Glucose tolerance tests (GTTs) and insulin tolerance tests (ITTs)

For the GTT, mice were unfed overnight (14 h); for the ITT, mice were unfed for 3 h. Glucose (1.2 g/kg body weight) or human recombinant insulin (HFD: 1.4 U/kg; ND: 0.75 U/kg) was injected intraperitoneally. Blood glucose concentrations were determined from tail using the FreeStyle Lite glucometer (Abbott).

Histology and cell-size measurement

Freshly isolated epididymal WAT and liver tissue from mice fed HFD was fixed in 4% formalin and embedded in paraffin. Sections were stained with hematoxylin and eosin (H&E) or Oil Red O. Adipocytes were photographed with a Leica DMR microscope (Leica Microsystems, Glattbrugg, Switzerland) and cell morphology and size were analyzed using the Leica IM 1000 software. Liver photographs were recorded using an Olympus AH-2 microscope (Olympus, Tokyo, Japan) equipped with an Axiocam camera (Carl Zeiss, Oberkochen, Germany).

RESULTS

ARTD1$^{-/-}$ mice fed HFD have increased liver weight and hepatic lipid deposition

To determine the role of ARTD1 in metabolic disorders, we analyzed 6–8 wk old *WT* and *ARTD1*$^{-/-}$ mice in the C57BL/6J background that were fed ND or HFD. *WT* and *ARTD1*$^{-/-}$ mice fed ND had identical body weights (Supplemental Fig. S1*A*). Both *WT* and *ARTD1*$^{-/-}$ mice fed HFD gained significantly more body weight as compared to those fed ND (identified as week 0; **Fig. 1***A*). Furthermore, in comparison to *ARTD1*$^{-/-}$ mice fed HFD, *WT* mice were heavier, which was not attributable to differences in food intake (Supplemental Fig. S1*B*). A pathological analysis revealed that the most apparent phenotype of the *ARTD1*$^{-/-}$ mice fed HFD was the significantly increased liver weight (Fig. 1*B*). Histological examination (H&E and Oil Red O staining) of liver sections revealed markedly increased hepatic lipid deposition in *ARTD1*$^{-/-}$ mice fed HFD, as compared to the *WT* controls (Fig. 1*C*), while no apparent difference was observed in mice fed ND (data not shown). H&E staining of skeletal muscle tissue of *WT* and *ARTD1*$^{-/-}$ mice did not reveal any difference (Fig. 1*C*).

ARTD1$^{-/-}$ mice fed HFD exhibit altered PPARγ2 target gene expression and dyslipidemia

Hepatic lipid accumulation is often associated with an ectopic induction of *PPARγ2* and PPARγ2-dependent gene expression in the liver and muscle (17). We therefore tested whether the increased lipid deposition in livers of *ARTD1*$^{-/-}$ mice correlated with alterations in PPARγ2 target gene expression in the liver. The expression of *PPARγ2* in *ARTD1*$^{-/-}$ livers was increased but not significantly different as compared to *WT* samples (**Fig. 2***A*). However, the PPARγ2 target genes *aP2* (fatty acid binding protein) and *LPL* (lipoprotein lipase) were significantly up-regulated in *ARTD1*$^{-/-}$ livers of mice fed HFD. Significantly increased compensatory expression was also observed for *PPARα*, a key regulator involved in fatty acid catabolism. Lipin, another highly inducible enzyme that is involved in triglyceride metabolism, was unaffected between the two genotypes, indicating that not all factors involved in lipid metabolism were changed in the livers of *ARTD1*$^{-/-}$ mice. These results, and in particular the strongly elevated expression of *aP2*, revealed that livers of *ARTD1*$^{-/-}$ mice fed HFD show gene expression

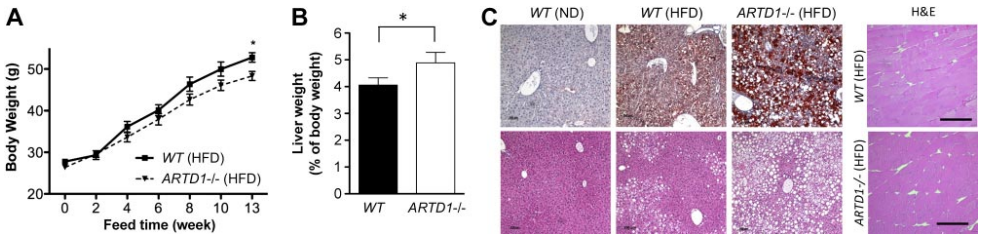

Figure 1. *ARTD1*$^{-/-}$ mice fed HFD display decreased weight gain and have reduced adipocyte size. *A*) Body weight of *WT* and *ARTD1*$^{-/-}$ mice that were fed HFD. HFD feeding started when mice were 6–8 wk old (time point 0; n=8–9 mice/group). *$P < 0.05$. *B*) Liver weight was measured and normalized with body weight (n=8–9 mice/group, means±SE). *$P < 0.05$, 14 wk after HFD. *C*) Representative images of Oil Red O-stained (top panels) or H&E-stained (bottom panels) sections of paraffin-embedded liver tissue from *WT* or *ARTD1*$^{-/-}$ mice fed HFD (n=4). H&E-stained skeletal muscle sections are shown as a control and for comparison (right panel).

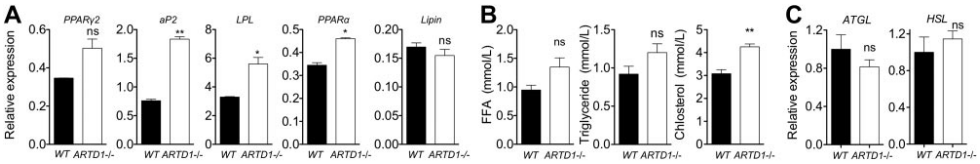

Figure 2. *ARTD1*$^{-/-}$ mice fed HFD exhibit altered PPARγ2 target gene expression and dyslipidemia. *A*) Real-time RT-PCR analysis of *PPARγ2* and PPARγ2 target genes in liver tissue obtained from *WT* and *ARTD1*$^{-/-}$ mice that were fed HFD (RNA of 7 mice pooled, means±SD of technical duplicates, 14 wk after HFD). *B*) Serum free fatty acid (FFA), triglyceride, and cholesterol levels were measured from independent samples of 5 *WT* and 4 *ARTD1*$^{-/-}$ mice. *C*) Real-time RT-PCR analysis of *ATGL* and *HSL* expression in WAT of *WT* and *ARTD1*$^{-/-}$ mice (RNA of 5–6 mice pooled, technical replicates, means±SD).

patterns typically associated with adipocytes and adipogenesis (17).

The hepatic lipid accumulation observed in *ARTD1*$^{-/-}$ mice suggested that the metabolic analytes might be altered in these animals. We therefore measured the plasma levels of free fatty acids (FFAs), triglycerides, and cholesterol. Indeed, *ARTD1*$^{-/-}$ mice displayed a marginal elevation in FFA and triglyceride levels as well as significantly increased cholesterol amounts, which also hinted at a disturbed lipid homeostasis in *ARTD1*$^{-/-}$ mice (Fig. 2*B*). However, lipolysis was likely not the cause for these alterations in lipid levels, since neither adipose triglyceride lipase (*ATGL*) nor hormone sensitive lipase (*HSL*) mRNA levels were significantly affected by the *ARTD1* deletion (Fig. 2*C*).

ARTD1$^{-/-}$ mice fed HFD exhibit defective glucose homeostasis

The increased FFA blood concentration and hepatic lipid accumulation can generate metabolic signals that impair the metabolization of glucose (18). To determine whether the hepatic lipid accumulation and dyslipidemia in *ARTD1*$^{-/-}$ mice is accompanied by abnormalities in glucose homeostasis, we performed GTTs in *WT* and *ARTD1*$^{-/-}$ mice fed HFD. Mice were injected with 1.2 g glucose/kg body weight, and glucose levels were quantified over a period of 2 h. Overall, *ARTD1*$^{-/-}$ mice had an 18% increased glucose content (area under curve) and required more time to clear the injected glucose, although the basal glucose levels were not significantly altered (**Fig. 3*A, B***). Since this analysis was performed with mice that experienced 14 h of food withdrawal, the differences between *WT* and *ARTD1*$^{-/-}$ mice may be underestimated (19). To explore the potential mechanism causing impaired glucose tolerance in *ARTD1*$^{-/-}$ mice, we examined aspects of insulin secretion in mice with and without *ARTD1*. A significant increase in plasma insulin was observed in *ARTD1*$^{-/-}$ mice as compared to *WT* mice following an i.p. glucose injection (Fig. 3*C*), thus indicating that β-cell function is unlikely to be impaired in *ARTD1*$^{-/-}$ mice. This insulin burst, which was not observed in *WT* mice, may hide elevated glucose levels in the *ARTD1*$^{-/-}$ mice at earlier time points. We next asked whether insulin sensitivity contributes to this phenotype. To assess whole-body insulin sensitivity, ITTs were performed in mice after 12 wk of exposure to HFD. Mice were injected with 1.4 U insulin/kg body weight, and glucose levels were determined during 90 min. Serum glucose levels of *ARTD1*$^{-/-}$ mice were 20% higher as compared to the *WT* control (area under curve), which is suggestive of a tendency toward insulin resistance, but this effect was not significant (Fig. 3*D*).

Comparable analysis with animals fed the ND revealed that glucose levels and response to GTTs and ITTs did not significantly change between the two genotypes (Supplemental Fig. S1*C–E*). Furthermore, insulin-stimulated AKT phosphorylation in muscle and WAT tissue from *WT* and *ARTD1*$^{-/-}$ mice fed ND was

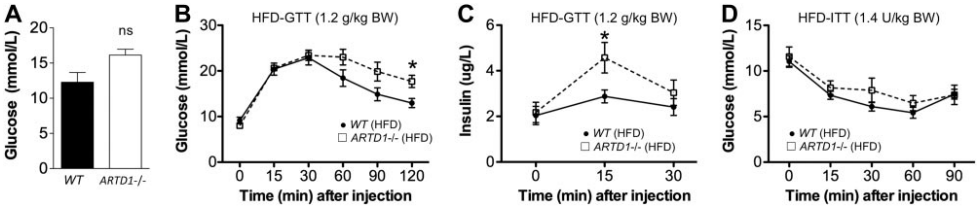

Figure 3. *ARTD1*$^{-/-}$ mice exhibit deteriorated glucose homeostasis. *A*) Serum glucose levels were measured from *WT* and *ARTD1*$^{-/-}$ mice. *B*) GTT: mice were injected with glucose (1.2 g/kg body weight), and glucose levels were quantified over a period of 2 h. *C*) Serum insulin levels during the GTT shown in *B*. *D*) ITT: mice were injected with insulin (1.4 U/kg body weight), and glucose levels were determined over a period of 90 min. Values are means ± SE, $n = 5–6$ mice/group. $*P < 0.05$, 12 wk after HFD.

also comparable (Supplemental Fig. S1*F*) suggesting that ARTD1 does not have a direct role in glucose homeostasis and insulin signaling under ND, but that the changes observed with HFD were rather the consequence of dyslipidemia and excessive lipid accumulation in the liver.

Adipocyte size and poly-ADP-ribose (PAR) formation in *ARTD1*$^{-/-}$ mice

We have recently reported that ARTD1 regulates adipogenesis *in vitro* (14), and PPARγ deletion in mouse adipose tissue was shown to cause increased lipid deposition in the livers (20). Our results on hepatic lipid accumulation and the dyslipidemic phenotype in *ARTD1*$^{-/-}$ mice fed HFD encouraged us to investigate the role of ARTD1 on adipocyte and WAT function *in vivo*. We therefore analyzed WAT from *WT* and *ARTD1*$^{-/-}$ mice. Surprisingly, neither the expression of *PPARγ2* or its target genes *aP2* and *CD36* nor the inflammatory genes *IL-1β*, *IL-13ra*, and *MCP1* differed between the *WT* and *ARTD1*$^{-/-}$ WAT samples from mice fed HFD (**Fig. 4*A*** and Supplemental Fig. S2). However, *ARTD1*$^{-/-}$ WAT tissue from mice fed HFD expressed less *IL-6*, which is a main regulator of inflammation. In addition, relative mRNA levels of the inflammatory genes *IL-10* and *IL-12* and of the macrophage specific genes *Pu.1* and *MPEG 1* were also reduced, while *SAA3* transcription was elevated. These results showed that a subset of the inflammatory genes was affected. Moreover, histological analysis of epididymal WAT from *ARTD1*$^{-/-}$ mice revealed a profound change in adipose tissue morphology, as evidenced by the significant reduction in adipocyte size (Fig. 4*B*, *C*). These results suggest that altered adipose tissue morphology likely impaired the storage of excess lipids in *ARTD1*$^{-/-}$ mice fed HFD and thus caused a pathological lipid accumulation in the liver. This significant effect of *ARTD1* deficiency on lipid metabolism and on the size of adipocytes from *ARTD1*$^{-/-}$ mice fed HFD suggests a fundamental role for ARTD1 in adipocyte function. Since we have recently shown that PAR formation is strongly induced in 3T3-L1 cells after 7 d of adipogenic induction (14), we investigated whether PAR was also formed in mature adipocytes *in vivo*. We could not detect PAR formation in WAT of *WT* mice that were fed ND (data not shown), but a distinct PAR signal was observed in the WAT extracts of *WT* mice (but not in the WAT of *ARTD1*$^{-/-}$ mice) that were maintained on HFD (Fig. 4*D*), suggesting that high energy diet (nutrient availability) induced ADP-ribosylation in WAT *in vivo* and in an ARTD1-dependent manner.

Adipogenic gene expression in differentiating aASCs is dependent on ARTD1

The *in vivo* results obtained from the studies with *ARTD1*$^{-/-}$ mice suggested that ARTD1 and PAR formation are centrally involved in adipose tissue activities. In addition, ARTD1 and PAR formation have been implicated in chromatin regulation (21) and were shown to affect PPARγ2-dependent gene expression and adipocyte function in differentiating 3T3-L1 cells (14, 21). We therefore hypothesized that ARTD1 may also affect the differentiation and development of functional adipocytes *in vivo*.

We tested this hypothesis by using ASCs, which can be easily isolated and expanded and have the ability to differentiate into several types of mesenchymal tissue. Differentiating ASCs are an established experimental system to study adipocyte differentiation (22). To study the role of ARTD1 and poly-ADP-ribosylation in adipogenesis, we compared ASCs from *ARTD1*$^{-/-}$ and from *WT* mice. In uninduced ASCs from *WT* mice, *ARTD1* expression levels were high and increased further at d 10 after the induction of adipogenesis (**Fig. 5*A***). Transcripts of the adipogenesis marker genes *PPARγ2*, *aP2*, and *GLUT4* were not detectable prior to the induction of adipogenesis but increased significantly on adipogenic induction in *WT* mice (Fig. 5*B–D*). In contrast, *PPARγ2*, *aP2*, and *GLUT4* expression remained at significantly lower levels in ASCs from *ARTD1*$^{-/-}$ mice throughout adipogenesis (Fig. 5*B–D*). The marked

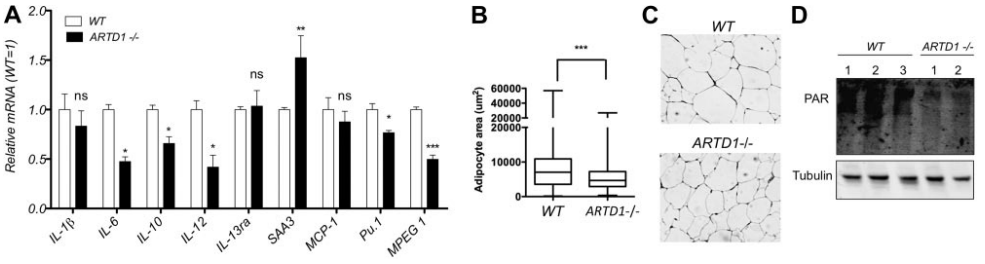

Figure 4. Adipocyte size and PAR formation in *ARTD1*$^{-/-}$ mice. *A*) Real-time RT-PCR analysis in total cell extracts from epididymal WAT of *WT* and *ARTD1*$^{-/-}$ mice that were fed HFD. mRNA levels were normalized with c*yclophilin A*. Results are means of 5–6 pooled mice, means ± SD of technical replicates. ns, not significant. $*P < 0.05$; $**P < 0.01$; $***P < 0.0001$. *B*) Whisker plot of adipocyte area from evaluation of 450 adipocytes from 4–5 independent mice. $***P < 0.0001$ comparing mean adipocyte area. *C*) Representative images of H&E-stained epididymal adipose tissue from *WT* and *ARTD1*$^{-/-}$ mice. *D*) PAR detection in total cell extracts from epididymal WAT of *WT* and *ARTD1*$^{-/-}$ mice that were fed HFD. All panels: 14 wk after HFD.

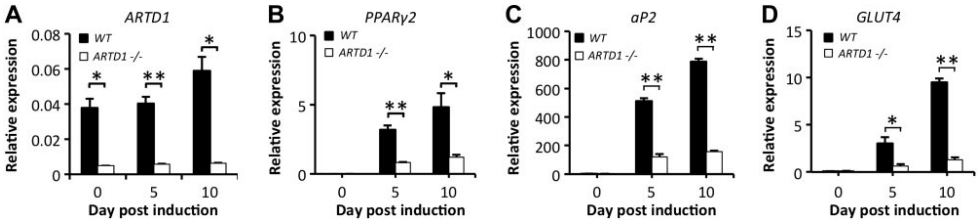

Figure 5. Adipogenesis is impaired in ASCs from *ARTD1*$^{-/-}$ mice. Expression levels of *ARTD1* (*A*) *PPARγ2* (*B*), *aP2* (*C*), and *GLUT4* (*D*) were evaluated by qRT-PCR over 0, 5, and 10 d of adipogenic differentiation. Expression value of each gene was normalized to the amount of ribosomal protein S12 (*RPS12*) RNA in order to calculate relative amounts of mRNA. $*P < 0.05$, $**P < 0.01$.

effect of *ARTD1* deletion on adipogenic gene expression suggests that ARTD1 is a major regulator of normal ASC differentiation.

Functional characterization of adipogenic ASCs isolated from *ARTD1*$^{-/-}$ mice

After 10 d of adipogenic differentiation, Oil Red O staining revealed a significantly higher percentage of mature adipocytes in ASC cultures isolated from *WT* mice as compared to *ARTD1*$^{-/-}$ mice (**Fig. 6A**). To further study the link between *ARTD1* and adipogenesis, we assessed ASC differentiation in the presence of the three PARP inhibitors (PJ34, olaparib, and nicotinamide) by Oil Red O staining (Fig. 6*B–D*). All three compounds significantly reduced the percentage of Oil Red O-positive cells in a concentration-dependent manner. Interestingly, the detrimental effect of *ARTD1* loss of function on ASC adipogenesis was much less apparent in ASCs undergoing osteogenesis, thus suggestive of a lineage-specific role for ARTD1 in mesenchymal stem cell differentiation (Supplemental Fig. S3). These results are in agreement with the strong and specific influence of the *ARTD1* deletion on PPARγ2-dependent gene expression in adipose tissue and thus further highlight the importance of ADP-ribosylation in adipogenesis.

Taken together, these results demonstrate that *ARTD1*$^{-/-}$ deficiency in mice affects adipocyte function *in vivo*, and lipid deposition in the liver. This correlates with the up-regulated expression of hepatic *PPARγ2* and its target genes involved in fatty acid metabolism in *ARTD1*$^{-/-}$ mice. The effect of ARTD1 and PAR formation on the adipogenic differentiation process may represent the underlying cause for the *in vivo* effects on WAT function and lipid deposition in *ARTD1*$^{-/-}$ mice.

DISCUSSION

In the present study, *ARTD1*$^{-/-}$ mice of the C57BL/6 background were fed HFD, and adipocyte and WAT function were analyzed. Several independent groups have previously reported significant differences in the body weight of adult *WT* and *ARTD1*$^{-/-}$ mice from various backgrounds (15, 23). While we and others (10) have observed a decreased body weight in C57BL/6 *ARTD1*$^{-/-}$ mice fed HFD, *ARTD1*$^{-/-}$ mice of the

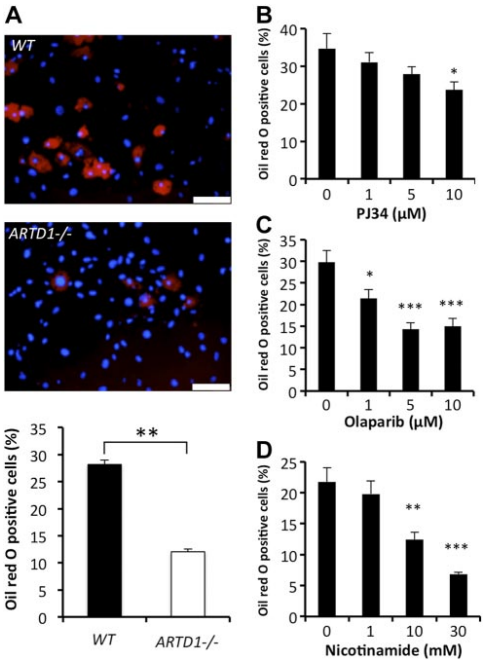

Figure 6. Triglyceride accumulation is decreased in adipogenic ASCs from *ARTD1*$^{-/-}$ mice. *A*) Representative fluorescent images of ASCs stained with Oil Red O (red) and Hoechst 33342 nuclear stain (blue). Scale bars = 150 μm. Percentage of cells demonstrating triglyceride accumulation was quantified in ASCs at d 10. *B–D*) ASCs from *WT* mice were induced to adipogenic differentiation in the presence of the ARTD1 inhibitors PJ34 (*B*), olaparib (*C*), and nicotinamide (*D*), and the percentage of cells demonstrating triglyceride accumulation was quantified at d 10. All differentiation studies were carried out using ASCs at passage 3 to 4 and were performed in triplicate. $*P < 0.05$, $**P < 0.01$, $***P < 0.01$.

SV129 background have been shown to be more susceptible to HFD-induced obesity (11). However, mice of the C57BL/6 background are readily susceptible to diet-induced obesity, irrespective of the presence or absence of ARTD1 (12). Our findings of lower body weight, increased liver weight, smaller adipocytes, elevated serum cholesterol levels, and impaired glucose tolerance in *ARTD1*$^{-/-}$ mice suggest that lipid allocation is impaired. These results differ from recently published observations with *ARTD1*$^{-/-}$ mice of the same strain background (10), although hepatic lipid accumulation was not assessed in this study. However, it should be noted that the two C57BL/6 *ARTD1*$^{-/-}$ mouse strains were created independently by targeting different *ARTD1* exons (15, 23), and as such, have given rise to certain age-related disparities, as evidenced by alterations in telomere lengths (24, 25). Whether such differences also account for the contradicting effects of the *ARTD1* deletion on lipid metabolism remains to be determined. In addition, the metabolic differences between the two studies using C57BL/6 *ARTD1*$^{-/-}$ mice might also be due to the fact that we started HFD feeding earlier (when the mice were 6–8 wk old), performed our analysis later (after 12 wk of HFD feeding) and used an HFD preparation from a different supplier with slightly different composition (10).

In the present study, PAR formation was only observed in *WT* mice and on HFD feeding. The absence of PAR formation in the WAT of *ARTD1*$^{-/-}$ animals indicated that PAR formation in WAT was dependent on nutrient availability and on ARTD1. Alterations in PAR formation due to *ARTD1* deletion could potentially change NAD^+ metabolism in these animals and thereby cause the activation of sirtuin 1 (SIRT1; ref. 10). Altered sirtuin activity may, in turn, affect adipocyte gene expression and function, metabolism, or number of mitochondria, for example, through the deacetylation of Forkhead box protein O1 (FOXO1; refs. 10, 26–28). Such indirect effects cannot be excluded, but our results describing the effects of *ARTD1* deletion on ASC adipogenesis also point to a direct effect of ARTD1 and ADP-ribosylation. These findings are in agreement with our earlier *in vitro* observation, where ARTD1 activity and ADP-ribosylation were induced at d 7 during adipogenesis and crucial for the sustained expression of PPARγ2 and CCAAT/enhancer-binding protein α (C/EBP-α), but not for the upstream regulator C/EBP-β (14). In the current study, ASCs from *ARTD1*$^{-/-}$ mice differentiated less efficiently into mature adipocytes but were capable of undergoing normal osteogenesis, thus confirming that ARTD1 plays a lineage-specific role in ASC differentiation. Further studies are needed to confirm the involvement of PAR formation in adipogenesis and also its role in the regulation of PPARγ2-dependent gene expression in WAT. The fact that three of the analyzed inflammatory genes (*IL-6*, *IL-10*, and *IL-12*) were affected by the *ARTD1* deletion suggests a limited and specific effect on only a subset of the genes expressed in WAT *in vivo*. Interestingly, two macrophage-specific genes (*Pu.1* and *MPEG 1*) exhibited reduced mRNA levels, alluding to a possible involvement of ARTD1 in macrophage differentiation.

The results presented here point to a direct and specific involvement of ARTD1 in adipogenesis *in vivo*. However, other genes or compensatory mechanisms seem to assure WAT formation in the absence of ARTD1. Apart from this, our results suggest that ARTD1 is required for efficient adipogenesis and that *ARTD1* ablation limits lipid storage in adipocytes, restricts adipocyte size, and causes hepatic lipid deposition. It therefore appears that ARTD1 may regulate adipocyte turnover and thereby indirectly affect adipocyte number and the response to different nutritional schemes. It will be interesting to investigate the metabolism and the long-term effect of HFD on *ARTD1*$^{-/-}$ mice. *ARTD1* deficient mice may thus become a useful model to study how adipocyte differentiation and function affect pathological responses to HFD and lead to diet-induced obesity.

Although the storage of excess energy in the form of triglycerides and the release of FFAs is the principal function of adipocytes (29), the liver is the organ of fatty acid uptake, synthesis, and circulation and can therefore be considered a hub of fatty acid metabolism (30). In humans, components of the metabolic syndrome, such as obesity, insulin resistance or dyslipidemia, are associated with fatty liver syndrome, which is one characteristic of NAFLD (31, 32). One consequence of NAFLD is an excessive release of FFAs into the bloodstream, which exacerbates peripheral insulin resistance. Our findings of significantly increased hepatic lipid accumulation, elevated serum cholesterol levels, and impaired glucose tolerance in *ARTD1*$^{-/-}$ mice, despite the unaffected insulin response, suggests that other lipid mediators or related mechanisms, such as inflammation, may be required for the development insulin resistance. Alternatively, it can be speculated that the hepatic insulin resistance is compensated for during the whole-body insulin resistance test. To explore insulin sensitivity more specifically at the level of the liver, hyperinsulinemic-euglycemic clamp studies could be employed, since the majority of endogenously produced glucose comes from hepatocytes. Currently, it is also not clear whether elevated cholesterol levels are only a consequence of the changes in WAT or whether they are also caused and exacerbated by the *ARTD1* deficiency in liver tissue, which might affect other metabolic processes. Further studies using conditional knockout mice with reduced expression of *ARTD1* either in WAT or liver would certainly provide additional insights into this interdependency. FJ

The authors thank I. Mittner and M. Wanner (University of Zurich) for FFA measurements. F. Freimoser (University of Zurich) provided editorial assistance and critical input during the writing. This work was supported in part by the University Research Priority Program, Integrative Human Physiology, at the University of Zurich; a Forschungskredit of the University of Zurich (to M.H.); Swiss National Science Foundation grants 31-122421 and 310030B-138667; and the Kanton of Zurich (to M.O.H.). The authors declare no conflicts of

interest. Author contributions: S.E., A.M., M.H., P.J.R., R.K., M.Y.D., and M.O.H. designed the experiments; S.E., A.M., M.H., A.N.T., and H.E. performed the experiments; P.J.R. and M.O.H. supervised the study; M.O.H., S.E., and P.J.R. wrote and edited the manuscript.

REFERENCES

1. Bluher, M. (2009) Adipose tissue dysfunction in obesity. *Exp. Clin. Endocrinol. Diabetes* **117,** 241–250
2. Trayhurn, P., and Beattie, J. H. (2001) Physiological role of adipose tissue: white adipose tissue as an endocrine and secretory organ. *Proc. Nutr. Soc.* **60,** 329–339
3. Trayhurn, P., and Wood, I. S. (2004) Adipokines: inflammation and the pleiotropic role of white adipose tissue. *Br. J. Nutr.* **92,** 347–355
4. Gregor, M. F., and Hotamisligil, G. S. (2011) Inflammatory mechanisms in obesity. *Annu. Rev. Immunol.* **29,** 415–445
5. Hotamisligil, G. (2006) Inflammation and metabolic disorders. *Nature* **444,** 860–867
6. Hottiger, M., Hassa, P., Lüscher, B., Schüler, H., and Koch-Nolte, F. (2010) Toward a unified nomenclature for mammalian ADP-ribosyltransferases. *Trends Biochem. Sci.* **35,** 208–219
7. Hassa, P., Haenni, S., Elser, M., and Hottiger, M. (2006) Nuclear ADP-ribosylation reactions in mammalian cells: where are we today and where are we going? *Microbiol. Mol. Biol. Rev.* **70,** 789–829
8. Krishnakumar, R., and Kraus, W. (2010) The PARP side of the nucleus: molecular actions, physiological outcomes, and clinical targets. *Mol. Cell* **39,** 8–24
9. Hassa, P., and Hottiger, M. (2008) The diverse biological roles of mammalian PARPS, a small but powerful family of poly-ADP-ribose polymerases. *Front. Biosci.* **13,** 3046–3082
10. Bai, P., Canto, C., Oudart, H., Brunyanszki, A., Cen, Y., Thomas, C., Yamamoto, H., Huber, A., Kiss, B., Houtkooper, R. H., Schoonjans, K., Schreiber, V., Sauve, A. A., Menissier-de Murcia, J., and Auwerx, J. (2011) PARP-1 inhibition increases mitochondrial metabolism through SIRT1 activation. *Cell Metab.* **13,** 461–468
11. Devalaraja-Narashimha, K., and Padanilam, B. (2010) PARP1 deficiency exacerbates diet-induced obesity in mice. *J. Endocrinol.* **205,** 243–252
12. Surwit, R. S., Kuhn, C. M., Cochrane, C., McCubbin, J. A., and Feinglos, M. N. (1988) Diet-induced type II diabetes in C57BL/6J mice. *Diabetes* **37,** 1163–1167
13. Bai, P., Canto, C., Brunyanszki, A., Huber, A., Szanto, M., Cen, Y., Yamamoto, H., Houten, S. M., Kiss, B., Oudart, H., Gergely, P., Menissier-de Murcia, J., Schreiber, V., Sauve, A. A., and Auwerx, J. (2011) PARP-2 Regulates SIRT1 expression and whole-body energy expenditure. *Cell Metab.* **13,** 450–460
14. Erener, S., Hesse, M., Kostadinova, R., and Hottiger, M. O. (2012) Poly(ADP-ribose)polymerase-1 (PARP1) controls adipogenic gene expression and adipocyte function. *Mol. Endocrinol.* **26,** 2011–1163
15. Wang, Z., Auer, B., Stingl, L., Berghammer, H., Haidacher, D., Schweiger, M., and Wagner, E. (1995) Mice lacking ADPRT and poly(ADP-ribosyl)ation develop normally but are susceptible to skin disease. *Genes Dev.* **9,** 509–520
16. Mirsaidi, A., Kleinhans, K. N., Rimann, M., Tiaden, A. N., Stauber, M., Rudolph, K. L., and Richards, P. J. (2011) Telomere length, telomerase activity and osteogenic differentiation are maintained in adipose-derived stromal cells from senile osteoporotic SAMP6 mice. [E-pub ahead of print] *J. Tissue Eng. Regen. Med.* doi: 10.1002/term.440
17. Vidal-Puig, A., Jimenez-Linan, M., Lowell, B. B., Hamann, A., Hu, E., Spiegelman, B., Flier, J. S., and Moller, D. E. (1996) Regulation of PPAR gamma gene expression by nutrition and obesity in rodents. *J. Clin. Invest.* **97,** 2553–2561
18. Samuel, V. T., Petersen, K. F., and Shulman, G. I. (2010) Lipid-induced insulin resistance: unravelling the mechanism. *Lancet* **375,** 2267–2277
19. Andrikopoulos, S., Blair, A. R., Deluca, N., Fam, B. C., and Proietto, J. (2008) Evaluating the glucose tolerance test in mice. *Am. J. Physiol. Endocrinol. Metab.* **295,** E1323–1332
20. Jones, J. R., Barrick, C., Kim, K. A., Lindner, J., Blondeau, B., Fujimoto, Y., Shiota, M., Kesterson, R. A., Kahn, B. B., and Magnuson, M. A. (2005) Deletion of PPARgamma in adipose tissues of mice protects against high fat diet-induced obesity and insulin resistance. *Proc. Natl. Acad. Sci. U. S. A.* **102,** 6207–6212
21. Messner, S., and Hottiger, M. O. (2011) Histone ADP-ribosylation in DNA repair, replication and transcription. *Trends Cell Biol.* **21,** 534–542
22. Zuk, P. A., Zhu, M., Ashjian, P., De Ugarte, D. A., Huang, J. I., Mizuno, H., Alfonso, Z. C., Fraser, J. K., Benhaim, P., and Hedrick, M. H. (2002) Human adipose tissue is a source of multipotent stem cells. *Mol. Biol. Cell* **13,** 4279–4295
23. Ménissier de Murcia, J., Niedergang, C., Trucco, C., Ricoul, M., Dutrillaux, B., Mark, M., Oliver, F. J., Masson, M., Dierich, A., LeMeur, M., Walztinger, C., Chambon, P., and de Murcia, G. (1997) Requirement of poly(ADP-ribose) polymerase in recovery from DNA damage in mice and in cells. *Proc. Natl. Acad. Sci. U.S.A.* **94,** 7303–7307
24. D'Adda di Fagagna, F., Hande, M. P., Tong, W. M., Lansdorp, P. M., Wang, Z. Q., and Jackson, S. P. (1999) Functions of poly(ADP-ribose) polymerase in controlling telomere length and chromosomal stability. *Nat. Genet.* **23,** 76–80
25. Samper, E., Goytisolo, F. A., Menissier-de Murcia, J., Gonzalez-Suarez, E., Cigudosa, J. C., de Murcia, G., and Blasco, M. A. (2001) Normal telomere length and chromosomal end capping in poly(ADP-ribose) polymerase-deficient mice and primary cells despite increased chromosomal instability. *J. Cell Biol.* **154,** 49–60
26. Picard, F., Kurtev, M., Chung, N., Topark-Ngarm, A., Senawong, T., Machado De Oliveira, R., Leid, M., McBurney, M. W., and Guarente, L. (2004) Sirt1 promotes fat mobilization in white adipocytes by repressing PPAR-gamma. *Nature* **429,** 771–776
27. Qiao, L., and Shao, J. (2006) SIRT1 regulates adiponectin gene expression through Foxo1-C/enhancer-binding protein alpha transcriptional complex. *J. Biol. Chem.* **281,** 39915–39924
28. Wang, F., and Tong, Q. (2009) SIRT2 suppresses adipocyte differentiation by deacetylating FOXO1 and enhancing FOXO1's repressive interaction with PPARgamma. *Mol. Biol. Cell* **20,** 801–808
29. Sethi, J. K., and Vidal-Puig, A. J. (2007) Thematic review series: adipocyte biology. Adipose tissue function and plasticity orchestrate nutritional adaptation. *J. Lipid Res.* **48,** 1253–1262
30. Nguyen, P., Leray, V., Diez, M., Serisier, S., Le Bloc'h, J., Siliart, B., and Dumon, H. (2008) Liver lipid metabolism. *J. Anim. Physiol. Anim. Nutr. (Berl.)* **92,** 272–283
31. Cortez-Pinto, H., Camilo, M. E., Baptista, A., De Oliveira, A. G., and De Moura, M. C. (1999) Non-alcoholic fatty liver: another feature of the metabolic syndrome? *Clin. Nutr.* **18,** 353–358
32. Marchesini, G., Brizi, M., Bianchi, G., Tomassetti, S., Bugianesi, E., Lenzi, M., McCullough, A. J., Natale, S., Forlani, G., and Melchionda, N. (2001) Nonalcoholic fatty liver disease: a feature of the metabolic syndrome. *Diabetes* **50,** 1844–1850

Received for publication November 11, 2011.
Accepted for publication February 28, 2012.

Supplementary Material

Supplementary Figure S1

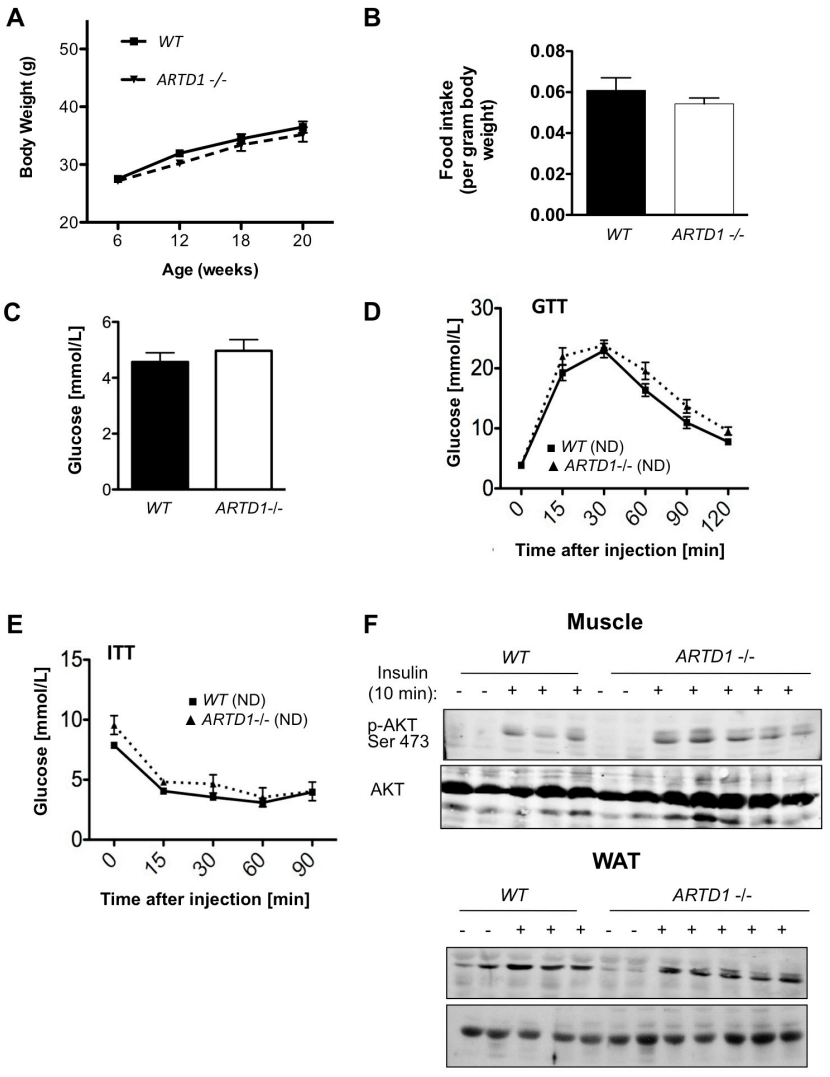

Supplementary Figure S2

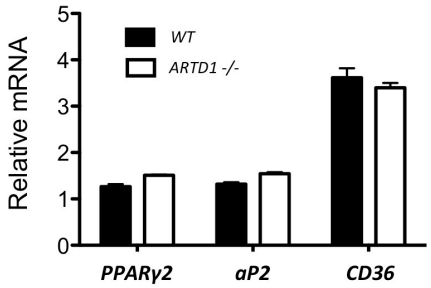

Supplementary Figure S3

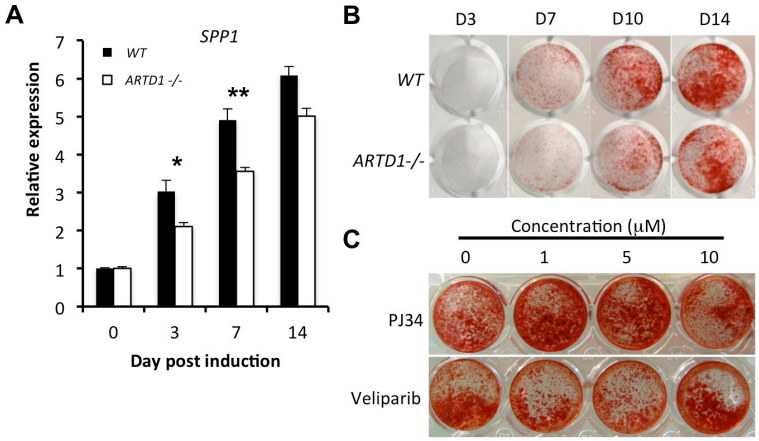

Suppl. Figure S1. *ARTD1 -/-* mice on ND exhibit reduced expression of adipogenic gene markers in WAT. (A-E) *ARTD1 -/-* mice display comparable sensitivity with *WT* mice to GTT and ITTs. **(A)** Body weight **(B)** Food intake (**C)** Starving glucose levels of *WT* and *ARTD1 -/-* mice. n=6 mice per group, mean ±SE. **(D)** Glucose tolerance test (GTT) measured after 14 h fasting *WT* and *ARTD1 -/-* mice. 6 weeks old mice were injected 0.75 g glucose per kg body weight. n = 5 mice per group, mean ±SE. **(E)** Insulin tolerance test (ITT) measured after 3 hr fasting *WT* and *ARTD1 -/-* mice. Mice were injected 0.75 U insulin per kg body weight n = 5 mice per group, mean ±SE. **(F)** Western blot analysis of phosphorylated Akt (p-Akt) from muscle and WAT of insulin (0.75 U/kg, 10 min) injected *WT* and *ARTD1 -/-* mice (14 h fast).

Suppl. Figure S2. PPARγ and PPARγ - dependent gene expression in WAT from *ARTD1 -/- mice on HFD*. Real-time RT-PCR analysis in total cell extracts from epididymal WAT of *WT* and *ARTD1 -/-* mice that were fed with HFD. mRNA levels were normalized with *Cyclophilin A.* Results represent mean ±SD of technical replicates.

Suppl. Figure S3. Osteogenic differentiation of ASCs is not adversely affected by *ARTD1* deletion. Analysis of osteogenic differentiation in ASCs isolated from wild type (*WT*) and *ARTD1*$^{-/-}$ mice. **(A)** The expression level of osteopontin (*Spp1*) was evaluated by qRT-PCR over 0, 3, 7 and 14 days of osteogenic differentiation. The expression value of each gene was normalized to the amount of ribosomal protein S12 (*RPS12*) RNA in order to calculate relative amounts of mRNA. **(B)** Mineral deposition was identified in mouse ASCs by Alizarin red S staining (red) at various stages during osteogenic differentiation. **(C)** The effect of ARTD1 inhibition on the osteogenic differentiation of ASCs isolated from *WT* mice was evaluated after 14 days using Alizarin red S staining. *$P < 0.05$, **$P < 0.01$.

Supplemental table S1. Primers used for real-time RT-PCR analyses.

The sequences of forward (F) and reverse (R) primers used for PCR are given in 5`-3`direction.

Gene	Sequence (F, R; 5`-3`)
aP2	F: ATGGGTGAAACTCTGGGAGATTCT R: CTTGGAGCTTCAGGTCATATTTGTA
Arginase 1	F: CAGAAGAATGGAAGAGTCAG R: CAGATATGCAGGGAGTCACC
ATGL	F: TGTGGCCTCATTCCTCCTAC R: TCGTGGATGTTGGTGGAGCT
CD36	F: ACAACAGGGTTTCAGCAGAAAGAGG R: GGTCTCTGACACCTGAGCCAAATG
Cyclophilin A	F: TCACCATTTCCGACTGTGGA R: AATGCCCGCAAGTCAAAAGA
HSL	F: GCTGGGCTGTCAAGCACTGT R: GTAACTGGGTAGGCTGCCAT
IL-10	F: GCTCTTACTGACTGGCATGAG R: CGCAGCTCTAGGAGCATGTG
IL-12	F: GAAGTTCAACATCAAGAGCAGTAG R: AGGGAGAAGTAGGAATGGGG
IL-13ra	F: TGCTGCTACTGTGGACCGCCA R: CCTTCAGGAGGACTCCACGTCCA
IL-1β	F: AAGGAGAACCAAGCAACGACAAAA R: TGGGGAACTCTGCAGACTCAAACT
IL-6	F: CTGCAAGAGACTTCCATCCAGTT R: GAAGTAGGGAAGGCCGTGG
IP-10	F: GCACGAACTTAACCACCATCTTCC R: CTACCCATTGATACATACTTGATGACAC
Lipin	F: AGCGCCAAAGAATAACCTGG R: TGAAGACTCGCTGTGAATGG
LPL	F: AGGACCCCTGAAGACAC R: GGCACCCAACTCTCATA
MCP-1	F: TTAAAAACCTGGATCGAACCAA R: GCATTAGCTTCAGATTTACGGGT
MPEG-1	F: GTGAAACAAAAGCCAGACAGAGCCT R: TCATGGCGCAGATGGTTTTGGC
PPARα	F: CGGGAAAGACCAGCAACAAC R: TGGCAGCAGTGGAAGAATCG
PPARγ2	F: ATGGGTGAAACTCTGGGAGATTCT R: CTTGGAGCTTCAGGTCATATTTGTA
Pu.1	F: GATCCGCCTTGATCCCCACCG R: TCTCCATCGCTGCCCACGAA
SAA3	F: TGCCATCATTCTTTGCATCTTGA R: CCGTGAACTTCTGAACAGCCT
aP2	Mm00445878_m1
ARTD1	Mm01321084_m1
GLUT4	Mm00436615_m1
PPARγ2	Mm00440940_m1
RPS12	Mm00488728_m1

STEM CELLS®

TISSUE-SPECIFIC STEM CELLS

Human Serine Protease HTRA1 Positively Regulates Osteogenesis of Human Bone Marrow-Derived Mesenchymal Stem Cells and Mineralization of Differentiating Bone-Forming Cells through the Modulation of Extracellular Matrix Protein

André N. Tiaden[1], Maike Breiden[2], Ali Mirsaidi[1,3], Fabienne A. Weber[4], Gregor Bahrenberg[1,3], Stephan Glanz[1,3], Paolo Cinelli[4], Michael Ehrmann[2], Peter J. Richards[1,3*]

[1]Bone and Stem Cell Research Group, CABMM, University of Zurich, Switzerland. [2]Centre for Medical Biotechnology, Faculty of Biology and Geography, University Duisburg-Essen, Germany. [3]Institute of Physiology and Zurich Center for Integrative Human Physiology (ZIHP), University of Zurich, Switzerland. [4]Institute of Laboratory Animal Science, University of Zurich, Switzerland.

Key words. HTRA1 protein • mesenchymal stem cell • differentiation • bone mineralization

ABSTRACT

Mammalian HTRA1 is a secreted member of the trypsin family of serine proteases which can degrade a variety of bone matrix proteins and as such, has been implicated in musculoskeletal development. In the present study, we have investigated the role of HTRA1 in mesenchymal stem cell (MSC) osteogenesis and suggest a potential mechanism through which it controls matrix mineralization by differentiating bone-forming cells. Osteogenic induction resulted in a significant elevation in the expression and secretion of HTRA1 in MSCs isolated from human bone marrow (hBMSCs), mouse adipose tissue (mASCs), and mouse embryonic stem cells (mESCs). Recombinant HTRA1 enhanced the osteogenesis of hBMSCs as evidenced by significant changes in several osteogenic markers including integrin-binding sialoprotein (*IBSP*), bone morphogenetic protein 5 (*BMP5*) and sclerostin (*SOST*), and promoted matrix mineralization in differentiating bone-forming osteoblasts. These stimulatory effects were not observed with proteolytically inactive HTRA1 and were abolished by small interfering RNA (siRNA) against *HTRA1*. Moreover, loss of HTRA1 function resulted in enhanced adipogenesis of hBMSCs. HTRA1 Immunofluorescence studies showed co-localization of HTRA1 with IBSP protein in osteogenic mASC spheroid cultures and was confirmed as being a newly identified HTRA1 substrate in cell cultures and in proteolytic enzyme assays. A role for HTRA1 in bone regeneration *in vivo* was also alluded to in bone fracture repair studies where HTRA1 was found localized predominantly to areas of new bone formation in association with IBSP. These data therefore implicate HTRA1 as having a central role in osteogenesis through modification of proteins within the extracellular matrix.

Author contributions: A.N.T.: Collection and/or assembly of data, data analysis and interpretation, manuscript writing; M.B.: Collection and/or assembly of data; A.M.: Collection and/or assembly of data; F.W.: Collection and/or assembly of data; G.B.: Collection and/or assembly of data; S.G.: Collection and/or assembly of data; P.C.: data analysis and interpretation; M.E.: Data analysis and interpretation, manuscript writing; P.J.R: conception and design, financial support, collection and/or assembly of data, data analysis and interpretation, manuscript writing.

*Corresponding Author: Dr. Peter J. Richards, CABMM, University of Zurich, Winterthurerstrasse 190, CH-8057 Zürich, Switzerland, Tel: +41-44-635-3801; Fax: +41-44-635-6840; peter.richards@cabmm.uzh.ch; Received May 04, 2012; accepted for publication July 21, 2012; 1066-5099/2012/$30.00/0 doi: 10.1002/stem.1190

This article has been accepted for publication and undergone full peer review but has not been through the copyediting, typesetting, pagination and proofreading process which may lead to differences between this version and the Version of Record. Please cite this article as doi: 10.1002/stem.1190

INTRODUCTION

Mammalian high temperature requirement serine protease A1 (HTRA1) belongs to a well-defined group of serine proteases originally identified in bacteria [1, 2]. They share many common features including a highly conserved trypsin-like serine protease domain and at least one PDZ domain at the C-terminus. To date, four HTRA1 family members have been identified and are termed HTRA1, -2, -3, and -4. HTRA2 is the best characterized of the four and exists as a membrane protein primarily involved in mitochondrial quality control [2, 3]. Both HTRA1 and -2 are primarily regarded as being key regulators of tumor development and subsequent malignancies [4-6], although a growing body of evidence now exists to suggest that HTRA1 may also play a central role in musculoskeletal development and disease through its proteolytic actions on proteins within the extracellular matrix (ECM) [7-10].

The skeletal ECM is a structurally dynamic scaffold which provides a well organized framework for mineralization and orchestrates many of the cellular processes required for maintaining bone integrity. The bone tissue ECM comprises of 70-90% mineral and 10-30% protein, the major proportion of which being glycoproteins such as collagen, fibronectin, and non-collagenous small integrin-binding ligand, N-linked glycoproteins (SIBLINGs) [11]. A direct interaction between these proteins and bone progenitor cells is essential for the development of a mineralized matrix [12-14]. Furthermore, degradation of specific glycoproteins within the ECM by serine proteases is also thought to play a central role in controlling mineral deposition by osteoblasts [15].

Bone remodeling and regeneration is a strictly regulated process, being reliant on the activities of resident osteoblasts originating from bone marrow-derived mesenchymal stem cells (BMSCs) through the process of osteogenic differentiation [16]. Osteogenesis is governed by a complex series of well orchestrated events involving numerous different transcription factors, signaling pathways and growth factors [17, 18]. The potential involvement of HTRA1 in osteogenesis and bone development has already been alluded to in studies examining the expression profile of *HTRA1* in developing mouse embryos and adult mouse bone where it was identified in osteocytes and osteoblasts within the bone matrix [10, 19]. More recently, it was suggested that HTRA1 may actually play a negative role in bone and mineral development through its ability to inhibit osteoblastic differentiation in the mouse 2T3 cell line [20]. However, no studies have yet sought to determine the influence of HTRA1 on the osteogenic differentiation potential of MSCs.

In the present study, we examined the effects of recombinant HTRA1 on the osteogenesis of human BMSCs (hBMSCs) and matrix mineralization by differentiating bone-forming cells with an aim to establishing a role for HTRA1 in bone formation. Our results demonstrate that HTRA1 is an essential requirement for osteogenesis and that its effects are mediated primarily through its proteolytic actions on ECM proteins.

MATERIALS AND METHODS

Materials

4-(2-Aminoethyl) benzenesulfonyl fluoride hydrochloride (AEBSF) was from Sigma-Aldrich. Recombinant IBSP was purchased from R & D Systems (Abingdon, UK). Monoclonal mouse anti-IBSP, C-terminal region (clone ID1.2) and polyclonal donkey anti-collagen type 1 were from LabForce (Switzerland), polyclonal rabbit anti-IBSP, N-terminal region was from Enzo Life Sciences (Lausen, Switzerland), and polyclonal rabbit anti-HTRA1 was generated as previously described [9]. The biotinylated polyclonal swine anti-rabbit IgG was from DAKO. All anti-IgG horseradish peroxidase (HRP)-conjugated and fluorescence-conjugated

secondary antibodies were from Jackson ImmunoResearch (Suffolk, UK).

Animals

Experiments were performed using 5-month-old senescence accelerated resistant mice (SAMR1) (n = 27) (Harlan, Netherlands). All animal research procedures were approved by the Animal Experimentation Committee of the Veterinary Office of the Canton of Zürich, Switzerland (Project License 140/2005 and 151/2010), and followed the guidelines of the Swiss Federal Veterinary Office for the use and care of laboratory animals.

Cell Culture

Mouse ASCs were isolated from the inguinal fat pads of SAMR1 mice (n = 4) and purity confirmed by fluorescence activated cell sorting (Sca1, 98%; CD29, 100%; CD105, 42%; CD34, 5%; CD45, 0.5%) as previously reported [21]. Mouse ESCs (E14 129/Ola) are a well-established cell line and were maintained as previously described [22, 23]. Human BMSCs were obtained from Lonza Verviers (Belgium) and were confirmed as being positive for CD105, CD166, CD44 and CD26, and negative for CD14, CD34 and CD45 as stated by the manufacturer. Cells were maintained in normal growth medium consisting of Dulbecco's modified eagle medium (DMEM-low glucose, with Glutamax) (Invitrogen AG, Basel, Switzerland), supplemented with 10% fetal bovine serum (FBS) (Invitrogen AG, Basel, Switzerland) and penicillin (50 units/ml) and streptomycin (50 µg/ml) (Invitrogen AG, Basel). Cells were used between passage 2 and 6 unless otherwise stated. In some cases, hBMSCs undergoing osteogenic differentiation were treated with recombinant active or inactive HTRA1 (5 µg/ml) for up to 18 days. For protease inhibition studies, AEBSF (20 µg/ml) was also included where indicated. For 3D-spheroids, mASCs were cultured in 25 µl hanging drops in in normal growth medium as described above, using Terasaki plates (VWR, Switzerland) at 2,500 cells/drop.

Induction and Analysis of Differentiation

Well established differentiation protocols were used to induce and analyze either osteogenesis or adipogenesis in mASCs and E14 129/Ola cells [21] and hBMSCs [24]. For differentiation assays, a starting density of 5'000 and 10'000 cells/cm^2 was used for human and mouse cells respectively. For osteogenic 3D-spheroid preparations, mASCs were pre-differentiated in 2D cultures for 3 days and cultured in hanging drops containing osteogenic culture medium for a further 2, 4 or 6 days, after which time they were harvested and processed for histological analysis using previously described techniques [25]. Mineralization induced by osteogenic differentiation was identified using Alizarin Red S (Sigma-Aldrich). Adipocyte formation was confirmed by positive staining for oil red O (Sigma-Aldrich). Differentiation markers specific to either osteogenesis or adipogenesis were also quantified by reverse-transcription polymerase chain reaction (qRT-PCR) using TaqMan Gene Expression Assays (Applied Biosystems) (Supplementary Table 1). Total RNA was harvested from cells at given time points during differentiation and 0.5µg total RNA reverse-transcribed using Superscript II (Life Technologies) and an equivalent of 10ng total RNA applied as cDNA template in the successive qRT-PCR reaction using the StepOnePlus (Life Technologies).

Recombinant HTRA1 Production

Purified recombinant active HTRA1 (HTRA1Δmac) and inactive HTRA1 (HTRA1ΔmacSA), were produced in *Escherichia coli* and purified using metal-affinity chromatography as previously described [26].

SDS-PAGE and Western Blotting

Protein was analyzed by SDS-PAGE using 4-15% precast Tris-HCl gels (BioRad) under reducing conditions and electroblotted onto PVDF membranes using the Trans-Blot Turbo blotting system (BioRad). IBSP was identified using antibodies raised against either the N-terminal (1:800) or C-terminal (1:500) regions of

human IBSP and detected using HRP-conjugated secondary antibodies (1:10'000) followed by incubation in SuperSignal West Pico Chemiluminescent Substrate (Pierce) and exposure to x-ray film..

Immunofluorescence

Cells in either 2D or 3D cultures were fixed in PBS buffered formaldehyde (4%) or ice cold methanol, blocked with normal goat serum (1:10) and incubated with polyclonal rabbit anti-HTRA1 (1:50), polyclonal donkey anti-collagen type 1 (1:50) or monoclonal mouse anti-IBSP (1:50) in phosphate buffered saline (PBS) containing 1% BSA overnight at 4°C. For paraffin wax sections, staining reactions were performed at 37°C for 1 h. In the case of double immunostaining procedures, samples were incubated with both polyclonal rabbit anti-HTRA1 (1:50) and monoclonal mouse anti-IBSP (1:50) using the conditions described above. Samples were then washed and incubated with either goat anti-rabbit-Cy3 (1:400), goat anti-donkey-Cy3 (1:400), or goat anti-mouse-Cy5 (1:400) for 1 hour and mounted in DAPI containing mounting solution and images captured using the Leica DMI6000B automated inverted research microscope system (Leica Microsystems).

Immunohistochemistry. Dewaxed paraffin sections (8 μm) were rehydrated and blocked with normal swine serum (DAKO) for 30 min. Sections were then incubated with polyclonal rabbit anti-HTRA1 (1:50) for 1 h at 37°C. Sections were then washed in PBS and incubated with biotinylated swine anti-rabbit IgG (1:500) for 1 h at room temperature followed by washing and a further incubation for 30 min with Vectastain (Vectorlabs). Sections were then developed using 3,3' diaminobenzidine tetrahydrochloride (DAB), counterstained with Harris' Hematoxylin and mounted in DPX.

Proteolytic Enzyme Assays

Degradation of IBSP by HTRA1 was determined using methods previously described [9]. Briefly, HTRA1 (45 nM) and IBSP (476 nM) were incubated in 50 mM Tris-HCl, pH 8.5, 150 mM NaCl for up to 24 h at 37 °C. In some reactions, active HTRA1 was replaced by proteolytically inactive HTRA1. Proteins were separated on a 4-15% SDS-PAGE gel and analysed by Western blot as described above. The proteolytic activity of HTRA1 was also investigated in hBMSC cultures using immunofluorescence staining. Cells were incubated in osteogenic induction medium either without or with active or inactive HTRA1 (5 μg/ml), fixed in methanol and IBSP or collagen type 1 detected with specific antibodies using methods as described above.

HTRA1 ELISA

The HTRA1 ELISA was performed using HTRA1 specific monoclonal and polyclonal antibodies as previously described [9].

***HTRA1* siRNA**

Specific knock down of *HTRA1* expression was performed with Silencer Select siRNA oligos, (Ambion, Life Technologies) according to the manufacturer's protocol. Human BMSCs ($1x10^5$ cells) were transfected with 100 nM *HTRA1*-specific (s11279, s11280) or negative control siRNA (Negative Control-1) using the NEON Transfection System (Life Technologies). Following transfection, cells were seeded in cell culture plates with fresh growth medium (without antibiotics) and incubated for 24 h at 37°C, 5% CO_2. Medium was then replaced with either fresh growth medium or differentiation medium and total RNA and supernatants harvested at selected time points for further analysis.

Fracture Model

A rigidly stabilized, unilateral mid diaphyseal osteotomy gap was created in the femurs of SAMR1 mice (n = 5-6 per time point) using a 0.22mm gigli saw as previously described [24]. The immunohistochemical and immunofluorescence techniques described above were used to detect both HTRA1 and IBSP protein in decalcified paraffin wax sections (8μm) from mouse femora at various stages of repair (n = 3 per time point).

Statistical Analysis

All statistical analyses were carried out using SPSS18.0 (SPSS Inc., Chicago, IL). Parametric analysis of normally distributed data was performed using the two-tailed unpaired Student's *t*-test for comparison of two groups or one-way analysis of variance (ANOVA) followed by Tukey's post-hoc test for multiple group comparisons. The sample size used in each study was based upon the observed level of variation between individual experiments and the need for sufficient sample numbers to allow for accurate statistical analyses. In all cases, a *p*-value of < 0.05 was considered statistically significant, and all data were expressed as mean ± standard deviation (S.D).

RESULTS

HTRA1 Production is Upregulated During Osteogenic Induction of MSCs

Differentiation studies conducted using hBMSCs demonstrated a small, but significant increase in the expression of *HTRA1* during the early phases of osteogenic induction with a greater than 1.5-fold ($p < 0.01$) increase in gene expression being attained by day 14 (Fig. 1A). However, unlike *HTRA1*, expression levels of the closely related HTRA family member, *HTRA3*, decreased during osteogenesis and remained significantly downregulated throughout the course of the study. The early induction of *HTRA1* gene expression was accompanied by significant increases in the expression of the well-known osteogenic markers runt-related transcription factor 2 (*RUNX2*), alkaline phosphatase (*ALP*), integrin-binding sialoprotein (*IBSP*) and Collagen type 1A1 (*COL1A*) (Fig. 1A). The expression level of the late osteogenic marker secreted phosphoprotein 1/osteopontin (*SPP1*) was actually downregulated during early osteogenesis, but became significantly increased during the late phase of osteogenesis at day 21, along with noticeable increases in mineralized matrix deposition beginning at day 10 as determined by alizarin red staining (Fig. 1B). As HTRA1 functions primarily as a secreted protease, we also investigated the effect of osteogenic differentiation on HTRA1 protein secretion from hBMSCs using an HTRA1 specific ELISA and immunofluorescence staining. In accordance with increases in its gene expression, secreted HTRA1 protein levels were also elevated in both the supernatant (Fig. 1C) and in the cell matrices (Fig. 1D) of hBMSC cultures undergoing osteogenic differentiation. Clearly therefore, induction of osteogenesis in hBMSCs has a major stimulatory effect on HTRA1 production resulting in both enhanced gene expression as well as protein secretion.

In order to investigate whether such effects were limited to adult human stem cells only, we extended these studies to include both mouse embryonic stem cells (mESCs) and mouse adipose-derived stromal cells (mASCs). *HtrA1* expression was also significantly upregulated in a time dependent manner in mESCs (Fig. 2A) and mASCs grown in either 2D- (Fig. 2B) or 3D- (Fig. 2C) culture systems in response to osteogenic stimuli. These increases in *HtrA1* expression were associated with mineralization of differentiating bone-forming cells derived from 2D-culutres of either mESCs (Fig. 2D) or mASCs (Fig. 2E), as well as 3D-cultures composed of osteogenic mASCs (Fig. 2F). Furthermore, immunofluorescence staining of paraffin wax sections from mASC 3D-spheroids identified HtrA1 protein in tissues undergoing mineralization, but not in uninduced controls (Fig. 2G), thus giving a first hint as to its role in stem cell osteogenesis.

Silencing of the *HTRA1* Gene Impairs hBMSC Osteogenesis and Enhances Adipogenesis

In order to investigate the role of *HTRA1* gene expression in the regulation of osteogenesis, we next performed loss of function studies by means of RNA interference in hBMSC cultures. The transfection of hBMSCs with small interfering RNA (siRNA) specific for *HTRA1* prior to osteogenic induction, resulted in a significant downregulation of *HTRA1* gene expression (Fig. 3A) and HTRA1 protein secretion (Fig. 3B) which was sustained throughout the first 2 weeks

of osteogenic differentiation. HTRA1 protein levels both within cells and the ECM were also markedly reduced (Supplementary Fig. 1). This was accompanied by a noticeable reduction in alizarin red staining at day 14, indicative of reduced mineral deposition in differentiating bone-forming cells (Fig. 3C). Biochemical analysis using the ALP activity assay revealed that these deficits in mineralization were accompanied by significant reductions in ALP protein activity, which were maintained for up to 14 days (Fig. 3D). Furthermore, *ALP* expression was also significantly downregulated in these cells at an early time point, although expression levels of the osteogenic markers *SPP1* and *RUNX2* were not significantly affected by *HTRA1* silencing (Fig. 3E).

Through the course of our studies, it became apparent that not only was osteogenesis reduced in hBMSCs following *HTRA1* gene silencing, but that adipogenesis appeared to actually be increased. Evidence of this was first realized in late-stage osteogenic cultures of hBMSC treated with *HTRA1* siRNA, where phase contrast microscopy revealed increased numbers of cells containing lipid droplets, reminiscent of mature adipocytes although control siRNA cultures continued to demonstrate matrix mineralization (Fig. 3F). In order to confirm this finding, hBMSCs transfected with either *HTRA1* siRNA or control siRNA were induced to undergo adipogenic differentiation and adipogenic gene expression measured by qRT-PCR (Fig. 3G) and triglyceride accumulation visualized by oil red O staining (Fig. 3H). As anticipated, silencing of the *HTRA1* gene greatly enhanced the number of oil red O positive cells present with the hBMSC culture and significantly enhanced the expression of specific adipogenic gene markers, peroxisome proliferator-activated receptor gamma 2 (*PPARG2*) and fatty acid binding protein 4 (*FABP4*), thereby supporting a differential role for HTRA1 in hBMSC lineage commitment.

Recombinant HTRA1 Protein Enhances hBMSC Osteogenesis

As previously mentioned, HTRA1 also exists as a secreted protease and thus, may have an extracellular role in the osteogenic differentiation of hBMSCs. We therefore next investigated whether exogenously added recombinant human HTRA1 protein could also influence osteogenic differentiation. hBMSCs undergoing osteogenic differentiation were initially treated every three days with either active or inactive HTRA1 for up to 14 days and mineralization determined by Alizarin red staining. Indeed, mineral deposition by differentiating bone-forming cells was greatly enhanced following stimulation with active, but not inactive, HTRA1 (Fig. 4B). Additional studies confirmed that these effects could be reproduced in late stage (day 10) cultures of osteogenic hBMSCs treated for only four days with HTRA1 (Fig. 4C). However, short term treatment with HTRA1 during the first week of osteogenic differentiation only, failed to elicit any noticeable increase in mineralization (Supplementary Fig. 2), thus implying that the stimulatory actions of HTRA1 were dependent not only on its protease activity, but also on the differentiation status of the cells. Further studies using the broad spectrum serine protease inhibitor, AEBSF, confirmed the stimulatory effects of HTRA1 to be dependent on its proteolytic activity (Fig. 4D). Although matrix mineralization was clearly enhanced in differentiating bone-forming cells treated with HTRA1, the expression of several well-known osteogenic markers including *ALP*, *RUNX2* and *SPP1* remained unaltered at the time point tested (day 10) (Fig. 4E). However, significant increases were observed in the expression levels of *IBSP* and bone morphogenetic protein 5 (*BMP5*). Furthermore, a significant decrease in the expression level of sclerostin (*SOST*) was also observed in cells treated with HTRA1.

Integrin-Binding Sialoprotein (IBSP) Represents a Novel HTRA1 Substrate During Osteogenic Differentiation of MSCs *in vitro*.

In the current study, we demonstrated that although *IBSP* expression was significantly enhanced in hBMSCs following the addition of HTRA1, IBSP protein was almost completely abolished from the cellular matrix of these cultures, an effect not observed with inactive HTRA1 (Fig. 5A). This was regarded as being specifically due to the HTRA1 protein added due to the fact that collagen Type 1, a proteoglycan not degraded by HTRA1 [20], remained unaffected within the cell matrices (Supplementary Fig. 3). The potential for proteolytically active HTRA1 to degrade IBSP was further confirmed by *in vitro* enzyme assays, where a noticeable reduction in recombinant human IBSP (476 nM) was evident after 8 hours incubation with HTRA1 (45 nM) as determined by Western blot analysis (Fig. 5B). We next utilized the mASC spheroid culture system to investigate whether endogenous HTRA1 protein could be localized to IBSP directly within differentiating MSCs. Paraffin wax sections of mASCs were stained for HTRA1 and IBSP at various stages of osteogenic differentiation, and overlays produced to determine whether HTRA1 could be localized to areas of IBSP protein expression. IBSP was detected within mASC spheroids during the early phase of osteogenesis (day 5), although HTRA1 remained at very low levels and mineral deposition was not detected using Alizarin red staining (Fig. 5C, *upper panel* and Supplementary Fig. 4A). By day 9, levels of HTRA1 had greatly increased and it was regularly found co-localized with IBSP in the tissue matrix (Fig. 5C, *lower panel*). In addition, mineralization of differentiating bone-forming cells within 3D-spheroids was also apparent at this time point as identified by intense Alizarin red staining (Supplementary Fig. 4B). Sections incubated with isotype-matched IgG antibodies stained negative and served as controls (Supplementary Fig. 4C).

Localization of HTRA1 and IBSP to Areas of New Bone Formation in Mice

In order to assess the potential involvement of HTRA1 in the reparative process of bone tissue, we utilized a previously well-established mouse femur osteotomy model (Fig. 6A) [24]. HTRA1 protein was identified in thin paraffin wax bone sections taken from mice at various stages of fracture repair using immunohistochemical staining. At day 7, early osteoid formation was observed within the bone marrow at the osteotomy site and was associated with intense staining for HTRA1 (Fig. 6B). At this time point, HTRA1 was also located within the cells and tissue of the overlying periosteal layer (Supplementary Fig. 5A). By day 14, the non-mineralized callus had increased greatly in size with numerous HTRA1-positive fibroblast-like cells present throughout the tissue as well as in cells of the newly forming callus (Fig. 6C and Supplementary Fig. 5B). Large numbers of HTRA1-positive chondrocytes were also evident within intact lacunae, and represented the early stages of endochondral ossification. By day 28, a substantial proportion of the callus had been replaced by new bone and HTRA1 was now localized to specific areas of active bone formation (Fig. 6D) in association with cuboidal osteoblasts (Supplementary Fig. 5C). By day 42, the osteotomy gap was almost completely healed (Fig. 6E) and the bone resembled that of a non-operative control femur (Fig. 6F). In both cases, HTRA1 was almost completely absent, being localized to only a small number of osteocytes within the bone matrix.

Having confirmed that HTRA1 protein was indeed present within actively forming bone tissue, we conducted further investigations to determine whether HTRA1 could also be localized to IBSP within these bone sections, thus providing a potential mode of action for HTRA1 in the context of osteogenesis *in vivo*. Indeed, co-localization of HTRA1 and IBSP was identified in paraffin wax bone sections from 28 day postoperative mice by double immunofluorescence staining, being confined to

areas previously identified as undergoing active regeneration (Fig. 7 and supplementary Fig. 6).

DISCUSSION

A complex molecular network of signaling pathways and regulatory factors govern the osteogenesis of multipotent MSCs [17, 18, 27], being reliant on the activation and regulation of a number of key molecular targets including *RUNX2, ALP, SPP1* and *IBSP* [28]. Although there have been significant advances in our understanding of the molecular mechanisms involved in controlling osteogenic differentiation, the influence of serine proteases on such processes remains relatively obscure. In the present study, we have shown for the first time that the serine protease HTRA1 is a positive regulator of MSC osteogenesis and its presence is required for the efficient mineralization of differentiating bone cells.

The expression of *HTRA1* was upregulated in hBMSCs upon osteogenic induction and was associated with significant increases in the levels of its secreted protein product. Furthermore, HTRA1 production increased in a time dependent manner throughout the course of osteogenic differentiation, and was closely associated with the appearance of mineralized matrix. Interestingly, expression levels of the closely related HTRA family member, *HTRA3*, were actually downregulated during osteogenesis. This was of particular interest as HTRA1 and HTRA3 are considered to have over-lapping functions due to close structural similarities [29]. It may well be therefore, that HTRA1 and HTRA3 play differential roles in mediating the osteogenesis of hBMSCs. This pattern of HTRA1 production during osteogenesis of hBMSCs was recapitulated in cultures composed of either mASCs or mESCs, where significant increases in *HtrA1* expression coincided with the appearance of HtrA1 protein and mineralized matrix. Although previous investigations have alluded to the involvement of HTRA1 in mouse osteogenesis [19, 20], our study is the first to report the potential role of HTRA1 in human osteogenesis. Based on earlier reports of HTRA1 imparting a negative influence over mineral deposition by murine 2T3 osteoblasts [20], initial expectations were for HTRA1 to inhibit osteogenesis of hBMSCs and thus prevent mineralization of differentiating human bone-forming cells. On the contrary, we found that siRNA-induced loss of HTRA1 function in hBMSCs, effectively suppressed the stimulatory effects of osteogenic culture medium on *ALP* expression and intracellular ALP protein activity by hBMSCs, as well as the formation of a mineralized matrix. Although *ALP* expression levels were compromised in cells lacking *HTRA1*, some of the key regulatory factors involved in osteogenesis, including *RUNX2* and *SPP1*, remained intact. It is possible therefore that HTRA1 mediates its effects through specific pathways, independent of these particular elements. In addition to its effects on osteogenesis, *HTRA1* silencing had a profound effect on hBMSC adipogenesis as evidenced by increases in adipogenic gene expression and oil droplet formation. Such observations would suggest that HTRA1 may in fact represent a decisive factor in determining stem cell lineage commitment and that its involvement in stem cell differentiation go somewhat beyond it simply being a mediator of osteoblast formation. Further investigations into the role of HTRA1 in other differentiation pathways, such as chondrogenesis, myogenesis or even tenogenesis, would therefore represent a logical progression of these studies and may hold particular relevance with regards to the involvement of HTRA1 in musculoskeletal development as has previously been inferred [19].

Based on the fact that HTRA1 is a secreted serine protease, we next directed our attention to the possible influence of HTRA1 on hBMSC osteogenesis by way of its extracellular effects. A specific role for HTRA1 in the osteogenesis of hBMSCs and mineralization of differentiating bone-forming cells was confirmed in studies using both proteolytically active and inactive recombinant forms of human HTRA1, as well

the broad spectrum serine protease inhibitor AEBSF. An increase in mineralized matrix formation was observed in cells treated with active HTRA1 only, and was dependent on HTRA1 being present during the initiation phase of mineralization, as short duration treatments prior to the onset of mineralization proved ineffective. This would therefore infer that the stimulatory effects of exogenously added HTRA1 protein on hBMSC osteogenesis and mineralization of differentiating bone-forming cells may be reliant on its ability to regulate factors present within the actively mineralizing ECM. In addition to its ability to affect ECM mineral content, HTRA1 also induced a significant upregulation in the expression of several positive regulators of mineralization, including *BMP5* and *IBSP* [30, 31], although a large proportion of well-known osteogenic genes such as *RUNX2*, *ALP*, and *SPP1* remained unaffected. In addition, the expression level of a potent negative-regulator of mineral formation, sclerostin/*SOST* [32, 33], was markedly downregulated in hBMSCs treated with HTRA1 and may thus represent an additional mechanism by which mineral deposition is enhanced in differentiating bone-forming cells. It is possible therefore, that the effects of HTRA1 protein on hBMSC mineralization may be mediated indirectly through its ability to modulate the production of both activators and inhibitors of osteogenic differentiation and/or mineralization. These results are in stark contrast to the findings presented in a previous report by Hadfield et al [20], where HTRA1 was shown to impart a negative influence over mineralized matrix formation by mouse 2T3 osteoblasts. One possible explanation may lie within the fact that 2T3 cells are derived from transgenic mice overexpressing the simian virus 40 (SV40) T antigen and as such, are immortalized [34]. The fact that *HTRA1* gene expression is known to be significantly affected in SV40 transformed cells [35], would imply that modifications of the osteogenic status of these cells brought about by changes in HTRA1 expression and activity, may not be truly representative of non-immortalized, primary cells. Further studies aimed at determining the effects of *HtrA1* gene silencing or exogenously added recombinant HTRA1 on primary mASC osteogenesis, may help to clarify this point.

Of the osteogenic genes that were regulated by HTRA1, *IBSP* held particular relevance to the current study due to the fact that its ability to regulate mineral deposition has previously been reported to be dependent on the actions of serine proteases [15]. Attention was therefore focused on IBSP and its potential involvement in mediating the effects of HTRA1 on both osteogenesis of MSCs and mineralization of differentiating bone-forming cells. IBSP belongs to the family of SIBLING proteins which also includes osteopontin, dentin matrix protein 1 (DMP1), dentin siaolophosphoprotein (DSPP) and matrix extracellular phosphoglycoprotein (MEPE) [36]. IBSP, along with other SIBLING proteins, is found almost exclusively in bone and dentin and is a major constituent of the mineralizing matrix during new bone formation [37-39]. The primary biological function of IBSP is unclear, although it has been reported to be involved in the initiation of matrix mineralization through the nucleation of hydroxyapatite crystals [40, 41]. Furthermore, it has been proposed that IBSP is required to undergo fragmentation, possibly through the actions of serine proteases, in order to allow for efficient matrix mineralization [15, 42, 43]. In the current report, we were able to demonstrate co-localization of HTRA1 and IBSP in osteo-induced mASC spheroid cultures, thus confirming the potential for endogenous HTRA1 to interact with IBSP under osteogenic culture conditions. Additional immunofluorescence analyses of hBMSCs treated with exogenous HTRA1 revealed that this interaction most likely resulted in the digestion and subsequent removal of IBSP protein from the mineralizing matrix. These results would therefore suggest that the stimulatory effects of secreted HTRA1 protein on matrix mineralization *in vitro* are mediated, at least in part, through its proteolytic actions on IBSP within the ECM. The potential for HTRA1-induced IBSP proteolysis was further

confirmed by Western bot analysis where proteolytically active HTRA1 effectively digested recombinant human IBSP protein at equivalent concentrations to those used in the cell culture studies. However, despite us using two different antibodies raised against either the N- or C-terminal regions of IBSP, we were unable to detect any HTRA1 digest fragments. This was somewhat unexpected, as findings from previous studies suggest that IBSP fragmentation plays an important role in its function as an instigator of mineral nodule formation [15]. This is based on the assumption that IBSP facilitates mineralization predominantly through its ability to bind and nucleate hydroxyapatite, although evidence exists to suggest that both intact and fragmented IBSP can also inhibit hydroxyapatite seeded crystal growth [44]. It is possible therefore that HTRA1 contributes to osteogenesis through the controlled turnover of IBSP within the mineralizing ECM. This is further supported by the observation that *IBSP* gene expression is upregulated by exogenous HTRA1 at the expense of its protein product, and may thus constitute a novel feedback mechanism through which HTRA1 regulates matrix mineralization.

The osteogenic differentiation of BMSCs towards mature bone-forming osteoblasts is a critical step in the development and repair of bone tissue. In the present study, we utilized a previously well-established mouse osteotomy model to investigate the expression of HTRA1 protein during bone healing. Immunohistochemical analysis identified high levels of HTRA1 protein within areas of active bone formation at various stages of bone repair although no positive staining was observed in tissue sections from intact bone, thus confirming it to be primarily involved in *de novo* bone formation. Furthermore, strong positive staining for HTRA1 was also evident in callus tissue harboring large numbers of chondrocytes, and is thus suggestive of its role in both chondrogenesis and endochondral ossification. Such findings could be of significant importance to fracture healing and possibly even cartilage formation, and as such, warrant further investigation. Immunofluorescence analysis of these sections revealed a close association of HTRA1 with IBSP in areas considered to be undergoing active bone regeneration. This lends support to the theory that HTRA1 regulates both osteogenesis of MSCs and mineralization of differentiating bone-forming cells through its interactions with IBSP, although it doesn't exclude the possibility that HTRA1 mediates its actions through the proteolytic processing of other SIBLING members [45-48].

SUMMARY

The findings from this study therefore implicate HTRA1 as a positive regulator of both osteogenesis of MSCs and mineralization of differentiating bone-forming cells, possibly at the expense of adipogenic differentiation. Based on these properties, HTRA1 may be deemed a key factor in determining the outcome of diseases such as age-related osteoporosis, where impaired BMSC osteogenesis and upregulated adipogenesis is believed to be a major contributor to the underlying pathology [24, 49].

ACKNOWLEDGMENTS

This study was supported in part by the Swiss National Science Foundation grant 31003A-134935; CABMM Start-up Grant; Forschungskredit of the University of Zurich; Novartis Foundation, formerly Ciba-Geigy-Jubilee-Foundation; and Uniscientia Foundation.

Disclosure of Potential Conflicts of Interest
The authors indicate no potential conflicts of interest.

REFERENCES

1. Clausen T, Southan C, Ehrmann M. The HtrA Family of Proteases: Implications for Protein Composition and Cell Fate. Mol Cell 2002;10:443-455.
2. Clausen T, Kaiser M, Huber R, et al. HTRA proteases: regulated proteolysis in protein quality control. Nat Rev Mol Cell Biol 2011;12:152-162.
3. Vande Walle L, Lamkanfi M, Vandenabeele P. The mitochondrial serine protease HtrA2/Omi: an overview. Cell Death Diff 2008;15:453-460.
4. Zurawa-Janicka D, Skorko-Glonek J, Lipinska B. HtrA proteins as targets in therapy of cancer and other diseases. Expert Opin Ther Targets 2010;14:665-79.
5. Chien J, Staub J, Hu SI, et al. A candidate tumor suppressor HtrA1 is downregulated in ovarian cancer. Oncogene 2004;23:1636-44.
6. Baldi A, De Luca A, Morini M, et al. The HtrA1 serine protease is down-regulated during human melanoma progression and represses growth of metastatic melanoma cells. Oncogene 2002;21:6684-8.
7. Hu SI, Carozza M, Klein M, et al. Human HtrA, an evolutionarily conserved serine protease identified as a differentially expressed gene product in osteoarthritic cartilage. J Biol Chem 1998;273:34406–12.
8. Wu J, Liu W, Bemis A, et al. Comparative proteomic characterization of articular cartilage tissue from normal donors and patients with osteoarthritis. Arthritis Rheum 2007;56:3675-84.
9. Grau S, Richards PJ, Kerr B, et al. The role of human HtrA1 in arthritic disease. J Biol Chem 2006;281:6124-9.
10. Tsuchiya A, Yano M, Tocharus J, et al. Expression of mouse HtrA1 serine protease in normal bone and cartilage and its upregulation in joint cartilage damaged by experimental arthritis. Bone 2005;37:323-3.
11. Marcus R, Feldman D, Nelson DA, et al. Osteoporosis: Third Edition 2007, 191-240.
12. Kundu AK, Putnam AJ. Vitronectin and collagen I differentially regulate osteogenesis in mesenchymal stem cells. Biochem Biophys Res Commun 2006;347:347-57.
13. Huang CH, Chen MH, Young TH, et al. Interactive effects of mechanical stretching and extracellular matrix proteins on initiating osteogenic differentiation of human mesenchymal stem cells. J Cell Biochem 2009;108:1263-73
14. Klees RF, Salasznyk RM, Kingsley K, et al. Laminin-5 induces osteogenic gene expression in human mesenchymal stem cells through an ERK-dependent pathway. Mol Biol Cell 2005;16:881-90
15. Huffman NT, Keightley JA, Chaoying C, et al. Association of specific proteolytic processing of bone sialoprotein and bone acidic glycoprotein-75 with mineralization within biomineralization foci. J Biol Chem 2007;282:26002-13.
16. Bruder SP, Fink DJ, Caplan AI. Mesenchymal stem cells in bone development, bone repair, and skeletal regeneration therapy. J Cell Biochem 1994;56:283-94.
17. Marie PJ. Transcription factors controlling osteoblastogenesis. Arch Biochem Biophys 2008;473:98-105.
18. Komori T. Regulation of bone development and maintenance by Runx2. Front Biosci 2008;13:898-903.
19. Oka C, Tsujimoto R, Kajikawa M, et al. HtrA1 serine protease inhibits signaling mediated by Tgfbeta family proteins. Development 2004;131:1041-53.
20. Hadfield KD, Rock CF, Inkson CA, et al. HtrA1 inhibits mineral deposition by osteoblasts: requirement for the protease and PDZ domains. J Biol Chem 2008;283:5928-38.
21. Mirsaidi A, Kleinhans KN, Rimann M, et al. Telomere length, telomerase activity and osteogenic differentiation are maintained in adipose-derived stromal cells from senile osteoporotic SAMP6 mice. J Tissue Eng Regen Med 2012;6:378-90.
22. Casanova EA, Shakhova O, Patel SS, et al. Pramel7 mediates LIF/STAT3-dependent self-renewal in embryonic stem cells. Stem Cells 2011;29:474-85.
23. Hooper M, Hardy K, Handyside A, et al. HPRT-deficient (Lesch-Nyhan) mouse embryos derived from germline colonization by cultured cells. Nature 1987;326:292-95.
24. Egermann M, Heil P, Tami A, et al. Influence of defective bone marrow osteogenesis on fracture repair in an experimental model of senile osteoporosis. J Orthop Res 2010;28:798-804.
25. Kelm JM, et al. In vitro vascularization of human connective microtissues. In: Hauser H, Fussenegger M, eds. Tissue Engineering. Series: Methods in Molecular Medicine, 2nd ed. Humana Press, 2007:162-164.
26. Grau S, Baldi A, Bussani R, et al. Implications of the serine protease HtrA1 in amyloid precursor protein processing and Alzheimer's disease. Proc Natl Acad Sci U S A 2005;102:6021-6.
27. Deng ZL, Sharff KA, Tang N, et al. Regulation of osteogenic differentiation during skeletal development. Front Biosci 2008; 13:2001-21.
28. Nishimura R, Hata K, Ikeda F, et al. Signal transduction and transcriptional regulation during mesenchymal cell differentiation. J Bone Miner Metab 2008;26:203-12.
29. Tocharus J, Tsuchiya A, Kajikawa M, et al. Developmentally regulated expression of mouse HtrA3 and its role as an inhibitor of TGF-beta signaling. Dev Growth Differ 2004;46:257-74.
30. Mailhot G, Yang M, Mason-Savas A, et al. BMP-5 expression increases during chondrocyte differentiation in vivo and in vitro and promotes proliferation and cartilage matrix synthesis in primary chondrocyte cultures. J Cell Physiol 2008;214:56-64.

31. Gordon JA, Tye CE, Sampaio AV, et al. Bone sialoprotein expression enhances osteoblast differentiation and matrix mineralization in vitro. Bone 2007;41:462-73.
32. ten Dijke P, Krause C, de Gorter DJ, et al. Osteocyte-derived sclerostin inhibits bone formation: its role in bone morphogenetic protein and Wnt signaling. J Bone Joint Surg Am 2008;90 Suppl 1:31-5.
33. Krause C, Korchynskyi O, de Rooij K, et al. Distinct modes of inhibition by sclerostin on bone morphogenetic protein and Wnt signaling pathways. J Biol Chem 2010;285:41614-26.
34. Ghosh-Choudhury N, Windle JJ, Koop BA, et al. Immortalized murine osteoblasts derived from BMP 2-T-antigen expressing transgenic mice. Endocrinology 1996;137:331-9.
35. Zumbrunn J, Trueb B. Primary structure of a putative serine protease specific for IGF-binding proteins. FEBS Lett 1996;398:187-92.
36. Qin C, Baba O, Butler WT. Post-translational modifications of sibling proteins and their roles in osteogenesis and dentinogenesis. Crit Rev Oral Biol Med 2004;15:126-36.
37. Fisher LW, Whitson SW, Avioli LV, et al. Matrix sialoprotein of developing bone. J Biol Chem 1983;258:12723-7.
38. Chen JK, Shapiro HS, Wrana JL, et al. Localization of bone sialoprotein (BSP) expression to sites of mineralized tissue formation in fetal rat tissues by in situ hybridization. Matrix 1991;11:133-43.
39. Bianco P, Fisher LW, Young MF, et al. Expression of bone sialoprotein (BSP) in developing human tissues. Calcif Tissue Int 1991;49:421-6.
40. Hunter GK, Goldberg HA. Nucleation of hydroxyapatite by bone sialoprotein. Proc Natl Acad Sci U S A 1993;90:8562-5.
41. Tye CE, Rattray KR, Warner KJ, et al. Delineation of the hydroxyapatite-nucleating domains of bone sialoprotein. J Biol Chem 2003;278:7949-55.
42. Kobayashi D, Takita H, Mizuno M, et al. Time-dependent expression of bone sialoprotein fragments in osteogenesis induced by bone morphogenetic protein. J Biochem 1996;119:475-81.
43. Gorski JP, Huffman NT, Cui C, et al. Potential role of proprotein convertase SKI-1 in the mineralization of primary bone. Cells Tissues Organs. 2009;189:25-32.
44. Stubbs JT 3rd, Mintz KP, Eanes ED, et al. Characterization of native and recombinant bone sialoprotein: delineation of the mineral-binding and cell adhesion domains and structural analysis of the RGD domain. J Bone Miner Res 1997;12:1210-22.
45. Nagata T, Bellows CG, Kasugai S, et al. Biosynthesis of bone proteins [SPP-1 (secreted phosphoprotein-1, osteopontin), BSP (bone sialoprotein) and SPARC (osteonectin)] in association with mineralized-tissue formation by fetal-rat calvarial cells in culture. Biochem J 1991;274:513-20.
46. Tsuchiya S, Simmer JP, Hu JC, et al. Astacin proteases cleave dentin sialophosphoprotein (Dspp) to generate dentin phosphoprotein (Dpp). J Bone Miner Res 2011;26:220-8.
47. Steiglitz BM, Ayala M, Narayanan K, et al. Bone morphogenetic protein-1/Tolloid-like proteinases process dentin matrix protein-1. J Biol Chem 2004;279:980-6.
48. Guo R, Rowe PS, Liu S, et al. Inhibition of MEPE cleavage by Phex. Biochem Biophys Res Commun 2002;297:38-45.
49. Rodriguez JP, Garat S, Gajardo H, et al. Abnormal osteogenesis in osteoporotic patients is reflected by altered mesenchymal stem cells dynamics. J Cell Biochem 1999;75:414–423.

See www.StemCells.com for supporting information available online.

Figure 1. The expression and secretion of HTRA1 is significantly enhanced in hBMSCs undergoing osteogenic differentiation. **(A):** Quantitative polymerase chain reaction analysis of genes regulated during osteogenic differentiation of hBMSCs. Data were normalized to *GUSB* and expressed as fold change as compared to non-induced controls at day 0 (value 1) using the comparative C_T method. Data are representative of two independent experiments performed in triplicate ± S.D. * $p < 0.05$, ** $p < 0.01$ as determined by 1-way ANOVA. **(B):** Representative images of Alizarin red stained hBMSC cultures at various time points following osteogenic induction. Scale bar = 2 mm. **(C):** Secretion of HTRA1 by hBMSCs during osteogenic differentiation as determined by HTRA1-specific ELISA (n = 4). * $p < 0.05$, ** $p < 0.01$ as determined by 1-way ANOVA. **(D):** Representative fluorescence images of anti-HTRA1 (red) and DAPI (blue) stained hBMSCs undergoing osteogenic differentiation. Scale bar = 25 µm. Abbreviations: HTRA1, high temperature requirement protease A1; hBMSCs, human bone marrow-derived mesenchymal stem cells; *GUSB*, beta glucuronidase; ELISA, enzyme-linked immunosorbent assay; ECM, extracellular matrix; DAPI, 4,6-diamidino-2-phenylindole.

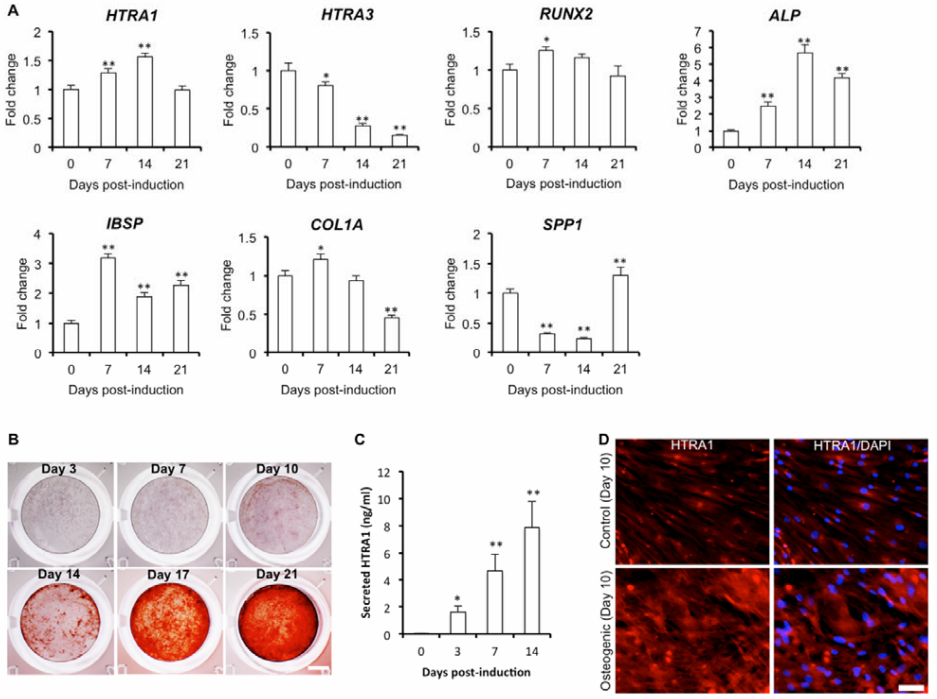

Figure 2. *HtrA1* gene expression is significantly increased in osteogenic mESCs and mASCs. **(A-C):** *HtrA1* gene expression during osteogenic differentiation of mESCs (A), mASCs (B) and mASC spheroids (day 7) (C) was determined by quantitative polymerase chain reaction and data normalized to *Mrps12* and expressed as fold change as compared to non-induced controls (Day 0 and control; value 1) using the comparative C_T method. Data are representative of at least two independent experiments performed in triplicate ± S.D. * $p < 0.05$, ** $p < 0.01$ as determined by 1-way ANOVA. **(D-E):** Representative images of Alizarin red stained mESCs (D) and mASCs (E) at various time points following osteogenic induction. Scale bar = 5 mm. **(F):** Representative images of Alizarin red and fast green stained paraffin wax sections of mASC spheroids incubated without (control) or with osteogenic media (osteogenic) for 7 days. Scale bar = 100 µm. **(G):** Representative immunofluorescence images of HTRA1 (red) and DAPI (blue) in paraffin wax sections of osteogenic mASC spheroids incubated without (control) or with osteogenic media (osteogenic) for 7 days. Scale bar = 25 µm. Abbreviations: HTRA1, high temperature requirement protease A1; mESCs, mouse embryonic stem cells; mASCs, mouse adipose-derived stromal cells; *GUSB*, beta glucuronidase; DAPI, 4,6-diamidino-2-phenylindole.

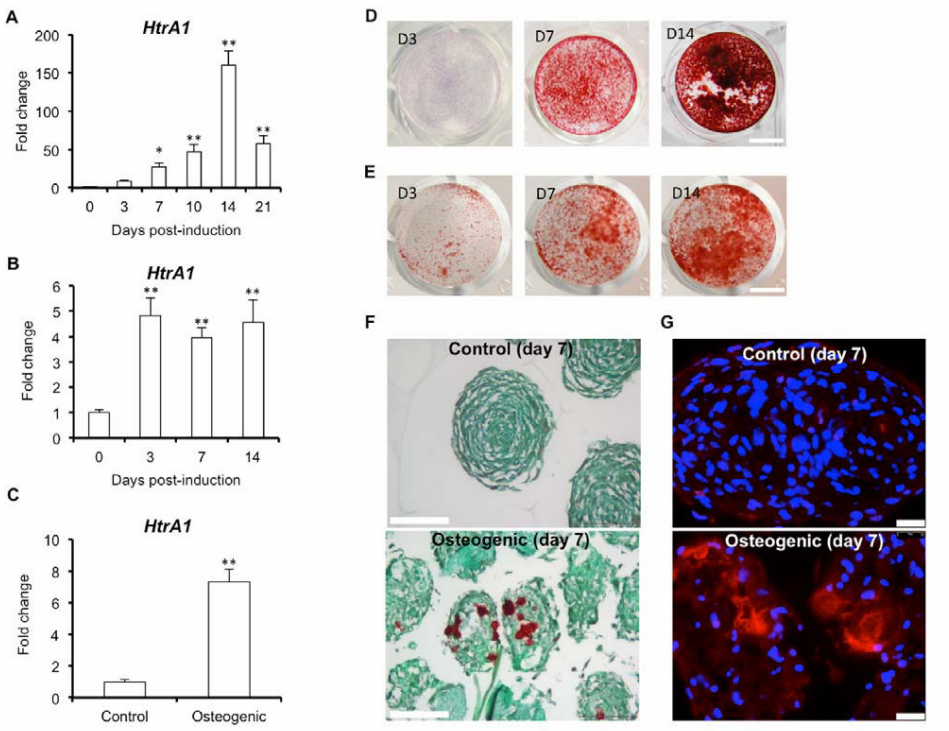

Figure 3. Repression of *HTRA1* gene expression alters lineage commitment of differentiating hBMSCs. **(A):** Quantitative polymerase chain reaction analysis of *HTRA1* gene expression in hBMSCs transfected with *HTRA1* siRNAs (siRNA (H1) or (H2)) or control siRNA (siRNA (C)) at 3 and 10 days post-osteogenic induction. Data was normalized to *GUSB* and expressed as fold change (Log10 scale) as compared to cells transfected with control siRNA using the comparative C_T method. * $p <$ 0.01 as determined by 1-way ANOVA. n = 3 separate experiments, ± S.D. **(B):** ELISA measurement of secreted HTRA1 from hBMSCs transfected with *HTRA1* siRNAs or control siRNA at various time points post-osteogenic induction. * $p < 0.01$ as determined by 1-way ANOVA. n = 3 separate experiments, ± S.D. **(C):** Representative images of Alizarin red stained hBMSCs transfected with *HTRA1* siRNAs or control siRNA at 14 days post-osteogenic induction. **(D):** ALP activity in protein lysates from hBMSC transfected with *HTRA1* siRNA or control siRNA at various time points post-osteogenic induction. * $p < 0.01$ as determined by 1-way ANOVA. n = 3 separate experiments, ± S.D. (E): Quantitative polymerase chain reaction analysis of *ALP, SPP1 and RUNX2* gene expression in hBMSCs transfected with *HTRA1* siRNA or control siRNA at 3 and 10 days post-osteogenic induction. Data was normalized to *GUSB* and expressed as fold change as compared to cells transfected with a control siRNA (value 1) using the comparative C_T method. n = 3 separate experiments, ± S.D. **(F):** Representative phase contrast micrographs of hBMSCs transfected with control siRNA or *HTRA1* siRNA at 14 days post-osteogenic induction. *Arrows*, mineral deposits. Scale bar = 10μm. **(G):** Quantitative polymerase chain reaction analysis of *PPARG2* and *FABP4* gene expression in hBMSCs transfected with *HTRA1* siRNA or control siRNA at day 6 post-adipogenic induction. Data was normalized to *GUSB* and expressed as fold change as compared to cells transfected with a control siRNA (value 1) using the comparative C_T method. Data is representative of two separate experiments, ± S.D. * $p < 0.01$ as determined by 1-way ANOVA. **(H):** Microscopic images of Oil red O stained hBMSCs transfected with *HTRA1* siRNA or control siRNA at 7 days post-adipogenic induction. Scale bar = 20 μm. Images are representative of two separate experiments. Abbreviations: HTRA1, high temperature requirement protease A1; hBMSCs, human bone marrow-derived mesenchymal stem cells; *GUSB*, beta glucuronidase; ELISA, enzyme-linked immunosorbent assay; siRNA, small interfering ribonucleic acid; *ALP*, alkaline phosphatase; *SPP1*, Secreted phosphoprotein 1; *RUNX2*, Runt-related transcription factor 2; *PPARG2*, peroxisome proliferator-activated receptor gamma 2; *FABP4*, fatty acid binding protein 4.

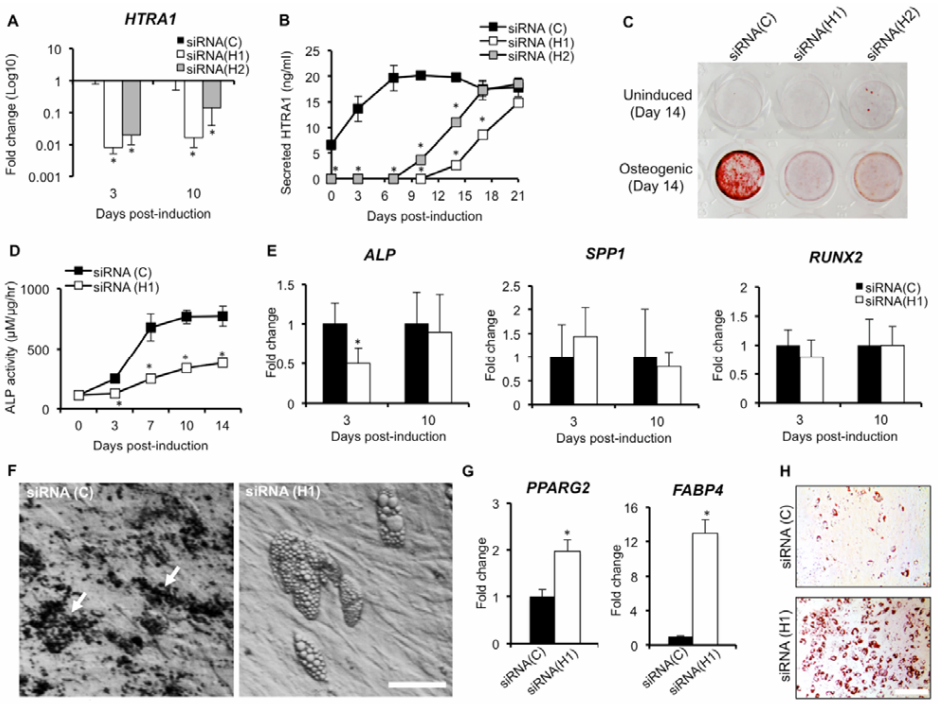
A
HTRA1
siRNA(C)
siRNA(H1)
siRNA(H2)
Fold change (Log10)
Days post-induction
B
siRNA (C)
siRNA (H1)
siRNA (H2)
Secreted HTRA1 (ng/ml)
Days post-induction
C
siRNA(C)
siRNA(H1)
siRNA(H2)
Uninduced (Day 14)
Osteogenic (Day 14)
D
siRNA (C)
siRNA (H1)
ALP activity (μM/μg/hr)
Days post-induction
E
ALP
SPP1
RUNX2
Fold change
Days post-induction
F
siRNA (C)
siRNA (H1)
G
PPARG2
FABP4
Fold change
H
siRNA (C)
siRNA (H1)

Figure 4. Exogenously added HTRA1 protein enhances hBMSC osteogenic differentiation. **(A-D):** Representative images of Alizarin red stained day 14 cultures of non-induced hBMSCs (non-induced control) and osteogenic induced hBMSCs (A), osteogenic induced hBMSCs previously treated with either proteolytically active (HTRA1ΔmacSA) or inactive (HTRA1ΔmacSA) HTRA1 (5 µg/ml) for 14 days (B) or 4 days (C), and osteogenic induced hBMSCs previously treated with proteolytically active HTRA1 (5 µg/ml) for 14 days in the presence or absence of AEBSF (20 µg/ml) (D). Data is representative of 3 independent experiments. Scale bar = 2 mm. **(E):** Quantitative polymerase chain reaction analysis of osteogenic gene expression in hBMSCs treated at day 7 with active HTRA1 (5 µg/ml) and harvested at day 10 post-osteogenic induction. Data was normalized to *GUSB* and expressed as fold change as compared to untreated cells (value 1) using the comparative C_T method. n = 3 separate experiments, ± S.D. * $p < 0.05$, ** $p < 0.01$ as determined by Student's *t*-test. Abbreviations: HTRA1, high temperature requirement protease A1; hBMSCs, human bone marrow-derived mesenchymal stem cells; AEBSF, 4-(2-Aminoethyl) benzenesulfonyl fluoride hydrochloride; *GUSB*, beta glucuronidase.

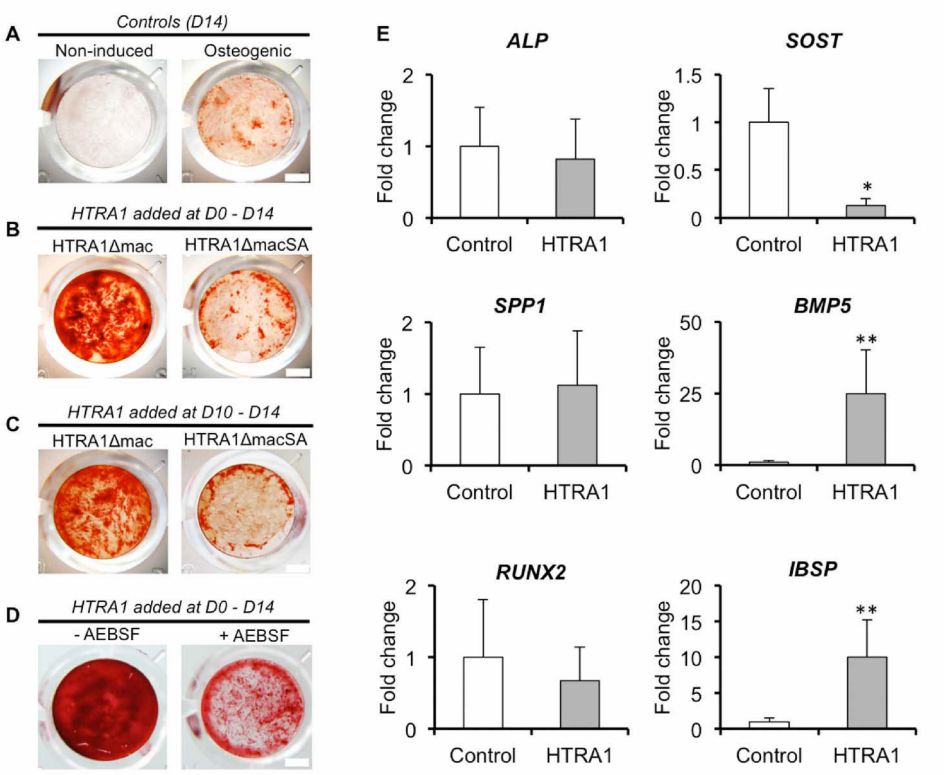

Figure 5. IBSP is an HTRA1 substrate in osteogenic MSC cultures. **(A):** Representative immunofluorescence micrographs of anti-IBSP (ID1.2) (green) and DAPI (blue) stained day 14 osteogenic hBMSCs cultures previously treated for 4 days with 5 µg/ml of either inactive HTRA1 (HTRA1ΔmacSA) or active HTRA1 (HTRA1Δmac). Scale bar = 75 µm. **(B):** Western blot analysis of an *in vitro* enzyme assay using recombinant human IBSP (476 nM) and HTRA1ΔmacSA (45 nM) or HTRA1Δmac (45 nM), incubated together for up to 24 h. Equal sample volumes were loaded onto an SDS-PAGE gel and IBSP protein detected using antibodies directed against either the N- or C-terminal regions of human IBSP. **(C):** Representative fluorescence images of anti-IBSP (ID1.2) (green), anti-HTRA1 (red) and DAPI (blue) stained mASC spheroids at 5 and 9 days post-osteogenic induction. Scale bar = 25 µm. Data is representative of 2 independent experiments. Abbreviations: HTRA1, high temperature requirement protease A1; hBMSCs, human bone marrow-derived mesenchymal stem cells; *IBSP,* Integrin-binding sialoprotein; DAPI, 4,6-diamidino-2-phenylindole; mASCs, mouse adipose-derived stromal cells.

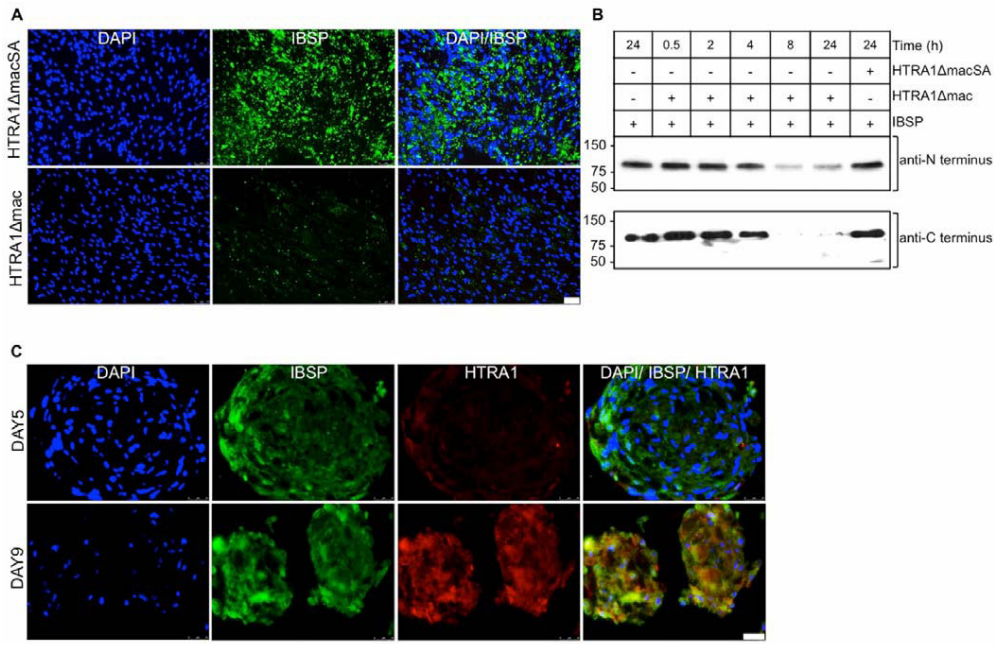

Figure 6. HTRA1 protein levels are increased during bone regeneration. **(A):** Representative micrograph of a hematoxylin and eosin stained paraffin wax section of decalcified mouse femur 7 days following a 0.22 µm osteotomy. Scale bar = 250 µm. **(B-F):** Representative micrographs of anti-HTRA1 (brown) stained paraffin wax sections of decalcified mouse femora (representative of n = 3) at 7 (B), 14 (C), 28 (D) and 42 (E) days following osteotomy. Non-operative femora served as controls (F). HTRA1 was visualized using horseradish peroxidase-diaminodenzidine and sections counterstained with hematoxylin. HTRA1 positive staining is identified in osteoid (*closed arrow heads*) at day 7 (B), in chondrocyte lacunae (*open arrow heads*) and soft tissue, *t,* at day 14 (C) and in sites of active bone regeneration (*arrows*) at day 28 (D). Scale bar = 100 µm. Abbreviations: *f*, fracture gap; *bm*, bone marrow; *cb*, cortical bone; HTRA1, high temperature requirement protease A1; DAPI, 4,6-diamidino-2-phenylindole.

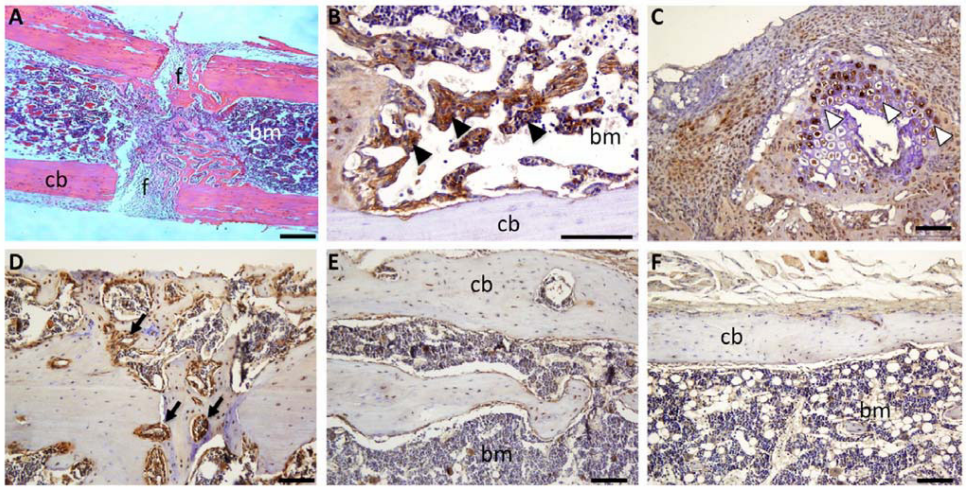

Figure 7. HTRA1 and IBSP co-localize during bone regeneration. Representative immunofluorescence micrographs of paraffin wax sections of decalcified mouse femora at 28 days following osteotomy stained with DAPI (blue), anti-IBSP (ID1.2) (green), and anti-HTRA1 (red). Scale bar = 50 µm. Abbreviations: *bm*, bone marrow; *cb*, cortical bone; HTRA1, high temperature requirement protease A1; IBSP, Integrin-binding sialoprotein; DAPI, 4,6-diamidino-2-phenylindole.

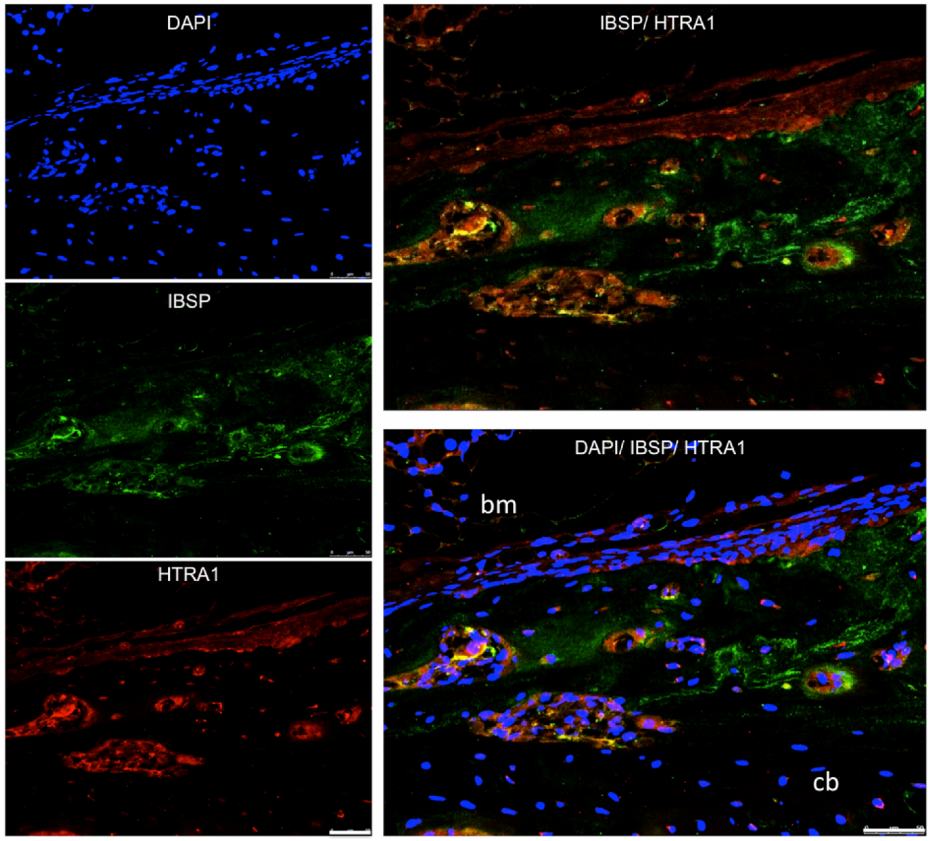

Supplementary Fig. 1. siRNA HTRA1 reduces HTRA1 protein within the ECM of hBMSCs. Representative immunofluorescence images of double staining for HTRA1 (red) and DAPI (blue) in HTRA1 siRNA (HTRA1 (H1)) or control siRNA (siRNA (C)) transfected hBMSCs after 10 days without (non-induced) or with (osteogenic) osteogenic induction. Scale bar = 75 µm. Abbreviations: HTRA1, high temperature requirement protease A1; ECM, extracellular matrix; hBMSCs, human bone marrow-derived mesenchymal stem cells; DAPI, 4,6-diamidino-2- phenylindole; siRNA, small interfering ribonucleic acid.

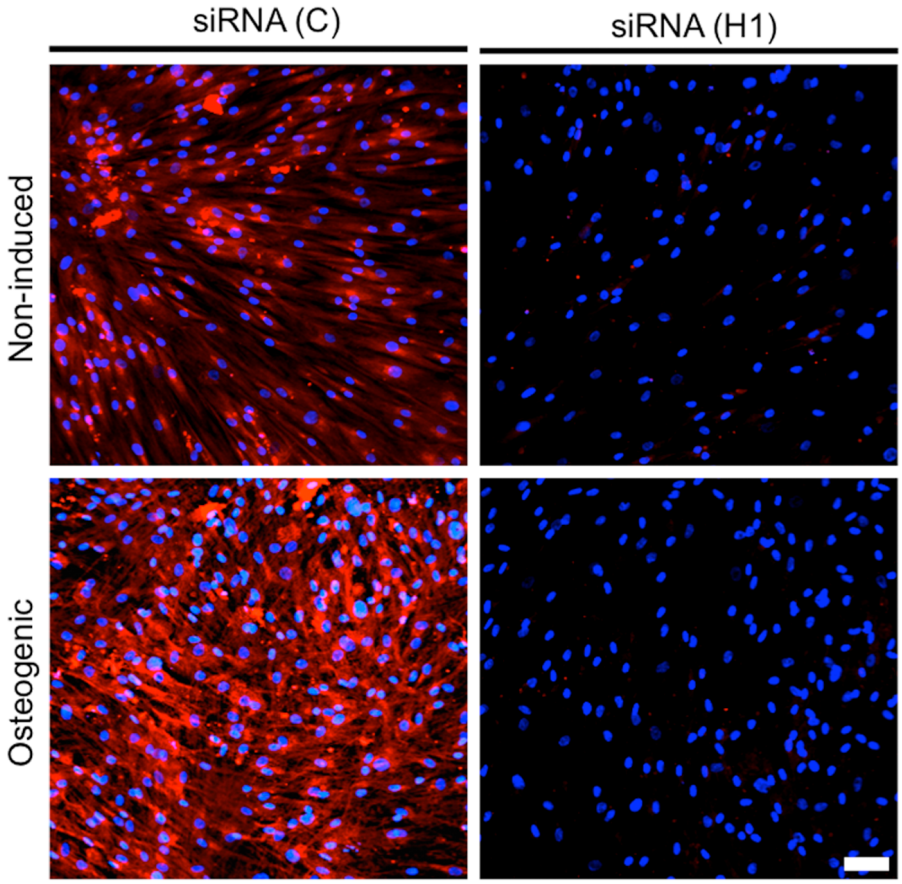

Supplementary Fig. 2. Exogenously added HTRA1 protein enhances hBMSC mineralization during the later stages of osteogenic differentiation only. Representative images of Alizarin red stained day 18 (D18) cultures of non-induced hBMSCs (non-induced) and osteogenic induced hBMSCs previously treated either without (osteogenic) or with proteolytically active HTRA1 (5 µg/ml) for the various times indicated. Data is representative of 3 independent experiments. Scale bar = 2 mm. Abbreviations: HTRA1, high temperature requirement protease A1; hBMSCs, human bone marrow-derived mesenchymal stem cells.

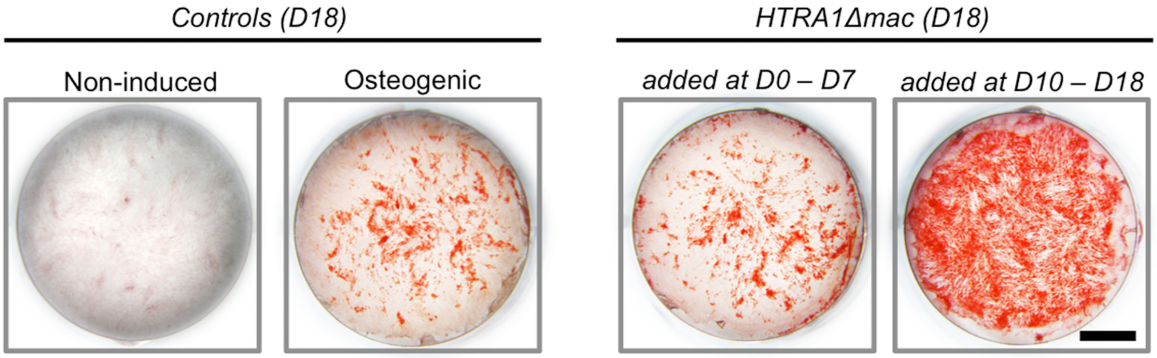

Supplementary Fig. 3. HTRA1 does not degrade collagen type I within the ECM of hBMSCs. Representative immunofluorescence images of COL1A1 (green) and DAPI (blue) in day 14 cultures of non-induced hBMSCs and osteogenic induced hBMSCs treated for 4 days without (untreated) or with 5 µg/ml of active (HTRA1 Δ mac) or inactive (HTRA1 Δ macSA) HTRA1. Scale bar = 75 µm. Abbreviations: HTRA1, high temperature requirement protease A1; hBMSCs, human bone marrow-derived mesenchymal stem cells; COL1A, collagen Type I; DAPI, 4,6- diamidino-2-phenylindole.

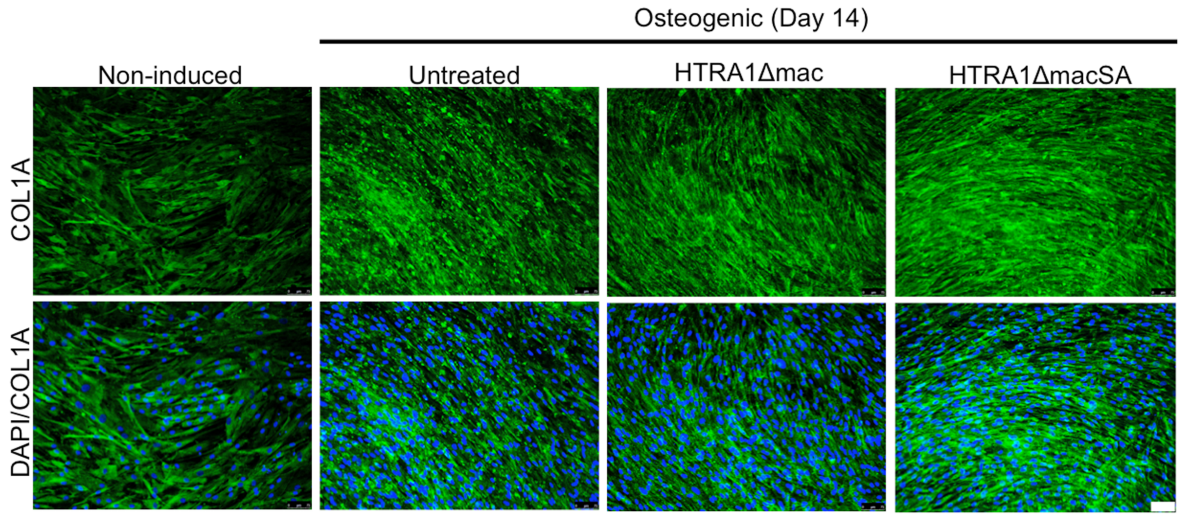

Supplementary Fig. 4. Osteogenic differentiation of mASC 3D-spheroids. (A-B): Alizarin red staining of mASC 3D-spheroids at 5 (A) and 9 (B) days post-osteogenic induction. Scale bar = 100 µm (C): Control immunofluorescence staining for HTRA1 and IBSP in mASC spheroids at 5 and 9 days post-osteogenic induction. Representative immunofluorescence images of spheroids stained with mouse IgG (M-IgG; green), rabbit IgG (R-IgG; red) and DAPI (blue). Data is representative of 2 independent experiments. Scale bar = 25 µm. Abbreviations: HTRA1, high temperature requirement protease A1; IBSP, Integrin-binding sialoprotein; mASC, mouse adipose-derived stromal cells; DAPI, 4,6-diamidino-2-phenylindole.

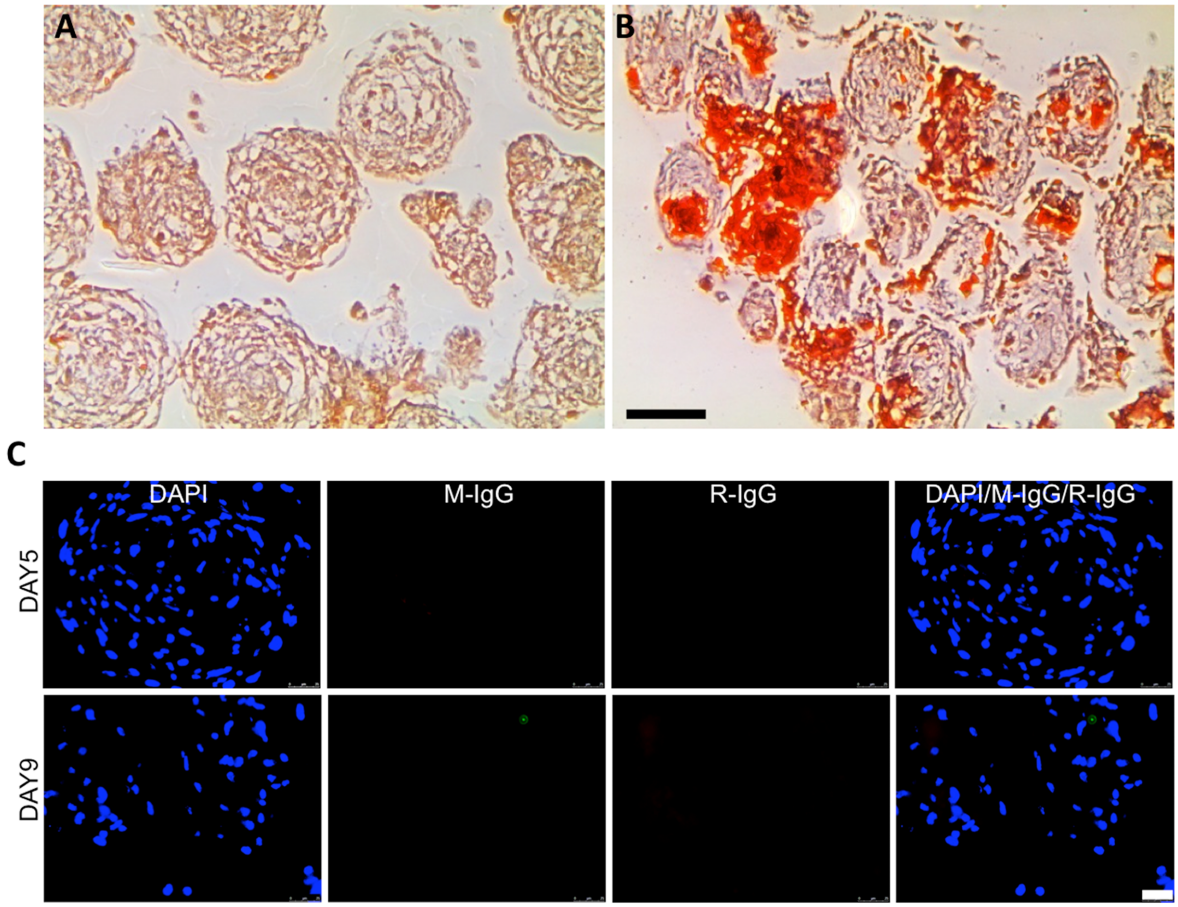

Supplementary Fig. 5. Immunohistochemical staining of HTRA1 in paraffin wax sections of mouse bone. (A-C): Representative micrographs of anti-HTRA1 (brown) stained paraffin wax sections of decalcified mouse femora (representative of n = 3) at 7 (A), 14 (B) and 28 (C) days following osteotomy. HTRA1 was detected in the periosteal layer, p, (A), non-mineralized callus tissue (B) and cuboidal cells localized within areas of active bone regeneration (white arrows) (C). HTRA1 was visualized using horseradish peroxidase-diaminodenzidine and sections counterstained with hematoxylin. Scale bar = 100 µm. Abbreviations: cb, cortical bone; HTRA1, high temperature requirement protease A1.

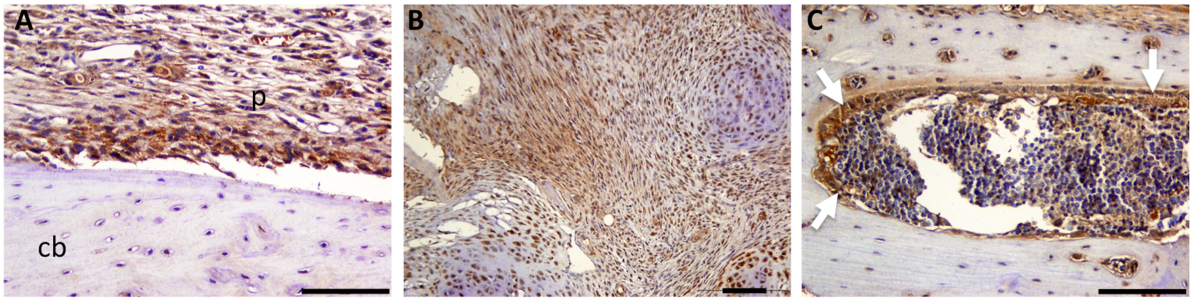

Supplementary Fig. 6. Control immunofluorescence staining for HTRA1 and IBSP in paraffin wax sections of mouse bone. Representative immunofluorescence images of paraffin wax sections of decalcified mouse femora (representative of n = 3) at 28 days following osteotomy stained with DAPI (blue), mouse IgG (M-IgG; green) or rabbit IgG (R-IgG; red). Scale bar = 50 μm. Abbreviations: HTRA1, high temperature requirement protease A1; IBSP, Integrin-binding sialoprotein; DAPI, 4,6-diamidino-2-phenylindole.

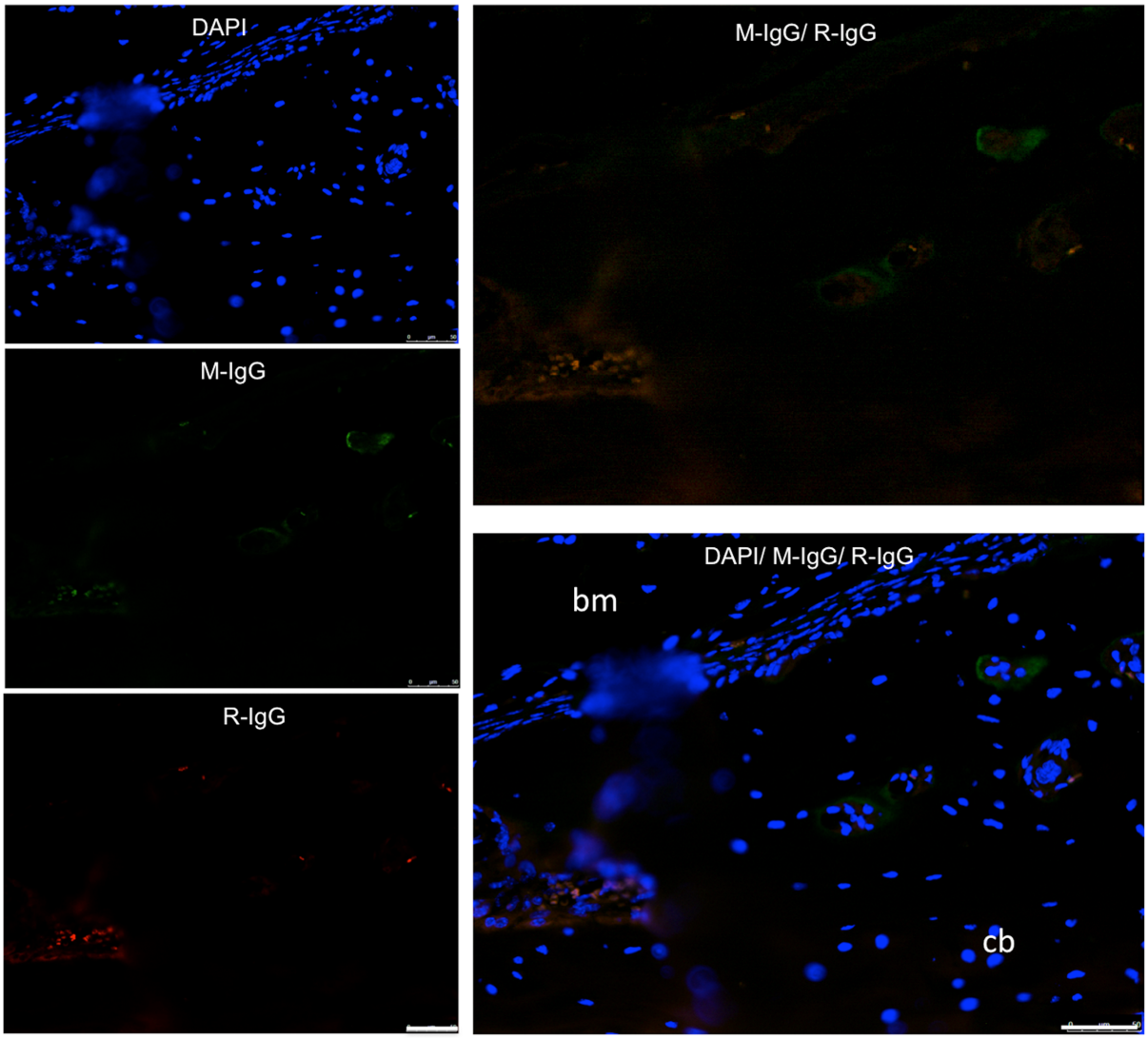

Supplementary Table 1. List of TaqMan Gene Expression Assays used in RT-PCR

Gene Symbol	Protein Product	Assay ID [a]
Mrps12	Mitochondrial ribosomal protein S12	Mm00488728_m1
HtrA1	High temperature requirement protease A1	Mm00479887_m1
GUSB	Beta glucuronidase	Hs99999908_m1
HTRA1	High temperature requirement protease A1	Hs01016151_m1
HTRA3	High temperature requirement protease A3	Hs01099710_m1
RUNX2	Runt-related transcription factor 2	Hs01047976_m1
ALP	Alkaline phosphatase	Hs00758162_m1
IBSP	Integrin-binding sialoprotein	Hs00173720_m1
SPP1	Secreted phosphoprotein 1/osteopontin	Hs00960942_m1
COL1A1	Collagen type 1A1	Hs00164004_m1
SOST	Sclerostin	Hs00228830_m1
BMP5	Bone morphogenetic protein 5	Hs00234930_m1
PPARG2	Peroxisome proliferator-activated receptor gamma 2	Hs01115513_m1
FABP4	Fatty acid binding protein 4	Hs01086177_m1

[a] *TaqMan Expression Assay identity code according to supplier (Applied Biosystems, Rotkreuz, Switzerland).*

Molecular Bases of Disease:

Detrimental Role for Human High Temperature Requirement Serine Protease A1 (HTRA1) in the Pathogenesis of Intervertebral Disc (IVD) Degeneration

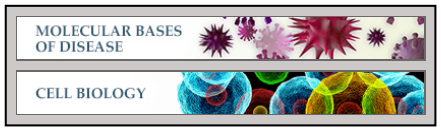

André N. Tiaden, Marina Klawitter, Vanda Lux, Ali Mirsaidi, Gregor Bahrenberg, Stephan Glanz, Lilian Quero, Thomas Liebscher, Karin Wuertz, Michael Ehrmann and Peter J. Richards

J. Biol. Chem. 2012, 287:21335-21345.
doi: 10.1074/jbc.M112.341032 originally published online May 3, 2012

THE JOURNAL OF BIOLOGICAL CHEMISTRY VOL. 287, NO. 25, pp. 21335–21345, June 15, 2012

Detrimental Role for Human High Temperature Requirement Serine Protease A1 (HTRA1) in the Pathogenesis of Intervertebral Disc (IVD) Degeneration*[S]

Received for publication, January 24, 2012, and in revised form, April 30, 2012 Published, JBC Papers in Press, May 3, 2012, DOI 10.1074/jbc.M112.341032

André N. Tiaden[‡1], Marina Klawitter[‡§1,2], Vanda Lux[¶], Ali Mirsaidi[‡‖3], Gregor Bahrenberg[‡‖2], Stephan Glanz[‡‖2], Lilian Quero[§4], Thomas Liebscher[**], Karin Wuertz[§‖‡‡4], Michael Ehrmann[¶], and Peter J. Richards[‡‖5]

From the [‡]Bone and Stem Cell Research Group and the [§]Spine Research Group, Center for Applied Biotechnology and Molecular Medicine, University of Zurich, 8057 Zurich, Switzerland, the [¶]Centre for Medical Biotechnology, Faculty of Biology and Geography, University Duisburg-Essen, 45117 Essen, Germany, the [‖]Institute of Physiology and Zurich Center for Integrative Human Physiology (ZIHP), University of Zurich, 8057 Zurich, Switzerland, the [**]Department of Spinal Surgery, SRH Klinikum Karlsbad-Langensteinbach, 76307 Karlsbad, Germany, and the [‡‡]AOSpine Research Network, 8600 Duebendorf, Switzerland

Background: HTRA1 has been associated with intervertebral disc (IVD) degeneration although its role is unknown.
Results: HTRA1 up-regulated matrix metalloproteinase (MMP) production by IVD cells via the generation of fibronectin fragments.
Conclusion: HTRA1 plays a detrimental role in the pathogenesis of IVD degeneration.
Significance: HTRA1 may represent a novel therapeutic target for the treatment of spinal disc degeneration.

Human HTRA1 is a highly conserved secreted serine protease that degrades numerous extracellular matrix proteins. We have previously identified HTRA1 as being up-regulated in osteoarthritic patients and as having the potential to regulate matrix metalloproteinase (MMP) expression in synovial fibroblasts through the generation of fibronectin fragments. In the present report, we have extended these studies and investigated the role of HTRA1 in the pathogenesis of intervertebral disc (IVD) degeneration. *HTRA1* mRNA expression was significantly elevated in degenerated disc tissue and was associated with increased protein levels. However, these increases did not correlate with the appearance of rs11200638 single nucleotide polymorphism in the promoter region of the *HTRA1* gene, as has previously been suggested. Recombinant HTRA1 induced MMP production in IVD cell cultures through a mechanism critically dependent on MEK but independent of IL-1β signaling. The use of a catalytically inactive mutant confirmed these effects to be primarily due to HTRA1 serine protease activity. HTRA1-induced fibronectin proteolysis resulted in the generation of various sized fragments, which when added to IVD cells in culture, caused a significant increase in MMP expression. Furthermore, one of these fragments was identified as being the amino-terminal fibrin- and heparin-binding domain and was also found to be increased within HTRA1-treated IVD cell cultures as well as in disc tissue from patients with IVD degeneration. Our results therefore support a scenario in which HTRA1 promotes IVD degeneration through the proteolytic cleavage of fibronectin and subsequent activation of resident disc cells.

Degeneration of the intervertebral disc (IVD)[6] is now regarded as one of the major causes of lower back pain, which is a highly prevalent, debilitating, and costly disorder (1, 2). The pathogenesis of degeneration is a highly complex and poorly understood process with many different genetic, biological, and mechanical influences playing key roles in the breakdown of extracellular matrix (ECM) components (3). The predominant means by which ECM is degraded is thought to be due to the proteolytic actions of matrix metalloproteinases (MMPs) and aggrecanases (ADAMTS). A number of MMPs, including MMP-1, -3, -7, -9, and -13, as well as ADAMTS-4, have been shown to increase in the IVD during disc degeneration and are responsible for the breakdown of several matrix components, the most notable being aggrecan and collagen (4–7). Both MMPs and their inhibitors (TIMP-1, -2, and -3) have been localized to the resident chondrocyte-like cells of the nucleus pulposus and inner fibrosus compartments of the IVD (4), thus implicating these cells in disease pathogenesis. The secretion of MMPs by human IVD cells is mediated in part through the stimulatory effects of various pro-inflammatory cytokines, the most prominent of which is IL-1β (8). In addition, fibronectin peptide fragments of the ECM have also been shown to induce MMP production by IVD cells (9) and are potent instigators of experimental disc degeneration (10). Moreover, fibronectin fragments have been shown to accumulate in the IVD during

* This work was supported by a grant from the Center for Applied Biotechnology and Molecular Medicine Start-up Grant/Mäxi Foundation.
[S] This article contains supplemental Table 1 and Figs. 1–4.
[1] Both authors contributed equally to this work.
[2] Supported by grants from the Swiss National Science Foundation.
[3] Supported by grants from the Stiftung Osteoporose Schweiz and Forschungskredit UZH, University of Zurich.
[4] Supported by grants from AOSpine. We thank Dr. Jurgen Klasen (University Hospital Balgrist, University of Zurich, Zurich, Switzerland) for providing fresh human disc biopsies used for all cell culture experiments.
[5] To whom correspondence should be addressed: Center for Applied Biotechnology and Molecular Medicine, University of Zürich, Winterthurerstrasse 190, Zürich 8057, Switzerland. Tel.: 41-44-635-3801; Fax: 41-44-635-6840; E-mail: peter.richards@cabmm.uzh.ch.

[6] The abbreviations used are: IVD, intervertebral disc; ECM, extracellular matrix; SNP, single nucleotide polymorphism; MMP, matrix metalloproteinase; IL-1RA, IL-1 receptor antagonist; ANOVA, analysis of variance; qRT-PCR, quantitative RT-PCR.

degeneration (11), although the proteases responsible for their formation remain elusive.

Human HTRA1 (high temperature requirement serine protease A1) belongs to a well defined family of serine proteases originally identified in bacteria (12). Although primarily regarded as a key regulator of tumor development and subsequent malignancies (13–15), a growing body of evidence now exists to suggest that HTRA1 may also play a central role in determining the outcome of various musculoskeletal disease pathologies, including Duchenne muscular dystrophy (16), osteoarthritis (17–19), and rheumatoid arthritis (19, 20). It has recently been shown in a Japanese population study that a single nucleotide polymorphism (SNP) located within the HTRA1 promoter is associated with spinal disc degeneration, where increases in spinal disc narrowing were observed in patients without the G allele (AA) as compared with those bearing at least one G allele (GG + GA) (21). It would therefore appear that HTRA1 may also play a role in disc pathology, although its influence on disease and its mechanism of action have not yet been elucidated.

Observations from our own studies examining the role of HTRA1 in osteoarthritis imply that HTRA1 may actually have a detrimental effect on the pathogenesis of musculoskeletal disease. Elevated levels of HTRA1 protein were measured in the synovial fluid from osteoarthritic patients, and primary synovial fibroblasts isolated from diseased patients were identified as being a major source of HTRA1 (19). The addition of proteolytically active HTRA1 to fibroblast cultures resulted in marked up-regulation of various MMPs, including MMP-1 and MMP-3, both of which have been implicated in cartilage and joint destruction in arthritic patients. Further experiments confirmed that the stimulatory effects of HTRA1 on MMP expression were protease-dependent and were related to the formation of fibronectin fragments due to extracellular degradation. Such observations are therefore strongly suggestive of a central role for HTRA1 in joint degeneration through its proteolytic actions on ECM components and thus may also be indicative of its role in other disease pathologies, such as disc degeneration.

In the current study, we used IVD tissue and cell samples from surgical patients in order to further investigate the potential involvement of HTRA1 in IVD degeneration. Our findings implicate HTRA1 as a key factor in the underlying pathology associated with IVD degeneration. HTRA1 may therefore represent a novel target for the development of more effective therapeutic strategies to treat this debilitating condition.

EXPERIMENTAL PROCEDURES

Materials—Human fibronectin and rabbit IgG were purchased from R & D Systems (Abingdon, UK). IL-1 receptor antagonist (IL-1RA) was obtained from Abcam (Cambridge, UK), and MEK1/2 inhibitors PD98059 and U0126 were from Sigma-Aldrich (Buchs, Switzerland). Monoclonal antibodies against the fibronectin carboxyl-terminal heparin-binding domain (Mab1935) and the amino-terminal fibrin- and heparin-binding domain (Mab1936) were from Chemicon International. A polyclonal anti-HTRA1 antibody was generated as described previously (19). All anti-IgG horseradish peroxidase (HRP)-conjugated, fluorescence-conjugated secondary antibodies and normal serum were from Jackson ImmunoResearch (Suffolk, UK). DAPI was purchased from Sigma-Aldrich. Collagenase NB4 was purchased from Serva/Promega (Duebendorf, Switzerland), and dispase II was from Roche Applied Science (Rotkreuz, Switzerland).

Tissue Harvesting—IVD tissue and/or blood was obtained from a total of 39 patients undergoing spinal surgery for symptomatic degenerative disc disease, disc herniation, or spinal trauma following informed consent in accordance with the local ethical guidelines (carried out at the SRH Clinic Karlsbad-Langensteinbach, Karlsbad, Germany). The degree of IVD degeneration in patients was assessed prior to surgical intervention by magnetic resonance imaging (MRI) using a four-level grading system based on Pfirrmann's classification of disc degeneration (22). Degeneration grades were assigned as follows: grade 1, non-degenerated (normal disc height); grade 2, mild degeneration (slight decrease in disc height); grade 3, moderate degeneration (moderate decrease in disc height); grade 4, severe degeneration (collapsed disc space).

Isolation and Culture of IVD Cells—Human IVD cells were isolated from the discs of a total of 14 patients undergoing spinal surgery for disc herniation (carried out at Balgrist University Hospital, Zürich, Switzerland) as described previously (23). Briefly, IVD tissue was enzymatically digested (0.2% collagenase NB4, 0.3% dispase II) for 4–8 h, and cells were thereafter cultured in growth medium consisting of DMEM/F-12 supplemented with 10% FCS, penicillin (50 units/ml), streptomycin (50 μg/ml), and amphotericin B (25 μg/ml) and incubated at 37 °C with 5% CO_2 and used at passages 2–3.

Recombinant Human HTRA1—Purified recombinant His-tagged HTRA1 in which the amino-terminal mac25 homology domain was absent (termed HTRA1Δmac) was produced in *Escherichia coli* and purified using Ni^{2+}-NTA chromatography as described previously (19, 24). The enzymatically inactive mutated form of HTRA1Δmac, termed HTRA1ΔmacSA, was generated through conversion of residue serine 328 to alanine by mutagenesis.

Stimulation of IVD Cells with Recombinant HTRA1—IVD cells were cultured in 6-well plates at 3.5×10^5 cells/well and serum starved for 2 h prior to stimulation. Cells were incubated in medium alone or in medium supplemented with either HTRA1Δmac (5 μg/ml) or HTRA1ΔmacSA (5 μg/ml) for up to 24 h. Concentrations used were based on previous observations using human synovial fibroblasts (19). After this time, RNA and culture supernatants were harvested for further analysis. In the case of inhibition studies, IVD cells were preincubated with either PD98059 (10 μM), U0126 (10 μM), or IL-1RA (250 ng/ml) for 2 h prior to stimulation.

Quantitative RT-PCR (qRT-PCR)—Total RNA was isolated from either intact IVD tissue or cells and purified using TRIzol reagent (Invitrogen AG, Basel, Switzerland) according to the manufacturer's instructions. RNA (0.5 μg) was reverse transcribed to cDNA using Superscript II (Invitrogen AG) and random hexanucleotide primers (Promega AG, Dübendorf, Switzerland). Quantification of mRNA expression was performed with TaqMan Gene Expression Assays (Applied Biosystems, Rotkreuz, Switzerland) (supplemental Table 1) using the StepOnePlus real-time PCR system (Applied Biosystems), and

values were normalized to *GAPDH* mRNA levels and presented as -fold change according to the $2^{-\Delta\Delta}C_T$ method. In cases where individual patients ($n = 36$) were compared for expression levels of *HTRA1* and *FN* mRNA in IVD tissue, data were normalized to *TBP* and presented as $2^{-\Delta}C_T$. Each 10-μl reaction consisted of 1× TaqMan fast universal PCR master mix (Applied Biosystems), 1× TaqMan gene expression assay, and 10 ng of cDNA (based upon initial RNA concentrations). All reactions were performed in triplicate in fast optical 96-well reaction plates (Applied Biosystems) at 95 °C for 20 s and 40 cycles of 95 °C for 1 s and 60 °C for 20 s.

SNP Analysis—A total of 35 patients were genotyped using a TaqMan SNP genotyping assay specific for the SNP, rs11200638, according to the manufacturer's instructions (Applied Biosystems). Patients were grouped according to their individual genotypes, and association studies were performed in order to determine the influence of the rs11200638 (A) risk allele on susceptibility to IVD degeneration. The influence of rs11200638 on *HTRA1* expression in IVD tissue was also assessed in patients from whom both RNA and DNA samples were obtained ($n = 32$).

Western Blot Analysis of Patient IVD Tissue—Patient IVD samples ($n = 12$) were selected based on degeneration grade. Protein was extracted using CelLytic M (Sigma-Aldrich) containing a protease inhibitor mixture (Sigma-Aldrich), and protein amounts were determined initially by a Bio-Rad protein assay (Bio-Rad, Reinach, Switzerland). Protein samples were boiled for 5 min in loading buffer (50 mM Tris-HCl, pH 6.8, 2% SDS, 10% glycerol, 100 mM DTT, 0.002% bromphenol blue), and equal amounts of protein were loaded onto 12% SDS-polyacrylamide gels. Further corrections to the loading volumes were made following densitometric analysis of Coomassie Blue-stained gels, thus allowing for accurate comparisons to be made between individual patient samples. Protein was then electroblotted onto PVDF membranes using the Trans-Blot Turbo blotting system (Bio-Rad) and incubated in 5% skim milk, 50 mM Tris-HCl, pH 7.6, 150 mM NaCl, 0.1% Tween 20 (TBST) for 1 h at room temperature. Membranes were then incubated for 1 h at room temperature with either rabbit anti-human HTRA1 (1:2000) or mouse anti-fibronectin amino-terminal fibrin- and heparin-binding domain (Mab1936) (1 μg/ml). After washing in TBST three times for 5 min each, membranes were incubated with a HRP-conjugated anti-mouse or anti-rabbit IgG (1:10,000) for 1 h at room temperature. Following a further washing step, peroxidase activity was detected using SuperSignal West Pico Chemiluminescent Substrate (Thermo Scientific, Lausanne, Switzerland).

Immunofluorescence Microscopy—Unfixed frozen IVD tissue sections were air-dried for 20 min, blocked with normal goat serum (1:10), and incubated with polyclonal anti-HTRA1 (1:50) or control rabbit IgG (2 μg/ml) in phosphate-buffered saline (PBS), pH 7.3, 1% BSA for 16 h at 4 °C. Tissue samples containing HTRA1 were then identified using goat anti-rabbit-Cy3 (1:400). Sections were mounted in Mowiol/DABCO (1,4-diazabicyclo[2.2.2]octane) (Sigma-Aldrich) containing DAPI (0.5 g/ml), and images were captured using the Leica DMI6000B automated inverted research microscope system (Leica Microsystems).

Quantification of Secreted MMP-3—MMP-3 protein levels in culture supernatants were determined using an MMP-3-specific ELISA kit according to the manufacturer's instructions (R & D Systems).

Proteolytic Enzyme Assays—Degradation of fibronectin by HTRA1Δmac was determined using methods described previously (19). Briefly, HTRA1Δmac and recombinant human fibronectin, in an equimolar ratio, were incubated together in Tris-buffered saline (TBS), pH 8.5, for 16 h at 37 °C. In some reactions, HTRA1Δmac was replaced by proteolytically inactive HTRA1ΔmacSA. Fibronectin, HTRA1Δmac, and HTRA1ΔmacSA were also incubated separately under the same conditions and served as controls. In order to assess whether HTRA1Δmac could also generate fibronectin fragments in IVD cell cultures, supernatants (20 ml) were harvested from cells treated with HTRA1Δmac (5 μg/ml) or HTRA1ΔmacSA (5 μg/ml) for 24 h and concentrated using Amicon Ultra-15, 10,000 molecular weight cut-off filter units (Millipore). Fibronectin fragments were analyzed on 4–15% Mini-PROTEAN TGX Precast gels (Bio-Rad) by Coomassie Blue staining and immunoblotting using either mouse anti-fibronectin carboxyl-terminal heparin-binding domain (Mab1935) (1 μg/ml) or mouse-anti-fibronectin amino-terminal fibrin- and heparin-binding domain (Mab1936) (1 μg/ml) as described above. The EnzCheck elastase kit (Molecular Probes, Basel, Switzerland) was used to confirm the proteolytic activity of recombinant HTRA1 proteins according to the manufacturer's protocol.

Effect of Fibronectin Fragments on MMP Expression—Equimolar concentrations of fibronectin (20 μg) and HTRA1Δmac (5 μg) were incubated under the conditions described above. Control reactions were also performed and included TBS, pH 8.5, alone or in combination with either fibronectin or HTRA1Δmac. Samples were then diluted into equilibration buffer containing TBS, pH 7.6, with 20 mM imidazole and incubated with 50 μl of pre-equilibrated HisPur Ni^{2+}-NTA resin (Qiagen, Hombrechtikon, Switzerland) in spin columns (Thermo Scientific) for 1 h at 4 °C. Columns were then centrifuged for 5 min at 1600 rpm, and the affinity column flow-through fraction was collected, dialyzed in TBS for 4 h at 4 °C using Slide-A-Lyzer MINI dialysis devices (3500 molecular weight cut-off) (Thermo Scientific), and then incubated with IVD cells for up to 24 h, after which time MMP expression was evaluated by qRT-PCR.

Statistical Analysis—All statistical analyses were carried out using SPSS19.0 (SPSS Inc., Chicago, IL). Parametric analysis of normally distributed data were performed using the two-tailed unpaired Student's t test or one-way analysis of variance (ANOVA) followed by Tukey's post hoc tests for multiple-group comparisons. Pearson's correlation coefficient was used to evaluate the relationship between the expression levels of selected genes in patient tissue samples. The χ^2 test was used to compare allele frequencies in patients with or without IVD degeneration (1 degree of freedom). In all cases, a p value of <0.05 was considered statistically significant.

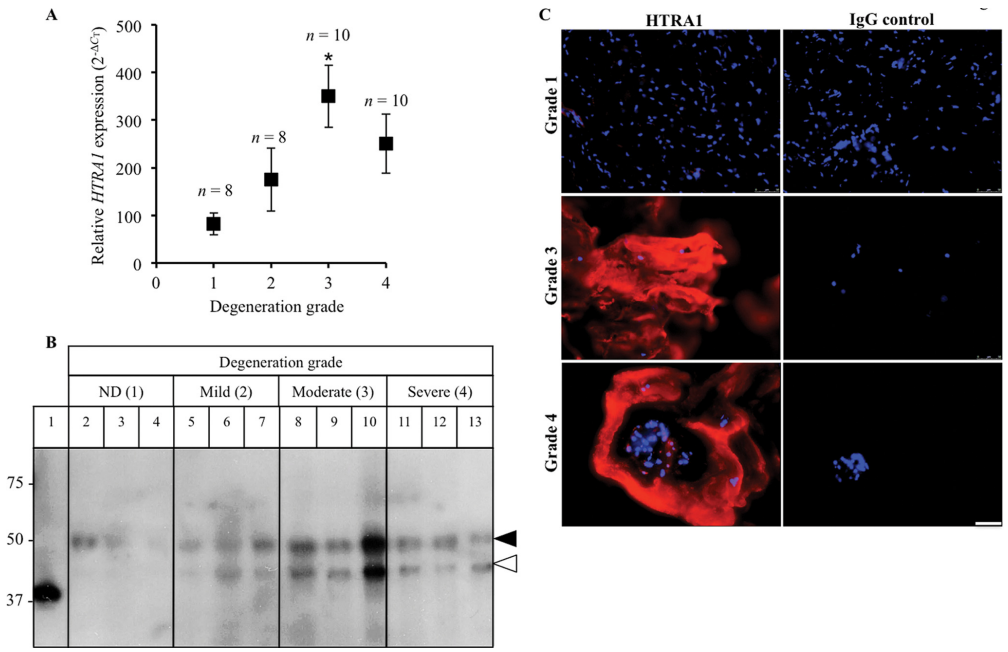

FIGURE 1. **Detection of HTRA1 in human IVD tissue.** *A*, *HTRA1* mRNA levels in intact IVD tissue samples from patients ($n = 36$) with varying degrees of IVD degeneration were determined by qRT-PCR and presented as $2^{-\Delta}C_T$. *, $p < 0.05$, as determined by one-way ANOVA *Error bars*, S.E. *B*, protein extracts from patient IVD tissues ($n = 12$) were loaded onto a 12% SDS-polyacrylamide gel, and immunoblotting was performed using a polyclonal antibody specific for HTRA1. *Lane 1*, *HTRA1Δmac* (4 ng); *lanes 2–4*, non-degenerated (*ND*) discs; *lanes 5–7*, mildly degenerated discs; *lanes 8–10*, moderately degenerated discs; *lanes 11–13*, severely degenerated discs. *Closed arrowhead*, 50-kDa HTRA1; *open arrowhead*, 42-kDa HTRA1. *C*, representative images of HTRA1 protein within frozen IVD tissue sections as identified by immunofluorescence staining. HTRA1 was detected using a Cy3-labeled secondary antibody (*red*), and nuclei were labeled with DAPI (*blue*). The specificity of staining was confirmed through the use of a nonspecific rabbit IgG control (*IgG*). Grade 1 represents a normal, non-degenerated IVD, whereas grades 3 and 4 signify moderate and severe degeneration, respectively. *Scale bar*, 50 μm.

RESULTS

We have previously demonstrated that HTRA1 plays a central role in the regulation of MMP expression in synovial fibroblasts from arthritic patients and that its stimulatory effects may be linked to the generation of fibronectin fragments (19). In the present report, we further investigated this property of HTRA1 in IVD cell cultures and aimed to establish its potential role in IVD degeneration.

Identification of HTRA1 in Patient Tissue—HTRA1 mRNA levels within IVD tissue samples from patients with varying degrees of disc degeneration were normalized to *TBP* and presented as $2^{-\Delta}C_T$. Expression levels significantly correlated ($r = 0.375$; $p = 0.024$) with patient degeneration grade and were found to be markedly increased in patients with severity scores of 3 (4-fold; $p = 0.015$) and 4 (3-fold; $p = 0.2$) as compared with control patients (Fig. 1*A*). Western blot analysis of IVD protein samples using a polyclonal antibody against HTRA1 identified two main species of HTRA1 protein migrating at ~50 kDa (*closed arrowhead*) and ~42 kDa (*open arrowhead*), which most likely represented the full-length and processed forms of HTRA1, respectively (Fig. 1*B* and supplemental Fig. 1) (25). The 50-kDa HTRA1 was found at varying levels in the majority samples tested, whereas the 42-kDa form of HTRA1 was identified in degenerated IVD protein samples only and was noticeably increased in the more severely affected discs. HTRA1 protein was also identified within both the cells and ECM of frozen IVD tissue sections, as determined by immunofluorescence staining, and levels were found to be increased in the more severely affected patients as compared with the control trauma patients (Fig. 1*C*).

Analysis of Patient rs11200638 SNP Genotype—In light of the recent evidence linking the rs11200638 SNP (G>A) in the *HTRA1* gene promoter and spinal disc degeneration in Japanese women (21), we investigated whether the rs11200638 risk allele frequency between patient groups used in the current study was associated with susceptibility to IVD degeneration. DNA from a total of 35 patients was subjected to SNP genotyping using the TaqMan SNP genotyping assay specific for rs11200638 SNP. Contrary to previous expectations, we were unable to demonstrate any significant differences in SNP allele frequencies between control patients without disc degeneration (25%) and patients with degeneration grades of 2 (14.3%; $p = 0.4$), 3 (15%; $p = 0.37$), or 4 (15%; $p = 0.37$) (Table 1). We also performed a comparative analysis of *HTRA1* expression levels in IVD tissue from 32 patients of known genotype. However, no significant associations could be made between

TABLE 1
rs11200638 SNP Genotyping of European patients with and without IVD degeneration

	Degeneration grade						
Genotype	**1 (n = 8)**	**2 (n = 7)**	**3 (n = 10)**	**4 (n = 10)**	**n**	**Relative *HTRA1* expression[a]**	**p value[b]**
GG	5	5	7	7	23	204.1 ± 35.6	
GA	2	2	3	3	8	307 ± 87.3	0.20
AA	1	0	0	0	1	14.9	
GA + AA	3	2	3	3	9	274.5 ± 83.5	0.37
G allele	12	12	17	17			
A allele[c]	4 (25%)	2 (14.3%) $p = 0.4$[d]	3 (15%) $p = 0.37$[d]	3 (15%) $p = 0.37$[d]			

[a] Comparisons were made between *HTRA1* expression levels ± S.E. in IVD tissue and genotype frequency in patients where both RNA and DNA samples were available (n = 32).
[b] Student's t test was used to compare *HTRA1* expression levels between patients carrying the risk allele (GA/AA) and those homozygous for the wild type allele (GG).
[c] Percentages refer to risk allele (A) frequency.
[d] The χ^2 test was used to evaluate the significance of differences in risk allele (A) frequency between patients with IVD degeneration (grades 2–4) and control patients without IVD degeneration (grade 1) (n = 35).

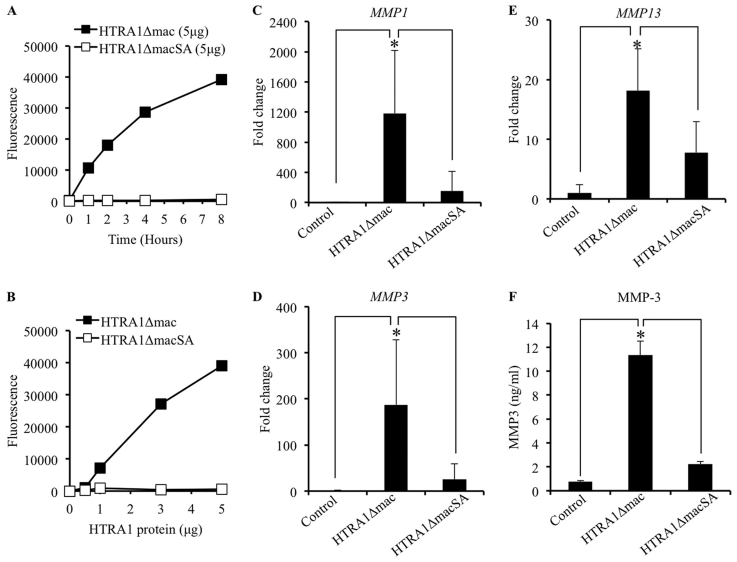

FIGURE 2. **Regulation of MMP expression in IVD cells by recombinant HTRA1.** *A* and *B*, recombinant HTRA1 proteolytic activity was determined using soluble bovine BODIPY FL-labeled DQ-elastin (100 μg/ml) as a substrate. Digestion of the DQ-elastin yielded fluorescent fragments detectable at 530 nm by a fluorescence microplate reader. The amount of DQ-elastin digestion was measured at selected time points (0, 1, 2, 4, and 8 h) using a defined amount of HTRA1 (5 μg) (*A*) or was determined after incubation for 8 h with varying amounts of HTRA1 (0, 0.5, 1, 3, and 5 μg) (*B*). *C–E*, the effects of recombinant HTRA1 (5 μg/ml) on MMP expression levels in IVD cells after a 24-h incubation period were determined by qRT-PCR, and the -fold change as compared with untreated controls was determined using the $2^{-\Delta\Delta C_T}$ method (n = 4–6 patients). *F*, a specific MMP-3 ELISA was used to investigate the effects of recombinant HTRA1 on MMP protein secretion in supernatants obtained from IVD cells. Shown are results of triplicate determinations ± S.D. (*error bars*). *, $p < 0.01$, as determined by one-way ANOVA.

HTRA1 expression levels and the rs11200638 genotype (Table 1).

Effect of Recombinant HTRA1 on MMP Production by IVD Cells—In order to investigate how HTRA1 may contribute to IVD degeneration, we generated both proteolytically active and inactive recombinant forms of HTRA1 lacking the amino-terminal mac25 homology domain as described previously (19). The protease activity of the active protein, termed HTRA1Δmac, was confirmed by its ability to cleave purified bovine elastin and was dependent on both incubation time (Fig. 2*A*) and protein amount (Fig. 2*B*). No such activity was observed with the proteolytically inactive form of HTRA1 (HTRA1ΔmacSA) in which serine 328, part of the serine protease catalytic triad domain, had been substituted for alanine. The effects of these recombinant proteins on MMP production by cultured IVD cells were then investigated. Cells were incubated for up to 24 h with either HTRA1Δmac (5 μg/ml) or HTRA1ΔmacSA (5 μg/ml), and the -fold change in mRNA expression levels of *MMP1*, *MMP3*, and *MMP13* was determined by qRT-PCR. HTRA1Δmac induced a significant increase in the expression levels of MMPs tested as compared with untreated cells and cells treated with the proteolytically inactive HTRA1ΔmacSA (Fig. 2, *C–E*). In addition, HTRA1Δmac also enhanced the expression of *ADAMTS4* (aggrecanase-1), although no increase was observed in *MMP2* (gelatinase A) expression, and *ACAN* (aggrecan) expression was actually reduced (supplemental Fig. 2). MMP expression was also up-regulated in HTRA1ΔmacSA-treated cells,

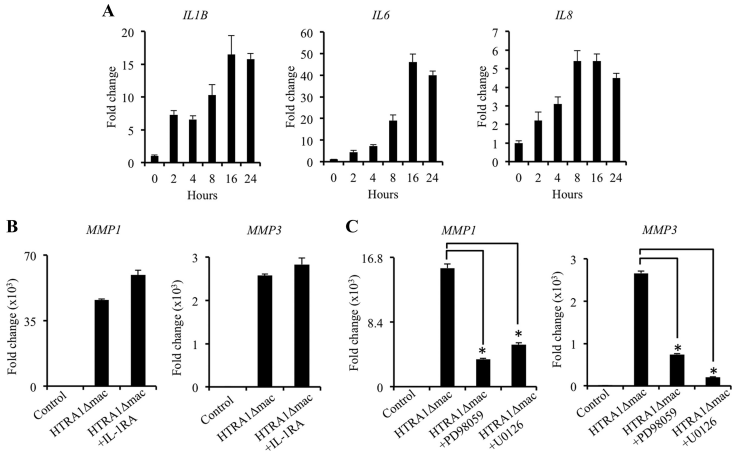

FIGURE 3. **Down-regulation of HTRA1-induced MMP expression in IVD cells by MEK inhibition.** *A*, *IL1B*, *IL6*, and *IL8* mRNA expression levels were measured in IVD cell cultures by qRT-PCR in response to HTRA1Δmac (5 μg/ml) stimulation over the course of 24 h, and the -fold change as compared with untreated cells was determined using the $2^{-\Delta\Delta}C_T$ method. *B*, the influence of IL-1β inhibition on HTRA1-induced *MMP1* and *MMP3* expression by IVD cells was evaluated by qRT-PCR after a 24-h incubation with HTRA1Δmac (5 μg/ml) in combination with the IL-1RA (250 ng/ml), and the -fold change as compared with untreated controls was determined using the $2^{-\Delta\Delta}C_T$ method. *C*, the effects of MEK inhibitors PD98059 (10 μM) and U0126 (10 μM) on HTRA1-induced *MMP1* and *MMP3* expression by IVD cells were evaluated by qRT-PCR after a 24-h incubation, and the -fold change as compared with untreated controls was determined using the $2^{-\Delta\Delta}C_T$ method. In each case, data are representative of at least two separate experiments performed using IVD cells isolated from a total of $n = 5$ patients. Shown are results of triplicate determinations ± S.D. (*error bars*). *, $p < 0.01$, as determined by one-way ANOVA.

although expression levels were over 3–7-fold less than those observed in cells incubated with HTRA1Δmac and were not deemed statistically significant as compared with untreated control cells (*MMP1*, $p = 0.19$; *MMP3*, $p = 0.41$; *MMP13*, $p = 0.41$). Clearly, therefore, HTRA1-induced MMP expression in IVD cells is primarily a protease-dependent phenomenon, although it would appear that other routes of activation may also exist. In addition to its stimulatory effects on MMP mRNA expression, HTRA1Δmac also enhanced MMP protein production, as evidenced by results obtained from the MMP-3 ELISA (Fig. 2*F*). Low levels of secreted MMP-3 were detected in the supernatants of untreated cells (0.76 ng/ml ± 0.04) but became significantly elevated following stimulation with HTRA1Δmac (11.33 ng/ml ± 0.68; $p < 0.001$). As with our previous findings, these stimulatory effects of HTRA1 were significantly diminished following inactivation of its protease activity, although levels remained elevated as compared with untreated cells (2.23 ± 0.13 ng/ml; $p = 0.089$).

Influence of MEK and IL-1β Inhibition on HTRA1-induced MMP Production—Of the known instigators of MMP expression by IVD cells, IL-1β is considered to be the most potent and, as such, is centrally involved in both IVD cell activation and IVD degeneration (8). Furthermore, IL-1β has previously been shown to play a central role in mediating MMP production by fibronectin fragments in cultures of bovine articular cartilage (26). We therefore investigated if the expression of IL-1β, along with several other cytokines, including IL-6 and IL-8, was up-regulated in IVD cells by HTRA1Δmac and whether this had any influence on the induction of MMP expression by HTRA1Δmac. Indeed, expression levels of the cytokines tested were up-regulated in IVD cells stimulated with HTRA1Δmac (5 μg/ml) in a time-dependent manner (Fig. 3*A*). However, additional studies focusing on the inhibition of IL-1β signaling using the IL-1RA (250 ng/ml) failed to demonstrate any significant alterations in the ability of HTRA1 to induce MMP expression in IVD cells (Fig. 3*B* and supplemental Fig. 3). This would suggest that HTRA1 does not mediate its stimulatory effects through IL-1β production, although we cannot exclude the possibility that other cytokines may be involved.

We have previously demonstrated that MMP expression by human synovial fibroblasts is up-regulated in response to HTRA1 stimulation and that this was at least partly dependent on the generation of fibronectin fragments (19). Furthermore, fibronectin fragments were recently confirmed as being potent inducers of MMP expression in IVD cells, mediating their effects through activation of the MEK pathway (27). We therefore investigated whether inhibition of MEK could influence the actions of HTRA1 on IVD MMP expression. Indeed, inclusion of either of the specific MEK inhibitors PD98059 (10 μM) or U0126 (10 μM) 2 h prior to treatment with HTRA1Δmac (5 μg/ml) significantly abrogated its stimulatory effects on the expression of *MMP1* and *MMP3* (Fig. 3*C*), thereby supporting the theory that fibronectin fragments may represent one possible route through which HTRA1 mediates its stimulatory effects on IVD cells.

Effect of Fibronectin Fragments on MMP Expression by IVD Cells—Based on the above results, we further investigated the potential involvement of fibronectin fragments in mediating the actions of HTRA1 on IVD cells. We observed a noticeable increase in the level of a 27–29-kDa fibronectin fragment containing the amino-terminal fibrin- and heparin-binding domain in the supernatants from IVD cell cultures previously treated with HTRA1Δmac (5 μg/ml) as compared with cells incubated in medium alone or with the inactive

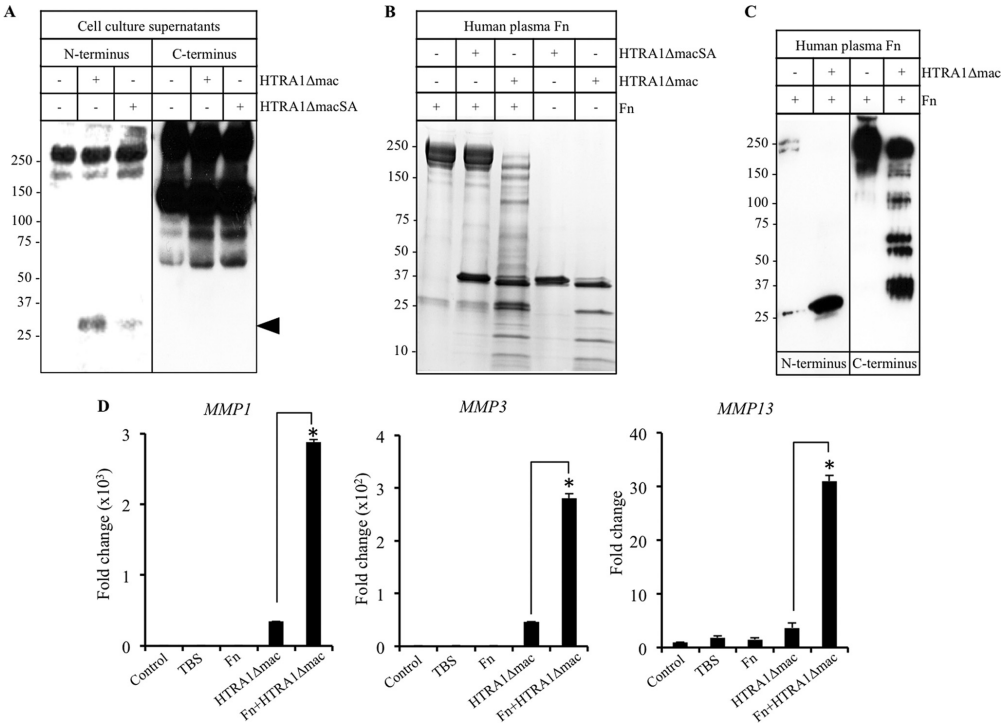

FIGURE 4. **Stimulation of IVD cells with HTRA1-generated fibronectin fragments.** *A*, concentrated protein supernatants (15 μg) from IVD cells treated for 24 h without or with HTRA1Δmac (5 μg/ml) or HTRA1ΔmacSA (5 μg/ml) were subjected to immunoblotting using antibody Mab1935 specific for the fibronectin carboxyl-terminal heparin-binding domain (*C terminus*) or Mab1936 specific for the fibronectin amino-terminal fibrin- and heparin-binding domain (*N terminus*). Fibronectin fragments containing the amino-terminal fibrin- and heparin-binding domain are identified by the *closed arrowhead*. *B*, purified human plasma-derived fibronectin (*Fn*) was incubated with HTRA1Δmac or HTRA1ΔmacSA at equimolar concentrations in TBS, pH 8.5, for 16 h at 37 °C, and samples were loaded onto a 4–15% gradient gel and stained with Coomassie Blue. Fibronectin and recombinant HTRA1 alone were also loaded and served as controls. *C*, an equimolar concentration of human plasma-derived fibronectin and HTRA1Δmac were incubated for 16 h, and fibronectin fragments were visualized by Western blot analysis using the antibodies described in *A*. *D*, equimolar concentrations of fibronectin (20 μg) and HTRA1Δmac (5 μg) were incubated for 16 h, and fibronectin fragments were purified by affinity chromatography. IVD cells were incubated with purified HTRA1-digested fibronectin (*Fn+HTRA1Δmac*) for 24 h, and expression levels of *MMP1*, *MMP3*, and *MMP13* mRNA were determined by qRT-PCR and the -fold change as compared with untreated controls was determined using the $2^{-\Delta\Delta C_T}$ method. Additional cultures were incubated with either affinity-purified Tris-buffered saline, pH 7.6 (*TBS*), fibronectin (*Fn*), or HTRA1 (*HTRA1Δmac*) or left untreated (*Control*). Data are representative of two separate experiments performed using IVD cells from two patients. Shown are results of triplicate determinations ± S.D. *, $p < 0.01$, as determined by one-way ANOVA.

HTRA1ΔmacSA (5 μg/ml) (Fig. 4*A* and supplemental Fig. 4*A*). Interestingly, increases in fibronectin fragments containing the carboxyl-terminal heparin-binding domain were evident in both HTRA1Δmac- and HTRA1ΔmacSA-treated cell cultures as compared with untreated controls. Further analyses confirmed that HTRA1Δmac, but not HTRA1ΔmacSA, could digest equimolar concentrations of human plasma-derived fibronectin after a 16-h incubation period, resulting in various sized fragments being generated, as determined by SDS-PAGE (Fig. 4*B*). The appearance of HTRA1Δmac as several bands is due to its autoproteolytic activity, as described previously (19), an effect not observed with HTRA1ΔmacSA. Western blot analysis of the products generated from HTRA1Δmac-induced fibronectin proteolysis revealed the presence of numerous fragments containing the carboxyl-terminal heparin-binding domain as well as the 27–29-kDa fragment containing the amino-terminal fibrin- and heparin-binding domain previously identified in the supernatants from HTRA1Δmac-treated IVD cells (Fig. 4*C*). We next investigated whether the fibronectin fragments generated by HTRA1 were also capable of activating IVD cells. Following an overnight incubation of human plasma-derived fibronectin with HTRA1Δmac (equimolar concentration), digested and undigested fibronectin was purified by affinity chromatography using Ni^{2+}-NTA to remove the majority of His-tagged HTRA1Δmac (supplemental Fig. 4*B*) and then incubated for up to 24 h with IVD cells. The expression levels of *MMP1*, *MMP3*, and *MMP13* (Fig. 4*D*) were all significantly increased in IVD cells incubated with the purified mixture of fibronectin fragments. By comparison, MMP expression in control cultures stimulated with the affinity column flow-through fraction from HTRA1Δmac samples in the absence of fibronectin was 6–9-fold less ($p < 0.01$), thus confirming that fibronectin fragments were the predominant cause of IVD cell activation.

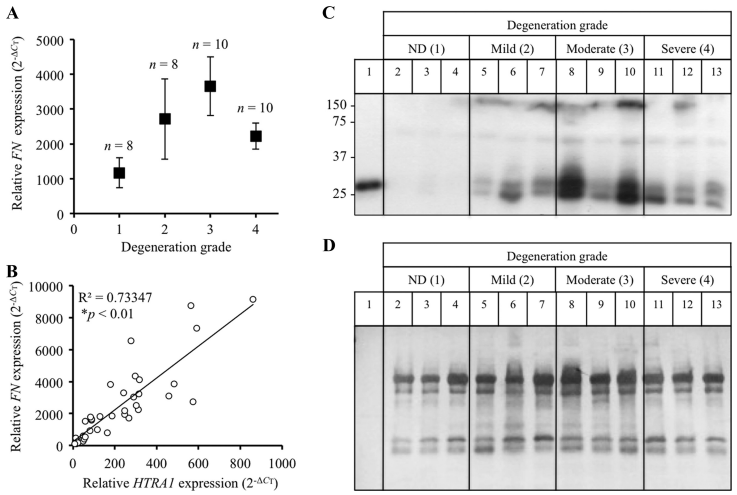

FIGURE 5. **Detection of fibronectin fragments in degenerated IVD tissue.** *A*, fibronectin (*FN*) mRNA levels in intact IVD tissue samples from patients ($n = 36$) with varying degrees of IVD degeneration were determined by qRT-PCR and presented as $2^{-\Delta}C_T \pm$ S.E. (*error bars*). *B*, correlation study between *FN* and *HTRA1* mRNA levels ($2^{-\Delta}C_T$) in patient IVD tissue samples ($n = 36$). R^2, square of correlation coefficient; $p < 0.01$ as determined from Pearson's correlation coefficient. *C*, protein extracts from patient IVD tissues ($n = 12$) were loaded onto a 12% SDS-polyacrylamide gel, and immunoblotting was performed using a monoclonal antibody (Mab1936) specific for the amino-terminal fibrin- and heparin-binding domain. *D*, the PVDF membrane used in *C* was stained with Coomassie Blue in order to confirm equal protein loading. *Lane 1*, HTRA1-digested human plasma-derived fibronectin; *lanes 2–4*, non-degenerated (*ND*) discs; *lanes 5–7*, mildly degenerated discs; *lanes 8–10*, moderately degenerated discs; *lanes 11–13*, severely degenerated discs.

Association of Fibronectin Fragments with Disc Degeneration—Both fibronectin and fibronectin fragments are known to increase with increasing disc degeneration and are thus considered to be an integral part of the underlying pathology (11). In the present study, fibronectin mRNA levels within IVD tissue samples from patients with varying degrees of disc degeneration were normalized to *TBP* and presented as $2^{-\Delta}C_T$. Fibronectin expression levels within patient disc tissue samples were indeed elevated in response to increases in degeneration grade (Fig. 5*A*) and correlated significantly with *HTRA1* mRNA expression levels ($r = 0.856$; $p < 0.01$) (Fig. 5*B*). Furthermore, Western blot analysis of IVD protein samples revealed an increase in fibronectin fragments containing the amino-terminal fibrin- and heparin-binding domain (Fig. 5*C*) in degenerated discs. Moreover, the majority of amino-terminal fragments identified were found to be of a similar size (27–29 kDa) to the fragment identified within samples of HTRA1-digested human fibronectin (*lane 1*). Membranes were counterstained with Coomassie Blue to confirm equal protein loading (Fig. 5*D*).

DISCUSSION

In the current study, we have identified HTRA1 mRNA and protein in the IVDs of human subjects and demonstrated an association between expression levels and severity of IVD degeneration. HTRA1 has previously been linked with disc degeneration following the association of a single nucleotide polymorphism, rs11200638, in the *HTRA1* gene and loss of disc height in postmenopausal Japanese women (21). In the present study, we were unable to show any significant association between the frequency of the risk allele (A) of SNP rs11200638 and IVD degeneration in a small European surgical patient population ($n = 35$). Furthermore, we found no evidence to suggest that the A allele of SNP rs11200638 has any significant influence on *HTRA1* expression levels in IVD tissue. This is supported by findings from studies investigating the role of HTRA1 in age-related macular degeneration, where, although closely associated with disease risk, rs11200638 alone was unable to significantly alter *HTRA1* expression (28, 29). It was subsequently reported that the additional disruption of the adjacent gene, *LOC387715*, was necessary in order for rs11200638 to have a positive influence on *HTRA1* expression (28).

We have previously shown that HTRA1 has the potential to stimulate MMP production by human synovial fibroblasts, thus implicating it in the pathogenesis of arthritis (19). As in the joints of arthritic patients, MMPs play a central role in orchestrating ECM breakdown in discs of patients with IVD degeneration (4–7). Therefore, we next investigated whether HTRA1 could also influence MMP production in human IVD cells. Consistent with our earlier findings with human synovial fibroblasts, recombinant HTRA1 was able to induce the expression of *MMP1*, *MMP3*, and *MMP13* mRNA, as well as MMP-3 protein, in short term IVD cell cultures. In addition, we also observed a significant increase in *ADAMTS4* expression in IVD cells stimulated with HTRA1. As with MMP-1, -3, and -13, ADAMTS-4 is also up-regulated in degenerated discs (4) and may therefore represent an additional route through which HTRA1 could influence ECM breakdown. These stimulatory effects were found to be primarily reliant on HTRA1 protease activity as evidenced by the fact that the proteolytically inactive form of HTRA1 (HTRA1ΔmacSA) was unable to significantly enhance MMP production. Neverthe-

less, increases in MMP production were apparent in cultures treated with HTRA1ΔmacSA and may be indicative of an additional, and as yet unidentified, protease-independent mechanism through which HTRA1 mediates its stimulatory effects. It is possible that further studies utilizing other mutant forms of HTRA1 may further assist in trying to decipher the exact cause of these stimulatory effects.

Degradation of the ECM within degenerated IVDs can give rise to fibronectin fragments of various sizes, which themselves are capable of activating resident disc cells to produce matrix-degrading proteases in a MEK-dependent manner (9, 27). Furthermore, the stimulatory properties of certain fibronectin fragment species on cellular MMP production are known to be mediated through the actions of IL-1β (26). In the current report, we demonstrated that the stimulatory effects of HTRA1 on MMP production by IVD cells were indeed MEK-dependent. Moreover, despite the fact HTRA1 induced the expression of *IL1B*, along with several other cytokines, inhibition of IL-1β signaling through the use of the IL-1RA failed to have any significant impact on HTRA1-induced MMP expression in IVD cells. On closer examination, it was revealed that IVD cell cultures and purified human plasma-derived fibronectin incubated with HTRA1Δmac both consisted of increased levels of a fibronectin fragment containing the 27–29-kDa amino-terminal fibrin- and heparin-binding domain. Furthermore, MMP expression was enhanced in IVD cells following stimulation with the proteolytic products of HTRA1-digested human plasma-derived fibronectin. Considering this, together with the additional observation that HTRA1-induced MMP expression was also dependent on MEK activity, we conclude that the stimulatory effects of HTRA1 on MMP production by IVD cells are mediated, at least in part, through the generation of fibronectin fragments. Interestingly, increases in fibronectin fragments containing the carboxyl-terminal heparin-binding domain, were also evident in the culture supernatants of cells treated with the HTRA1ΔmacSA. The fact that HTRA1ΔmacSA was proteolytically inactive and only able to generate fibronectin fragments in the presence of cells would suggest that these effects were most likely mediated through the stimulated secretion of other active proteases. This may therefore offer some explanation as to why MMP production by IVD cells was enhanced with HTRA1ΔmacSA, although the mechanism of action still remains to be determined. Furthermore, the observation that levels of the 27–29-kDa fibronectin fragment containing the amino-terminal fibrin- and heparin-binding domain were elevated predominantly in cell cultures treated with HTRA1Δmac would further imply that these fragment species are of particular relevance with regard to IVD cell activation.

Increased production of fibronectin by resident IVD cells has been observed within degenerated disc tissue samples and is considered to be central to the ongoing reparative and remodeling processes associated with IVD degeneration (30, 31). In the present study, we observed a marked increase in fibronectin expression in IVD tissue from patients with moderate to severe disc degeneration, which correlated significantly with changes in *HTRA1* expression levels. At present, it is not known whether fibronectin and HTRA1 share common regulatory pathways,

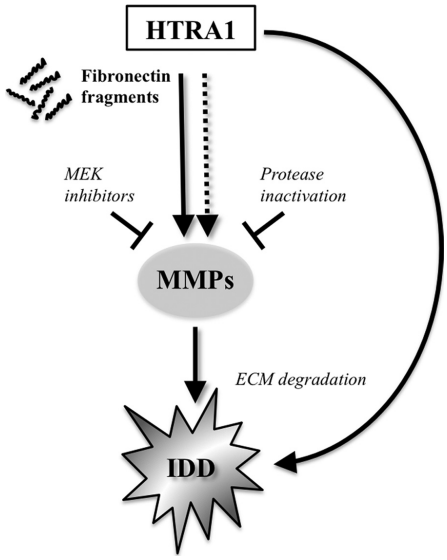

FIGURE 6. **A theoretical model for the role of HTRA1 in IVD degeneration.** Based on our findings, we propose that HTRA1 accumulates in IVD tissue undergoing degeneration and stimulates MMP production by resident cells in a predominantly protease-dependent manner, via activation of the MEK pathway. Furthermore, we suggest that the stimulatory effects of HTRA1 on IVD cells are mediated indirectly through its ability to generate fibronectin fragments, although other routes of cellular activation cannot be ruled out. *IDD*, intervertebral disc degeneration.

although it would appear that both of their expression patterns are dependent on factors intrinsic to the degenerative process. Given the fact that HTRA1-generated fibronectin fragments serve as potent inducers of MMP production, overexpression of fibronectin and *HTRA1* within IVDs is likely to have a significant influence on the development of disc degeneration. This is supported by our finding that small molecular mass fragments (27–29 kDa) containing the amino-terminal fibrin- and heparin-binding domain of fibronectin could also be identified within degenerated disc samples. The involvement of such fragments in disc degeneration has already been alluded to in a recent report by Anderson *et al.* (32), where a single fibronectin fragment with an estimated size of 25 kDa was detected in degenerated discs by immunoblotting with the same monoclonal antibody as used in the current study. It is possible, therefore, that HTRA1 protease activity may in fact be one of the main causative agents responsible for generating such fibronectin fragments within degenerated discs.

Taken together, these findings led us to propose a working model for the biological role of HTRA1 in IVD degeneration (Fig. 6). In addition to its already well characterized ability to directly degrade ECM proteins known to be present within IVDs (19, 20, 33–35), HTRA1 may also further modulate ECM breakdown indirectly through fibronectin fragment production and subsequent up-regulation of MMPs by resident disc cells. Clearly, further investigations are required in order to identify which particular fragments are responsible for the activation of

Role of HTRA1 in Intervertebral Disc Degeneration

IVD cells *in vitro* and to clarify the involvement of fibronectin fragments in IVD degeneration. Furthermore, additional studies are needed to fully evaluate the potential stimulatory effects of other soluble mediators (*e.g.* cytokines) released by IVD cells following incubation with HTRA1. Moreover, examination of the possible interplay between inflammatory mediators and fibronectin fragments in the regulation of Toll-like receptor signaling pathways in IVD cells may also lend further insight into how HTRA1 contributes to the catabolic response in IVD degeneration (36). These results therefore encourage the design of specific HTRA1 inhibitors for the treatment of patients with disc degeneration, an endeavor that will no doubt be facilitated by information gleaned from the recently solved crystal structure of HTRA1 (37).

REFERENCES

1. Peterson, C. K., Bolton, J. E., and Wood, A. R. (2000) A cross-sectional study correlating lumbar spine degeneration with disability and pain. *Spine* **25,** 218–223
2. Luoma, K., Riihimäki, H., Luukkonen, R., Raininko, R., Viikari-Juntura, E., and Lamminen A. (2000) Low back pain in relation to lumbar disc degeneration. *Spine* **25,** 487–492
3. Freemont, A. J., Watkins, A., Le Maitre, C., Jeziorska, M., and Hoyland, J. A. (2002) Current understanding of cellular and molecular events in intervertebral disc degeneration. Implications for therapy. *J. Pathol.* **196,** 374–379
4. Le Maitre, C. L., Freemont, A. J., and Hoyland, J. A. (2004) Localization of degradative enzymes and their inhibitors in the degenerate human intervertebral disc. *J. Pathol.* **204,** 47–54
5. Le Maitre, C. L., Freemont, A. J., and Hoyland, J. A. (2006) Human disc degeneration is associated with increased MMP 7 expression. *Biotech. Histochem.* **81,** 125–131
6. Roberts, S., Caterson, B., Menage, J., Evans, E. H., Jaffray, D. C., and Eisenstein, S. M. (2000) Matrix metalloproteinases and aggrecanase. Their role in disorders of the human intervertebral disc. *Spine* **25,** 3005–3013
7. Bachmeier, B. E., Nerlich, A., Mittermaier, N., Weiler, C., Lumenta, C., Wuertz, K., and Boos, N. (2009) Matrix metalloproteinase expression levels suggest distinct enzyme roles during lumbar disc herniation and degeneration. *Eur. Spine J.* **18,** 1573–1586
8. Millward-Sadler, S. J., Costello, P. W., Freemont, A. J., and Hoyland, J. A. (2009) Regulation of catabolic gene expression in normal and degenerate human intervertebral disc cells. Implications for the pathogenesis of intervertebral disc degeneration. *Arthritis Res. Ther.* **11,** R65
9. Anderson, D. G., Li, X., and Balian, G. (2005) A fibronectin fragment alters the metabolism by rabbit intervertebral disc cells *in vitro*. *Spine* **30,** 1242–1246
10. Greg Anderson, D., Li, X., Tannoury, T., Beck, G., and Balian, G. (2003) A fibronectin fragment stimulates intervertebral disc degeneration *in vivo*. *Spine* **28,** 2338–2345
11. Oegema, T. R., Jr., Johnson, S. L., Aguiar, D. J., and Ogilvie, J. W. (2000) Fibronectin and its fragments increase with degeneration in the human intervertebral disc. *Spine* **25,** 2742–2747
12. Clausen, T., Kaiser, M., Huber, R., and Ehrmann, M. (2011) HTRA proteases. Regulated proteolysis in protein quality control. *Nat. Rev. Mol. Cell Biol.* **12,** 152–162
13. Shridhar, V., Sen, A., Chien, J., Staub, J., Avula, R., Kovats, S., Lee, J., Lillie, J., and Smith, D. I. (2002) Identification of underexpressed genes in early and late stage primary ovarian tumors by suppression subtraction hybridization. *Cancer Res.* **62,** 262–270
14. Chien, J., Staub, J., Hu, S. I., Erickson-Johnson, M. R., Couch, F. J., Smith, D. I., Crowl, R. M., Kaufmann, S. H., and Shridhar, V. (2004) A candidate tumor suppressor HtrA1 is down-regulated in ovarian cancer. *Oncogene* **23,** 1636–1644
15. Baldi, A., De Luca, A., Morini, M., Battista, T., Felsani, A., Baldi, F., Catricalà, C., Amantea, A., Noonan, D. M., Albini, A., Natali, P. G., Lombardi, D., and Paggi, M. G. (2002) The HtrA1 serine protease is down-regulated during human melanoma progression and represses growth of metastatic melanoma cells. *Oncogene* **21,** 6684–6688
16. Bakay, M., Zhao, P., Chen, J., and Hoffman, E. P. (2002) A Web-accessible complete transcriptome of normal human and DMD muscle. *Neuromuscul. Disord.* **12,** S125–S141
17. Hu, S. I., Carozza, M., Klein, M., Nantermet, P., Luk, D., and Crowl, R. M. (1998) Human HtrA, an evolutionarily conserved serine protease identified as a differentially expressed gene product in osteoarthritic cartilage. *J. Biol. Chem.* **273,** 34406–34412
18. Wu, J., Liu, W., Bemis, A., Wang, E., Qiu, Y., Morris, E. A., Flannery, C. R., and Yang, Z. (2007) Comparative proteomic characterization of articular cartilage tissue from normal donors and patients with osteoarthritis. *Arthritis Rheum.* **56,** 3675–3684
19. Grau, S., Richards, P. J., Kerr, B., Hughes, C., Caterson, B., Williams, A. S., Junker, U., Jones, S. A., Clausen, T., and Ehrmann, M. (2006) The role of human HtrA1 in arthritic disease. *J. Biol. Chem.* **281,** 6124–6129
20. Tsuchiya, A., Yano, M., Tocharus, J., Kojima, H., Fukumoto, M., Kawaichi, M., and Oka, C. (2005) Expression of mouse HtrA1 serine protease in normal bone and cartilage and its up-regulation in joint cartilage damaged by experimental arthritis. *Bone* **37,** 323–336
21. Urano, T., Narusawa, K., Kobayashi, S., Shiraki, M., Horie-Inoue, K., Sasaki, N., Hosoi, T., Ouchi, Y., Nakamura, T., and Inoue, S. (2010) Association of HTRA1 promoter polymorphism with spinal disc degeneration in Japanese women. *J. Bone Miner. Metab.* **28,** 220–226
22. Pfirrmann, C. W., Metzdorf, A., Zanetti, M., Hodler, J., and Boos, N. (2001) Magnetic resonance classification of lumbar intervertebral disc degeneration. *Spine* **26,** 1873–1878
23. Wuertz, K., Urban, J. P., Klasen, J., Ignatius, A., Wilke, H. J., Claes, L., and Neidlinger-Wilke, C. (2007) Influence of extracellular osmolarity and mechanical stimulation on gene expression of intervertebral disc cells. *J. Orthop. Res.* **25,** 1513–1522
24. Grau, S., Baldi, A., Bussani, R., Tian, X., Stefanescu, R., Przybylski, M., Richards, P., Jones, S. A., Shridhar, V., Clausen, T., and Ehrmann, M. (2005) Implications of the serine protease HtrA1 in amyloid precursor protein processing. *Proc. Natl. Acad. Sci. U.S.A.* **102,** 6021–6026
25. Nie, G., Li, Y., and Salamonsen, L. A. (2005) Serine protease HtrA1 is developmentally regulated in trophoblast and uterine decidual cells during placental formation in the mouse. *Dev. Dyn.* **233,** 1102–1109
26. Yasuda, T., and Poole, A. R. (2002) A fibronectin fragment induces type II collagen degradation by collagenase through an interleukin-1-mediated pathway. *Arthritis Rheum.* **46,** 138–148
27. Xia, M., and Zhu, Y. (2011) Fibronectin fragment activation of ERK increasing integrin α and β subunit expression to degenerate nucleus pulposus cells. *J. Orthop. Res.* **29,** 556–561
28. Yang, Z., Tong, Z., Chen, Y., Zeng, J., Lu, F., Sun, X., Zhao, C., Wang, K., Davey, L., Chen, H., London, N., Muramatsu, D., Salasar, F., Carmona, R., Kasuga, D., Wang, X., Bedell, M., Dixie, M., Zhao, P., Yang, R., Gibbs, D., Liu, X., Li, Y., Li, C., Li, Y., Campochiaro, B., Constantine, R., Zack, D. J., Campochiaro, P., Fu, Y., Li, D. Y., Katsanis, N., and Zhang, K. (2010) Genetic and functional dissection of HTRA1 and LOC387715 in age-related macular degeneration. *PLoS Genet.* **6,** e1000836
29. Kanda, A., Chen, W., Othman, M., Branham, K. E., Brooks, M., Khanna, R., He, S., Lyons, R., Abecasis, G. R., and Swaroop, A. (2007) A variant of mitochondrial protein LOC387715/ARMS2, not HTRA1, is strongly associated with age-related macular degeneration. *Proc. Natl. Acad. Sci. U.S.A.* **104,** 16227–16232
30. Nerlich, A. G., Bachmeier, B. E., and Boos, N. (2005) Expression of fibronectin and TGF-β1 mRNA and protein suggest altered regulation of extracellular matrix in degenerated disc tissue. *Eur. Spine J.* **14,** 17–26
31. Gruber, H. E., Hoelscher, G. L., Ingram, J. A., Bethea, S., Zinchenko, N., and Hanley, E. N. Jr. (2011) Variations in aggrecan localization and gene expression patterns characterize increasing stages of human intervertebral disk degeneration. *Exp. Mol. Pathol.* **91,** 534–539
32. Anderson, D. G., Markova, D., Adams, S. L., Pacifici, M., An, H. S., and Zhang, Y. (2010) Fibronectin splicing variants in human intervertebral disc and association with disc degeneration. *Spine* **35,** 1581–1588
33. Tocharus, J., Tsuchiya, A., Kajikawa, M., Ueta, Y., Oka, C., and Kawaichi,

M. (2004) Developmentally regulated expression of mouse HtrA3 and its role as an inhibitor of TGF-β signaling. *Dev. Growth Differ.* **46,** 257–274
34. Hadfield, K. D., Rock, C. F., Inkson, C. A., Dallas, S. L., Sudre, L., Wallis, G. A., Boot-Handford, R. P., and Canfield, A. E. (2008) HtrA1 inhibits mineral deposition by osteoblasts. Requirement for the protease and PDZ domains. *J. Biol. Chem.* **283,** 5928–5938
35. Chamberland, A., Wang, E., Jones, A. R., Collins-Racie, L. A., LaVallie, E. R., Huang, Y., Liu, L., Morris, E. A., Flannery, C. R., and Yang, Z. (2009) Identification of a novel HtrA1-susceptible cleavage site in human aggrecan. Evidence for the involvement of HtrA1 in aggrecan proteolysis *in vivo*. *J. Biol. Chem.* **284,** 27352–27359
36. Su, S. L., Tsai, C. D., Lee, C. H., Salter, D. M., and Lee, H. S. (2005) Expression and regulation of Toll-like receptor 2 by IL-1β and fibronectin fragments in human articular chondrocytes. *Osteoarthr. Cartil.* **13,** 879–886
37. Truebestein, L., Tennstaedt, A., Mönig, T., Krojer, T., Canellas, F., Kaiser, M., Clausen, T., and Ehrmann, M. (2011) Substrate-induced remodeling of the active site regulates human HTRA1 activity. *Nat. Struct. Mol. Biol.* **18,** 386–388

Supplementary Figure Legends

Supplementary Figure 1. Protein loading control for patient IVD samples. The PVDF membrane used in the Western blot analysis of HTRA1 protein within normal and degenerated discs was counter stained with Coomassie blue in order to visualize total protein and thus confirm equal sample loading. *Lane 1*, *HTRA1Δmac (4 ng)* ; *lanes 2 to 4*, non-degenerated (ND) disc; *lanes 5 to 7*, mildly degenerated discs; *lanes 8 to 10*, moderately degenerated discs; *lanes 11 to 13*, severely degenerated discs.

Supplementary Figure 2. Regulation of aggrecanase-1 (*ADAMTS4*), gelatinase A (*MMP2*) and aggrecan (*ACAN*) expression in IVD cells by recombinant HTRA1. *A–C*, the effects of HTRA1Δmac on *ADAMTS4, MMP2* and *ACAN* mRNA expression in IVD cells after a 24 h incubation period were determined by qRT-PCR and the fold change as compared to untreated controls determined using the $2^{-\Delta\Delta C_T}$ method. Data is representative of two independent experiments (±S.D. triplicates). * $p < 0.05$, ** $p < 0.01$, as determined by Student's *t*-test.

Supplementary Figure 3. Downregulation of IL-1β-induced MMP expression in IVD cells by IL-1RA. The inhibitory effects of IL-1RA (250 ng/ml) on IL-1β (5 ng/ml)-induced MMP expression in IVD cells after a 24 h incubation period were determined by qRT-PCR and the fold change as compared to untreated controls determined using the $2^{-\Delta\Delta C_T}$ method. * $p < 0.01$ as determined by Student's *t*-test (±S.D. triplicates).

Supplementary Figure 4. Generation of fibronectin fragments. *A*, The PVDF membrane used in the Western blot analysis of fibronectin fragments within concentrated IVD cell culture supernatants was counter stained with Coomassie blue in order to visualize total protein and thus confirm equal sample loading. *B*, Fibronectin (20 μg) (*Fn*), recombinant HTRA1 (5 μg) (*HTRA1Δmac)* or a combination of fibronectin and HTRA1 (*Fn+ HTRA1Δmac*) were incubated for 16 h at 37°C and then subjected to Ni^{2+}-NTA affinity chromatography in spin columns. The columns were initially centrifuged at 1600 rpm for 5 min and the flow through fraction (*FT*) containing unbound protein collected. Columns were then washed with TBS, pH 7.6, and the wash fraction (*W*) collected. Remaining protein bound to the column was then removed with TBS, pH 7.6, 300 mM imidazole and the elution fraction (*E*) collected. All samples were then loaded onto a 4-15% gradient gel and stained with Coomassie Blue. The *closed arrow* indicates the eluted his-tagged HTRA1Δmac (37 kDa). *M*, Protein marker.

Supplementary Figure 1

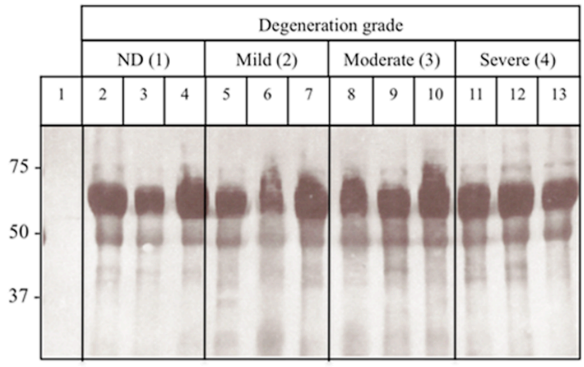

Supplementary Figure 2

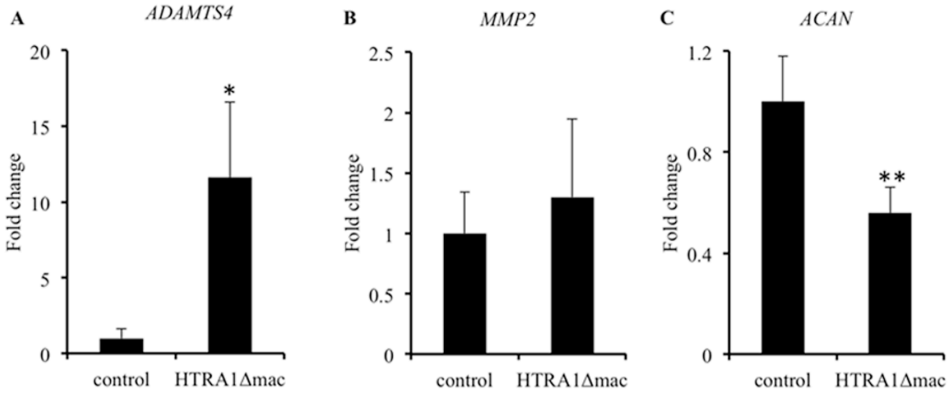

Supplementary Figure 3

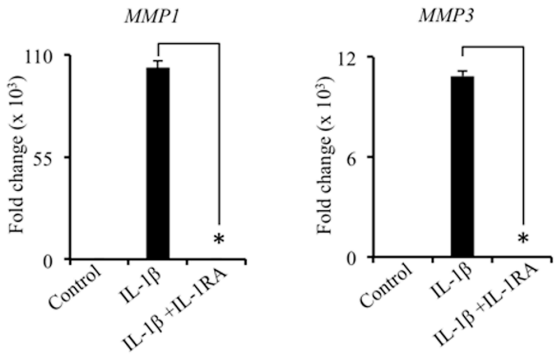

Supplementary Figure 4

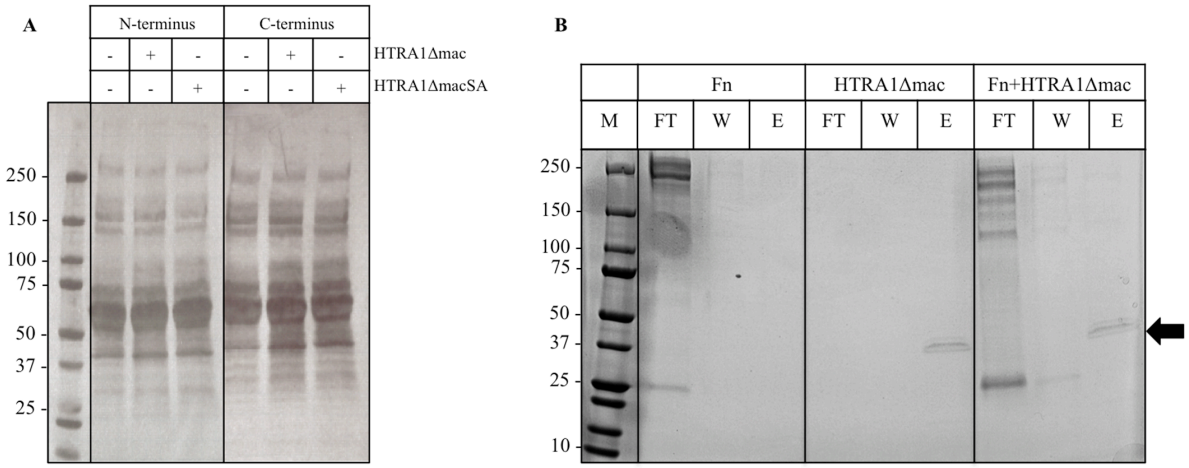

Supplementary Table 1. List of TaqMan Gene Expression Assays used in RT-PCR analysis

Gene Symbol	Protein Product	Assay ID [a]
ADAMTS4	Disintegrin and metalloproteinase with thrombospondin motifs 4	Hs00943031_g1
ACAN	Aggrecan	Hs00202971_m1
FN	Fibronectin	Hs01549976_m1
GAPDH	Glyceraldehyde 3-Phosphate Dehydrogenase	Hs02758991_g1
HTRA1	High Temperature Requirement Protease A1	Hs01016151_m1
IL1B	Interleukin-1 beta	Hs00174097_m1
IL6	Interleukin-6	Hs00174131_m1
IL8	Interleukin-8	Hs00174103_m1
MMP1	Matrix Metalloproteinase-1	Hs00233958_m1
MMP2	Matrix Metalloproteinase-2	Hs01548724_m1
MMP3	Matrix Metalloproteinase-3	Hs00968308_m1
MMP13	Matrix Metalloproteinase-13	Hs00233992_m1
TBP	TATA-box binding protein	Hs00427620_m1

[a] *TaqMan Expression Assay identity code according to supplier (Applied Biosystems, Rotkreuz, Switzerland).*

4 General discussion and perspectives

The number of patients experiencing bone fractures is expected to steadily rise due to changes in life style, increases in population growth and life expectancy [186]. The majority of patients who are eligible for bone replacement procedures are elderly, and their bones display poor mechanical properties and, most importantly, exhibit limited regeneration potential. Therefore, bone quality is an essential factor to prevent bone from fracture and reflects the incorporation of bone density and mechanical strength as well as architecture and mineralization [13, 77, 78], and is affected during aging by alterations in bone turnover through the process of bone remodeling. As such, fracture repair in aged and osteoporotic bone presents a major challenge to the orthopaedic surgery due to inferior properties of the cancellous bone [79-81]. Although bone has an intrinsic ability to regenerate itself, this capacity is limited to small fractures, and therapeutic alternatives are still necessary to improve bone healing as well as to treat bone deficiencies associated with degenerative disorders, such as osteoporosis.

The incidence and management of osteoporotic fractures is adversely affected by low bone mass and poor healing potential and thus results in higher complication rates. The importance of developing new therapies to counteract the effects of aging bone is highlighted by the fact that on average, 20% of the patients sustaining an osteoporotic-related fracture die within the first year due to complications caused by immobility. This figure is expected to rise due to shifts in the age pyramid. It is envisaged that the concept of local treatment of age-related osteoporosis by stem cells, harvested from autologous tissue samples addressed in this thesis, could be directly translated into clinical applications and has enormous potential for enhancing osteoporotic bone regeneration thereby reducing morbidity and health costs associated with this disorder.

Stem cells, and in particular MSCs, represent a promising tool for the development of clinical strategies for the repair of site specific bone defects, and could help reduce the prevalence of various bone disorders like osteoporosis [164]. To date a number of studies exist which support the role of BMSCs in the development and progression of age-related osteoporosis and subsequent alterations in the levels of bone quality [14, 15, 88]. BMSCs are considered as being key elements of the BMU due to their osteogenic potential, and therefore play an important role in the overall maintenance of bone quality. However, their general fitness appears to reduce with age and passage number *in vitro*, as demonstrated by increases in

cellular aging markers and an inability to maintain their osteogenic potential under normal conditions or following exposure to stress [187-189]. Additionally, alteration in the differentiation capacity of resident BMSCs in osteoporotic patients and animal models has led to the hypothesis that impaired BMSC osteogenesis may be involved in the development of age-related osteoporotic phenotypes, due inadequate numbers of active osteoblasts.

The idea of dysfunctional BMSCs as being a basic cause of age-related osteoporosis and impaired bone quality is supported by several reports for both human osteoporotic patients [3, 15], and also in experimental mouse models [88, 190, 191]. It has been shown that BMSCs isolated from *Sca-1*$^{-/-}$ mice have a reduced tendency to differentiate towards osteogenesis and that these mice displayed many of the phenotypes associated with age-related osteoporosis [192]. In a similar study, a low turnover osteoporosis was observed in the klotho mouse strain, where bone marrow osteogenesis was also significantly reduced [83]. Moreover, results from several investigations utilizing the senile osteoporotic SAMP6 model have revealed that the osteogenic differentiation potential of resident BMSCs is remarkably reduced as compared to BMSCs isolated from the age-matched SAMR1 control strain [88, 190, 191]. These observations therefore highlight the fact that age-related inadequacies in cellular differentiation must be taken into account when considering the potential impact of therapeutic strategies aimed at restoring bone quality in osteoporotic patients.

There are certain aspects apart from BMSC functionality that need to be taken into account when considering the use of BMSCs for therapeutic purposes. These include limitations in the amount of cells that can be harvested at any one time, plus the fact that collection of bone marrow is a painful and sometimes risky procedure [116, 149, 176]. As such, efforts have been made to identify other potential sources of multipotent bone progenitor cells. In this thesis, I studied the role of adipose tissue as an alternative autologous cell source from which a sufficient number of osteo-progenitor cells may be easily accessed. ASCs have a similar differentiation potential, morphology, phenotype and gene expression pattern as BMSCs, and may therefore represent a promising autologous cell source of osteoprogenitor cells for the treatment of age-related osteoporosis [193, 194].

In the first part of this thesis, I investigated the possibility of using the SAMP6 mouse as a model for senile osteoporosis. The results presented in this part confirmed that bone quality was significantly compromised in SAMP6 mice as compared to their age-matched non-osteoporotic counterparts, SAMR1 mice. Furthermore, the observation that SAMP6 mice have shorter telomere lengths is suggestive of an age-related osteoporotic phenotype. I was also able to harvest and purify ASCs from the subcutaneous inguinal fat pads of SAM mice

and could expand these cells in culture over several passages. They displayed similar characteristics to BMSCs, as they consistently expressed mesenchymal cell surface markers and readily differentiated into adipocyte, chondrocytes, and osteoblast cell lineages, thus confirming their multipotency. Additionally, in the same study, I also analyzed ASCs for various biological markers of premature aging, due to the premature aging-like features associated with the SAMP6 model. Although isolated from aged, osteoporotic mice, ASCs displayed no signs of cellular senescence or impaired osteogenic differentiation. Moreover, unlike BMSCs isolated from these mice, ASCs were not prone to excessive adipogenic differentiation [88].

Despite the intense excitement surrounding stem cells and their potential to revolutionize modern regenerative medicine, translation of stem cell research from bench to bedside has proceeded more slowly than expected. One possible reason for this may involve the culture conditions used. Classically, 2D culture systems have been used to grow, maintain and differentiate MSCs. However, the incorporation of cells within a 3D microstructure configuration is believed to be more representative of their natural physiological condition, where cells are surrounded by neighbouring cells and are embedded in an ECM which helps contribute to cellular communication pathways [195]. Therefore, in the second part of this thesis, I established a methodology for preparing ASCs in a 3D culture system, and investigated their potential for osteogenesis. I used the hanging drop method to culture ASCs in a scaffold-free 3D culture system, which allowed for gravity-enforced ASC microtissue spheroid formation (ASC-MTs). This method of culturing ASCs allowed me to investigate ASC osteogenesis in a more native cellular environment, and also offered me the possibility of an alternative means by which to deliver osteoprogenitor cells directly to sites of interest *in vivo*.

The concept of culturing ASCs in a 3D system was investigated further in the third part of this thesis. In the first approach, SAMP6-derived ASCs were cultured in a scaffold-free 3D culture system, ASC-MT, as introduced in the second part of this thesis. ASCs cultured in ASC-MTs were confirmed as being able to retain both their proliferative capacity as well as their osteogenic potential. This was considered to be of crucial importance if microtissues were to be used for the purpose of delivering ASCs to osteoporotic bone. In the second approach, SAMP6-derived ASCs were seeded on silk fibroin scaffolds and allowed to differentiate for up to 6 weeks. Not only did this enable further analysis of ASC behaviour under 3D culture conditions, but also better mimicked the environmental conditions found in trabecular bone. A steady increase in mineralized tissue formation was observed in ASC-

seeded scaffolds upon osteogenesis as determined by micro-CT. Taken together, these findings confirmed that SAMP6-derived ASCs were capable of maintaining their functional capacity for osteogenesis when cultured in 3D environments and thus encouraged me to further investigate their capacity to influence bone formation *in vivo*.

In order to evaluate the potential beneficial effects of SAMP6-derived ASCs on bone quality in the same mouse strain, I opted for a local delivery regime, whereby single cell suspensions of ASCs or ASC-MTs were injected directly into the tibia, and bone parameters compared with untreated contralateral tibia. Bones injected with PBS/EDTA served as controls. I observed a significant improvement in the trabecular bone quality of SAMP6 mice after 42 days following a single intratibial injection of either undifferentiated ASCs or pre-differentiated osteogenic ASC-MT in comparison to untreated contralateral bones. Furthermore, CM-Dil labeled ASCs could still be detected within the bone marrow of treated tibia even at this late time point. However, I unexpectedly encountered adverse effects of a single intratibial injection of pre-differentiated osteogenic ASCs when delivered as a cell suspension, which caused high mortality rates as a result of pulmonary embolism. It remains unclear as to why such adverse events should have occurred following the use of these cells, especially as other studies using pre-differentiated mouse ASCs reported no untoward effects [196]. This could in fact represent an important point of concern when considering such an approach in humans and may therefore required further investigation. However, it would appear that implementing ASC-MTs might represent one possible means by which to overcome this potentially detrimental effect of pre-differentiated osteogenic ASCs when injected directly into the bone marrow cavity.

In addition to improvements being made in trabecular bone, the elevation of gene expression profiles of several bone turnover markers in the tibia of ASC-treated mice was also observed as compared to PBS/EDTA-treated mice. This is in agreement with previous studies in which the positive effects of locally administered ASCs on mouse bone quality have been associated with alterations in genetic markers of osteogenesis [196]. However, it should be mentioned that in the experimental setup used in this thesis, the majority of genes tested were upregulated in both ASC- and PBS/EDTA-treated mice when compared to untreated contralateral bones, thus indicating that the mere act of intratibial injection alone was sufficient to upregulate gene expression, possibly due to the stimulation of bone formation caused by accessing the bone cavity during operation procedure.

It is interesting to note, that the capacity of pre-differentiated osteogenic ASC-MT to enhance trabecular bone quality was comparable to undifferentiated ASCs, despite them having

already been induced along the osteogenic lineage. This observation would therefore imply that the transplanted ASCs might have mediated their effects through the stimulation of resident cells, rather than instigating new bone formation directly by differentiating to osteoblasts. This concept of a paracrine effect was further tested *in vitro* utilizing ASCs and BMSCs isolated from human osteoporotic patients in collaboration with my colleagues in Innsbruck University Hospital. Initial results presented in this thesis confirmed that the osteogenic potential of osteoporotic BMSCs was significantly impaired as compared to normal, age-matched non-osteoporotic control samples. We could also demonstrate that conditioned media harvested from ASCs isolated from osteoporotic patients was able to better support mineralization of osteoporotic BMSCs as compared to cell cultures supplemented with media obtained from osteoporotic BMSCs. Although similar findings were reported in studies utilizing human ASCs with either human BMSCs or mouse osteoblastic cell lines [194, 197], as far as I'm aware, this is the first direct evidence that human osteoporotic ASCs have the capacity to impart a pro-osteogenic paracrine effect on human osteoporotic BMSCs *in vitro*. It is possible therefore, that the increases in SAMP6 trabecular bone quality following ASC treatment were partially due to the paracrine actions of injected ASCs on resident BMSC populations. These findings therefore support the use of isogeneic and possibly even autologous ASCs for the treatment of age-related bone loss.

Currently, several systemic-based pharmacotherapies are available to treat osteoporosis (e.g. bisphosphonates), although local therapeutic modalities may also be useful to treat bone loss. One possible alternative could be to treat bone loss with a local application of ASCs harvested from autologous tissue samples.

The isolation of human ASCs is now a well-established procedure worldwide, and as such, could easily be incorporated into the working practices of standard patient care in many different countries. In fact, a number of clinical studies are currently on-going, or have already been completed, in which ASCs are or have been augmented in a composite graft for the purposes of treating proximal humeral fractures (http://clinicaltrials.gov: NCT01532076). With this in mind, supplementation of osteoporotic bone with competent osteoprogenitor cells may therefore represent a viable means by which to re-establish normal bone homeostasis and enhance bone quality. Indeed, this concept has already been tested by several independent research groups and has been shown to have significant benefits in terms of preventing bone loss in various experimental OVX mouse models. Human ASCs demonstrated a protective effect on OVX-induced bone loss in nude mice when intravenously injected at the time of surgical intervention [197]. These effects were hypothesized as being

mediated mainly through paracrine effects of the transplanted ASCs based on the fact that no cells could be visualized within bone after 48 h post injection. Similarly, the systemic administration of genetically modified mouse ASCs restored normal bone parameters in immunocompetent mice after 28 days, although no data was presented to indicate whether ASCs could be detected within the bones of treated animals [198]. More recently, it was shown that a single intrafemoral injection of ASCs into OVX senescence-accelerated mouse prone 8 mice (SAMP8) resulted in significant increases in BMD as compared to control groups, which was evident at 4 months following the initial treatment [196]. However, these effects appeared to require the *in vitro* osteogenic differentiation of ASCs prior to implantation.

It was previously shown that in SAMP6 mice, BMSCs displayed a higher tendency for adipogenic differentiation [88], which is supposed to be one underlying reason for the deficiency of bone quality in human osteoporotic patients. This phenomenon may lead to increased fat deposition within the bone marrow of osteoporotic patients, which is undesired for normal physiological condition of bone. However, it should be noted that not all types of fat tissue within bone marrow may have a detrimental effect on bone homeostasis. In humans, it is known that the amount of adipose tissue in the bone marrow increases around the time of peak bone mass and may therefore play an important role in bone acquisition during this time of increased bone formation. Moreover, studies in some mouse strains with high bone mass have revealed the presence of BAT has the capacity to burn calories and decrease lipid stores [199]. As such, it would be interesting to assess the types of fat marrow found in osteoporotic versus healthy bones, and the putative involvement of BMSCs in this process. Additionally, stimulation of BMSCs towards brown adipocytes rather than white adipocytes may possibly provide another novel approach to positively affect bone metabolism.

In summary, results demonstrated in my thesis show that SAMP6-derived ASCs retain a high capacity for osteogenesis, display no alterations in adipogenic differentiation potential, maintain telomere length, and show no signs of premature cellular senescence. In addition, *in vivo* studies demonstrated that a single intrabone injection of isogenic undifferentiated ASCs or pre-differentiated ASC-MTs, significantly enhanced bone quality parameters in SAMP6 mice. Furthermore, *in vitro* data utilizing human osteoporotic BMSCs and ASCs is provided, which supports the concept that transplanted osteoporotic ASCs may influence bone formation in a paracrine manner. These observations therefore support the idea of using adipose tissue as a promising source for cell-based therapeutic strategy to treat age-related osteoporosis.

References

1. Goldstein, S.A., Matthews, L.S., Kuhn, J.L., and Hollister, S.J. (1991). Trabecular bone remodeling: an experimental model. J Biomech *24 Suppl 1*, 135-150.
2. Hill, P.A. (1998). Bone remodelling. Br J Orthod *25*, 101-107.
3. Manolagas, S.C. (2000). Birth and death of bone cells: basic regulatory mechanisms and implications for the pathogenesis and treatment of osteoporosis. Endocr Rev *21*, 115-137.
4. Lin, J.T., and Lane, J.M. (2004). Osteoporosis: a review. Clin Orthop Relat Res, 126-134.
5. Rodriguez, J.P., Astudillo, P., Rios, S., and Pino, A.M. (2008). Involvement of adipogenic potential of human bone marrow mesenchymal stem cells (MSCs) in osteoporosis. Curr Stem Cell Res Ther *3*, 208-218.
6. Rosen, C.J., and Bouxsein, M.L. (2006). Mechanisms of disease: is osteoporosis the obesity of bone? Nat Clin Pract Rheumatol *2*, 35-43.
7. Burge, R., Dawson-Hughes, B., Solomon, D.H., Wong, J.B., King, A., and Tosteson, A. (2007). Incidence and economic burden of osteoporosis-related fractures in the United States, 2005-2025. J Bone Miner Res *22*, 465-475.
8. Dontas, I.A., and Yiannakopoulos, C.K. (2007). Risk factors and prevention of osteoporosis-related fractures. J Musculoskelet Neuronal Interact *7*, 268-272.
9. Kanis, J.A., Borgstrom, F., De Laet, C., Johansson, H., Johnell, O., Jonsson, B., Oden, A., Zethraeus, N., Pfleger, B., and Khaltaev, N. (2005). Assessment of fracture risk. Osteoporos Int *16*, 581-589.
10. de Paula, F.J., Horowitz, M.C., and Rosen, C.J. (2010). Novel insights into the relationship between diabetes and osteoporosis. Diabetes Metab Res Rev *26*, 622-630.
11. Kawai, M., Devlin, M.J., and Rosen, C.J. (2009). Fat targets for skeletal health. Nat Rev Rheumatol *5*, 365-372.
12. Rosen, C.J., Ackert-Bicknell, C., Rodriguez, J.P., and Pino, A.M. (2009). Marrow fat and the bone microenvironment: developmental, functional, and pathological implications. Crit Rev Eukaryot Gene Expr *19*, 109-124.
13. Seeman, E., and Delmas, P.D. (2006). Bone quality--the material and structural basis of bone strength and fragility. N Engl J Med *354*, 2250-2261.
14. Rodriguez, J.P., Garat, S., Gajardo, H., Pino, A.M., and Seitz, G. (1999). Abnormal osteogenesis in osteoporotic patients is reflected by altered mesenchymal stem cells dynamics. J Cell Biochem *75*, 414-423.
15. Rodriguez, J.P., Montecinos, L., Rios, S., Reyes, P., and Martinez, J. (2000). Mesenchymal stem cells from osteoporotic patients produce a type I collagen-deficient extracellular matrix favoring adipogenic differentiation. J Cell Biochem *79*, 557-565.
16. Harvey, N., Dennison, E., and Cooper, C. (2010). Osteoporosis: impact on health and economics. Nat Rev Rheumatol *6*, 99-105.
17. Doetsch, F., Caille, I., Lim, D.A., Garcia-Verdugo, J.M., and Alvarez-Buylla, A. (1999). Subventricular zone astrocytes are neural stem cells in the adult mammalian brain. Cell *97*, 703-716.
18. Heaney, R.P. (2003). How does bone support calcium homeostasis? Bone *33*, 264-268.
19. Kanis, J.A. (1994). Calcium nutrition and its implications for osteoporosis. Part I. Children and healthy adults. Eur J Clin Nutr *48*, 757-767.
20. Hall, B.K., and Miyake, T. (2000). All for one and one for all: condensations and the initiation of skeletal development. Bioessays *22*, 138-147.
21. Bush, P.G., Hall, A.C., and Macnicol, M.F. (2008). New insights into function of the growth plate: clinical observations, chondrocyte enlargement and a possible role for membrane transporters. J Bone Joint Surg Br *90*, 1541-1547.
22. Aaron, J.E., Shore, P.A., Shore, R.C., Beneton, M., and Kanis, J.A. (2000). Trabecular architecture in women and men of similar bone mass with and without vertebral fracture: II. Three-dimensional histology. Bone *27*, 277-282.
23. Bonucci, E., Silvestrini, G., and Bianco, P. (1992). Extracellular alkaline phosphatase activity in mineralizing matrices of cartilage and bone: ultrastructural localization using a cerium-based method. Histochemistry *97*, 323-327.
24. Termine, J.D., Kleinman, H.K., Whitson, S.W., Conn, K.M., McGarvey, M.L., and Martin, G.R. (1981). Osteonectin, a bone-specific protein linking mineral to collagen. Cell *26*, 99-105.
25. Hauschka, P.V., Lian, J.B., Cole, D.E., and Gundberg, C.M. (1989). Osteocalcin and matrix Gla protein: vitamin K-dependent proteins in bone. Physiol Rev *69*, 990-1047.

26. Butler, W.T. (1989). The nature and significance of osteopontin. Connect Tissue Res *23*, 123-136.
27. Sodek, J., Ganss, B., and McKee, M.D. (2000). Osteopontin. Crit Rev Oral Biol Med *11*, 279-303.
28. http://www.cliffsnotes.com/sciences/anatomy-and-physiology/bones-and-skeletal-tissues/bone-tructure.
29. Ducy, P., Starbuck, M., Priemel, M., Shen, J., Pinero, G., Geoffroy, V., Amling, M., and Karsenty, G. (1999). A Cbfa1-dependent genetic pathway controls bone formation beyond embryonic development. Genes Dev *13*, 1025-1036.
30. Nakashima, K., Zhou, X., Kunkel, G., Zhang, Z., Deng, J.M., Behringer, R.R., and de Crombrugghe, B. (2002). The novel zinc finger-containing transcription factor osterix is required for osteoblast differentiation and bone formation. Cell *108*, 17-29.
31. Lee, M.H., Kwon, T.G., Park, H.S., Wozney, J.M., and Ryoo, H.M. (2003). BMP-2-induced Osterix expression is mediated by Dlx5 but is independent of Runx2. Biochem Biophys Res Commun *309*, 689-694.
32. Rawadi, G., Vayssiere, B., Dunn, F., Baron, R., and Roman-Roman, S. (2003). BMP-2 controls alkaline phosphatase expression and osteoblast mineralization by a Wnt autocrine loop. J Bone Miner Res *18*, 1842-1853.
33. Mao, J., Wang, J., Liu, B., Pan, W., Farr, G.H., 3rd, Flynn, C., Yuan, H., Takada, S., Kimelman, D., Li, L., et al. (2001). Low-density lipoprotein receptor-related protein-5 binds to Axin and regulates the canonical Wnt signaling pathway. Mol Cell *7*, 801-809.
34. Winkler, D.G., Sutherland, M.S., Ojala, E., Turcott, E., Geoghegan, J.C., Shpektor, D., Skonier, J.E., Yu, C., and Latham, J.A. (2005). Sclerostin inhibition of Wnt-3a-induced C3H10T1/2 cell differentiation is indirect and mediated by bone morphogenetic proteins. J Biol Chem *280*, 2498-2502.
35. Brunkow, M.E., Gardner, J.C., Van Ness, J., Paeper, B.W., Kovacevich, B.R., Proll, S., Skonier, J.E., Zhao, L., Sabo, P.J., Fu, Y., et al. (2001). Bone dysplasia sclerosteosis results from loss of the SOST gene product, a novel cystine knot-containing protein. Am J Hum Genet *68*, 577-589.
36. Teitelbaum, S.L. (2000). Osteoclasts, integrins, and osteoporosis. J Bone Miner Metab *18*, 344-349.
37. Rousselle, A.V., and Heymann, D. (2002). Osteoclastic acidification pathways during bone resorption. Bone *30*, 533-540.
38. Reinholt, F.P., Hultenby, K., Oldberg, A., and Heinegard, D. (1990). Osteopontin--a possible anchor of osteoclasts to bone. Proc Natl Acad Sci U S A *87*, 4473-4475.
39. Blair, H.C., Teitelbaum, S.L., Ghiselli, R., and Gluck, S. (1989). Osteoclastic bone resorption by a polarized vacuolar proton pump. Science *245*, 855-857.
40. Bromme, D., Okamoto, K., Wang, B.B., and Biroc, S. (1996). Human cathepsin O2, a matrix protein-degrading cysteine protease expressed in osteoclasts. Functional expression of human cathepsin O2 in Spodoptera frugiperda and characterization of the enzyme. J Biol Chem *271*, 2126-2132.
41. Salo, J., Lehenkari, P., Mulari, M., Metsikko, K., and Vaananen, H.K. (1997). Removal of osteoclast bone resorption products by transcytosis. Science *276*, 270-273.
42. Nesbitt, S.A., and Horton, M.A. (1997). Trafficking of matrix collagens through bone-resorbing osteoclasts. Science *276*, 266-269.
43. Andersson, G., Ek-Rylander, B., Hollberg, K., Ljusberg-Sjolander, J., Lang, P., Norgard, M., Wang, Y., and Zhang, S.J. (2003). TRACP as an osteopontin phosphatase. J Bone Miner Res *18*, 1912-1915.
44. Ek-Rylander, B., and Andersson, G. (2010). Osteoclast migration on phosphorylated osteopontin is regulated by endogenous tartrate-resistant acid phosphatase. Exp Cell Res *316*, 443-451.
45. Toyosawa, S., Shintani, S., Fujiwara, T., Ooshima, T., Sato, A., Ijuhin, N., and Komori, T. (2001). Dentin matrix protein 1 is predominantly expressed in chicken and rat osteocytes but not in osteoblasts. J Bone Miner Res *16*, 2017-2026.
46. Igarashi, M., Kamiya, N., Ito, K., and Takagi, M. (2002). In situ localization and in vitro expression of osteoblast/osteocyte factor 45 mRNA during bone cell differentiation. Histochem J *34*, 255-263.
47. Gowen, L.C., Petersen, D.N., Mansolf, A.L., Qi, H., Stock, J.L., Tkalcevic, G.T., Simmons, H.A., Crawford, D.T., Chidsey-Frink, K.L., Ke, H.Z., et al. (2003). Targeted disruption of the osteoblast/osteocyte factor 45 gene (OF45) results in increased bone formation and bone mass. J Biol Chem *278*, 1998-2007.
48. Yang, W., Lu, Y., Kalajzic, I., Guo, D., Harris, M.A., Gluhak-Heinrich, J., Kotha, S., Bonewald, L.F., Feng, J.Q., Rowe, D.W., et al. (2005). Dentin matrix protein 1 gene cis-regulation: use in osteocytes to characterize local responses to mechanical loading in vitro and in vivo. J Biol Chem *280*, 20680-20690.
49. Dierkes, C., Kreisel, M., Schulz, A., Steinmeyer, J., Wolff, J.C., and Fink, L. (2009). Catabolic properties of microdissected human endosteal bone lining cells. Calcif Tissue Int *84*, 146-155.
50. Everts, V., Delaisse, J.M., Korper, W., Jansen, D.C., Tigchelaar-Gutter, W., Saftig, P., and Beertsen, W. (2002). The bone lining cell: its role in cleaning Howship's lacunae and initiating bone formation. J Bone Miner Res *17*, 77-90.

51. Parfitt, A.M. (1994). Osteonal and hemi-osteonal remodeling: the spatial and temporal framework for signal traffic in adult human bone. J Cell Biochem *55*, 273-286.
52. Parfitt, A.M. (2002). Life history of osteocytes: relationship to bone age, bone remodeling, and bone fragility. J Musculoskelet Neuronal Interact *2*, 499-500.
53. Arai, F., Miyamoto, T., Ohneda, O., Inada, T., Sudo, T., Brasel, K., Miyata, T., Anderson, D.M., and Suda, T. (1999). Commitment and differentiation of osteoclast precursor cells by the sequential expression of c-Fms and receptor activator of nuclear factor kappaB (RANK) receptors. J Exp Med *190*, 1741-1754.
54. Hofbauer, L.C., and Heufelder, A.E. (2000). Clinical review 114: hot topic. The role of receptor activator of nuclear factor-kappaB ligand and osteoprotegerin in the pathogenesis and treatment of metabolic bone diseases. J Clin Endocrinol Metab *85*, 2355-2363.
55. Martin, T.J. (2004). Paracrine regulation of osteoclast formation and activity: milestones in discovery. J Musculoskelet Neuronal Interact *4*, 243-253.
56. Bord, S., Ireland, D.C., Beavan, S.R., and Compston, J.E. (2003). The effects of estrogen on osteoprotegerin, RANKL, and estrogen receptor expression in human osteoblasts. Bone *32*, 136-141.
57. Boyle, W.J., Simonet, W.S., and Lacey, D.L. (2003). Osteoclast differentiation and activation. Nature *423*, 337-342.
58. Hofbauer, L.C., Khosla, S., Dunstan, C.R., Lacey, D.L., Spelsberg, T.C., and Riggs, B.L. (1999). Estrogen stimulates gene expression and protein production of osteoprotegerin in human osteoblastic cells. Endocrinology *140*, 4367-4370.
59. Weilbaecher, K.N., Guise, T.A., and McCauley, L.K. (2011). Cancer to bone: a fatal attraction. Nat Rev Cancer *11*, 411-425.
60. Li, M., Liang, H., Shen, Y., and Wronski, T.J. (1999). Parathyroid hormone stimulates cancellous bone formation at skeletal sites regardless of marrow composition in ovariectomized rats. Bone *24*, 95-100.
61. Suda, T., Nakamura, I., Jimi, E., and Takahashi, N. (1997). Regulation of osteoclast function. J Bone Miner Res *12*, 869-879.
62. Erlebacher, A., Filvaroff, E.H., Ye, J.Q., and Derynck, R. (1998). Osteoblastic responses to TGF-beta during bone remodeling. Mol Biol Cell *9*, 1903-1918.
63. Kubota, K., Sakikawa, C., Katsumata, M., Nakamura, T., and Wakabayashi, K. (2002). Platelet-derived growth factor BB secreted from osteoclasts acts as an osteoblastogenesis inhibitory factor. J Bone Miner Res *17*, 257-265.
64. Udagawa, N., Takahashi, N., Yasuda, H., Mizuno, A., Itoh, K., Ueno, Y., Shinki, T., Gillespie, M.T., Martin, T.J., Higashio, K., et al. (2000). Osteoprotegerin produced by osteoblasts is an important regulator in osteoclast development and function. Endocrinology *141*, 3478-3484.
65. Cummings, S.R., Black, D.M., Nevitt, M.C., Browner, W., Cauley, J., Ensrud, K., Genant, H.K., Palermo, L., Scott, J., and Vogt, T.M. (1993). Bone density at various sites for prediction of hip fractures. The Study of Osteoporotic Fractures Research Group. Lancet *341*, 72-75.
66. Johnell, O., Kanis, J.A., Oden, A., Johansson, H., De Laet, C., Delmas, P., Eisman, J.A., Fujiwara, S., Kroger, H., Mellstrom, D., et al. (2005). Predictive value of BMD for hip and other fractures. J Bone Miner Res *20*, 1185-1194.
67. Eklund, F., Nordstrom, A., Neovius, M., Svensson, O., and Nordstrom, P. (2009). Variation in fracture rates by country may not be explained by differences in bone mass. Calcif Tissue Int *85*, 10-16.
68. Bono, C.M., and Einhorn, T.A. (2003). Overview of osteoporosis: pathophysiology and determinants of bone strength. Eur Spine J *12 Suppl 2*, S90-96.
69. Raisz, L.G. (1999). Physiology and pathophysiology of bone remodeling. Clin Chem *45*, 1353-1358.
70. Eghbali-Fatourechi, G., Khosla, S., Sanyal, A., Boyle, W.J., Lacey, D.L., and Riggs, B.L. (2003). Role of RANK ligand in mediating increased bone resorption in early postmenopausal women. J Clin Invest *111*, 1221-1230.
71. Akhter, M.P., Lappe, J.M., Davies, K.M., and Recker, R.R. (2007). Transmenopausal changes in the trabecular bone structure. Bone *41*, 111-116.
72. Justesen, J., Stenderup, K., Ebbesen, E.N., Mosekilde, L., Steiniche, T., and Kassem, M. (2001). Adipocyte tissue volume in bone marrow is increased with aging and in patients with osteoporosis. Biogerontology *2*, 165-171.
73. Pei, L., and Tontonoz, P. (2004). Fat's loss is bone's gain. J Clin Invest *113*, 805-806.
74. Gimble, J.M., Zvonic, S., Floyd, Z.E., Kassem, M., and Nuttall, M.E. (2006). Playing with bone and fat. J Cell Biochem *98*, 251-266.
75. Beresford, J.N., Bennett, J.H., Devlin, C., Leboy, P.S., and Owen, M.E. (1992). Evidence for an inverse relationship between the differentiation of adipocytic and osteogenic cells in rat marrow stromal cell cultures. J Cell Sci *102 (Pt 2)*, 341-351.

76. Klein, R.F., Allard, J., Avnur, Z., Nikolcheva, T., Rotstein, D., Carlos, A.S., Shea, M., Waters, R.V., Belknap, J.K., Peltz, G., et al. (2004). Regulation of bone mass in mice by the lipoxygenase gene Alox15. Science *303*, 229-232.
77. Lane, N.E. (2006). Epidemiology, etiology, and diagnosis of osteoporosis. Am J Obstet Gynecol *194*, S3-11.
78. Recker, R.R., and Barger-Lux, M.J. (2004). The elusive concept of bone quality. Curr Osteoporos Rep *2*, 97-100.
79. Barrios, C., Brostrom, L.A., Stark, A., and Walheim, G. (1993). Healing complications after internal fixation of trochanteric hip fractures: the prognostic value of osteoporosis. J Orthop Trauma *7*, 438-442.
80. Cornell, C.N. (2003). Internal fracture fixation in patients with osteoporosis. J Am Acad Orthop Surg *11*, 109-119.
81. Kim, W.Y., Han, C.H., Park, J.I., and Kim, J.Y. (2001). Failure of intertrochanteric fracture fixation with a dynamic hip screw in relation to pre-operative fracture stability and osteoporosis. Int Orthop *25*, 360-362.
82. Pignolo, R.J., Suda, R.K., McMillan, E.A., Shen, J., Lee, S.H., Choi, Y., Wright, A.C., and Johnson, F.B. (2008). Defects in telomere maintenance molecules impair osteoblast differentiation and promote osteoporosis. Aging Cell *7*, 23-31.
83. Kuro-o, M., Matsumura, Y., Aizawa, H., Kawaguchi, H., Suga, T., Utsugi, T., Ohyama, Y., Kurabayashi, M., Kaname, T., Kume, E., et al. (1997). Mutation of the mouse klotho gene leads to a syndrome resembling ageing. Nature *390*, 45-51.
84. Kawaguchi, H., Manabe, N., Miyaura, C., Chikuda, H., Nakamura, K., and Kuro-o, M. (1999). Independent impairment of osteoblast and osteoclast differentiation in klotho mouse exhibiting low-turnover osteopenia. J Clin Invest *104*, 229-237.
85. Suzuki, H., Amizuka, N., Oda, K., Li, M., Yoshie, H., Ohshima, H., Noda, M., and Maeda, T. (2005). Histological evidence of the altered distribution of osteocytes and bone matrix synthesis in klotho-deficient mice. Arch Histol Cytol *68*, 371-381.
86. Silva, M.J., Brodt, M.D., and Ettner, S.L. (2002). Long bones from the senescence accelerated mouse SAMP6 have increased size but reduced whole-bone strength and resistance to fracture. J Bone Miner Res *17*, 1597-1603.
87. Takeda, T. (1999). Senescence-accelerated mouse (SAM): a biogerontological resource in aging research. Neurobiol Aging *20*, 105-110.
88. Egermann, M., Heil, P., Tami, A., Ito, K., Janicki, P., Von Rechenberg, B., Hofstetter, W., and Richards, P.J. (2010). Influence of defective bone marrow osteogenesis on fracture repair in an experimental model of senile osteoporosis. J Orthop Res *28*, 798-804.
89. Weissman, I.L. (2000). Translating stem and progenitor cell biology to the clinic: barriers and opportunities. Science *287*, 1442-1446.
90. Polak, J.M., and Bishop, A.E. (2006). Stem cells and tissue engineering: past, present, and future. Ann N Y Acad Sci *1068*, 352-366.
91. Stadtfeld, M., Nagaya, M., Utikal, J., Weir, G., and Hochedlinger, K. (2008). Induced pluripotent stem cells generated without viral integration. Science *322*, 945-949.
92. Warren, L., Manos, P.D., Ahfeldt, T., Loh, Y.H., Li, H., Lau, F., Ebina, W., Mandal, P.K., Smith, Z.D., Meissner, A., et al. (2010). Highly efficient reprogramming to pluripotency and directed differentiation of human cells with synthetic modified mRNA. Cell Stem Cell *7*, 618-630.
93. Fuchs, E., Tumbar, T., and Guasch, G. (2004). Socializing with the neighbors: stem cells and their niche. Cell *116*, 769-778.
94. Joseph, N.M., and Morrison, S.J. (2005). Toward an understanding of the physiological function of Mammalian stem cells. Dev Cell *9*, 173-183.
95. Wagers, A.J., and Weissman, I.L. (2004). Plasticity of adult stem cells. Cell *116*, 639-648.
96. Schofield, R. (1978). The relationship between the spleen colony-forming cell and the haemopoietic stem cell. Blood Cells *4*, 7-25.
97. Preston, S.L., Alison, M.R., Forbes, S.J., Direkze, N.C., Poulsom, R., and Wright, N.A. (2003). The new stem cell biology: something for everyone. Mol Pathol *56*, 86-96.
98. Scadden, D.T. (2006). The stem-cell niche as an entity of action. Nature *441*, 1075-1079.
99. Song, L., Webb, N.E., Song, Y., and Tuan, R.S. (2006). Identification and functional analysis of candidate genes regulating mesenchymal stem cell self-renewal and multipotency. Stem Cells *24*, 1707-1718.
100. Sacchetti, B., Funari, A., Michienzi, S., Di Cesare, S., Piersanti, S., Saggio, I., Tagliafico, E., Ferrari, S., Robey, P.G., Riminucci, M., et al. (2007). Self-renewing osteoprogenitors in bone marrow sinusoids can organize a hematopoietic microenvironment. Cell *131*, 324-336.

101. Bianco, P., Robey, P.G., Saggio, I., and Riminucci, M. (2010). "Mesenchymal" stem cells in human bone marrow (skeletal stem cells): a critical discussion of their nature, identity, and significance in incurable skeletal disease. Hum Gene Ther *21*, 1057-1066.
102. Brazelton, T.R., Rossi, F.M., Keshet, G.I., and Blau, H.M. (2000). From marrow to brain: expression of neuronal phenotypes in adult mice. Science *290*, 1775-1779.
103. Kuznetsov, S.A., Mankani, M.H., Gronthos, S., Satomura, K., Bianco, P., and Robey, P.G. (2001). Circulating skeletal stem cells. J Cell Biol *153*, 1133-1140.
104. Rosada, C., Justesen, J., Melsvik, D., Ebbesen, P., and Kassem, M. (2003). The human umbilical cord blood: a potential source for osteoblast progenitor cells. Calcif Tissue Int *72*, 135-142.
105. Vandenabeele, F., De Bari, C., Moreels, M., Lambrichts, I., Dell'Accio, F., Lippens, P.L., and Luyten, F.P. (2003). Morphological and immunocytochemical characterization of cultured fibroblast-like cells derived from adult human synovial membrane. Arch Histol Cytol *66*, 145-153.
106. Miura, M., Gronthos, S., Zhao, M., Lu, B., Fisher, L.W., Robey, P.G., and Shi, S. (2003). SHED: stem cells from human exfoliated deciduous teeth. Proc Natl Acad Sci U S A *100*, 5807-5812.
107. Gronthos, S., Franklin, D.M., Leddy, H.A., Robey, P.G., Storms, R.W., and Gimble, J.M. (2001). Surface protein characterization of human adipose tissue-derived stromal cells. J Cell Physiol *189*, 54-63.
108. Igura, K., Zhang, X., Takahashi, K., Mitsuru, A., Yamaguchi, S., and Takashi, T.A. (2004). Isolation and characterization of mesenchymal progenitor cells from chorionic villi of human placenta. Cytotherapy *6*, 543-553.
109. Tsai, M.S., Lee, J.L., Chang, Y.J., and Hwang, S.M. (2004). Isolation of human multipotent mesenchymal stem cells from second-trimester amniotic fluid using a novel two-stage culture protocol. Hum Reprod *19*, 1450-1456.
110. Salingcarnboriboon, R., Yoshitake, H., Tsuji, K., Obinata, M., Amagasa, T., Nifuji, A., and Noda, M. (2003). Establishment of tendon-derived cell lines exhibiting pluripotent mesenchymal stem cell-like property. Exp Cell Res *287*, 289-300.
111. Seo, B.M., Miura, M., Gronthos, S., Bartold, P.M., Batouli, S., Brahim, J., Young, M., Robey, P.G., Wang, C.Y., and Shi, S. (2004). Investigation of multipotent postnatal stem cells from human periodontal ligament. Lancet *364*, 149-155.
112. in 't Anker, P.S., Noort, W.A., Scherjon, S.A., Kleijburg-van der Keur, C., Kruisselbrink, A.B., van Bezooijen, R.L., Beekhuizen, W., Willemze, R., Kanhai, H.H., and Fibbe, W.E. (2003). Mesenchymal stem cells in human second-trimester bone marrow, liver, lung, and spleen exhibit a similar immunophenotype but a heterogeneous multilineage differentiation potential. Haematologica *88*, 845-852.
113. Wagner, E.R., He, B.C., Chen, L., Zuo, G.W., Zhang, W., Shi, Q., Luo, Q., Luo, X., Liu, B., Luo, J., et al. (2010). Therapeutic Implications of PPARgamma in Human Osteosarcoma. PPAR Res *2010*, 956427.
114. Noth, U., Osyczka, A.M., Tuli, R., Hickok, N.J., Danielson, K.G., and Tuan, R.S. (2002). Multilineage mesenchymal differentiation potential of human trabecular bone-derived cells. J Orthop Res *20*, 1060-1069.
115. Nuttall, M.E., Patton, A.J., Olivera, D.L., Nadeau, D.P., and Gowen, M. (1998). Human trabecular bone cells are able to express both osteoblastic and adipocytic phenotype: implications for osteopenic disorders. J Bone Miner Res *13*, 371-382.
116. Pittenger, M.F., Mackay, A.M., Beck, S.C., Jaiswal, R.K., Douglas, R., Mosca, J.D., Moorman, M.A., Simonetti, D.W., Craig, S., and Marshak, D.R. (1999). Multilineage potential of adult human mesenchymal stem cells. Science *284*, 143-147.
117. MacDougald, O.A., and Lane, M.D. (1995). Transcriptional regulation of gene expression during adipocyte differentiation. Annu Rev Biochem *64*, 345-373.
118. MacDougald, O.A., and Mandrup, S. (2002). Adipogenesis: forces that tip the scales. Trends Endocrinol Metab *13*, 5-11.
119. Tontonoz, P., Graves, R.A., Budavari, A.I., Erdjument-Bromage, H., Lui, M., Hu, E., Tempst, P., and Spiegelman, B.M. (1994). Adipocyte-specific transcription factor ARF6 is a heterodimeric complex of two nuclear hormone receptors, PPAR gamma and RXR alpha. Nucleic Acids Res *22*, 5628-5634.
120. Spiegelman, B.M., Choy, L., Hotamisligil, G.S., Graves, R.A., and Tontonoz, P. (1993). Regulation of adipocyte gene expression in differentiation and syndromes of obesity/diabetes. J Biol Chem *268*, 6823-6826.
121. Barak, Y., Nelson, M.C., Ong, E.S., Jones, Y.Z., Ruiz-Lozano, P., Chien, K.R., Koder, A., and Evans, R.M. (1999). PPAR gamma is required for placental, cardiac, and adipose tissue development. Mol Cell *4*, 585-595.

122. Tontonoz, P., Hu, E., and Spiegelman, B.M. (1994). Stimulation of adipogenesis in fibroblasts by PPAR gamma 2, a lipid-activated transcription factor. Cell *79*, 1147-1156.
123. Rosen, E.D., Sarraf, P., Troy, A.E., Bradwin, G., Moore, K., Milstone, D.S., Spiegelman, B.M., and Mortensen, R.M. (1999). PPAR gamma is required for the differentiation of adipose tissue in vivo and in vitro. Mol Cell *4*, 611-617.
124. Franceschi, R.T., and Iyer, B.S. (1992). Relationship between collagen synthesis and expression of the osteoblast phenotype in MC3T3-E1 cells. J Bone Miner Res *7*, 235-246.
125. Jaiswal, N., Haynesworth, S.E., Caplan, A.I., and Bruder, S.P. (1997). Osteogenic differentiation of purified, culture-expanded human mesenchymal stem cells in vitro. J Cell Biochem *64*, 295-312.
126. Ducy, P., Schinke, T., and Karsenty, G. (2000). The osteoblast: a sophisticated fibroblast under central surveillance. Science *289*, 1501-1504.
127. Nakashima, K., and de Crombrugghe, B. (2003). Transcriptional mechanisms in osteoblast differentiation and bone formation. Trends Genet *19*, 458-466.
128. Kundu, M., Javed, A., Jeon, J.P., Horner, A., Shum, L., Eckhaus, M., Muenke, M., Lian, J.B., Yang, Y., Nuckolls, G.H., et al. (2002). Cbfbeta interacts with Runx2 and has a critical role in bone development. Nat Genet *32*, 639-644.
129. Miller, J., Horner, A., Stacy, T., Lowrey, C., Lian, J.B., Stein, G., Nuckolls, G.H., and Speck, N.A. (2002). The core-binding factor beta subunit is required for bone formation and hematopoietic maturation. Nat Genet *32*, 645-649.
130. Jaiswal, R.K., Jaiswal, N., Bruder, S.P., Mbalaviele, G., Marshak, D.R., and Pittenger, M.F. (2000). Adult human mesenchymal stem cell differentiation to the osteogenic or adipogenic lineage is regulated by mitogen-activated protein kinase. J Biol Chem *275*, 9645-9652.
131. Xiao, G., Jiang, D., Gopalakrishnan, R., and Franceschi, R.T. (2002). Fibroblast growth factor 2 induction of the osteocalcin gene requires MAPK activity and phosphorylation of the osteoblast transcription factor, Cbfa1/Runx2. J Biol Chem *277*, 36181-36187.
132. Ebert, T.R., Martin, D.T., Bullock, N., Mujika, I., Quod, M.J., Farthing, L.A., Burke, L.M., and Withers, R.T. (2007). Influence of hydration status on thermoregulation and cycling hill climbing. Med Sci Sports Exerc *39*, 323-329.
133. Jeon, E.J., Lee, K.Y., Choi, N.S., Lee, M.H., Kim, H.N., Jin, Y.H., Ryoo, H.M., Choi, J.Y., Yoshida, M., Nishino, N., et al. (2006). Bone morphogenetic protein-2 stimulates Runx2 acetylation. J Biol Chem *281*, 16502-16511.
134. Battula, V.L., Bareiss, P.M., Treml, S., Conrad, S., Albert, I., Hojak, S., Abele, H., Schewe, B., Just, L., Skutella, T., et al. (2007). Human placenta and bone marrow derived MSC cultured in serum-free, b-FGF-containing medium express cell surface frizzled-9 and SSEA-4 and give rise to multilineage differentiation. Differentiation *75*, 279-291.
135. Marie, P.J., Coffin, J.D., and Hurley, M.M. (2005). FGF and FGFR signaling in chondrodysplasias and craniosynostosis. J Cell Biochem *96*, 888-896.
136. Ornitz, D.M. (2005). FGF signaling in the developing endochondral skeleton. Cytokine Growth Factor Rev *16*, 205-213.
137. Ling, L., Murali, S., Dombrowski, C., Haupt, L.M., Stein, G.S., van Wijnen, A.J., Nurcombe, V., and Cool, S.M. (2006). Sulfated glycosaminoglycans mediate the effects of FGF2 on the osteogenic potential of rat calvarial osteoprogenitor cells. J Cell Physiol *209*, 811-825.
138. Choi, K.Y., Kim, H.J., Lee, M.H., Kwon, T.G., Nah, H.D., Furuichi, T., Komori, T., Nam, S.H., Kim, Y.J., and Ryoo, H.M. (2005). Runx2 regulates FGF2-induced Bmp2 expression during cranial bone development. Dev Dyn *233*, 115-121.
139. Quarto, N., and Longaker, M.T. (2006). FGF-2 inhibits osteogenesis in mouse adipose tissue-derived stromal cells and sustains their proliferative and osteogenic potential state. Tissue Eng *12*, 1405-1418.
140. Muruganandan, S., Roman, A.A., and Sinal, C.J. (2009). Adipocyte differentiation of bone marrow-derived mesenchymal stem cells: cross talk with the osteoblastogenic program. Cell Mol Life Sci *66*, 236-253.
141. Kuhn, N.Z., and Tuan, R.S. (2010). Regulation of stemness and stem cell niche of mesenchymal stem cells: implications in tumorigenesis and metastasis. J Cell Physiol *222*, 268-277.
142. Mendez-Ferrer, S., Michurina, T.V., Ferraro, F., Mazloom, A.R., Macarthur, B.D., Lira, S.A., Scadden, D.T., Ma'ayan, A., Enikolopov, G.N., and Frenette, P.S. (2010). Mesenchymal and haematopoietic stem cells form a unique bone marrow niche. Nature *466*, 829-834.
143. Yin, T., and Li, L. (2006). The stem cell niches in bone. J Clin Invest *116*, 1195-1201.
144. Imhoff, B.R., and Hansen, J.M. (2011). Differential redox potential profiles during adipogenesis and osteogenesis. Cell Mol Biol Lett *16*, 149-161.
145. Nuttall, M.E., and Gimble, J.M. (2004). Controlling the balance between osteoblastogenesis and adipogenesis and the consequent therapeutic implications. Curr Opin Pharmacol *4*, 290-294.

146. Jethva, R., Otsuru, S., Dominici, M., and Horwitz, E.M. (2009). Cell therapy for disorders of bone. Cytotherapy *11*, 3-17.
147. Duque, G. (2008). Bone and fat connection in aging bone. Curr Opin Rheumatol *20*, 429-434.
148. Takada, I., Kouzmenko, A.P., and Kato, S. (2009). Wnt and PPARgamma signaling in osteoblastogenesis and adipogenesis. Nat Rev Rheumatol *5*, 442-447.
149. Logeart-Avramoglou, D., Anagnostou, F., Bizios, R., and Petite, H. (2005). Engineering bone: challenges and obstacles. J Cell Mol Med *9*, 72-84.
150. Aggarwal, S., and Pittenger, M.F. (2005). Human mesenchymal stem cells modulate allogeneic immune cell responses. Blood *105*, 1815-1822.
151. Le Blanc, K., Rasmusson, I., Sundberg, B., Gotherstrom, C., Hassan, M., Uzunel, M., and Ringden, O. (2004). Treatment of severe acute graft-versus-host disease with third party haploidentical mesenchymal stem cells. Lancet *363*, 1439-1441.
152. Majumdar, M.K., Keane-Moore, M., Buyaner, D., Hardy, W.B., Moorman, M.A., McIntosh, K.R., and Mosca, J.D. (2003). Characterization and functionality of cell surface molecules on human mesenchymal stem cells. J Biomed Sci *10*, 228-241.
153. Petite, H., Viateau, V., Bensaid, W., Meunier, A., de Pollak, C., Bourguignon, M., Oudina, K., Sedel, L., and Guillemin, G. (2000). Tissue-engineered bone regeneration. Nat Biotechnol *18*, 959-963.
154. Kon, E., Muraglia, A., Corsi, A., Bianco, P., Marcacci, M., Martin, I., Boyde, A., Ruspantini, I., Chistolini, P., Rocca, M., et al. (2000). Autologous bone marrow stromal cells loaded onto porous hydroxyapatite ceramic accelerate bone repair in critical-size defects of sheep long bones. J Biomed Mater Res *49*, 328-337.
155. Shang, Q., Wang, Z., Liu, W., Shi, Y., Cui, L., and Cao, Y. (2001). Tissue-engineered bone repair of sheep cranial defects with autologous bone marrow stromal cells. J Craniofac Surg *12*, 586-593; discussion 594-585.
156. Pereira, R.F., Halford, K.W., O'Hara, M.D., Leeper, D.B., Sokolov, B.P., Pollard, M.D., Bagasra, O., and Prockop, D.J. (1995). Cultured adherent cells from marrow can serve as long-lasting precursor cells for bone, cartilage, and lung in irradiated mice. Proc Natl Acad Sci U S A *92*, 4857-4861.
157. Pereira, R.F., O'Hara, M.D., Laptev, A.V., Halford, K.W., Pollard, M.D., Class, R., Simon, D., Livezey, K., and Prockop, D.J. (1998). Marrow stromal cells as a source of progenitor cells for nonhematopoietic tissues in transgenic mice with a phenotype of osteogenesis imperfecta. Proc Natl Acad Sci U S A *95*, 1142-1147.
158. Horwitz, E.M., Prockop, D.J., Fitzpatrick, L.A., Koo, W.W., Gordon, P.L., Neel, M., Sussman, M., Orchard, P., Marx, J.C., Pyeritz, R.E., et al. (1999). Transplantability and therapeutic effects of bone marrow-derived mesenchymal cells in children with osteogenesis imperfecta. Nat Med *5*, 309-313.
159. Horwitz, E.M., Prockop, D.J., Gordon, P.L., Koo, W.W., Fitzpatrick, L.A., Neel, M.D., McCarville, M.E., Orchard, P.J., Pyeritz, R.E., and Brenner, M.K. (2001). Clinical responses to bone marrow transplantation in children with severe osteogenesis imperfecta. Blood *97*, 1227-1231.
160. Horwitz, E.M., Gordon, P.L., Koo, W.K., Marx, J.C., Neel, M.D., McNall, R.Y., Muul, L., and Hofmann, T. (2002). Isolated allogeneic bone marrow-derived mesenchymal cells engraft and stimulate growth in children with osteogenesis imperfecta: Implications for cell therapy of bone. Proc Natl Acad Sci U S A *99*, 8932-8937.
161. Cho, S.W., Sun, H.J., Yang, J.Y., Jung, J.Y., An, J.H., Cho, H.Y., Choi, H.J., Kim, S.W., Kim, S.Y., Kim, D., et al. (2009). Transplantation of mesenchymal stem cells overexpressing RANK-Fc or CXCR4 prevents bone loss in ovariectomized mice. Mol Ther *17*, 1979-1987.
162. Kumar, S., Nagy, T.R., and Ponnazhagan, S. (2010). Therapeutic potential of genetically modified adult stem cells for osteopenia. Gene Ther *17*, 105-116.
163. Zhang, X.S., Linkhart, T.A., Chen, S.T., Peng, H., Wergedal, J.E., Guttierez, G.G., Sheng, M.H., Lau, K.H., and Baylink, D.J. (2004). Local ex vivo gene therapy with bone marrow stromal cells expressing human BMP4 promotes endosteal bone formation in mice. J Gene Med *6*, 4-15.
164. Ichioka, N., Inaba, M., Kushida, T., Esumi, T., Takahara, K., Inaba, K., Ogawa, R., Iida, H., and Ikehara, S. (2002). Prevention of senile osteoporosis in SAMP6 mice by intrabone marrow injection of allogeneic bone marrow cells. Stem Cells *20*, 542-551.
165. Lien, C.Y., Chih-Yuan Ho, K., Lee, O.K., Blunn, G.W., and Su, Y. (2009). Restoration of bone mass and strength in glucocorticoid-treated mice by systemic transplantation of CXCR4 and cbfa-1 co-expressing mesenchymal stem cells. J Bone Miner Res *24*, 837-848.
166. Ailhaud, G., Grimaldi, P., and Negrel, R. (1992). Cellular and molecular aspects of adipose tissue development. Annu Rev Nutr *12*, 207-233.
167. Rosen, E.D., and Spiegelman, B.M. (2000). Molecular regulation of adipogenesis. Annu Rev Cell Dev Biol *16*, 145-171.

168. Lowell, B.B., and Flier, J.S. (1997). Brown adipose tissue, beta 3-adrenergic receptors, and obesity. Annu Rev Med *48*, 307-316.
169. Krug, A.W., and Ehrhart-Bornstein, M. (2005). Newly discovered endocrine functions of white adipose tissue: possible relevance in obesity-related diseases. Cell Mol Life Sci *62*, 1359-1362.
170. Trayhurn, P., Bing, C., and Wood, I.S. (2006). Adipose tissue and adipokines--energy regulation from the human perspective. J Nutr *136*, 1935S-1939S.
171. Cousin, B., Casteilla, L., Lafontan, M., Ambid, L., Langin, D., Berthault, M.F., and Penicaud, L. (1993). Local sympathetic denervation of white adipose tissue in rats induces preadipocyte proliferation without noticeable changes in metabolism. Endocrinology *133*, 2255-2262.
172. Wajchenberg, B.L. (2000). Subcutaneous and visceral adipose tissue: their relation to the metabolic syndrome. Endocr Rev *21*, 697-738.
173. de Meis, L., Arruda, A.P., da Costa, R.M., and Benchimol, M. (2006). Identification of a Ca2+-ATPase in brown adipose tissue mitochondria: regulation of thermogenesis by ATP and Ca2+. J Biol Chem *281*, 16384-16390.
174. Guerre-Millo, M. (2004). Adipose tissue and adipokines: for better or worse. Diabetes Metab *30*, 13-19.
175. Aust, L., Devlin, B., Foster, S.J., Halvorsen, Y.D., Hicok, K., du Laney, T., Sen, A., Willingmyre, G.D., and Gimble, J.M. (2004). Yield of human adipose-derived adult stem cells from liposuction aspirates. Cytotherapy *6*, 7-14.
176. Zuk, P.A., Zhu, M., Ashjian, P., De Ugarte, D.A., Huang, J.I., Mizuno, H., Alfonso, Z.C., Fraser, J.K., Benhaim, P., and Hedrick, M.H. (2002). Human adipose tissue is a source of multipotent stem cells. Mol Biol Cell *13*, 4279-4295.
177. Mirsaidi, A., Tiaden, A.N., and Richards, P.J. (2013). Preparation and osteogenic differentiation of scaffold-free mouse adipose-derived stromal cell microtissue spheroids (ASC-MT). Curr Protoc Stem Cell Biol *27*, Unit 2B 5.
178. Guilak, F., Lott, K.E., Awad, H.A., Cao, Q., Hicok, K.C., Fermor, B., and Gimble, J.M. (2006). Clonal analysis of the differentiation potential of human adipose-derived adult stem cells. J Cell Physiol *206*, 229-237.
179. Dragoo, J.L., Choi, J.Y., Lieberman, J.R., Huang, J., Zuk, P.A., Zhang, J., Hedrick, M.H., and Benhaim, P. (2003). Bone induction by BMP-2 transduced stem cells derived from human fat. J Orthop Res *21*, 622-629.
180. Mirsaidi, A., Kleinhans, K.N., Rimann, M., Tiaden, A.N., Stauber, M., Rudolph, K.L., and Richards, P.J. (2012). Telomere length, telomerase activity and osteogenic differentiation are maintained in adipose-derived stromal cells from senile osteoporotic SAMP6 mice. J Tissue Eng Regen Med *6*, 378-390.
181. Hattori, H., Sato, M., Masuoka, K., Ishihara, M., Kikuchi, T., Matsui, T., Takase, B., Ishizuka, T., Kikuchi, M., and Fujikawa, K. (2004). Osteogenic potential of human adipose tissue-derived stromal cells as an alternative stem cell source. Cells Tissues Organs *178*, 2-12.
182. Hicok, K.C., Du Laney, T.V., Zhou, Y.S., Halvorsen, Y.D., Hitt, D.C., Cooper, L.F., and Gimble, J.M. (2004). Human adipose-derived adult stem cells produce osteoid in vivo. Tissue Eng *10*, 371-380.
183. Liao, X., Li, F., Wang, X., Yanoso, J., and Niyibizi, C. (2008). Distribution of murine adipose-derived mesenchymal stem cells in vivo following transplantation in developing mice. Stem Cells Dev *17*, 303-314.
184. Peterson, B., Zhang, J., Iglesias, R., Kabo, M., Hedrick, M., Benhaim, P., and Lieberman, J.R. (2005). Healing of critically sized femoral defects, using genetically modified mesenchymal stem cells from human adipose tissue. Tissue Eng *11*, 120-129.
185. Cowan, C.M., Shi, Y.Y., Aalami, O.O., Chou, Y.F., Mari, C., Thomas, R., Quarto, N., Contag, C.H., Wu, B., and Longaker, M.T. (2004). Adipose-derived adult stromal cells heal critical-size mouse calvarial defects. Nat Biotechnol *22*, 560-567.
186. Mehrara, B.J., Disa, J.J., and Pusic, A. (2006). Scalp reconstruction. J Surg Oncol *94*, 504-508.
187. Roura, S., Farre, J., Soler-Botija, C., Llach, A., Hove-Madsen, L., Cairo, J.J., Godia, F., Cinca, J., and Bayes-Genis, A. (2006). Effect of aging on the pluripotential capacity of human CD105+ mesenchymal stem cells. Eur J Heart Fail *8*, 555-563.
188. D'Ippolito, G., Schiller, P.C., Ricordi, C., Roos, B.A., and Howard, G.A. (1999). Age-related osteogenic potential of mesenchymal stromal stem cells from human vertebral bone marrow. J Bone Miner Res *14*, 1115-1122.
189. Stolzing, A., Jones, E., McGonagle, D., and Scutt, A. (2008). Age-related changes in human bone marrow-derived mesenchymal stem cells: consequences for cell therapies. Mech Ageing Dev *129*, 163-173.

190. Jilka, R.L., Weinstein, R.S., Takahashi, K., Parfitt, A.M., and Manolagas, S.C. (1996). Linkage of decreased bone mass with impaired osteoblastogenesis in a murine model of accelerated senescence. J Clin Invest *97*, 1732-1740.
191. Silva, M.J., Brodt, M.D., Ko, M., and Abu-Amer, Y. (2005). Impaired marrow osteogenesis is associated with reduced endocortical bone formation but does not impair periosteal bone formation in long bones of SAMP6 mice. J Bone Miner Res *20*, 419-427.
192. Bonyadi, M., Waldman, S.D., Liu, D., Aubin, J.E., Grynpas, M.D., and Stanford, W.L. (2003). Mesenchymal progenitor self-renewal deficiency leads to age-dependent osteoporosis in Sca-1/Ly-6A null mice. Proc Natl Acad Sci U S A *100*, 5840-5845.
193. Yoon, E., Dhar, S., Chun, D.E., Gharibjanian, N.A., and Evans, G.R. (2007). In vivo osteogenic potential of human adipose-derived stem cells/poly lactide-co-glycolic acid constructs for bone regeneration in a rat critical-sized calvarial defect model. Tissue Eng *13*, 619-627.
194. Kim, K.I., Park, S., and Im, G.I. (2014). Osteogenic differentiation and angiogenesis with cocultured adipose-derived stromal cells and bone marrow stromal cells. Biomaterials *35*, 4792-4804.
195. Schenk, S., and Quaranta, V. (2003). Tales from the crypt[ic] sites of the extracellular matrix. Trends Cell Biol *13*, 366-375.
196. Liu, H.Y., Chiou, J.F., Wu, A.T., Tsai, C.Y., Leu, J.D., Ting, L.L., Wang, M.F., Chen, H.Y., Lin, C.T., Williams, D.F., et al. (2012). The effect of diminished osteogenic signals on reduced osteoporosis recovery in aged mice and the potential therapeutic use of adipose-derived stem cells. Biomaterials *33*, 6105-6112.
197. Cho, S.W., Sun, H.J., Yang, J.Y., Jung, J.Y., Choi, H.J., An, J.H., Kim, S.W., Kim, S.Y., Park, K.J., and Shin, C.S. (2012). Human adipose tissue-derived stromal cell therapy prevents bone loss in ovariectomized nude mouse. Tissue Eng Part A *18*, 1067-1078.
198. You, L., Pan, L., Chen, L., Chen, J.Y., Zhang, X., Lv, Z., and Fu, D. (2012). Suppression of zinc finger protein 467 alleviates osteoporosis through promoting differentiation of adipose derived stem cells to osteoblasts. J Transl Med *10*, 11.
199. Krings, A., Rahman, S., Huang, S., Lu, Y., Czernik, P.J., and Lecka-Czernik, B. (2012). Bone marrow fat has brown adipose tissue characteristics, which are attenuated with aging and diabetes. Bone *50*, 546-552.

Curriculum Vitae

Ali MIRSAIDI

Date of Birth: 06.02.1983
Citizenship: Iranian
Residency: Switzerland, B permit

+41 79 315 4802
ali.mirsaidi@uzh.ch
Herbstweg 74, CH–8050, Zürich

Education

03/2010 – 06/2014 **Doctor of Natural Science (PhD)**
Doctoral thesis: Therapeutic potential of adipose-derived stromal cells for the treatment of senile osteoporosis

University of Zürich, Faculty of Science, Switzerland
Life Science Zürich Graduate School

03/2007 – 02/2010 **Master of Science in Biomedical Engineering (MSc)**
Master thesis: Differentiation of mesenchymal stem cells on elastic matrices
Grade: magna cum laude

University of Bern, Faculty of Medicine, Switzerland

09/2001 – 09/2006 **Bachelor of Science in Mechanical Engineering (BSc)**
Bachelor thesis: Study the influence of bending moment on plane composite laminates and derive numerical solution for mechanical behavior
Grade: 20/20

Tehran University, Faculty of Mechanical Engineering, Iran

06/1997 – 06/2001 **Mathematics and Physics Discipline**

Danesh College, Tehran**,** Iran
Grade: 17/20

Research and Industrial Experience

03/2010 – 12/2014 **Ph.D. candidate and research assistant**
Center for Applied Biotechnology and Molecular Medicine *(CABMM)*
Bone and Stem Cell Research Group, University of Zürich

- Managing and leading collaborative animal projects
- Establishing intra-bone surgery for mice
- Micro computed tomography (*µCT)* scanning and evaluation
- Isolating and differentiating adult stromal cells
- Developing 3D culture systems for *in-vivo* & *vitro* applications
- Performing and optimizing immunostaining methods
- Histology and histomophometry analysis of tissue sections

06/2009 – 02/2010 **MSc candidate**
Department of Clinical Research
Bone Biology and Orthopaedic Research Group, University of Bern

- Establishing and processing coating techniques to grow primary cells on polymeric substrates
- Investigating the effect of matrix stiffness on the differentiation of human mesenchymal stromal cells
- Performing molecular biology and associated technique for gene and protein expression by RT-qPCR, Western Blot and ELISA

01/2005 – 02/2007 **Member of design and development unit**
SGI Co. (*Gas Valve Factory*), Iran

- Optimizing production planning process
- Establishing and supervising a new production line
- Modeling and designing layout of products using computer software

01/2004 – 12/2004 **Maintenance supervisor**
Faragir Plastic Co. (*Polyethylene Pipes & Joints Factory*), Iran

- Installing and operating new plastic injection molds
- Training operators and inspection of the machinery

Computer Skills

Programming Matlab, R, C++
Software SPSS, Abaqus, literature databases, MS Office

Language skills

English: fluent
Persian: native
German: upper intermediate
French: basics

Award

07/2013 **Travel grant for 7th EFF/ASBMR fellows, Baltimore, MD, USA**
Selected research work in the field of metabolic bone diseases

Interests and Hobbies

Reading, Ski, Basketball, Badminton, Swimming, Travelling

Articles in Peer – Reviewed Journal

1. **Mirsaidi A**, Genelin K, Vetsch JR, Stanger S, Theiss F, Lindtner RA, von Rechenberg B, Blauth M, Müller R, Kuhn GA, Hofmann-Boss S, Ebner HL, Richards PJ. Therapeutic potential of adipose-derived stromal cells in age-related osteoporosis. *Biomaterials 2014; 35(26):7326-35.*

2. **Mirsaidi A**, Tiaden AN, Richards, PJ. Preparation and osteogenic differentiation of scaffold-Free mouse adipose-derived stromal cell microtissue spheroids (ASC-MT). *Current Protocols in Stem Cell Biology 2013; 27:2B.5.1–2B.5.12.*

3. **Mirsaidi A**, Kleinhans KN, Rimann M, Tiaden AN, Stauber M, Rudolph KL, Richards PJ. Telomere length, telomerase activity and osteogenic differentiation are maintained in adipose tissue-derived stromal cells from senile osteoporotic SAMP6 mice. *J Tissue Eng Reg Med 2011; 6:378-90.*

4. Erener S, **Mirsaidi A**, Hesse M, Tiaden AN, Ellingsgaard H, Kostadinova R, Donath MY, Richards PJ, Hottiger MO. ARTD1 knockout mice on high-fat diet develop hepatic steatosis as a consequence of impaired adipocyte function. *FASEB J 2012; 26:2631-8.*

5. Tiaden AN, Breiden M, **Mirsaidi A**, Weber FA, Bahrenberg G, Glanz S, Cinelli P, Ehrmann M, Richards PJ. Human serine protease HTRA1 positively regulates osteogenesis of human bone marrow-derived mesenchymal stem cells and mineralization of differentiating bone-forming cells through the modulation of extracellular matrix protein. *Stem Cells 2012; 30:2271-2282.*

6. Tiaden AN, Klawitter M, Lux V, **Mirsaidi A,** Bahrenberg G, Glanz S, Quero L, Liebscher T, Wuertz K, Ehrmann M, Richards PJ. Detrimental role for human high temperature requirement serine protease A1 in the pathogenesis of intervertebral disc degeneration. *J Biol Chem 2012; 15; 287(25):21335-45.*

7. Lehmann M, Pirinen E, **Mirsaidi A**, Richards PJ, Auwerx J, Hottiger MO. ARTD1-induced poly-ADP-ribose formation enhances PPARγ ligand binding and co-factor exchange. *Nucleic Acids Res 2014; 43(1):129-42*.

8. Müller-Edenborn K, Léger K, Garzon JF, Oertli C, **Mirsaidi A**, Richards PJ, Rehrauer H, Spielmann P, Hoogewijs D, Borsig L, Hottiger MO, Wenger RH. Hypoxia attenuates the proinflammatory response in colon cancer cells by regulating IκB. *Oncotarget 2015; Epub ahead of print.*

Peer – Reviewed Conference Abstracts

1. **Mirsaidi A**, Kleinhans K, Tiaden AN, Rudolph KL, Richards PJ. Adipose tissue-derived stromal cell function is maintained in senile osteoporotic SAMP6 mice, proceedings of the 57th Annual Meeting of the *Orthopaedic Research Society*, Long Beach, CA, 2011.

2. **Mirsaidi A**, Vetsch JR, Müller R, Hofmann S, Richards PJ. Therapeutic potential of adipose-derived stromal cells for the treatment of age-related osteoporosis, proceedings of Annual Meeting of the *American Society for Bone and Mineral Research*, Baltimore, MD, 2013.

3. **Mirsaidi A**, Luginbuehl R, Hofstetter W, Egli RJ. Differentiation potential and molecular characterization of mesenchymal stem cells during long-term monolayer culture, proceedings of Annual Meeting of the *American Society for Bone and Mineral Research*, Baltimore, MD, 2013.

Acknowledgements

First and foremost I would like to express sincere acknowledgements to PD Dr. Peter Richards for giving me the opportunity to work on this project and for his excellent supervision and guidance through my Ph.D. thesis. I feel very privileged to have been selected 4 years ago as the first Ph.D. student in Bone and Stem Cell Research (BSR) group, and for the opportunity to conduct this challenging project within the BSR group. I am grateful to Pete for shaping a mechanical engineer (in biology) I am today.

I would also like to thank Prof. Dr. Hottiger for being my responsible faculty member, and also Prof. Dr. med. Verrey, and PD Dr. Cinelli for valuable discussions and input during my committee meetings. I would like to acknowledge PD Dr. Arnaud Scherberich who agreed to read my thesis as external reviewer.

A very special thank goes to Nicki for paving the way for me through the maze of the scientific world, for his valuable suggestions and fruitful discussions, and for the time dedicated. Many thanks to Lilian for being a great Ph.D. companion since the first day, listening to all my words. Sincere acknowledgements also to Felix for helping me during mice surgery, which was not easy to set up everything from scratch, very frustrating, but his patience and friendship helped greatly to finish the *in vivo* experiments. Additionally, I'm very thankful to Dr. Silke Kalchofner-Mark for the interesting scientific discussions during CABMM seminars, and for all the administrative help. I would also like to thank all the former and current members of the BSR group and IVBMB, not only for their scientific input, but also for lots of nice memories. I am very grateful to have such good colleagues and friends during tough time in my PhD.

I express a sincere appreciation to all my collaborators, especially Dr. Matthias Arlt, Dr. med. vet. Gisela Kuhn and Jolanda Vetsch, for sharing expertise, time and also lots of efforts to do this project.

Thanks to my best friends Nikrouz, Nima, Negin, and Mahsa. All their endless support and friendship kept me going day-in and day-out and giving me great time outside the lab.

Last but not least, I would also like to show my appreciation to my brothers, Hossi and Reza, who helped me a lot throughout my studies. Mom and Dad, thank you for supporting and encouraging me in conducting the research project far from home and all the cheering words in times I needed them.